Biological activity of palmitoylcarnitine in prostate cancer

Ala'a Al-Bakheit

Institute of Food Research

A thesis for the degree of Doctor of Philosophy to the University of East Anglia

2014

Abstract

Acylcarnitines are intermediates of fatty acid oxidation and accumulate as a result of a metabolic defect. Accumulation of palmitoylcarnitine (palcar), a long-chain acylcarnitine, has been observed in diabetes mellitus type II, obesity and kidney cancer. Certain dietary intervention studies have been shown to reduce serum and urinary levels of acylcarnitines.

It was shown that palcar accumulates in prostate cancer tissue, possibly indicative of the metabolic changes associated with cancer development, but that palcar at high concentrations may have activities that could be associated with cancer development. Through the use of cancerous (PC3, DU145) and non-cancerous (PNT1A, BPH) cell models, it was shown that high levels of palcar could induce gene expression of the inflammatory cytokine IL-6, and induce its secretion in PC3 cells. This was associated with the rapid influx of Ca^{2+}. Through the use of various metabolic inhibitors, it was shown that Ca^{2+} influx includes the activation of G-protein coupled receptors, L-type Ca^{2+} channels and PI3K pathway. However, it was shown through the use of global gene arrays that lower levels of palcar with uncorrected P value induced many changes in gene expression in PNT1A cells. A comparison with the global changes induced by DHT, an androgen linked to prostate cancer progression, revealed a significant overlap in activity between palcar and DHT, suggesting that palcar may have a potential role in promoting cancer progression. In PC3 cells through the use of real time RT-PCR palcar was shown to induce glycolysis.

In conclusion, it is suggested that palcar may represent a potential biomarker of the metabolic dysfunction associated with prostate cancer. At physiological levels palcar had no effects on the prostate cancer cells, however, at high levels palcar drive tumour development through inducing key inflammatory cytokine and inducing changes in gene expression associated with glycolysis.

Acknowledgements

I would like to express my deep gratitude to my supervisor, Professor Richard Mithen, for giving me the chance to do my PhD, for his help in making me settled in UK and for his enthusiastic encouragement and continued guidance throughout my PhD.

I would like to express my very great appreciation to my secondary supervisor, Ian Jonson, for his valuable and constructive suggestions during the development of my research work.

A special thanks to Dr. Antonietta Melchini for her support during my initial stages of my PhD and for her daily supervision. Her willingness to give her time so generously has been very much appreciated.

I would like to thank Dr. Maria Traka for her contribution in writing the protocol for the ethical approval of the prostate tissue form the NNUH Partners in Cancer Research Human Tissue Bank, which I also thank for providing these tissue samples. Also I would like to thank her for her help in the Affymetrix microarray analysis and her useful critiques and comments of this research work.

I would like to thank Dr. Shikha Saha for her assistance with the LC-MS/MS. Also, I would like to express my deepest appreciation to Dr. Charlotte Armah for her help in my early steps in UK and throughout my PhD and especially for her time in proof reading this thesis. I would also like to thank Dr. Joanne Doleman for her help with proof reading this thesis. In addition, I would like to acknowledge Dr. Jack Dainty for his statistical advice throughout my PhD.

From my research group, I would like to thank my friend and colleague, Danielle Folkard, for her help in real time RT-PCR, in addition to my colleague, Tharsini Sivapalan, for the microarray data. I also take this opportunity to thank all my other friends and colleagues for their support and for the nice memories that they have given me for the rest of my life.

Special thanks to Al-Balqa'a Applied University for their financial support granted through the PhD scholarship.

Finally, very huge thanks to my lovely family; my mum, dad and my siblings for their ongoing love, support, encouragement and massive amount of advice.

Contents

List of Figures

Chapter 1

Chapter 2

Chapter 3

List of Tables

Chapter 2

Chapter 3

Chapter 4

Chapter 5

Abbreviations

$[Ca^{+2}]_i$	Intracellular calcium concentration
ACAT	AcetylCoA acetyltransferase
ACC1	AcetylCoA carboxylase 1
ACLY	ATP citrate lyase
ADP	Adenosine diphosphate
ALDH1A3	Aldehyde dehydrogenase 1 family, member A3
AR	Androgen receptor
ASD	Autism spectrum disorder
ATP	Adenine nucleotide triphosphate
BCA	Bicinchoninic acid
BPH	Benign prostatic hyperplasia
Ca^{2+}	Calcium ion
cAMP	Cyclic adenosine monophosphate
CAT	Carnitine-acylcarnitine translocase
CoA	Co-enzyme A
Ctrl	Control
CPT	Carnitine palmitoyl acyltransferase
Cu^{2+}	Cupric ion
Cu^{1+}	Cuprous ion
CVD	Cardiovascular disease
DAG	Diacylglycerol
DAVID	Database for annotation, visualization and integrated discovery
DHT	Dihydrotestosterone
DM type 2	Diabetes mellitus type 2
DMSO	Dimethyl sulphoxide
DOC	Sodium deoxycholate
EDN1	Endothelin 1
ELISA	Enzyme-linked immune sorbent assay
ENO	Enolase
ESI	Electrospray ionization
ETC	Electron transport chain
$FADH_2$	Falvin adenine dinucleotide
FAM	6-Carboxyfluorescein
FASN	Fatty acid synthase
FBP aldolase	Fructose-bisphosphate aldolase

FBS	Fetal bovine serum
FC	Fold change
GA-II	Glutaric xivalonylC type II
GAPDH	Glyceraldehyde-3-phosphate dehydrogenase
GDP	Guanosine diphosphate
GPCR	G-protein coupled receptor
GSL	Glucosinolate
GTP	Guanosine triphosphate
$G_i\alpha$	Gα inhibitory subunit
hBPH	Human prostatic myofibroblast cells
HIF–1	Hypoxia–inducible factor–1
HK	Hexokinase
HMG	3-Hydroxy-3-methylglutaryl
HMGCR	HMG-CoA reductase
HMGCS	HMG-CoA synthase
HPLC	High performance liquid chromatography
HRP	Horseradish peroxidase
HVA	High voltage–activate
IL	Interleukin
IL-6Rα	IL-6 receptor α
IP3	Inositol-1,4,5-triphosphate
KEAP1	Kelch-like ECH-associated protein 1
LDH	lactate dehydrogenase
LDL	Low density lipoprotein
LPA	Lysophosphatidic acid
LPC	Lysophosphatidylcholine
LVA	Low voltage–activate
m/z	Mass to charge ratio
MAPK	Mitogen–activated protein kinase
MRM	Multiple reaction monitoring
MS	Mass spectrometer
Na^+/K^+	Sodium ion /potassium ion
NADH	Nicotinamide adenine dinucleotide
NFκB	Nuclear factor kappa-light-chain-enhancer of activated B cells
NNUH	Norwich and Norfolk University hospital
Nrf2	Nuclear factor E2-related factor 2
PAGE	Poly acrylamide gel electrophoresis

Palcar	Palmitoylcarnitine
PAP	Prostate acid phosphatase
PBS	Phosphate buffered saline
PDH	pyruvate dehydrogenase
PFK	Phosphofructokinase
PFKFB	6-phosphofructo-2-kinase/fructose-2,6-bisphosphatase
PGI	Phosphoglucose isomerase
PGK	Phosphoglycerate kinase
PGM	Phosphoglycerate mutase
PI3K	Phosphatidylinositol-3-kinase
PIP2	Phosphatidyl inositol-4,5-bi-phosphate
PK	Pyruvate kinase
PKA	Protein kinase A
PKB	Protein kinase B
PKC	Protein kinase C
PLC	Phospholipase C
PM	Perfect match
PPP	Pentose phosphate pathway
PSA	Prostate specific antigen
PTX	Pertussis toxin
RIPA	Radio Immuno Precipitation Assay
RMA	Robust multiple average
ROS	Reactive oxygen species
rpm	Round per minute
RQ	Respiratory quotient
RT-PCR	Real time polymerase chain reaction
SDS	Sodium dodecyl sulphate
SF	Sulforaphane
SR	Sarcoplasmic reticulum
STAT3	Signal transducer and activator of transcription 3
TAMRA	6-Carboxytetramethylrhodamine
TBST	Tris buffer saline Tween20
TCA	Tricarboxylic acid cycle
TG	Triacylglycerol
TIC	Total ion chromatogram
TIM	Triosephosphate isomerase
TLRs	Toll-like receptors

TNF-α	Tumour necrosis factor-α
TURP	Transurethral resection of the prostate
UV	Ultraviolet
VLCAD	Very long chain acylCoA dehydrogenase
WST-1	Water-soluble tetrazolium
ZDHHC22	Zinc finger DHHC-type containing 22

Chapter 1

General introduction

1.1. Introduction

Cancer is one of leading causes of deaths worldwide. In the UK, prostate cancer is second only to lung cancer as the leading cause of cancer related deaths in men [1]. According to the 2010 national statistics on the incidence of cancer in England, 25.6% of the newly diagnosed cancer cases in men over 50 years were found to be prostate cancer [2]. This number is expected to rise as the number of elderly population is rising with prostate cancer largely affecting men over 50 years [3].

The risk factors for developing prostate cancer have been associated with age, high fat diet and chronic disorders, such as obesity and diabetes mellitus type 2 (DM type 2) [4]. A common feature between all chronic disorders including cancer is metabolic dysfunction, where the metabolic defect has been linked to impaired mitochondrial function.

Prostate cancer is considered a metabolic disease, where the metabolism is re-programmed due to secretion of citrate into the cytosol to be used as a precursor for the lipogenesis that is essential for providing the building blocks required for the biology of cancer cells. Since citrate is an intermediate in the TCA cycle, prostate cancer cells rely on glutamate metabolism to replenish the TCA cycle. In these cells glycolysis is also stimulated to provide the carbon skeleton for the synthesis of pentose sugar, nucleic acids and the nicotinamide adenine dinucleotide (NADH)-phosphate through the pentose phosphate pathway (PPP). In these cells, pyruvate is converted into lactate. The stimulated lipogenesis aids in attenuating the effect of lactate production on cellular pH during the stimulated glycolysis and maintains redox balance [5]. This makes the fatty acid oxidation, through β-oxidation, an important source for energy. It is important to note that lipogenesis is process important during cancer progression, while fatty acid oxidation is important during cell transformation [5], but it is unlikely that both processes would occur simultaneously in prostate cancer.

As a consequence of the stimulation of these metabolic processes, the levels of the reactive oxygen species (ROS) increase, which can negatively affect the enzymatic activities involved in tricarboxylic acid (TCA) cycle. A defect in the latter can affect the integration with β-oxidation leading to a metabolic defect resulting from the mismatch between their rates. This is important when fatty acids overload β-oxidation as a result of persistent lipolysis, which would decrease the ability of the mitochondria to generate the intermediates of TCA cycle. As a result of stimulated lipolysis to cover the energy needs and the less efficient TCA cycle a spill over of intermediates of fatty acid oxidation, such as acylcarnitines, would be expected.

Accumulation of acylcarnitines has been observed in chronic diseases, such as obesity, DM type 2 [6, 7] and kidney cancer [8].

Metabolic defects could also include a dysfunctions in any of the components of the carnitine shuttle system, such as the carnitine palmitoyltransferase (CPT) II enzyme [8], as well as a defect in β-oxidation itself, any of which could lead to a mismatch with the TCA cycle. However, these are notions that are yet to be investigated in prostate cancer.

Fatty acid oxidation is considered one of the main energy sources for prostate normal and cancerous cells [9]. In this chapter a review of the general metabolism of lipids is described and the role of the acylcarnitines as markers for the metabolic dysfunction, in addition to the cellular effect of the accumulation of acylcarnitines is discussed. Since recently it has been found that a diet rich in high glucosinolates (GSLs) broccoli is able to reduce the accumulation of acylcarnitines, the effect of this diet in reducing the accumulation of acylcarnitines is described. Also in this chapter, the biology of the human prostate and the development of prostate cancer in addition to the cell lines used to study the biology of the prostate are discussed. Finally in this chapter, the metabolic changes in healthy and cancerous prostate are described.

1.2. General metabolism of lipids

1.2.1. Fatty acid oxidation

Fatty acids, either from dietary or endogenous sources, are generally considered an important source for energy production [10]. The endogenous sources include either *de novo* fatty acid synthesis through lipogenesis or fatty acid released during lipolysis. Lipolysis occurs under certain physiological conditions of low levels of glucose, such as fasting or starvation [11-13]. The dietary sources of fatty acids include the hydrolysis of the circulating triacylglycerol (TG) contained within lipoproteins by the action of the circulatory lipoprotein lipase. This occurs during the postprandial state. The main lipoprotein that contributes to this process is the low density lipoprotein (LDL), which is involved in transferring fatty acids from liver to cells [14].

In order to be utilised as an energy source, fatty acids need to cross the plasma membrane and then enter the mitochondria, which is the main machinery for energy production. Fatty acids can cross the cell plasma membrane by the aid of fatty acid binding protein, such as albumin, in a process called active transport. Small quantities of free fatty acids exist in equilibrium with albumin-bound fatty acids and can cross the

membrane via passive or facilitative diffusion [13, 15]. In prostate cells, it has been found that the process of fatty acid uptake is via active transport mediated by membrane receptor [9].

Once inside the cells, fatty acids are converted into a thioester to enable their crossing of the mitochondrial membrane and this is because the mitochondrial membrane is impermeable to fatty acids [15].

Structurally, the mitochondria have outer and inner membranes. The permeability of each membrane is different resulting in different metabolite concentrations, proteins, and redox state [16]. The outer membrane is permeable to a limited number of compounds, while the inner membrane is completely impermeable [16].

The conversion of fatty acids into a form that allows them to pass through the membrane is called fatty acid activation [17]. This activation step is a thioesterification reaction and involves the binding of fatty acids with co-enzyme A (CoA), to form fatty acylCoA (or simply called acylCoA) esters [15]. This reaction occurs at the cytosolic face of the outer mitochondrial membrane and is catalysed by acylCoA synthetase (figure 1.1) [15].

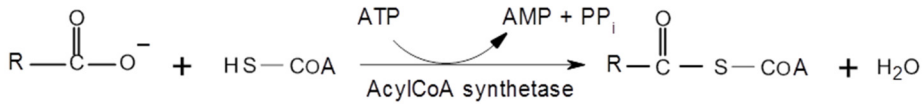

Figure 1.1: Fatty acid activation. Fatty acids in the cytosol are activated by binding to the –SH group of CoA catalysed by acylCoA synthetase. (Source: Devlin and Devlin, 1999 [13]).

CoA acts as an acyl group carrier, and is therefore considered to be a crucial co-factor in all living organisms. However, due to the impermeable nature of the inner mitochondrial membrane, CoA along with it esters cannot pass the inner mitochondrial membrane [16]. Therefore, a sequential trans-esterification reaction then follows, where the acyl group is transferred to carnitine to form the acylcarnitines by an enzyme called CPT I located on the external surface of the outer membrane [17, 18], which belongs to the carnitine acyltransferase family (figure 1.2).

The resultant acylcarnitine can then pass the inner mitochondrial membrane into the matrix via carnitine-acylcarnitine translocase (CAT), which is present in the inner

mitochondrial membrane [17, 18], where it catalyses the exchange of acylcarnitines with the free intramitochondrial carnitines. This enzyme transports carnitine and acylcarnitines with acyl chains of various lengths from 2 to 18 carbon atoms [18].

The driving force for this transport is the concentration gradient of the substrates across the membrane [19]. As the average carnitine concentration inside the organelle ranges from 2 to 5 mM and the affinity of carnitine for this enzyme on the matrix side is about 10 mM, the intramitochondrial carnitine concentration limits the overall rate of the acylcarnitine/carnitine exchange and, hence, represents a regulatory step of fatty acid β-oxidation. [20-22]

The consequence of this series of reactions is a net transport of fatty acyl units into the mitochondrial matrix [17, 18]. Having arrived in the mitochondrial matrix, acylcarnitine is trans-esterified a second time, where the transported acyl group is transferred from carnitine to a matrix CoA to generate acylCoA and carnitine. This reaction is catalysed by the CPT II enzyme present in the internal surface of the inner mitochondrial membrane [18]. The resultant carnitine is then transferred back into the cytosol by CAT, while the acylCoA is oxidized by β-oxidation (figure 1.2) [13]. This process of transferring fatty acyl groups from the cytosol into the mitochondrial matrix using the above enzymatic system is called the carnitine shuttle [18].

Studies have shown that deficiency or alteration to any of the molecular components of the carnitine shuttle system can lead to a defect in fatty acid oxidation resulting in the excretion of specific acylcarnitine esters [23, 24].

The activity of CPT I, CPT II and CAT is important for the regulation of the concentration of carnitines, acylCoA esters, and free CoA in each mitochondrial compartment, therefore affecting the carnitine acylation state in the cytosol [16]. It has been found that carnitine acylation state in the plasma can reflect the cytosolic acylcarnitine pool and serves as a diagnostic marker for altered equilibrium between acylCoA and acylcarnitines [16]. This suggests that the accumulation of acylcarnitines could be a good indicator for metabolic changes associated with defects in mitochondrial function.

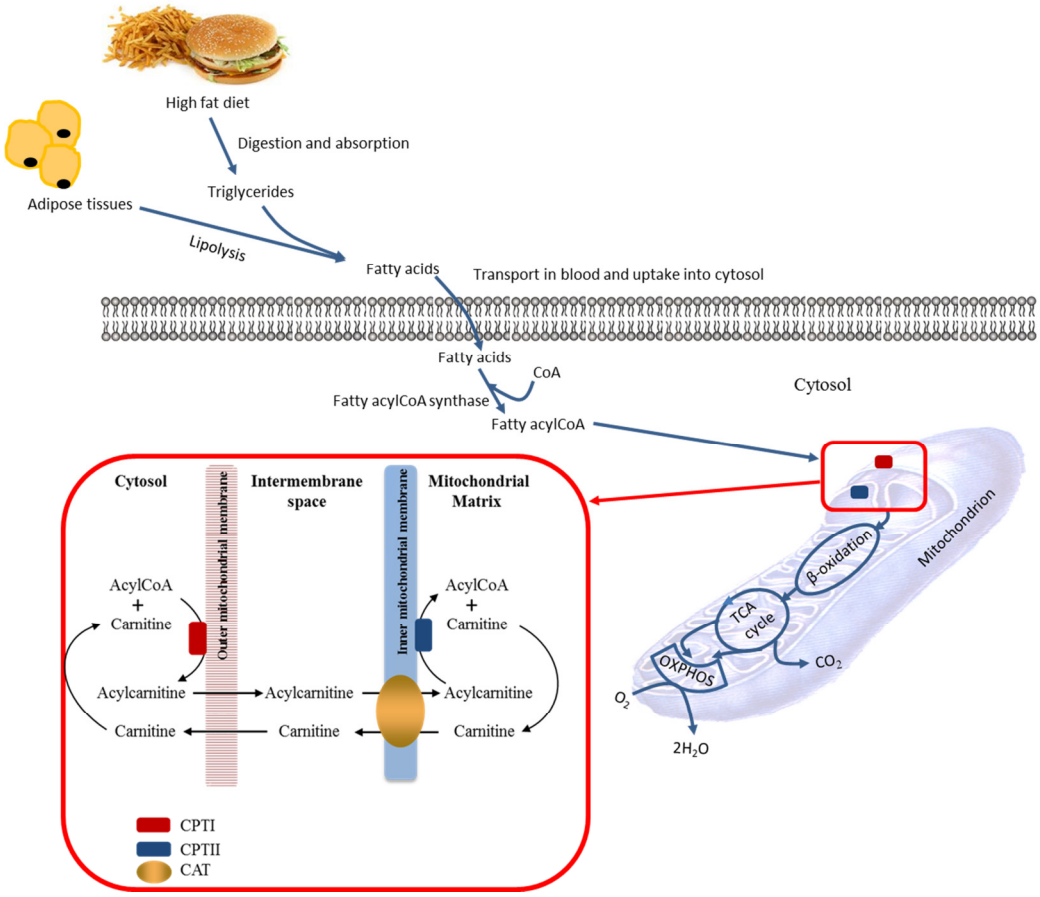

Figure 1.2: Oxidation of fatty acids. Fatty acids resulting from high fat diets and stimulated lipolysis are activated by fatty acylCoA synthase to form fatty acylCoA. The latter binds to carnitine by CPT I to form acylcarnitine, an intermediate that is transferred by CAT into the mitochondrial matrix to be converted back into acylCoA by CPT II. This enzymatic system of transferring acylcarnitines is called the carnitine shuttle (red box). OXPHOS; oxidative phosphorylation.

1.2.2. β-oxidation

In the mitochondrial matrix, acylCoA is oxidized by β-oxidation, in which the acylCoA is shortened by the removal of two carbon atoms at the β-carbon position of the fatty acylCoA molecule, hence the term β-oxidation [25]. This leads to the production of acetylCoA (C = 2) as a final product [26]. The process of β-oxidation can also occur in the peroxisome. Peroxisomal β-oxidation is involved in the initial oxidation of very long chain fatty acids and the shortened chains are then transferred to the mitochondria for further hydrolysis [27].

The process of β-oxidation is a cycle of four consecutive reactions: dehydrogenation (or oxidation), hydration, dehydrogenation (or oxidation) and thiolytic cleavage [26] (figure 1.3).

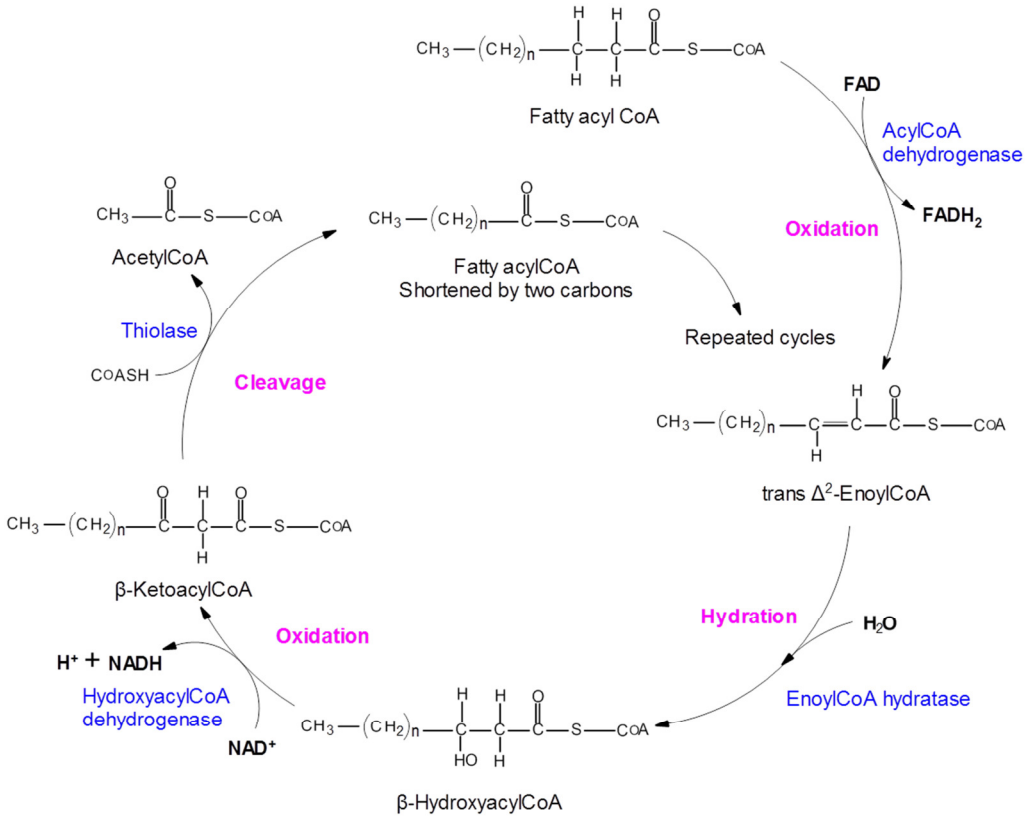

Figure 1.3: Reactions of β-oxidation. The process of β-oxidation is composed of four steps (highlighted in pink); oxidation, hydration, oxidation and cleavage. The enzymes are highlighted in blue. (Source: Devlin and Devlin 1999 [13]).

In the first reaction, the single bond is oxidized to a double bond and results in the formation of flavin adenine dinucleotide ($FADH_2$). This reaction is catalysed by acylCoA dehydrogenases, which are specific to the chain length of the fatty acid [26].

The second reaction is catalysed by enoylCoA hydrase. It catalyses the stereospecific hydration of the trans-double bond produced in the first reaction to form 3-L-HydroxyacylCoA. In the third reaction (the second oxidation step), the hydroxyl group at the β-position on carbon number three is oxidized into a ketone and generates NADH. This reaction is catalysed by 3-L-hydroxyacylCoA dehydrogenase. In the fourth reaction, β-ketoacylCoA produced in the previous step is cleaved into fatty acylCoA that is shortened by two carbons. This reaction is catalysed by thiolase and in the presence of

CoA. The fatty acylCoA that is shortened by two carbon atoms re-enters β-oxidation for further cleavage to form acetylCoA (figure 1.3) [25].

Regulation of β-oxidation depends on many factors; the substrate supply, the rate of oxidation of acetylCoA, the rate of CoA recycling, and the redox state [17]. Each cycle of β-oxidation produces one mole each of $FADH_2$, NADH, and acetylCoA [13].

1.2.3. TCA cycle

AcetylCoA produced by β-oxidation and glycolysis is oxidized via the TCA cycle. The TCA cycle is a consecutive series of enzyme-catalysed reactions that take place in the mitochondrial matrix. It starts with binding acetylCoA to oxaloacetate and end up with producing free hydrogen ions, CO_2, adenosine triphosphate (ATP), NADH and $FADH_2$. Therefore, a functioning TCA cycle is essential for the generation of reducing molecules that are not only important for energy production, but also for other anabolic processes, such as the PPP [13].

The transamination reactions within the cycle, which involve the reversible interconversion of glutamate into α-ketoglutarate and oxaloacetate into aspartate, ensure the availability of the TCA cycle intermediates, and thus a functioning cycle. The transamination reactions are catalysed by aspartate amino transferase (or also called aspartate transaminase) (figure 1.4) [28].

The activity of the TCA cycle is controlled by several factors. These include $NADH/NAD^+$ ratio, adenosine diphosphate (ADP)/ATP ratio, CoA availability, the rate limiting enzymes (citrate synthase, isocitrate and α-ketoglutarate dehydrogenase) and calcium (Ca^{2+}) concentration [28]. An increase in Ca^{2+} concentrations increases the activity of TCA cycle by activating Ca^{2+} sensitive dehydrogenases, such as pyruvate dehydrogenase (PDH) [29].

It has been found that certain deficiencies of the enzymes involved in the TCA cycle may lead to certain types of disorders, such as fumaric aciduria, which is an inborn metabolic disorder that is characterised by high levels of fumaric acid in the urine caused by a deficient activity of fumarase [30].

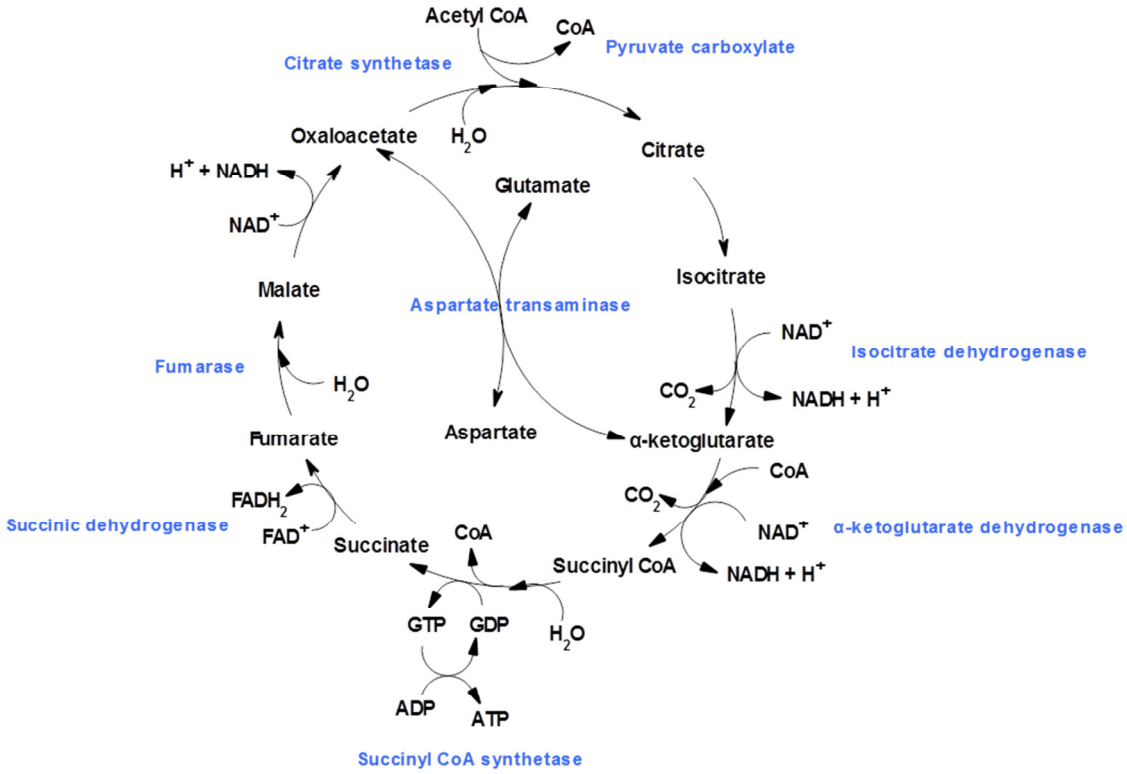

Figure 1.4: Reactions of TCA cycle. AcetylCoA is oxidised in a series of enzyme-catalysed reactions in the mitochondrial matrix. The enzymes are highlighted in blue. In the cycle CO_2, NADH and $FADH_2$ are produced. Transamination reaction within the cycle catalysed by aspartate transaminase keeps the cycle intermediates available for a functioning TCA cycle (based on Brie`re *et al* 2006 [28]).

1.2.4. Electron transport chain

The NADH and $FADH_2$ generated during the oxidation of acetylCoA in the TCA cycle and those generated from β-oxidation and glycolysis can enter the electron transport chain (ETC) for the production of ATP in a process called oxidative phosphorylation [13]. This process takes place within the inner mitochondrial membrane, where the electrons are transferred from the NADH and $FADH_2$ into electron carrier proteins called cytochromes, which contain iron and copper cofactors. The electrons from NADH and $FADH_2$ are transferred down the ETC from one cytochrome into another, usually to or from an iron or copper ion, to reach the terminal cytochrome C oxidase complex, which catalyses the transfer of electrons to atmospheric oxygen and combines them to hydrogen ions to form water [13, 14, 28]. After transferring the electrons from NADH and $FADH_2$, the energy generated is used to transfer the hydrogen ions across the inner mitochondrial membrane to the intermembrane space, thus generating a concentration gradient of hydrogen ions across the membrane. These hydrogen ions can

re-enter the mitochondrial matrix through ATP synthase, which is a protein channel for hydrogen ions that uses the energy derived from ion movement to catalyse the formation of ATP from ADP and inorganic phosphate ion. This process is called oxidative phosphorylation and it provides almost 90% of the total energy in the cells [13]. This process is also important for re-oxidation of the reduced molecules to generate NAD^+ and FAD. The availability of these molecules is important to accept more hydrogen ions from intermediates in the TCA cycle, glycolysis, and fatty acid oxidation [14].

The well balanced series of reactions outlined above can be perturbed during moments of metabolic stress affecting the co-ordination between β-oxidation, TCA cycle and the ETC , which lead to the accumulation of intermediates, such as acylcarnitines that could impair cellular functionality [7].

1.3. Acylcarnitines and chronic diseases

Metabolic dysfunction is a common feature between all chronic diseases including cancer. It has been shown that this metabolic dysregulation is associated with an increase in the plasma levels of acylcarnitines [6, 7, 23, 31, 32].

An *in vivo* study characterizing the acylcarnitine profile in human plasma from lean, obese and subjects with DM type 2 diabetic subjects revealed that in both obese and diabetic groups the levels of long, medium and short chain acylcarnitines were increased [7]. These findings were also observed in Adams *et al* study, where they found an accumulation of medium and short chains acylcarnitines in obese diabetic subjects compared to the obese non-diabetic subjects [6].

In metabolic syndrome and obesity, insulin resistance leads to persistent lipolysis and high levels of plasma non esterified fatty acids, leading to an increase in fatty acid oxidation. Tissues will use fatty acids as priority when their concentrations are raised in the plasma. However, in diabetic subjects, it has been reported that the metabolic defect is linked to impaired insulin signalling as well as a poor coordination between the TCA cycle and β-oxidation. This can be explained by the overload of mitochondria with fatty acids, which overload β-oxidation and decrease the ability of mitochondria to generate the intermediates of the TCA cycle, leading to less efficient TCA cycle and the accumulation of acetylCoA. To overcome this accumulation acetylCoA is converted into ketone bodies, which in turn inhibit enzymes involved in TCA cycle. Accumulation of acetylCoA also stimulates pyruvate dehydrogenase kinase, which inhibit PDH and stimulate pyruvate carboxylase, leading to an increase in the levels of oxaloacetate, which is a substrate for glucose synthesis. The increase in glucose levels induces the

secretion of insulin from the β-cells. A persist in insulin secretion can lead to insulin resistance [6, 13].

In Mihalik *et al* study, the increased concentrations of insulin in both obese and diabetic groups was associated with a lower concentration of short and long chain acylcarnitines, which indicates the importance of insulin in regulating the oxidation of fatty acids [7]. This was supported by measuring the respiratory quotient (RQ), which is a measure of the ratio of CO_2 eliminated to the amount of O_2 consumed during metabolism. It ranges from 1 (indicating a pure carbohydrate oxidation) to around 0.7 (indicating a pure fat oxidation) [14]. Higher insulin concentrations were associated with higher RQ, which suggest a switch from fatty acid oxidation to carbohydrate oxidation. This was not the case in the diabetic subjects, whose insulin levels were higher, where the levels of acylcarnitines were not changed in the same pattern as the obese or the lean subjects, indicating their inability to switch into more efficient fat oxidation. In addition, diabetic subjects showed a secondary accumulation of shorter chain acylcarnitines, which are produced from the second round of β-oxidation, suggesting that there is a poor co-ordination between β-oxidation and the TCA cycle [7]. Further evidence for the poor co-ordination in diabetic subjects is the increase in the levels of C3 carnitines as well as C4 dicarboxyl carnitine. The latter is a sum of both methylmalonylcarnitine and succinylcarnitine, which suggest that succinylCoA is poorly utilized by the TCA cycle [7]. The findings of these studies suggest that acylcarnitines could represent a possible biomarker for predicting the development of diabetes.

In a study involving subjects recently diagnosed with diabetes, the acylcarnitine decanoylcarnitine was positively correlated with LDL concentrations, which was significantly increased along with triglycerides, interleukin (IL)-6 and tumour necrosis factor-α (TNF-α) compared to the non-diabetic subjects [33].

It has been observed that there is a link between lipid and amino acid metabolic pathways. An increase in some amino acid metabolites has been associated with an increase in some acylcarnitines. Metabolomic profiling of obese versus lean human subjects reveals that in obese subjects, higher levels of short (C3) and medium (C5) chain acylcarnitines were detected, in addition to higher levels of branched chain amino acids [34]. The link between the accumulation of acylcarnitines and amino acids is that the metabolites of amino acids resulting from amino acid metabolism can be used to form acylcarnitines. C5 acylcarnitines are composed of α-methylbutyryl and isovalerylcarnitine that result from α-methylbutyrylCoA and isovalerylCoA respectively. Both α-methylbutyrylCoA and isovalerylCoA are intermediates of the mitochondrial

catabolism of isoleucine and leucine respectively, which are present in equilibrium with their cognate acylcarnitine esters. C3 acylcarnitine results from the catabolism of propionylCoA, which is a by-product of both isoleucine and valine catabolism [7, 34].

The link between the accumulation of acylcarnitines and amino acids also suggest an impaired TCA cycle. In chronic diseases the high levels of oxidative stress resulting from the accumulation of ROS can negatively affect the enzymes involved in the TCA cycle and thus affect its efficiency. Because the TCA cycle is a central process for many catabolic and anabolic processes including amino acid catabolism, reduction in the efficiency of the TCA cycle may lead to the accumulation of amino acids and their metabolites as well as affect its integration with other processes, such as β-oxidation leading to the accumulation of acylcarnitines.

Elevated levels of certain amino acid metabolites have been found to be correlated with insulin resistance, in that they can interfere with insulin mediated glucose uptake pathways leading to a reduction in glucose uptake and glycogen synthesis [35]. Because amino acids and lipid metabolism are linked through the TCA cycle, this suggests that acylcarnitine may also be indirectly linked to insulin resistance [34]. Another study by Ganti *et al* showed that acylcarnitines also accumulate in urine and tissue from kidney cancer [8]. Since metabolic dysfunction is a common feature between obesity, DM type 2 and cancer, accumulation of acylcarnitine has the potential to be used as a biomarker to detect the metabolic dysfunction associated with the chronic disease.

1.4. Cellular effect of acylcarnitines

Acylcarnitines including palmitoylcarnitine (palcar), the most abundant of the long chain acylcarnitines, are formed by transferring an acyl group of fatty acylCoA to carnitine (figure 1.5).

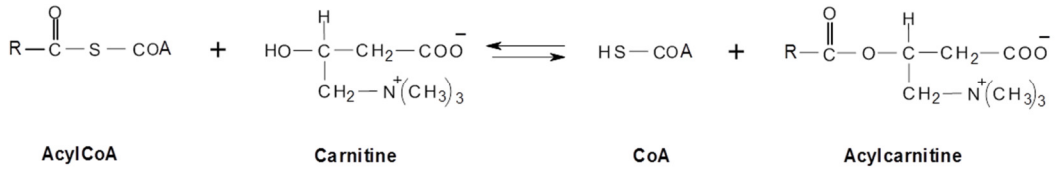

Figure 1.5: Acylcarnitine formation from acylCoA and carnitine. CPT I catalyse the binding of acylCoA to carnitine to form acylcarnitine. Acylcarnitine has an amphiphilic nature; the hydrocarbon chain that is specific for each acylcarnitine (R group) represents the hydrophobic part of the molecule, and both the carboxylic and amine group represent the hydrophilic part.

The resultant chemical structure contains both hydrophobic and hydrophilic groups. The hydrophobic group is the large hydrocarbon fraction of the compound (represented with R group in figure 1.5), with the hydrophilic group being the fraction containing the carboxylic and amine groups. This structure gives the acylcarnitines an important feature of being amphiphilic.

The amphiphilic nature of acylcarnitines allows them to induce many cellular changes that are related to cell membrane functionality. In the cell membrane microenvironment, amphiphiles have been reported to bind to target proteins in the cell membrane as well as to the phospholipid bilayer, and this led to a corresponding change in membrane fluidity and the corresponding state of the membrane and the protein lipid bilayer interface [15, 36-40]. This may cause conformational changes in the proteins involved in the interface. These proteins could be either ion channels, thus controlling transport of ions and membrane permeability, or receptors that are involved in many signalling pathways [13], therefore altering their activity and the ionic movement across the membrane, thus modifying cell membrane permeability [36, 39]. The ability of acylcarnitines to induce changes in membrane bound proteins have been realized for palcar by studying sodium (Na^+)/potassium (K^+)–ATPase and Ca^{2+}–ATPase activities in the sarcoplasmic reticulum (SR) [41-43].

Altering membrane permeability could be associated with changes in the homeostasis of ions that could act as secondary messengers, such as Ca^{2+}. In endothelial cells, palcar has been shown to induce the influx of Ca^{2+} [44]. The influx of Ca^{2+} has been also observed in response to dihydrotestosterone (DHT), which is a hormone essential for prostate growth and development, and associated with prostate cancer progression [45].

Changing the homeostasis of secondary ions, such as Ca^{2+} could be associated with the alteration of many signal transduction pathways, some of which are linked to inflammatory responses [45]. Acylcarnitines generally, have been shown to be associated with some pro-inflammatory responses. They were able to induce an increase in the levels of TNF- α and pro-inflammatory cytokines including IL-3, IL-16 and IL-23 [46, 47], in addition to an increase in nuclear factor kappa-light-chain-enhancer of activated B cells (NFκB); a downstream target of toll-like receptors (TLRs) that are known to regulate the synthesis of the IL-6 [6, 48]. The increase in IL-6 levels has been associated with the progression of prostate cancer [49-51].

1.5. The role of the diet in reducing acylcarnitines

One of the most important risk factors that influence human health is the diet. A diet high in fat and low in fruit and vegetables can affect the quality of life leading to the development of many chronic diseases, such as cardiovascular diseases (CVD), DM type 2 and cancer.

Recently, the use of natural product in cancer prevention has increased considerably [52]. There is an increasing volume of evidence demonstrating that a diet rich in fruit and vegetables including crucifers are beneficial to health. This kind of diet provides a variety of potentially health-promoting phytochemicals, such as vitamins, carotenoids, polyphenols and GSLs [53].

GSLs are distinctive phytochemicals that accumulate in cruciferous vegetables, which make them unique compared to other green vegetables [54]. The GSL containing vegetables belong to the family *Brassicaceae* and genus *Brassica.* The name of cruciferous vegetables is derived from the cross-shaped flower of the plant [52].

A diet rich in cruciferous vegetables has been linked to the reduced risk of many chronic diseases, such as CVD [55] and many types of cancers including lung [56], breast [57], colon [58, 59] bladder [60], and prostate [61]. The evidence of this link has come from a number of worldwide epidemiological studies including those carried out in the US [57, 58, 61, 62], Canada [62, 63], Netherland, [64], Shanghai [56, 59] and Western Australia [65].

Part of the cumulative evidence suggesting the protective role of cruciferous vegetables also comes from human intervention studies. Recently, a diet rich in high GSLs broccoli has been found to decrease the accumulation of acylcarnitines by rebalancing the metabolic processes of amino acid metabolism, TCA cycle and β-oxidation [66]. The beneficial health effect of such a diet is attributed to the GSL break down product sulforaphane (SF). SF is thought to exert its effect in rebalancing the integration between TCA cycle, fatty acid oxidation and amino acid catabolism through the induction of transcription factor nuclear factor E2-related factor 2 (Nrf2) [66]. Nrf2 is a transcription factor that regulates the expression of antioxidant genes involved in phase II detoxifying systems. When Nrf2 is released from the Kelch-like ECH-associated protein 1 (KEAP1), it binds to antioxidant response element sites in the genes and induces the expression of enzymes involved in the process of carcinogen detoxification [67]. SF was also found to induce the expression of glutathione-S-transferase enzyme involved in phase II enzyme [68]. Induction of phase II detoxifying systems reduces the

oxidative stress that cause the mitochondrial dysfunction and may enhance the redox-sensitive enzymes involved in TCA cycle, such as aconitase and α-ketoglutarate dehydrogenase [66], which results in a more efficient TCA cycle that is able to properly integrate with β-oxidation, thus reducing the accumulation of acylcarnitines.

The effect of a diet rich in fruit and vegetables on lowering the levels of acylcarnitines has been also observed after consuming a diet rich in citrus and soy [69]. Furthermore, low levels of acylcarnitines has been associated with the dietary intakes of garlic and coffee [70]; both of which induce Nrf2-mediated transcription [71, 72].

Recently, a WHO/FAO report recommended a minimum of 400g of fruit and vegetables per day for the prevention of chronic diseases, such as heart disease, cancer, diabetes and obesity, and also for the prevention of a number of micronutrient deficiencies [73]. However, a recommendation for the consumption of cruciferous vegetables has not been established. Epidemiological studies show that consumption of 24.1 – 72.9g/day of cruciferous vegetables is associated with a reduced risk in cancer [62, 63]. As mentioned previously, consuming a diet rich in broccoli (400g/week) has a positive effect on correcting the disrupted metabolic pathway through lowering the oxidative stress in people with moderate risk of developing CVD, therefore 400g serving per week (57g per day) could be suggested for this special group of vegetables.

Since prostate cancer is the second leading cause of male deaths in the UK, the next sections describe the prostate, how prostate cancer develops, and the role of DHT in cancer development, as well as the importance of using *in vitro* cell models for studying prostate biology. Furthermore, how metabolism is between the healthy and cancerous prostate is also discussed.

1.6. The biology of human prostate

The prostate is one of the organs belonging to the male reproductive system. It is a single “donut”-shaped gland that has the size of a walnut and is located in front of the rectum and underneath the bladder. It surrounds the upper part of the urethra, into which it secretes the semen, an acidic fluid that carries the sperm cells, through hundreds of small openings in the side of the urethra; the tube that carries the urine from the bladder (figure 1.6) [14].

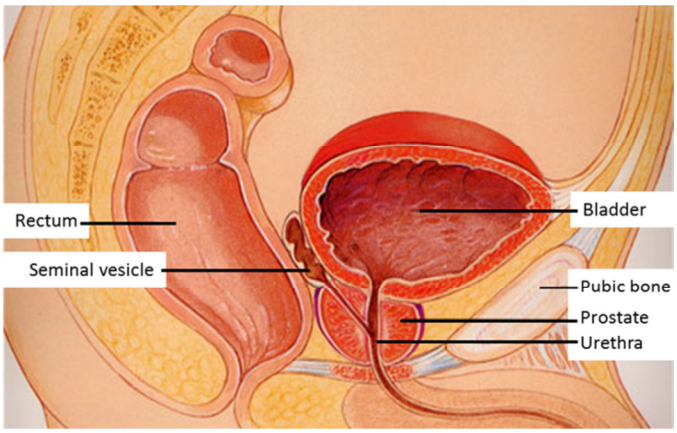

Figure 1.6: Anatomic view of the prostate gland. Prostate gland is located underneath the bladder and surrounds the urethra (source: Prostate Cancer Foundation of Australia; http://www.prostate.org.au).

The prostate gland consists of epithelial glands surrounded by fibromuscular tissue; in other words, a glandular and a stromal part. The stromal part of the prostate includes fibroblasts, myofibroblasts, and smooth muscle cells, whereas the glandular part is composed, anatomically, of three types of epithelial cells illustrated in figure 1.7:

1- The basement membrane

2- The prostatic proliferative basal cells, which form a layer along the basement membrane of each prostatic duct and contain the stem cells. This layer also contain some scattered neuroendocrine cells, and

3- The luminal epithelium secretory cells, which form a layer above the basal cells and express prostate specific antigen (PSA), prostate acid phosphatase (PAP) and androgen receptor (AR).

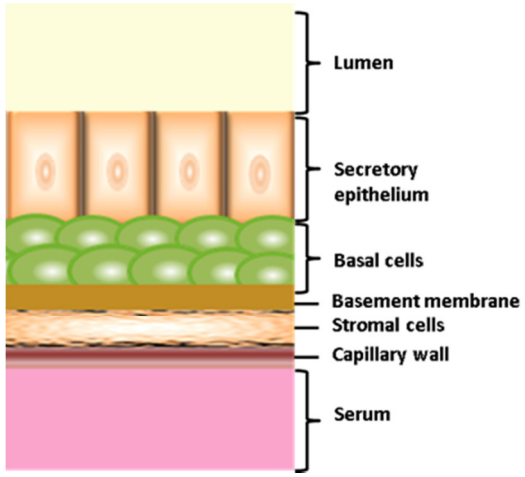

Figure 1.7: Cell layers in prostate gland. Normal columnar secretory epithelium is surrounded by basal cells that set on the basement membrane, which is supported by stromal cells. These tissue separate the prostate lumen from the capillary bed (source: Kirby and Patel 2011 [3]).

Cells that develop from the basal layer start to express ARs and become responsive to androgen, causing them to differentiate into columnar secretory luminal cells that are capable of producing PSA [74].

Testosterone is a male sex hormone that is secreted from the Leydig cells of testes and is important for the induction of the differentiation of male reproductive organs and the maintenance of their function [14]. The prostate gland develops after puberty as a result of the flow of testosterone [75]. Once in cytoplasm, 5α-reductase converts testosterone into 5α-DHT, or simply called DHT [3, 14], which then binds to ARs to induce their effects. In the absence of testosterone, prostate gland cells normally undergo apoptosis.

In the early stages of the development of prostate cancer, there is a dependence upon DHT. At this stage the cancer is described as androgen-dependent. As the cancer progresses, the presence of this hormone is not required for its growth, but the cells still respond, at this stage cells are described as androgen-sensitive. With time, these cancer cells then become androgen-insensitive due to increase or decrease in the number of the receptors [3, 14].

In some forms of prostate cancer that are sensitive to DHT, blocking the enzymes required for the transformation of testosterone to DHT represents a good approach for cancer therapy [14].

As a result of the positioning of the prostate, its size is of great importance. Any enlargement of this gland could result in the constriction of the urethra causing a cessation of the flow of urine. This has been observed in cases of benign prostatic hyperplasia (BPH), where an enlargement of the prostate, caused by the development of macroscopic nodules with hyperplasia of stromal and epithelial cells, lead to the obstruction of the bladder. BPH nodules develop due to chronic inflammation. The repetitive wound-healing of the tissue damaged by the activity of the autoimmune system that is stimulated by the proliferation of the stromal and epithelial cells in the prostate causes the formation of the nodules [76].

The main function of the prostate is to produce a liquid that contains both the semen and PSA. This liquid contributes to around 25–30% of the semen volume and PSA, and mainly produced from the luminal prostate epithelial cells to help liquefying the semen [74].

PSA is a glycoprotein with serine protease activity and regulated by androgen. It represents the major protein in the semen and is responsible for liquefying the semen allowing sperm cells to swim freely [3, 77]. It is secreted by the prostate epithelium as an inactive protein called pro-PSA and becomes activated by proteolytic hydrolysis in the lumen into free active PSA. The active PSA then can enter the circulation as an unbound form (free PSA). In the circulation, some of the free PSA can directly bind to protease inhibitors, such as α_1-antichymotrypsin and α_2-macroglobulin and circulate as a bound form. In prostate cancer, the secreted pro-PSA escape to the circulation as a result of the loss of basal cells, basement membrane, and normal lumen architecture resulting in an increase in the levels of bound PSA and pro-PSA in the serum [77, 78]. The ratio of serum free PSA to total PSA (free, pro- and bound PSA) is used to distinguish between the BPH and prostate cancer [77].

PSA is used as a diagnostic test for prostate cancer. Men without prostate cancer usually have low levels of PSA [75], these can range from 0 – 4.0ng/ml [3]. However, men diagnosed with BPH, prostatitis, urinary tract infection and cancer may be expected to achieve levels of between 4.0–10.0ng/ml [3]. Cancer is indicated if their free PSA < 25% of total PSA, as well as PSA levels between 4.0 – 10.0ng/ml [77]. The risk of cancer increases when patients have PSA levels > 10.0ng/mL [3, 77].

In order to confirm the occurrence of prostate cancer, other screening tests are used along with the determination of PSA concentrations. Some of these tests include digital rectal examination and transurethral resection of the prostate (TURP). Measuring the PSA density, that is the ratio of PSA to gland volume, also aids in distinguishing between

prostate cancer and BPH. This is because PSA is produced by both normal prostate and BPH, therefore, serum levels can be compared with the volume of the prostate gland, so that the PSA released into the serum per gram of cancer tissue is greater than per gram of BPH tissue [77].

To help evaluate the prognosis of men with prostate cancer, some pathological prognostic factors are used; the Gleason grade is one of them. This is a system named after Donald Gleason, who first described it in the 60s, where the grade of the prostate cancer is evaluated microscopically. The tissue thought to be cancerous is compared to that of normal tissue to detect any glandular differentiation. This helps to determine the aggressive nature of the cancer. Tumours that are very similar to normal tissue are considered well-differentiated and were given a score of 1 (low grade), whereas tumours that are clearly different are considered least differentiated and were given a score of 5 (high grade). Because tumours are heterogeneous and may have multiple levels of differentiation, a combined Gleason grade or score is used, which refer to use of two grades; primary (most dominant) and secondary (second most dominant). Thus Gleason score may range from 2 (1+1) to 10 (5+5) [75].

The prostate gland itself can also be divided into four major anatomical zones (figure 1.8) [74, 77]:

1. The transition zone, which is composed of two small lobules that surrounds the prostatic urethra. It is responsible for the prostate enlargement problems and represents the area where BPH mainly originates.

2. The central zone, which surrounds the transition zone and extends to the angle of the urethra and base of the bladder (surrounding the ejaculatory duct system).

3. The peripheral zone, which extends from the apex to the base of the gland and represents the most common site for the developing prostate carcinomas.

4. Anterior fibromuscular zone or stroma doesn't contain any glandular parts, but consists of a variety of cells including fibroblasts, nerves, infiltrating lymphocytes, macrophages, endothelial cells, and smooth muscle cells. It covers the area from the bladder neck to the external urethral sphincter.

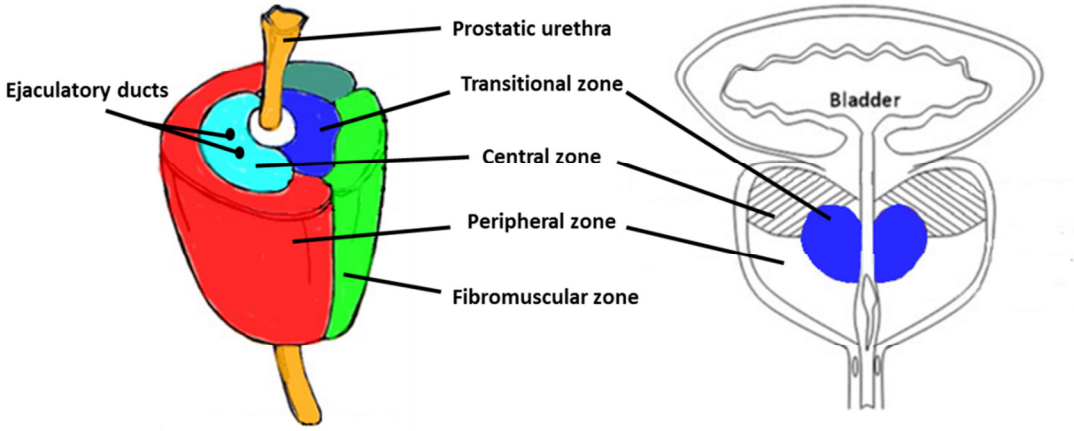

Figure 1.8: The anatomic zones of the prostate. To the right is the frontal view (coronal section) of the prostate and on the left is the 3D view of the whole prostate. The Prostate gland is located underneath the bladder and surrounds part of the urethra. It is divided into four main zones; central, transition, peripheral and an anterior fibromuscular zone. (based on: Notara and Ahmed, 2012 [74] and Manila Genitourinary Clinic, Philippines http://www.prostate.com.ph/anatomy.htm [79]).

1.7. The use of *in vitro* models for studying prostate biology

The similarities between the immortalised cell lines and the primary tumours from where they came, make the use of cell lines a good tool to attempt to understand the biological, molecular, and biochemical nature of cancer. Moreover, the flexibility of using cell-culturing may also aid in understanding the effect of many drug, chemical or food constituents on cancer and thus helps to formulate different hypotheses that could be further investigated in more appropriate *in vivo* systems [80]. There are many *in vitro* cell models of immortalized non-cancerous and cancerous human prostate epithelial cell lines that are used to investigate the tumour pathology of the prostate as well as assessing the beneficial health effects of many food constituents.

In order for the *in vitro* cultured cells to reflect the actual *in vivo* system, the cell line used must be pure; this is important during the initial isolation of the cell line and during sub-culturing because cross contamination with another cell line may cause a change in the genotype and phenotype of the cultured cells and thus affecting their stability, which is another important factors that affect the characteristics of the cultured cells and eventually leading to a compromised interpretation of the results [80]. Therefore, different methods have been used to distinguish different cell lines. Some of the prostate-derived cell lines were characterised using immunocytochemistry, which employ the use of antibodies to detect the presence of specific peptides or protein

antigens in the cell using different technique such as microscope. Some of the markers that are used are cytokeratins, which reflect the differentiation of the epithelial cells, E-cadherin and catenins, which reflect cell adhesion/anti-adhesion ability, PSA, PAP and AR, which are markers for prostatic differentiation [80].

Prostate cancer can spread into lymph nodes and bones [81] and because most human prostate cancer cell lines have been taken from metastatic deposits, the cell line models reflecting these two types have different characteristics. LNCaP cells are cells derived from a metastatic lesion of human prostatic cancer and derived from the lymph node metastasis. They were described in 1980 [82] and are positive for prostatic differentiation markers; PSA, PAP and AR [80], thus they are hormone sensitive. Whereas, DU145 and PC3 cells are human prostate cancer cells that are derived from brain and bone metastasis, respectively. They were described in 1977 [83] and in 1978 [84], respectively, and are positive for cell adhesion markers, but not for markers of prostatic differentiation; PSA, AR and PAP [80], therefore they are not hormone sensitive and do not express PSA.

PNT1A cells are immortalised benign prostatic epithelial cells and were described in 1991 [85]. They are positive for some epithelium differentiation and cell adhesion markers. These cells do not express AR and PSA. BPH-1 cells are another type of the immortalised benign prostatic epithelial cells and they were described in 1995 [86]. They are positive for cell adhesion and some epithelium differentiation markers, but they also do not express AR and PSA [80].

The work in this thesis, which involve investigating the effect of palcar accumulation was performed using *in vitro* cell models of prostate non-cancerous; PNT1A and BPH-1 cells, and cancerous; DU145 and PC3 cells.

1.8. Metabolic characteristics of the healthy prostate

Generally, the main energy source for all cells is the oxidation of glucose [13]. Glucose is transported into the cells by facilitative diffusion [13], which means down concentration gradient involving membrane proteins. Once inside the cells, glucose is phosphorylated by hexokinase to glucose–6–phosphate and used for various cellular processes depending on the cell needs. It can be used for energy production through glycolysis, stored as glycogen, enter PPP to produce pentose for nucleic acid synthesis, or used for the synthesis of structural glycoprotein. For energy production, glucose–6–phosphate is further phosphorylated and converted into pyruvate. The fate of pyruvate determines the fate of glycolysis; whether it is aerobic or anaerobic. In aerobic glycolysis,

pyruvate enters the mitochondria to be converted into acetylCoA and then metabolised by the TCA cycle, whereas in the anaerobic glycolysis, pyruvate is converted into lactate by lactate dehydrogenase (LDH) [13].

In aerobic glycolysis, hexokinase (HK) enzyme converts glucose into glucose-6-phosphate. Glucose-6-phophate is converted into fructose-6-phosphate, which is then phosphorylated by 6-phosphofructo-2-kinase/fructose-2,6-bisphosphatase (PFKFB) into 2,6-fructose bisphosphate [13]. PFKFB is an isoform of phosphofructokinase (PFK)-2 and it is encoded by four genes; PFKFB1, PFKFB2, PFKFB3 and PFKFB4. It has been found that PFKFB4 is expressed in the prostate non-cancer and cancer cells [87].

Fructose-2,6-bisphosphate regulates the activity of PFK1, which is responsible for the conversion of fructose-6-phoshate into fructose-1,6-bisphosphate (figure 1.9).

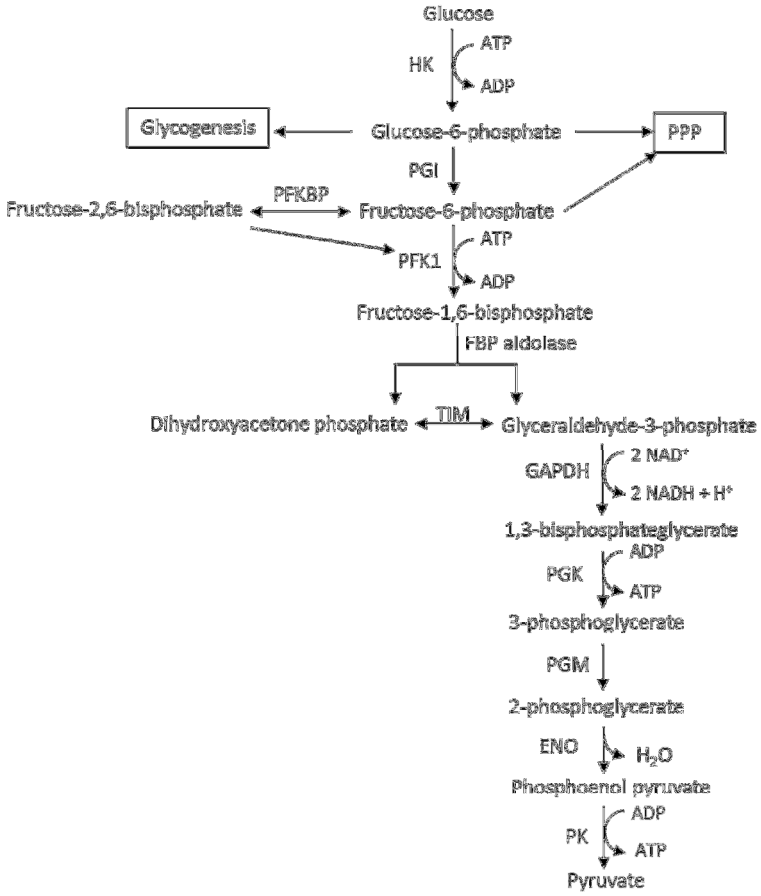

Figure 1.9: The steps of converting glucose into pyruvate during glycolysis. Glucose is converted into puruvate by series of enzyme-catalysed reactions. PGI, phosphoglucose isomerase; FBP aldolase, fructose-bisphosphate aldolase; TIM, triosephosphate isomerase; GAPDH, glyceraldehyde-3-phosphate dehydrogenase; PGK, phosphoglycerate kinase; PGM, phosphoglycerate mutase; ENO, enolase; PK, pyruvate kinase. (Based on Devlin and Devlin [13]).

Diverting glucose and pyruvate away from TCA cycle for other metabolic processes is a key characteristic of prostate cells and the driving force for the oxidation of fatty acids as an alternative energy source [10]. In both prostate non-cancer and cancer cell lines, it was found that the uptake of fatty acids is more dominant than the uptake of glucose and involves an active transport mechanism involving membrane receptor [9].

Fatty acids are oxidized by β-oxidation to produce acetylCoA, which is then converted into citrate in the TCA cycle. In prostate cells, the accumulation of zinc decreases the activity of aconitase, an enzyme that converts citrate into iso-citrate via *cis*-aconitate. This decreases the oxidation of citrate, leading to its accumulation and secretion into the cytosol [88] (figure 1.10).

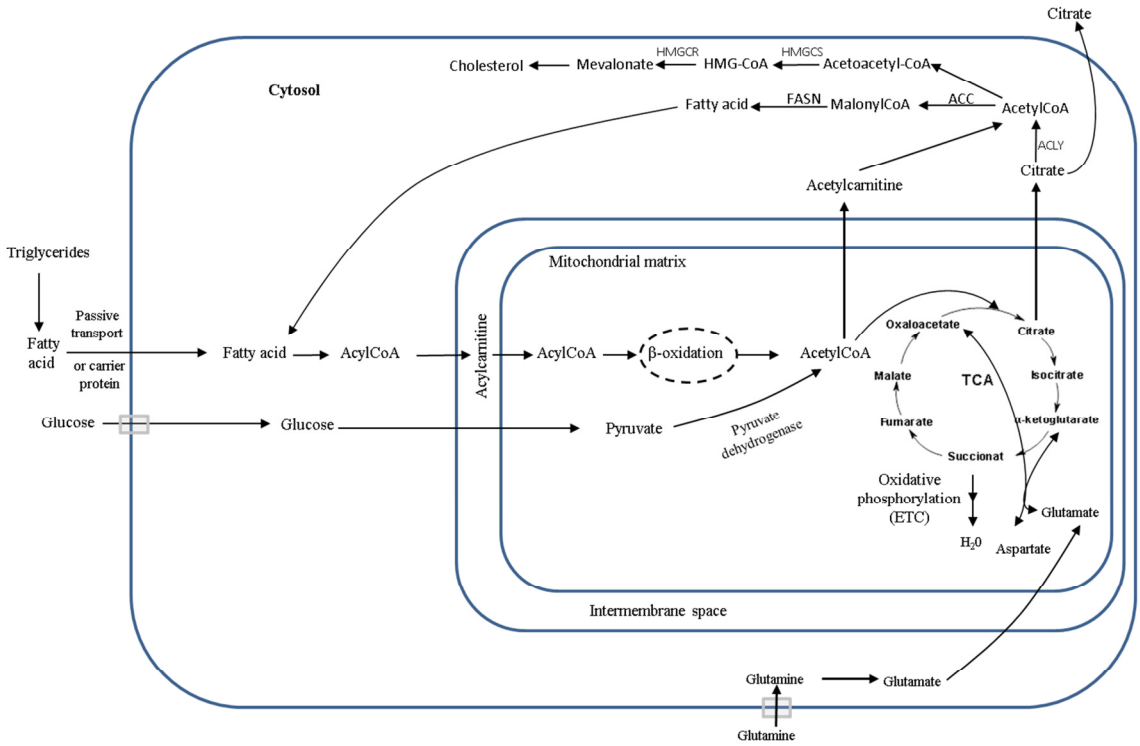

Figure 1.10: Metabolism of fatty acids in prostate normal cells. Fatty acids are converted into acylCoA and binds with carnitine to produce acylcarnitine. Acylcarnitines are transferred into the mitochondrial matrix and converted back to acylCoA to be oxidized by β-oxidation and TCA cycle. Zinc accumulation in these cells inhibit the activity of aconitase, leading to the accumulation of citrate and its excretion into the cytosol to be used for fatty acid and cholesterol synthesis. Glutamine is utilised to replace intermediates of TCA cycle. ACLY; ATP citrate lyase, ACAT; AcetylCoA acetyltransferase, HMGCS; 3-hydroxy-3-methylglutaryl (HMG)-CoA synthase, HMGCR; HMG-CoA reductase, ACC1; AcetylCoA carboxylase 1, FASN; fatty acid synthase.

Blocking the aconitase step is considered another characteristic feature of prostate cells. In order to replace intermediates of TCA cycle and keep it functioning, the uptake of glutamate is stimulated to be converted by deamination reaction into α-ketoglutarate, which transaminate with aspartate to produce oxaloacetate [5].

1.9. Metabolic characteristics of the cancerous prostate

In prostate cancer cells, the metabolic alterations include the induction of aerobic glycolysis and this is not for energy production, but rather for providing the carbon skeleton required for the PPP. This is due to the neoplastic growth and the poor blood supply for the newly formed cells, the levels of O_2 and nutrients decrease leading to hypoxic conditions and stimulation of cellular metabolism. This may increase the levels of ROS. High levels of ROS have been found to induce changes in the sulfhydryl group of pyruvate kinase [89], an enzyme that converts phosphoenol pyruvate into pyruvate [13]. This conversion leads to the oxidation of pyruvate kinase, which results in diverting the glucose from glycolysis toward the PPP [89]. PPP is essential in providing NADH phosphate, which is important for maintaining glutathione in the reduced form and thus protecting the cells from the oxidative stress resulting from ROS accumulation [89].

Under hypoxic conditions, high levels of ROS activate hypoxia–inducible factor–1 (HIF–1) [90]. Induction of HIF-1 has a role in diverting glucose away from glycolysis and pyruvate away from the TCA cycle. HIF–1 has been found to be expressed in prostate cancer cells [91]. HIF-1 has been found to induce the gene expression of PFKFB4 [92]. In PC3 cells the gene expression of HIF-1 and HK2 has been found to be induced under hypoxic conditions [93]. HK2 drives glycolysis to produce glucose-6-phosphate, but an increase in PFKFB4 decreases fructose-2,6-bisphosphate and since fructose-2,6-bisphosphate is a regulator of PFK1, this may cause a decrease the activity of PFK1, therefore, the resultant fructose-6-phosphate is diverted into the PPP, suggesting that glucose is diverted away from glycolysis in these cells [87].

Moreover, in cancerous cells, it was found that HIF–1 induces the expression of pyruvate dehydrogenase kinase 1 that is responsible for the phosphorylation of PDH, thus deactivating PDH [90]. Also, it was found that HIF–1 induces LDH, which converts pyruvate into lactate in anaerobic glycolysis [90]. Deactivation of PDH and activation of LDH decreases the entry of pyruvate into the TCA cycle and instead diverts pyruvate towards lactate production. Indeed, it has been found that lactate production is higher in prostate cancer than non-cancer cells and high levels of lactate are secreted in the media [94].

These observations suggest that the rate of aerobic glycolysis in the prostate cancer cells is decreased. Citrate production in these cells also account for the decreased rate of glycolysis by inhibiting PFK [95]. Therefore, in order to meet the energy need, fatty acid oxidation through β-oxidation is stimulated. In these cells, peroxisomal β-oxidation, which is specialised in oxidizing long and branched chain fatty acids has been found to be increased [27, 95].

Another metabolic characteristic of the prostate cancer cells is the oxidation of citrate due to the low zinc content, which is reflected in the increased activity of aconitase, therefore, increased oxidation of citrate in TCA cycle [5]. However, citrate in these cells is exported into the cytosol due the overexpression of citrate transporters; therefore, they are being used as a precursor for lipogenesis. In order to keep an efficient TCA cycle, glutamate is utilised and subsequently converted into α-ketoglutarate to replace the TCA intermediate [5].

In the cytosol, citrate is converted back into acetylCoA by ACLY and it was suggested that citrate acted as the main source for acetylCoA required for either cholesterol or fatty acids synthesis [10]. For cholesterol synthesis, the reformed acetylCoA is converted into acetoacetylCoA by ACAT and then into mevalonate, which is the precursor for cholesterol synthesis by HMGCS and HMGCR. Cholesterol is important for the production of hormones, such as testosterone, which is essential for prostate growth.

AcetylCoA can also be converted into malonylCoA by ACC1. AcetylCoA along with other molecules of malonylCoA can be bind to form fatty acids in multi-enzymatic processes [5] (figure 1.11). It is unlikely that the formation of malonylCoA is associated with the inhibition of CPTI enzyme since malonylCoA is not accumulated in case of prostate cancer, but rather consumed in the process of fatty acid synthesis, which are essential for the newly proliferated cells. In fact this assumption does not goes against fatty acid-glucose cycle as it has been shown that in prostate cancer cells silencing *PFKFB4* increases levels of Fru-2,6-BP, which is a regulator of PFK1, therefore diverting glucose 6-phosphate towards the glycolytic pathway, thus depleting the pentose phosphate pathway [87].

One of most abundant fatty acids is that synthesized in the cells is palmitic acid, which is a C16 fatty acid that represents approximately 80% of the total fatty acids synthesized in the cell [96].

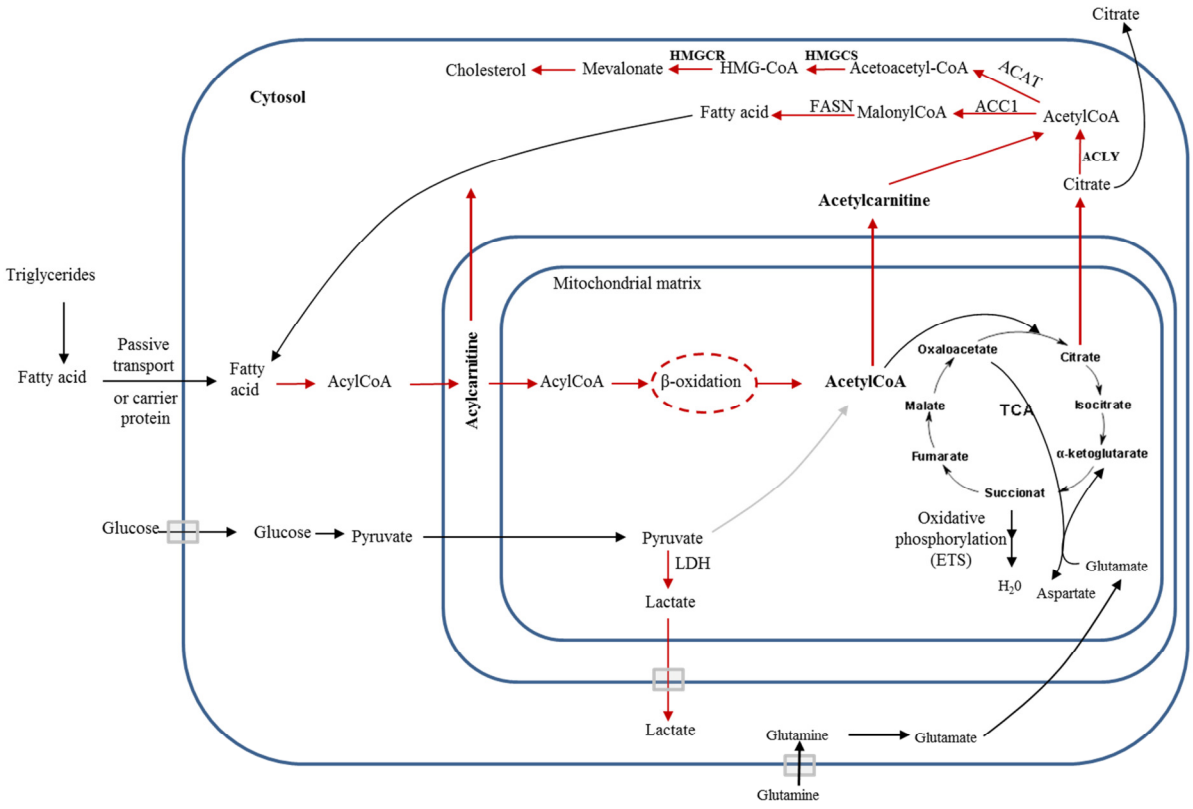

Figure 1.11: Metabolism of fatty acids in prostate cancer cells. In these cells, the main energy source is the oxidation of fatty acids. The mitochondrial defect results in a loss of co-ordination between β-oxidation and TCA cycle, leading to the accumulation of acylcarnitines. The latter are also produced due to the low efficiency of TCA cycle as a result of high levels of ROS. The produced acetylCoA enters the TCA cycle and is converted into citrate and further oxidized to eventually produce NADH and $FADH_2$, which are oxidized for energy production through the ETC. Citrate however, can also be excreted into the cytosol and used as a precursor for fatty acids and cholesterol synthesis. Red arrows indicate the stimulated processes.

It has been shown that the up-regulation of lipogenesis is linked to the development of prostate cancer [97, 98]. Generally, lipids are considered important for the biology of cancer. They provide the building blocks for membrane synthesis, they represent a form of energy storage, a source for synthesizing signalling molecules and they are involved in post-translational modification of proteins crucial for cell-signalling, and hormonal synthesis [5]. All these factors are important for the growth, proliferation and invasion of cancer cells.

These observations suggest that in prostate cancer cells, the up-regulation of the *de novo* lipogenesis as well as the increased amino acid metabolism could be associated with an increase in TCA activity to produce NADH and $FADH_2$ required for these two

processes. Since TCA cycle is a central process for many metabolic reactions, the stimulation of metabolic processes, such as β-oxidation and lipogenesis along with the stimulated fatty acid uptake, may lead to a less efficient TCA cycle. A less efficient TCA cycle could affect its co-ordination with β-oxidation, which may result in incomplete fatty acid oxidation leading to the accumulation of intermediates of fatty acid oxidation, such as acylcarnitines.

1.10. Thesis aims

Prostate cancer is a disease where metabolic processes, such as lipogenesis and glycolysis have been re-programmed in order to provide sufficient energy to support the growth of the proliferating cells. Induction of several metabolic processes is accompanied with an increase in the levels of ROS. One of the consequences of ROS accumulation is their effect on the enzymes efficiencies involved in metabolic processes, such as the TCA cycle, which could affect the balance between metabolic processes. A less efficient TCA cycle results in a poor co-ordination with β-oxidation leading to the accumulation of intermediates of fatty acid oxidation, the acylcarnitines. Among these acylcarnitines is palcar. The presence of palcar was associated with pro-inflammatory responses and Ca^{2+} influx in endothelial cells. However, the levels of palcar and the consequences of the presence of palcar have not been investigated in prostate cancer. Therefore, the purpose of this thesis is to investigate the levels of palcar in prostate cancer tissue and explore the biological consequences of palcar accumulation in prostate epithelial non-cancerous and cancerous cells. I accomplish this research goal by addressing and investigating the following aims:

- To test the hypothesis that palcar accumulates in the prostate cancer tissue as compared to the non-cancerous tissue, thus providing a biomarker for the metabolic dysfunction in prostate cancer (Chapter 2).

- To test the hypothesis that the accumulation of palcar is associated with induction of IL-6 and Ca^{2+} influx in prostate epithelial cancer cells (Chapter 3).

- To test the hypothesis that the mechanism by which palcar induces Ca^{2+} influx involves the activation of PTX-sensitive GPCR and L-type Ca^{2+} channels (Chapter 4).

- To investigate the hypothesis that low concentrations of palcar are associated with changes in gene expression in prostate epithelial cells (Chapter 5).

Chapter 2

Palmitoylcarnitine: A biomarker for metabolic disturbances associated with prostate cancer

2.1. Introduction

In this Chapter, the accumulation of palcar, as an example of long chain acylcarnitines, in prostate cancer tissue was investigated and compared to the levels of palcar in the benign non-cancerous tissue. As it has been reported that metabolism is disrupted in prostate cancer, this Chapter seeks to provide an answer to the question of whether palcar accumulation would represent a biomarker for metabolic dysfunction associated with prostate cancer.

Metabolism is a set of chemical transformations that includes both catabolic and anabolic reactions. The critical balance of both types of reactions is essential for the generation of new organic molecules and the release of energy required for cellular growth and development. However, accelerating the rate of one metabolic reaction at the expense of others may result in the loss of this balance leading to metabolic dysfunction. Chronic disorders, such as CVD [99], DM type 2 [6] and obesity [7], display this type of imbalance especially between β-oxidation and TCA cycle. Prostate cancer is another form of chronic disease that has seemingly unique metabolic features [5, 94]; one of them being the increase in fatty acid uptake. In prostate cancer cells despite the overexpression of glucose transporters [100], the uptake of fatty acids was more pronounced [9]. Fatty acids are transferred into the mitochondrial matrix for β-oxidation through the carnitine shuttle system. Very long chain and branched chain fatty acids have been found to be oxidized via peroxisomal β-oxidation to produce shortened chains that can be then transferred to mitochondria for further oxidation and energy production [27]. In prostate cancer, the rate of peroxisomal β-oxidation was up-regulated compared to normal prostate tissue [27].

A defect in the β-oxidation or alteration in any of the molecular components of the carnitine shuttle system involved in the transport of fatty acids into the mitochondria, for example CPT II and CAT, may result in a defect of fatty acid oxidation and the accumulation of intermediates, such as acylcarnitines [23, 24].

2.1.1. Acylcarnitines

Acylcarnitines have for some time been used as a biomarker to indicate an “inborn error of metabolism”, which is an inherited missing or inadequate enzyme that leads to an abnormality of metabolism [101, 102]. Higher levels of acylcarnitines were detected in the ischemic heart of animal models [103-105] as well as in the animal models of acquired mitochondrial dysfunction [106]. Also, it was noticed that high fat diets, obesity and DM type 2 were also associated with high plasma levels of acylcarnitines as a result

of impaired metabolic pathways caused by the loss of the integration between TCA cycle and β-oxidation [6]. The loss of the integration between these processes maybe caused by the less activity of TCA cycle without necessary affecting the rate of β-oxidation leading to the accumulation of acetylCoA. AcetylCoA is then converted into acetylcarnitine, which is a short chain acylcarnitines, and this is in order to reduce the toxic effect of the accumulated acetylCoA. Moreover, the loss of integration between TCA cycle and β-oxidation could also involve a less activity of β-oxidation due to a decrease in the activity of enzymes involved in β-oxidation leading to the accumulation of acylcarnitines, however this notion need further investigation.

The accumulation of acylcarnitines was also linked to some metabolic disorders of protein metabolism, where the inherited deficiencies of important enzymes involved in energy production, such as acylCoA dehydrogenase, can cause an increase in the levels of acylcarnitines. AcylCoA dehydrogenase is an enzyme that catalyses the first step in the β-oxidation [31].

2.1.2. Palmitoylcarnitine

Palmitoylcarnitine (palcar) is a C16:00 acylcarnitine (figure 2.1) that is synthesized from the fatty acid palmitic acid, which represents approximately 80% of the total fatty acids synthesized in the cell [96], therefore, it is one of the commonly studied acylcarnitines in human and animal models and used as an example of long chain acylcarnitine.

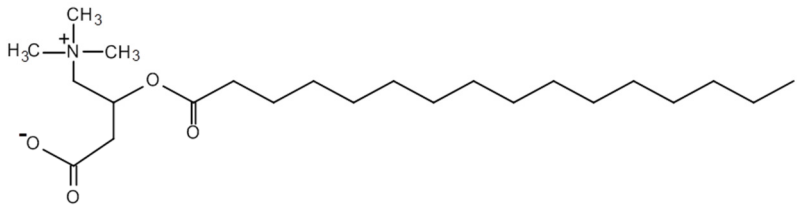

Figure 2.1: Structure of palcar. Palcar consist of a chain of 16 carbon atoms derived from the fatty acid palmitic acid, acyl group and carnitine molecule.

The high plasma levels of palcar associated with obesity and DM type 2 [6, 7] suggest that the accumulation of palcar may represent a biomarker for metabolic dysregulation. In DM type 2, long chain acylcarnitines have been associated with oxidative stress, arterial stiffness as well as being linked to the risk of developing DM type 2 itself [33]. Lately, palcar accumulation has been reported in kidney cancer tissue and urine samples [8].

The levels of palcar quantified in different matrices from both human and animal models are summarised in table 2.1. The difference between the observed levels of palcar in these studies is due to the different techniques used to quantify palcar. In Vieira Neto *et al* study, the subjects were babies who depends on milk as their main food and milk is known to have high levels of fatty acids, which indicate that the mitochondria is overload with fatty acids, therefore having high rate of fatty acid metabolism [102].

Table 2.1: Levels of palcar as reported in the literature.

Concentration of palcar		Sample (species)	Reference
Healthy levels	**Unhealthy levels**		
0.25µM	1.02 µmol/L (VLCAD)[1] 1.55µmol/L (GA-II)[2]	Plasma (Human)	Peng *et al*. *Chromatography B*, 2013. 932: 12– 18 [31].
1.70 µM	-	Cord blood samples (Human)	Vieira Neto *et al*. *Braz J Med Biol Res*, 2012, 45(6): 546-556 [102].
2.16 µM	-	Heel-prick blood samples (Human)	Vieira Neto *et al. Braz J Med Biol Res*, 2012, 45(6): 546-556 [102].
0.04 ± 0.02 µM (non-diabetic lean)	0.07 ± 0.02 µM (obese) 0.06 ± 0.03 µM (diabetic)	Plasma (Human)	Mihalik *et al*. *Obesity,* 2010. 18(9): 1695-700 [7].
0.352 ± 0.148 µM	0.404 ± 0.220 µmole/L (chronic fatigue syndrome)	Plasma (Human)	Reuter & Evans. *J Intern Med, 2011. 270(1): 76-84 [23].*
0.87 µM	-	Whole blood (Human)	Minkler *et al. Clin Chem, 2008. 54(9): 1451-62 [32].*
0.92 µM	-	Blood spot (Human)	Minkler *et al*. Clin Chem, 2008. 54(9): 1451-62 [32].
≈ 12 µM	-	Skeletal muscle (Human)	Minkler *et al*. Clin Chem, 2008. 54(9): 1451-62 [32]
≈ 17µM	≈ 19µM (high fat diet)	Adipose tissue (Rat)	Sampey *et al. PloS ONE,* 2012. 7(6): e38812 [46].
≈ 6 µM	≈ 12 µM (high fat diet)	Muscles (Rat)	Sampey *et al. PloS ONE,* 2012. 7(6): e38812 [46]
-	60 µM (ischemic heart)	Heart (rabbit)	Moore *et al*. J Clin Invest. 1982. 69(2): 377-83 [103]

[1] VLCAD: very long chain acyl-CoA dehydrogenase; [2]GA-II: glutaric acidemia type II.

2.2. Aims

- To quantify the levels of palcar in both non-cancerous and cancerous prostate tissue.
- To investigate the possibility that palcar may represent a potential biomarker for the metabolic dysregulation associated with prostate cancer.

2.3. Materials and methods

2.3.1. Tissue collection and sample preparation

Prostate tissue samples were obtained from Norwich and Norfolk University Hospital (NNUH) Partners in Cancer Research Human Tissue Bank. A total of 20 tissue samples were used for method optimization and measurement of palcar. The protocol was approved by the Faculty of Medicine and Health Science Research Ethics Committee (reference: 2012/2013 – 10HT and 2012/2013 – 37), University of East Anglia.

Clinical information (procedure, diagnosis and Gleason grade) was obtained for all tissue. Benign samples were obtained from either prostate glands with no cancer present obtained from a cystoprostatectomy, or from prostate glands with cancer. In the latter case the Gleason grade is reported.

The tissue samples were received frozen and immediately pulverized to a fine powder under liquid nitrogen using tissue BioPulverizer (Cat. # YO-36903-00, Cole-Parmer, UK). The resultant frozen powder was stored immediately at -80°C for later analysis.

Levels of palcar were measured based on a previously published method [107] with slight modifications, optimised by Dr. Shikha Saha at the Institute of Food Research. These modifications are outlined below. Approximately 20 mg of the frozen tissue samples were placed in 2 ml screw cap centrifuge tubes. Fifty microliters of freshly prepared 1M potassium phosphate monobasic (KH_2PO_4) solution and 10µl of 100ng/ml of each of the deuterated internal standards solutions, D_3-octanoylcarnitine (C8:0) and D_3-palmitoylcarnitine (C16:0), were added to the sample. Then, 500µl of freshly prepared extraction solution of 3:1 acetonitrile:methanol (v/v) was added. The resulting mixture was vortexed for 30 seconds and further homogenised with a mechanical grinder for 30 seconds, then another 500µl of the freshly prepared extraction solution was added to each sample and homogenised for an additional 30 seconds and vortexed again. The mixture was centrifuged at 13000 round per minute (rpm) for 5 minutes at 4°C and the supernatants were transferred into insert vials to be analysed using a liquid chromatography-tandem mass spectrometry (LC-MS/MS) system.

The use of a mixture of labelled internal standards (figure 2.2) eliminates the issues associated with common ion fragmentation, which could result in an overestimation of palcar concentrations. Common ion fragmentation means the production of the same fragment ion of 85 mass to charge ratio (m/z) by all acylcarnitines (figure 2.3). This

means that palcar present in the tissue samples and the internal standard will produce the same fragment ion of 85 m/z and will be eluted at the same retention time, so the resulted peaks of palcar may sometimes represent an overestimation. To prevent the overestimation of palcar coming from internal standard, the deuterated octanoylcarnitine was used for accurate quantification because octanoylcarnitine has a different retention time.

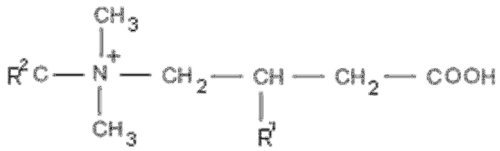

Figure 2.2: Chemical structures of D_3-octanoylcarnitine and D_3-palmitoylcarnitine. R^1 and R^2 are:

R^2	R^1	Name	Transition (m/z)
D_3	$OCO(CH_2)_6CH_3$	D_3-octanoylcarnitine	291.2 →229.0 + 85.1
D_3	$OCO(CH_2)_{14}CH_3$	D_3-palmitoylcarnitine	403.4 → 85
H_3	$OCO(CH_2)_{14}CH_3$	Palcar	400.0 → 85

(Source: based on Sun *et al* [107]).

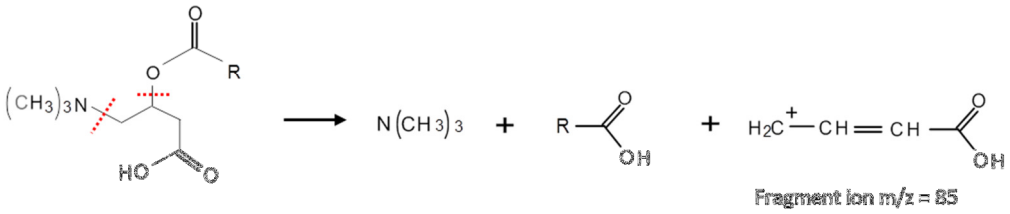

Figure 2.3: Fragmentation of acylcarnitines. All acylcarnitines can be fragmented by breaking the bond indicated with red dashed line to produce a characteristic product (fragment) ion of 85 m/z.

2.3.2. Preparation of internal standards and standard curve

Stock solutions of internal standards of D_3-palmitoylcarnitine (Cat. # DLM-1263-0.01, Cambridge Isotope Laboratories, USA) and D_3-octanoylcarnitine (Cat. # DLM-755-0, Cambridge Isotope Laboratories, USA) were prepared by dissolving the corresponding compounds into DMSO to obtain a final concentration of 1mg/ml. These solutions were further diluted to 10µg/ml and 100ng/ml using freshly prepared extraction solution of acetonitrile and methanol (3:1). Internal standard work solution of 100ng/ml was used for standard and sample preparation. The standard curve was prepared using serial dilutions of a synthetic palcar stock solution (27mM) and following the same steps for sample preparation. Both the peak areas and the concentrations of the standards were used to

obtain an equation with a response factor. This equation was used to quantify the concentrations of palcar in the prostate tissue samples.

2.3.3. LC-MS/MS determination and quantification of palcar

The high performance liquid chromatography (HPLC) system used was Agilent 1200 series LC combined with Agilent 6490 triple Quad LC/MS with electrospary interference (ESI) built in, in addition to a quaternary pump, degasser, auto-sampler, thermo-stated column compartment and a wide range of wavelength ultraviolet (UV) detector. The separation was performed using reverse phase HPLC silica column (Acquity UPLC, 2.1 x 50mm, 1.7 µm, BEHC8 column, Waters Ireland).

The column temperature was maintained at 37°C and 15°C for the autosampler. A small aliquot (10µl) was automatically injected into the LC-MS/MS and eluted with 10% of mobile phase A (0.1% ammonium acetate in de-ionized water) and 90% of mobile phase B (0.1% ammonium acetate in methanol), at a rate of 0.5ml/minute. Mobile phase A was prepared by dissolving 0.2g of mass spectrometer (MS) grade ammonium acetate (Cat. # 01244153, Biosolve BV, Netherland) and 0.535g of 0.05% heptafluorobutyric acid (Cat. # 52411-5ML-F, Sigma-Aldrich, UK) in de-ionised water. Mobile phase B was prepared in the same way as mobile phase A, but dissolved in HPLC-grade methanol (Cat. # 1691935328, Merk, Germany). A positive ion mode ESI was used as ionization source. The nebulizer gas used was nitrogen with a flow of 12 L/min, pressure 60 psi and temperature of 200°C.

The system lines were purged for 5 minutes at 0.5ml/minute using the prepared mobile phase A & B prepared as described above. The operating parameters used are shown in Table 2.2.

Table 2.2: LC-MS/MS parameters for operation

LC – system	
Injection volume	10µl
Mobile phase	90% methanol 10% water
Flow rate	0.5ml/min
Syringe/system wash	Acetonitrile: Methanol: water (25:50:25)
MS–MS system	
Scan mode	multiple reaction monitoring (MRM)
Q2 precursor ion	400 m/z
Product ion	85 m/z
Polarity	Positive

In the MRM mode of analysis, that utilizes a triple quadrupole MS, the mass (m/z) of desired parent ion, which was 400 m/z, was selected in the first quadrupole. The second quadrupole generates fragment ion(s) through collisional induced dissociation, while in the third quadrupole, the product (fragment) ion, which was 85 m/z, was monitored. Therefore, the three mass analysers (triple quadrupole) of the MS, cycle through a series of transitions (the specific pair of 400/ 85 m/z selected) and record the signal of each transition as a function of elution time to give a peak that represent the presence of palcar.

The peak area of palcar was then integrated for each tissue sample and palcar concentration was calculated using the response factor obtained from the equation created by performing the standard curve (section 2.3.2). For example, if the peak area of palcar obtained from a tissue was 251929.24, and the standard curve gives the following equation: y = 2470070.31x – 2909.50, then the concentration of palcar would be (251929.24+ 2909.5)/2470070.31, which is equal to 0.103µM.

2.3.3.1. Data processing

All standard and tissue samples were analysed in triplicate. Mass Hunter B.06 software was used to integrate the chromatographic peaks and calculate the area under the curves. Calibration curves were generated using Excel 2010 and a linear regression of the peak areas of the serial dilutions of palcar stock solution was obtained. The response factor was used to indirectly calculate the concentration of palcar in the prostate tissue samples.

2.3.3.2. Statistical analysis

Tissue levels of palcar were quantified from 20 prostatic tissue samples; 10 non-cancerous (benign) and 10 cancerous tissue. The levels represent mean ± SEM. To compare the mean levels of palcar in cancerous tissue to non-cancerous (benign) tissue statistical analysis was performed with unpaired t-test using GraphPad Prism version 5.00 for Windows (GraphPad Software, San Diego California USA, www.graphpad.com).

2.4. Results

A fragment ion of 85 m/z was detected in the two internal standards that were used to detect the presence of palcar in the prostate tissue (figure 2.4). Total ion chromatogram (TIC) showed the peaks of both D_3-octanoylcarnitine and D_3-palmitoylcarnitine internal standards, where the retention times for the D_3-octanoylcarnitine and D_3-palmitoylcarnitine were 1.678 and 2.063 minutes, respectively. Since the tissue samples

were mixed with the D_3-palmitoylcarnitine during sample preparation, the peak of the C16:00 represent palcar detected from both the internal standard (403.0/85 m/z) and the tissue sample (400.0/85 m/z).

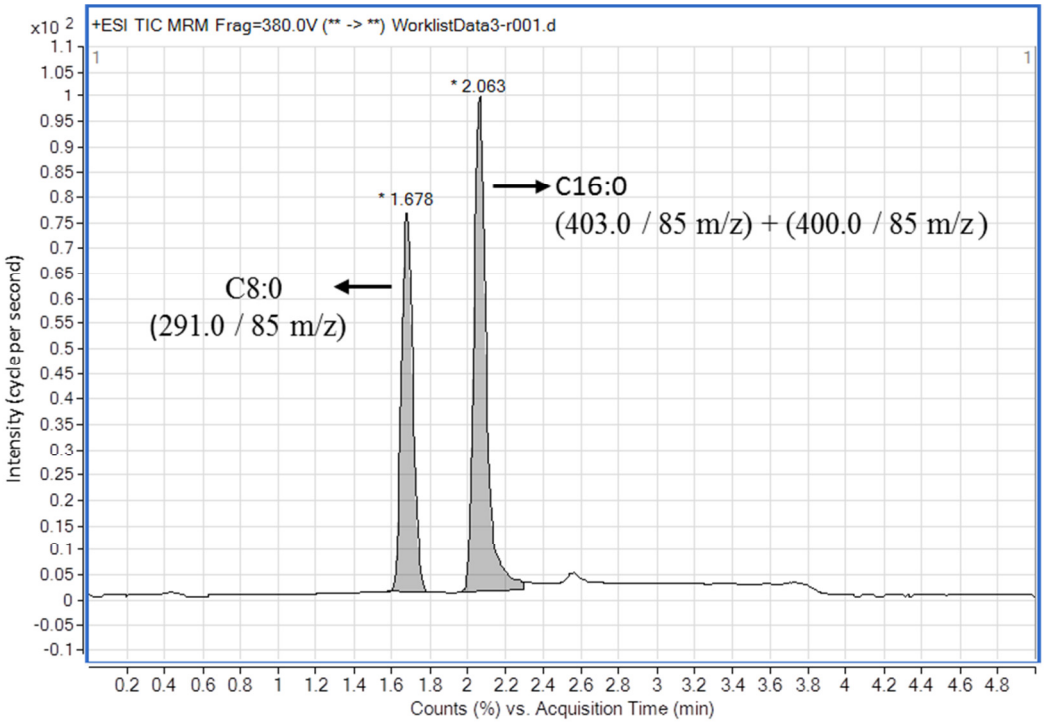

Figure 2.4: TIC of D_3-octanoylcarnitine and D_3-palmitoylcarnitine from a representative prostate tissue sample. The retention time for D_3-octanoylcarnitine (C8:0) is 1.678 minutes detected using selected scan of 291.0/85 m/z, and 2.063 minutes for D_3-palmitoylcarnitine (C16:0) with scan of 403.0/85 m/z.

The MRM chromatogram was extracted from the TIC. D_3-Palmitoylcarnitine was identified by the mass screening of 403.0/85 m/z (figure 2.5), while palcar detected in prostate both non-cancerous and cancerous tissue was identified by the mass screening of m/z 400.0/85 (figure 2.6), which has a retention time similar to the palcar internal standard.

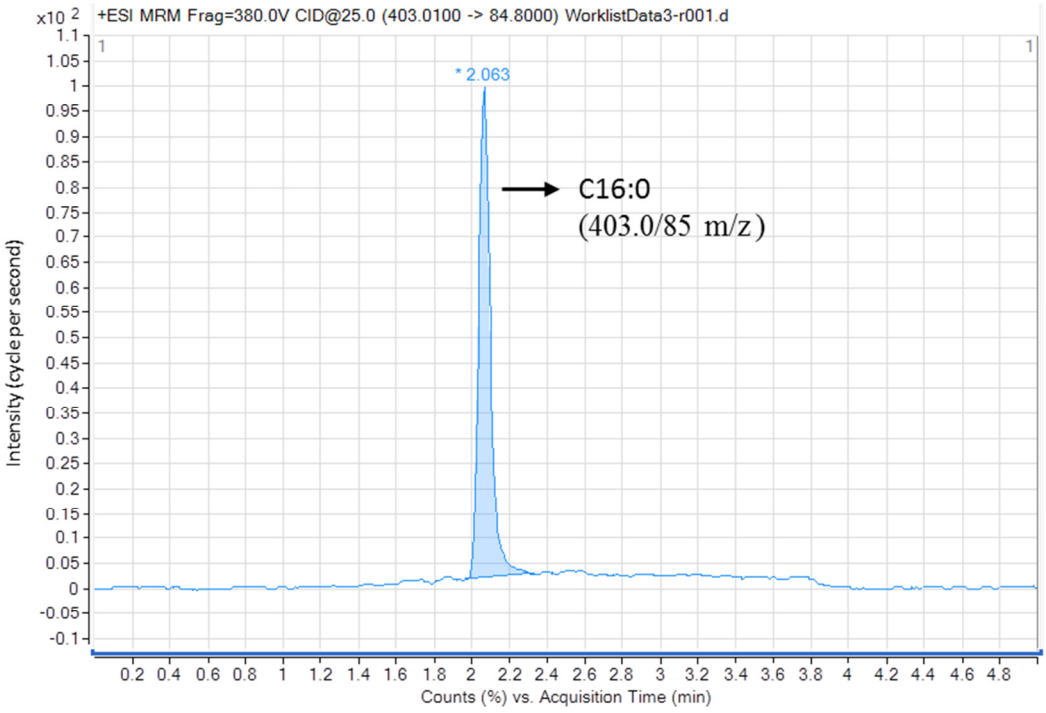

Figure 2.5: LC–MS/MS chromatogram of D_3-palmitoylcarnitine from a representative prostate tissue sample. Palcar (C16:0) from internal standard was detected using selected MRM scan of 403.0/85 m/z.

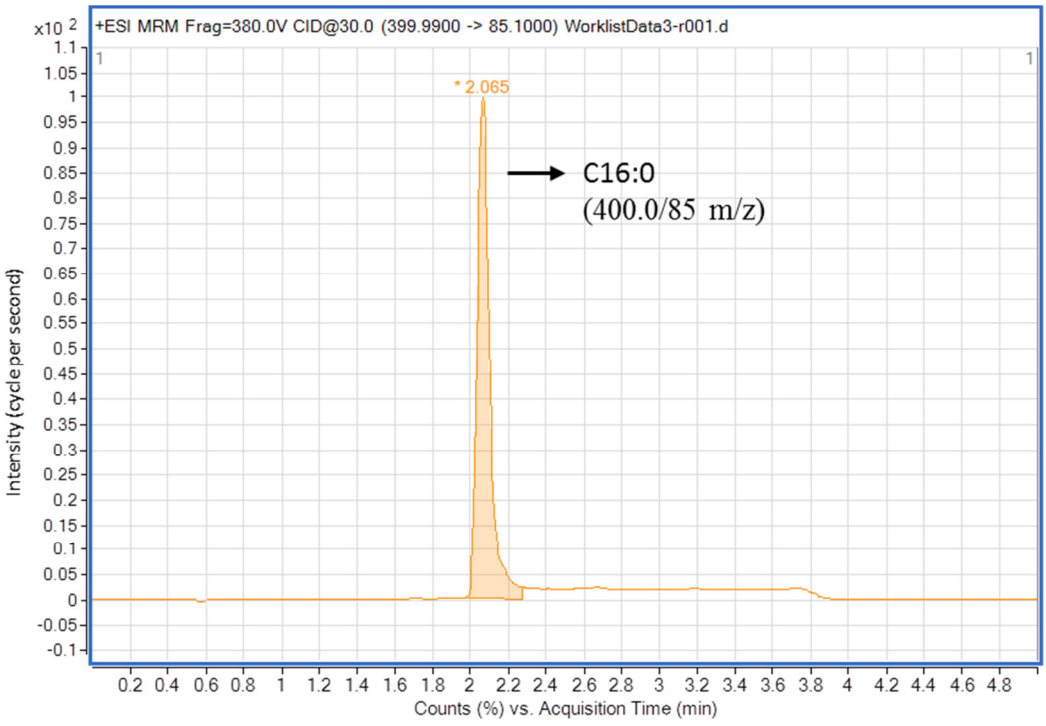

Figure 2.6: LC–MS/MS chromatogram of palcar from a representative prostate tissue sample. Palcar was detected using selected MRM scan of 400.0/85 m/z.

Analysis of palcar levels in prostate tissue using LC-MS/MS showed significantly higher levels of palcar in the prostate cancerous tissue compared to the non-cancerous benign tissue (P=0.0135, figure 2.7A). There were individual differences in the quantified levels of palcar in both non-cancerous benign and cancerous prostate tissue, these values ranged from almost zero to approximately 0.0747±0.0234µM for the benign tissue with an average of 0.0329±0.0234µM, and from approximately 0.02167±0.0319µM to 0.1030±0.0319µM for the cancerous tissue with an average of 0.0671±0.0319µM (figure 2.7B). The characteristics of each tissue used are depicted in Table 2.3.

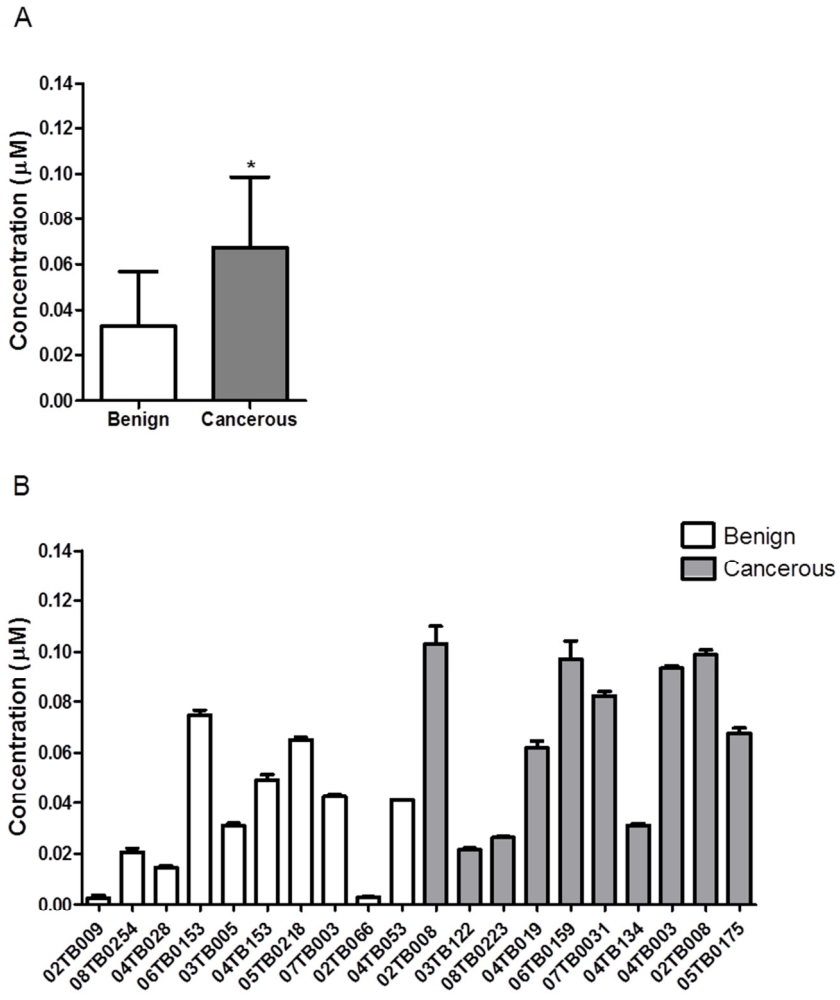

Figure 2.7: Concentrations of palcar (µM) in prostate benign and cancerous tissue. Tissue samples were obtained from NNUH Partners in Cancer Research Human Tissue Bank. A) The mean concentrations of palcar (µM) ± SEM from 10 benign and 10 cancerous tissue samples. B) Palcar concentrations (µM) ± SEM from each individual tissue. The x-axis represents the individual tissue code. Statistical analysis in A was performed with unpaired t-test. *P = 0.0135.

Table 2.3: Characteristics of prostate benign and cancerous tissue.

Tissue code	Procedure*	Diagnosis	Gleason grade
08TB0254	Cystoprostatectomy	Normal	-
04TB153	TURP	Hyperplasia	-
04TB053	TURP	Benign	-
03TB005	Cystoprostatectomy	Benign	-
05TB0218	Radical prostatectomy	Benign	7
07TB0033	Radical prostatectomy	Benign	7
06TB0153	Radical prostatectomy	Benign	7
02TB066	TURP	Benign	7
02TB009	Radical prostatectomy	Benign	7
04TB28	Radical prostatectomy	Benign	10
02TB008	Radical prostatectomy	Adenocarcinoma	7
04TB019	Radical prostatectomy	Adenocarcinoma	7
06TB0159	Radical prostatectomy	Adenocarcinoma	7
07TB0031	Radical prostatectomy	Adenocarcinoma	7
04TB134	Radical prostatectomy	Adenocarcinoma	7
02TB008	Radical prostatectomy	Adenocarcinoma	7
05TB0175	Radical prostatectomy	Adenocarcinoma	7
03TB122	TURP	Adenocarcinoma	Not provided
04TB003	TURP	Adenocarcinoma	9
08TB0223	Radical prostatectomy	Adenocarcinoma	4+3+5

* Cystoprostatectomy: the removal of the urinary bladder and prostate gland. TURP: the removal of a section of the prostate gland. Radical prostatectomy: the removal of the prostate and the surrounding tissue.

2.5. Discussion

In this study, the levels of palcar in both non-cancerous and cancerous prostate tissue were quantified to investigate the possibility that palcar may represent a potential biomarker for the metabolic dysregulation associated with prostate cancer. The levels of palcar in prostate cancer tissues were higher than the levels in the non-cancerous tissue.

In this study, levels of palcar were measured using an LC-MS/MS method. This method is a significant improvement to a previously published method [107] as it does not include a derivatisation step. Many studies have analysed carnitine and acylcarnitines from different matrices using LC-MS/MS techniques, however, they all have used the derivatisation technique before sample injection. The purpose of derivatisation is to change the chemical structure of the tested compound to include ionic or charged groups in order to increase the intensity of the signal detected on the positive mode, or to change the hydrophobicity of the test compound, thus improving the detection [108]. Therefore, derivatisation technique is applied for unstable compounds that are not easily detected.

Palcar is a stable compound [109]. Its stability was verified and tested by LC-MS/MS in our lab in the Institute of Food Research, where it was found that palcar was stable at 15°C for at least 24 hours. The inclusion of a derivatisation step may have some drawbacks including the partial hydrolysis of the test compound and/or incomplete reaction [31], which may result in an underestimation of its presence. Due to the small size of the obtained prostate tissue samples, it was difficult to use the tissue samples to perform both the derivatisation and non-derivatisation steps to compare palcar tissue levels between derivatised and non-derivatised tissue samples, which could provide more confidence in the data.

Accumulation of acylcarnitines has previously been measured in animal tissue of kidney [8], liver, skeletal muscle and heart [110]. Following the review of the relevant literature, the levels of acylcarnitines, specifically palcar, have not been published in human prostate tissue, therefore, in this thesis it is the first time that the levels of palcar were measured in human prostate tissue. In this study increased levels of palcar were observed in prostate cancerous tissue compared to non-cancerous benign tissue. The levels of palcar in the cancerous tissue ranged from 0.02 µM to 0.1µM with an average of 0.07µM compared to 0.034µM average of the non-cancerous benign tissue (figure 2.7A). These results were obtained from 20 prostate cancer and non-cancer tissue samples. This limited number of tissue samples is in accordance with the ethical approval for performing this study, which limits the number of the tissue samples to 20 samples. For further analysis with additional samples additional ethical approval would be required. However, due to the time limitation for the completion of this work, this study was not further investigated. Nevertheless, the results from the 20 tissue samples indicate the utility of prostate tissue palcar levels as a diagnostic tool for distinguishing prostate cancer from non-cancer tissues. It is important to note that having more tissue samples would give a robust assessment of the potential use of palcar as a diagnostic tool for prostate cancer.

There are possible hypotheses that may explain the increased levels of palcar in cancer tissue. One explanation is that a higher degree of tissue lipid metabolism is occurring in the cancerous tissue. This might indicate mitochondrial overload of the long chain fatty acid (palmitic acid), which could be an indication of stimulated lipolysis. Stimulated lipolysis is a characteristic feature of cancer cells [111, 112]. *In vitro* models of prostate cells revealed that the uptake of palmitic acid by both malignant and benign cells was significantly higher than that of glucose [9], which suggests that fatty acid oxidation is a dominant energy source for the prostate cells.

Overload with fatty acids either as a result of lipolysis or high fat diet may lead to the production of high levels of acetylCoA by β-oxidation. It has been found that acetylCoA is a precursor for acetylcarnitine and ketone bodies [113] and it has been suggested that formation of ketone bodies may inhibit or reduce the efficiency of TCA cycle as the mitochondria is unable to synthesize the intermediate of TCA cycle [6]. A less efficient TCA cycle would result in a mismatch between the rates of β-oxidation and TCA cycle, leading to a metabolic defect that results in an incomplete fatty acid oxidation and the accumulation of other acylcarnitines, such as palcar [6]. In prostate cancerous tissue, it has been found that peroxisomal β-oxidation was up-regulated [27]. Alpha-methylacylCoA racemase and its downstream enzymes pristanoylCoA oxidase and D-bifunctional protein, involved in peroxisomal β-oxidation, were overexpressed in prostate cancer tissue [27]. Peroxisomal β-oxidation is important for the initial oxidation of branched and very long chain acylcarnitine. The resultant chain-shortened products can then be transported to the mitochondrion for complete degradation. However, a defect in mitochondrial β-oxidation may result in the accumulation of fatty acid intermediates, such as acylcarnitines, which is another explanation for the accumulation of palcar in the prostate cancerous tissue observed in this study.

In this study the accumulation of palcar in prostate cancer tissue was hypothesized to be a result of a metabolic defect. A metabolic defect not only imply a mismatch between the rate of β-oxidation and TCA cycle, but also a defect in mitochondrial transport system of fatty acids through the mitochondrial membrane, which provide another explanation for the observed increased levels of palcar in prostate cancer tissue. There are two enzymes responsible for this process, CPT I and CPT II. It seems unlikely that a CPT I defect would result in palcar accumulation, as this enzyme is involved in transferring the acyl group from fatty acylCoA to carnitine to form palcar. In support of this, accumulation of acylcarnitines found in other metabolic disorders, such as obesity and DM type 2 was not related to a defect in CPT I enzyme since all fatty acids were found to be converted into acylcarnitines and then into long chain hydroxyl acylcarnitines [7]. Hydroxyl acylcarnitines are intermediates of β-oxidation occurring as a result of the activity of very-long-chain acylCoA dehydrogenase (VLCAD) and long chain 3-hydroxyacyl-CoA dehydrogenase [7]. However, accumulation of palcar in prostate cancer tissue could be a result of an inadequate activity of CPT II enzyme, which is involved in transferring the acyl group from acylcarnitines to the mitochondrial CoA. This assumption was suggested in diabetic subjects who have high plasma levels of palcar compared to non-diabetic subjects [7]. Nevertheless, since the activity of this enzyme was not determined in prostate tissues, further research is needed to investigate

this notion. The explanations for the accumulation of palcar in prostate cancer tissue samples are hypotheses and need further investigations to determine the nature of this accumulation.

The levels of palcar detected in the prostate non-cancer and cancer tissue were in the range of the plasma levels from non-diabetic lean subjects and diabetic and obese subjects, respectively [6, 7]. It is important to note that accumulation of palcar may start in tissue prior to its leakage to the plasma and since the tissue content of carnitine is higher than in plasma [114], the expected tissue levels of palcar should be higher than that in the plasma. In this study, the plasma levels of palcar from the same prostate tissue donors were not measured, and therefore were not possible to compare the levels of palcar in tissue samples with that in plasma. However, in this study, when comparing the levels of palcar in prostate cancer tissue with that reported in the plasma from diabetic and obese subjects, the levels of palcar in prostate cancer tissue samples were not higher than that reported in the plasma samples and this might be related to different tissue type where the metabolic defect occur. In diabetic and obese subjects the metabolic defect occur in the liver and the carnitine content in these tissue were reported to be higher than the plasma levels [114].

Accumulation of acylcarnitines has been positively correlated with mitochondrial dysfunction associated with a high fat diet [46]. Rats fed with a high fat diet induced an increase in the serum levels of palmitic acid to approximately 80μM as well as an increase in medium and long chain acylcarnitines in muscle and adipose tissue. Also this was accompanied with an increase in the levels of triglycerides, which is a marker for metabolic syndrome [46]. Moreover, there is a growing body of evidence suggesting that accumulation of acylcarnitines may represent a potential biomarker for metabolic dysfunction associated with insulin resistance and obesity [12, 33]. High plasma levels of long chain acylcarnitines were detected in obese and diabetic subjects during fasting. This was suggested to be as a result of a limitation in fatty acid β-oxidation, which could results in a mismatch with the rate of TCA cycle. This leads to an incomplete fatty acid oxidation and the accumulation of acylcarnitines. During fasting, fatty acid oxidation is activated, which increases the levels of acylcarnitines. These levels were decreased by a short-term insulin clamp in obese subjects indicating a switch from fat to carbohydrate metabolism. This was in contrast to diabetic subjects, who have an increase in short and medium chain acylcarnitines indicating a defect in fatty acid oxidation that was associated with insulin resistance [7]. In diabetes type 2, the increase in fatty acid oxidation leads to an increase in blood glucose levels because of the glucose fatty acid cycle and because glucose is not being used as an energy source, fatty acids are being

consumed, however, because of the metabolic defect resulting from the mismatch between β-oxidation and TCA cycle, intermediates of fatty acid oxidation including the short and medium chain acylcarnitines are accumulated.

Accumulation of acylcarnitines were detected in kidney and liver cancer and it has been shown that this accumulation was associated with cancer grade; the higher the cancer grade, the higher the levels of acylcarnitines [8]. In prostate cells, cancer is reflected by the Gleason grade; the more aggressive the cancer, the higher the Gleason grade. In the work presented in this chapter, most of the tissue obtained from the human tissue bank had a Gleason grade of 7 (table 2.3). The results showed that there were variations in the levels of palcar between these tissue (figure 2.7B), which could be due to inter-individual variability. This variability can be explained by the fact that Gleason score of 7 is a sum of two figures that represent the most dominant and second most dominant tumour according to the degree of cells differentiation (as discussed in Chapter 1). A Gleason score of 7 may mean 4+3 or 3+4, which are both different. This means different tissue level of metabolism between the two samples. The tissue samples obtained for this study were only provided with the combined Gleason score without specifying each figure of the score. In addition, these donors may have other complications, such as diabetes that could affect their metabolism and therefore affecting the levels of palcar.

Having some of the cancer samples with normal levels of palcar and some of the normal samples with high levels suggests the need for further investigation using a higher number of tissue samples with more variable Gleason grade in order to validate the use of palcar as a candidate for diagnostic purposes in addition to explore whether the increase in palcar levels is correlated with the increase in Gleason grade.

2.6. Conclusion

In this study palcar was found to accumulate in prostate cancerous tissue in levels that were higher than benign non-cancerous tissue. The presence of high levels of palcar in the cancerous prostate tissue may indicate that palcar could represent a potential biomarker for the metabolic disturbance associated with prostate cancer. However analysis of higher number of tissue samples is needed in order to confirm the validity of using palcar as a diagnostic tool. The reason behind the accumulation of palcar was not investigated and therefore further studies are needed to determine the nature of the metabolic disturbance.

Accumulation of palcar in cancerous prostate tissue may influence the biological activities of the cancer cells prior to their leakage into the surrounding environment. These activities may include changing membrane permeability, thus changing the homeostasis of small intracellular mediators, which have a role in other signalling pathways that can be linked to the induction of pro-inflammatory responses and altering gene regulating proteins. Therefore, whether the presence of palcar is only a biomarker for the metabolic disturbances in prostate cancer or induces other physiological roles in the cells is to be addressed in the next chapter, where the effect of palcar on IL-6 secretion and Ca^{2+} influx as possible biological consequences are studied *in vitro* using prostate cell lines.

Chapter 3

Effect of palmitoylcarnitine on cellular IL-6 secretion and calcium influx

3.1. Introduction

Previously in Chapter 2, the accumulation of palcar was observed in prostate cancer tissue at levels that were higher than in non-cancer tissue. This accumulation may have biological consequences. In this Chapter, the secretion of the pro-inflammatory cytokine IL-6 and changes in membrane permeability, measured as the induction of Ca^{2+} influx, were investigated. Palcar-induced Ca^{2+} influx was compared to that induced by DHT, the hormone that is associated with prostate cancer progression. These properties were studied *in vitro* using prostate non-cancerous PNT1A and BPH-1, and cancerous DU145 and PC3 cells.

3.1.1. Acylcarnitines and pro-inflammatory responses

Acylcarnitines have been associated with pro-inflammatory responses including the secretion of TNF-α and pro-inflammatory cytokines, such as IL-3, IL-16 and IL-23 [46, 47]. This was in addition to their effect on inducing an increase in the levels of NFκB, which is one of the downstream targets of TLRs that are known to regulate the synthesis of the IL-6 [6, 48].

3.1.2. IL-6 and prostate cancer

Pro-inflammatory cytokines, such as IL-6, have been associated with the development and progression of prostate cancer [49-51]. The mode of action of IL-6 involves its binding with its membrane-bound receptor, IL-6 receptor α (IL-6Rα), that has been found in prostate cancer tissue [115], LNCaP, DU145 and PC3 cancerous cell lines [116]. The mode of action of IL-6 involves the binding of IL-6 with IL-6Rα to form a complex, then this complex binds to glycoprotein 130 to initiate cellular responses [49]. These responses include the induction of different growth phenotypes depending on the type of cultured cells and the activated signalling pathways. These phenotypes could be growth-inhibitory or growth-stimulatory phenotypes. In PC3 and DU145 cells, IL-6 induced growth and proliferation via the activation of phosphatidylinositol-3-kinase (PI3K) pathway [117, 118], while in LNCaP cells; it induced growth arrest via the activation of signal transducer and activator of transcription 3 (STAT3) and Mitogen–activated protein kinase (MAPK) pathways [117].

3.1.3. Acylcarnitines and Ca^{2+} influx

Due to their chemical nature, acylcarnitines have been shown to alter membrane permeability by changing the activity of membrane associated ion channels [41-43]. Alterations in a cell membrane permeability could lead to changes in the homeostasis of

ions, such as Ca^{2+}. In endothelial cells, palcar has been shown to induce Ca^{2+} influx [44]. This has also been observed in response to DHT in prostate cancer cells [45].

3.1.4. DHT and inflammation in prostate cancer

DHT exerts its effect by binding with the AR to form a complex. This complex translocates into the nucleus to bind with the androgen response element. The DHT-AR complex acts as a transcription factor that is able to alter inflammatory responses. In human prostatic myofibroblast cells (hBPH), DHT acts as an anti-inflammatory agent, where it reduces the secretion of IL-6 and IL-8 in response to oxidized LDL [119]. However, in different cell lines, different concentrations of DHT have been found to induce a variety of effects; either pro- or anti-inflammatory. In HUVEC cells, 10nM DHT decreased the endotoxin–induced adhesion molecule, cyclooxygenase-2, IL-6 and TLR4 expression [120]. Whereas higher concentration (400nM) were found to enhance the activation of NFκB due to its suppressing effect on NFκB inhibitory protein, which leads to an increase in the activity of vascular cell adhesion molecule-1promoter [121], thus acting as a pro-inflammatory agent.

3.2. Aims

- To investigate *in vitro* the biological consequences of palcar accumulation in prostate cancerous and non-cancerous cell lines, through investigating:
    - Palcar pro-inflammatory activity via the induction of IL-6 secretion.
    - The effect of palcar on changing membrane permeability assessed by measuring the induction of Ca^{2+} influx.
- To compare the effects of palcar and DHT on IL-6 secretion and Ca^{2+} influx.

3.3. Materials and methods

3.3.1. Cell-culturing techniques

3.3.1.1. Cell lines

Human epithelial cell line from normal post pubertal prostate (PNT1A) (Cat # 95012614), human prostate adenocarcinoma (PC3) (Cat # 90112714) and human Caucasian prostate carcinoma (LNCaP) (Cat # 89110211) cell lines were obtained from the European Collection of Cell Culture. The human Caucasian prostate adenocarcinoma (DU145) cell line was obtained from the American Type Culture Collection (Cat # HTB-

81). The benign hyperplastic prostatic epithelial (BPH-1) cell line was obtained from the German collection of microorganism and cell cultures (No. ACC 143, DSMZ, Germany).

3.3.1.2. Cells resuscitation

All cell-culture work was carried out in laminar flow biological safety cabinet using sterilised equipment and aseptic techniques. PC3, DU145, PNT1A and BPH-1 cells were suspended in fetal bovine serum (FBS, Cat # 10270, Life Technologies, UK) containing 20% dimethyl sulphoxide (DMSO; Cat # 276855, Sigma-Aldrich, UK) and kept in cryovials in liquid nitrogen at -80˚C. The cryovial was transferred to cell culture room in dry ice. A small piece of tissue paper sprayed with 70% ethanol was used to sterilize, partially opened and re-tightened the cryovial. These steps were carried out in the safety cabinet. The cryovial was placed in the water bath at 37˚C for approximately one minute to defrost the cells.

PNT1A, BPH-1 and LNCaP cells were routinely resuscitated and cultured in RPMI media (Cat # E15-885, PAA cell-culture Company, UK). DU145 and PC3 cells were cultured in EMEM (Cat # M2279, Sigma-Aldrich, UK) and HAMS (Cat # BE02-014F, Lonza Verviers sprl, UK) media, respectively. All media were supplemented with 10% FBS, 1% glutamine and 100 units/ml penicillin and streptomycin (Cat # 10378-016, Life Technologies, UK).

The cell suspension was mixed gently and centrifuged at 1500 rpm for 3 minutes to remove the DMSO. The cell pellet was re-suspended in the warmed FBS-supplemented media, seeded into T-25 flask and incubated at 37˚C and 5% CO_2. The medium was changed after 48 hours to remove the non-adherent cells and subsequently every two days until the cell growth reached 70-80% confluence and ready for sub-culturing. Figure 3.1 shows the cell morphology.

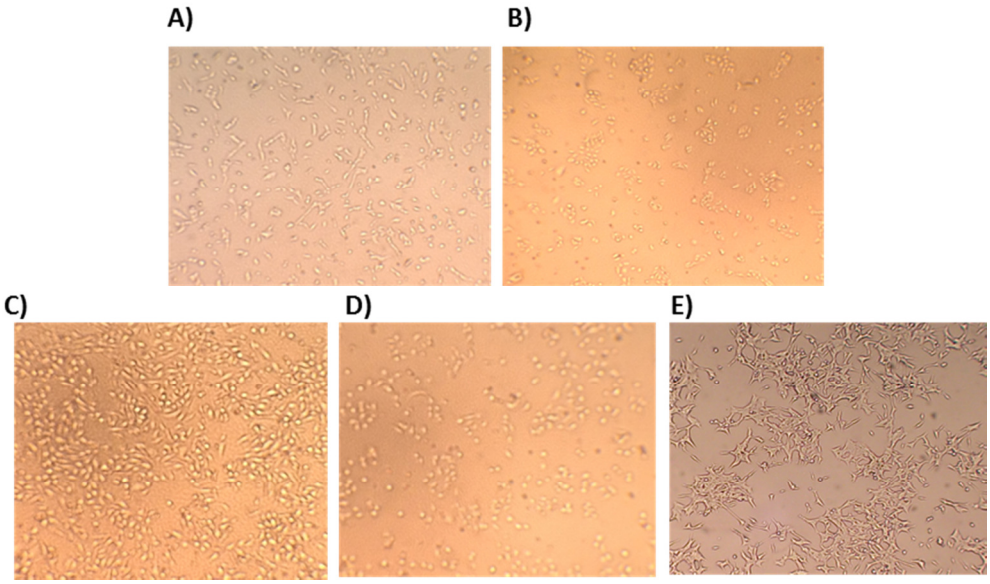

Figure 3.1: Cell morphology of prostate non-cancerous and cancerous cell lines. A) PNT1A, B) BPH-1, C) PC3, D) DU145 and E) LNCaP cells.

3.3.1.3. Cells sub-culturing

Cells were sub-cultured by removing the media followed by washing with 1x Dulbecco's Phosphate Buffered Saline (PBS; Cat # 14200059, Gibco, UK) twice. Then cells were trypsinized using 2ml of 0.05% EDTA trypsin (1x)/10cm (Cat # 25300054, Life Technologies, UK) at 37°C for 3 minutes. The cells were then collected using FBS-supplemented media. The cells suspension were seeded into 10cm dishes and incubated at 37˚C and 5% CO_2. The media was then changed every 48 hours and then after two days until the growth reached 70 – 80% confluence.

3.3.2. Viability assays

3.3.2.1. Water-soluble Tetrazolium (WST-1) viability assay

3.3.2.1.1. Background

The principle of water-soluble tetrazolium (WST-1) assay relies on measuring the intensity of the formazan dye formed by converting a tetrazolium salt, contained within the WST-1 reagent, by the mitochondrial dehydrogenase enzyme present in the cells. As the number of viable cells increases the activity of the mitochondrial dehydrogenase increases, therefore the intensity of the dye formed is directly proportional to the amount of mitochondrial dehydrogenase [122].

3.3.2.1.2. Measurement of cell viability using WST-1

A range of palcar concentrations (5, 10, 50 or 100µM) was selected to test their effect of cells viability. This range was selected based on the levels of plasma acylcarnitines reported under metabolic dysfunction [31, 103]. Palcar at 50µM was above the concentrations reported in human plasma, but within the range reported in ischemic heart of animal model [103], whereas 100µM was above the reported levels in human and animal models. However, both 50 and 100µM palcar have been previously investigated in cardiac sarcolemmal membrane under ischemic conditions [41, 123], which is another form of metabolic dysfunction that include a dysfunction of fatty acid metabolism, but were not investigated in human prostate cells. The effect of 50µM was compared to that of 100µM.

PNT1A and PC3 cells were seeded on 96-well culture plate. Once the cells reached 70% confluence, cells were treated with DMSO or 5, 10, 50 or 100µM palcar for 24hour at 37°C and 5%CO_2. Then, 10µl of cell proliferation reagent WST-1 (Cat # 11644807001, Roche, UK) was added to each treatment and incubated for 30 minutes at 37°C and 5% CO_2. The spectrophotometric absorbance, which corresponds to the cell metabolic activity or viability, was then measured at a wavelength of 450nm.

3.3.2.2. Trypan blue based viability assay

3.3.2.2.1. Background

Trypan blue is a dye used to measure cell viability based on the integrity of the cell membrane. Viable cells have an intact cell membrane and thus will exclude the dye and upon visual examination under microscope, cells will appear clear and non-stained as their cytoplasm is clear. Nonviable cells, lacking an intact membrane, will appear blue under microscopic examination as the dye is able to penetrate into the cytoplasm.

3.3.2.2.2. Measurement of cell viability using trypan blue

The PC3 cell suspension was collected and centrifuged at 1500rpm for 3 minutes at room temperature. The cell pellet was washed, re-suspended in media supplemented with 10% FBS and left for one hour at 37°C to recover from trypsin, then the suspension was seeded into 96 well plate. Palcar (50µM) was then added to the cell suspension and incubated for 5 minutes at 37°C. A volume of 50µl of cell suspension was transferred to a 1.5ml eppendorf tube containing 400µl media, supplemented with 10% FBS, and 50µl trypan blue (1:1 v/v). The mixture was mixed and incubated at room temperature for 2 minutes to allow the dye to penetrate the cells. During the 2 minutes incubation time, the

haemocytometer and the cover slip were prepared for cell. Both unstained (viable) and blue stained (non-viable) cells were counted. The percentage (%) of cell viability was calculated using the following equation.

$$The\ \%\ viability = \frac{Average\ number\ of\ unstained\ cells}{(Average\ number\ of\ unstained + average\ \ number\ of\ stained\ cells)} \times 100$$

3.3.3. Measuring IL-6 secretion using enzyme-linked immunosorbant assay (ELISA)

3.3.3.1. Background

The principle of using the enzyme-linked immune sorbent assay (ELISA) depends on the special binding between the proteins (antigens) of interest and the antibodies attached to a solid surface/support, where a solution of the antigen molecules to be assayed is added, so that the antigen binds to their specific antibody. Then, a second antibody is then added, which has an enzyme attached and specific for the antigen. Finally a substrate solution specific for the enzyme is added that produces a fluorescent compound on interaction with the enzyme. The intensity of the fluorescence is then measured, which gives a direct indication of the amount of antigen present in the sample.

3.3.3.2. Measurement of IL-6 secretion

PNT1A and PC3 cells were seeded in 24-well culture plate and once cell growth reached 70% confluence, they were treated with DMSO, palcar (5, 10, 50 and 100µM), lysophosphatidylcholine (LPC; 5, 10, 50 and 100µM) or DHT (1, 10, 100 and 1000nM) for 24 hours at 37°C and 5% CO_2. The media was then collected in labelled 1.5ml eppendorf tubes and stored at -20°C until analysis. IL-6 secretion was measured using the commercially available Human IL-6 Quantikine ELISA kit (Cat # D6050, R & D Systems, UK) following the manufacturer's protocol. Diagram 3.1 show the steps followed to measure IL-6 in the media.

Diagram 3.1: Steps of measuring IL-6 secretion using ELISA kit.

3.3.4. Measuring gene expression

3.3.4.1. Background

Measuring gene expression depends on using RNA extracted from the cells by disturbing the plasma membranes using highly denaturing buffer. This results in the inactivation of the other RNAs (mRNA, rRNA and tRNA) and ensures the purification of intact RNA. A homogenization step is applied in order to reduce the viscosity occurring as a result of the presence of genomic DNA and other high molecular weight cellular components. The mRNA is selectively separated using silica-based membrane present within a spin column in presence of ethanol and eluted using RNA free water.

3.3.4.2. Extraction of total RNA

PNT1A and PC3 cells were seeded in 6-well culture plate and once growth reached 70% confluence, the cells were treated with 5, 10, 50 or 100µM palcar and incubated for 24 hours at 37°C and 5% CO_2. Cell culture media were removed and cells were rinsed

twice with cold PBS (1x). Then, cells were collected using rubber scrappers and total RNA was extracted using RNeasy mini kit (Cat # 74104, Qiagen, UK) following the manufacturer's procedure (diagram 3.2). The extracted RNA was used as a template for measuring gene expression.

Diagram 3.2: RNA extraction using RNeasy mini kit

3.3.4.3. Determination of RNA quantity and quality using Nanodrop

The quantity and quality of RNA present in the cell sample was measured using UV absorbance as determined by RNA Nanodrop 1000 (Life Technologies, UK). The two wavelengths used is 260 and 280nm. An absorbance reading at 260nm reflects the quantity of RNA; an absorbance of one unit at 260nm corresponds to 40µg/ml RNA, while absorbance readings at 280nm are used to measure the amount of protein in the sample. The ratio of the readings at 260nm and 280nm provides an estimate of purity of RNA with respect to proteins, thus reflecting the quality of the RNA. Pure RNA has a ratio of 1.9 – 2.1. The ratio for All RNA samples used in the experiments needed for conducting the work in this thesis were within this ratio.

3.3.4.4. Quantification of gene expression of IL-6 using real-time reverse-transcription-polymerase chain reaction (RT-PCR)

IL-6 gene expression was measured by real time RT-PCR performed using an Applied Biosystems OneStep Plus real time RT-PCR system on an optical 96-well plate in a total volume of 20 µl/well, consisting of TaqMan 1-step RT-PCR master mix reagent kit (Applied Biosystems), 20 ng total RNA, and IL-6 primers and probes: IL-6 forward sequence 5'-CTCTTCAGAACGAATTGACAAACAAAT-3, 100µM, reverse sequence 5'-ATGTTACTCTTGTTACATGTCTTCTTTCTC-3, 100µM and probe 5' TACATCCTCGACGGCATCTCAGCCC-3', 100µM. All were designed and purchased from Eurofins, UK. Reverse transcription was performed for 30 minutes at 48°C, amplification Taq activation for 10 min at 95°C, followed by 40 PCR cycles of denaturation at 95°C for 15 seconds and annealing/extension at 60°C for 1 minute.

Reactions were carried out in triplicate and were normalized against an endogenous housekeeping gene, 18S ribosomal RNA. The 18S ribosomal RNA was quantified using 18S primers and probes: forward sequence 5'-GGCTCATTAAATCAGTTATGGTTCCT-3, 100µM, reverse sequence 5'-GTATTAGCTCTAGAATTACCACAGTTATCCA-3, 100µM, and probe 5'-TGGTCGCTCGCTCCTCTCCCAC-3, 100µM. All were designed and purchased from Sigma-Aldrich, UK.

The probes used in this study were labelled with a 5' reporter dye FAM (6-carboxyfluorescein) and a 3' quencher dye TAMRA (6-carboxytetramethylrhodamine).

The amount of mRNA and thus gene expression was quantified based on a standard curve method. Standard curves were produced for each set of primers and probes using 5, 10, 20, 40, and 80 ng total RNA/reaction.

3.3.5. Plate reader-based kinetic measurement of intracellular calcium levels using the fluorescent dye FURA-2AM

3.3.5.1. Background

Kinetic measurement of Ca^{2+} influx in response to various reagents used in this thesis was performed using a fluorescent plate reader; FLUROstar optima (Cat # NP-RFM-048, BMG labtech, UK), where Ca^{2+} influx was measured by monitoring fluorescence. This technique was chosen due to its availability and low cost. The fluorescence was measured by using FURA, which is a ratiometric dye that has two excitation wavelengths; 340nm, representing the Ca^{+2}–saturated FURA and 380nm,

representing the Ca^{+2}–free FURA [124, 125], thus allows the representation of the fluorescence as a ratio to reflect the amount of the Ca^{2+} in the cells [124]. It is used in the form of FURA-2AM, which is the acetoxymethyl ester of the fluorescent Ca^{2+} probe FURA. The presence of ester groups facilitates the movement of the dye through the cellular plasma membrane [126, 127]. Once applied to the cells, FURA-2AM can cross the cell membrane into the cytosol where the intracellular esterases cleave the ester group to release the polar FURA that is sensitive to Ca^{2+}. In this form it cannot re-cross the cell membrane and the carboxyl groups of the free FURA can bind with the Ca^{2+} to form the FURA-Ca^{2+} complex (figure 3.2A). The binding of Ca^{2+} to FURA results in a change in the wavelength and fluorescence intensity [125], excitation at 340nm increases the fluorescence emission detected at 510nm, while excitation at 380nm decreases the fluorescence emission detected at 510nm (figure 3.2B). The ratio of fluorescence therefore, can be used to indicate the intracellular Ca^{2+} concentration ($[Ca^{2+}]_i$).

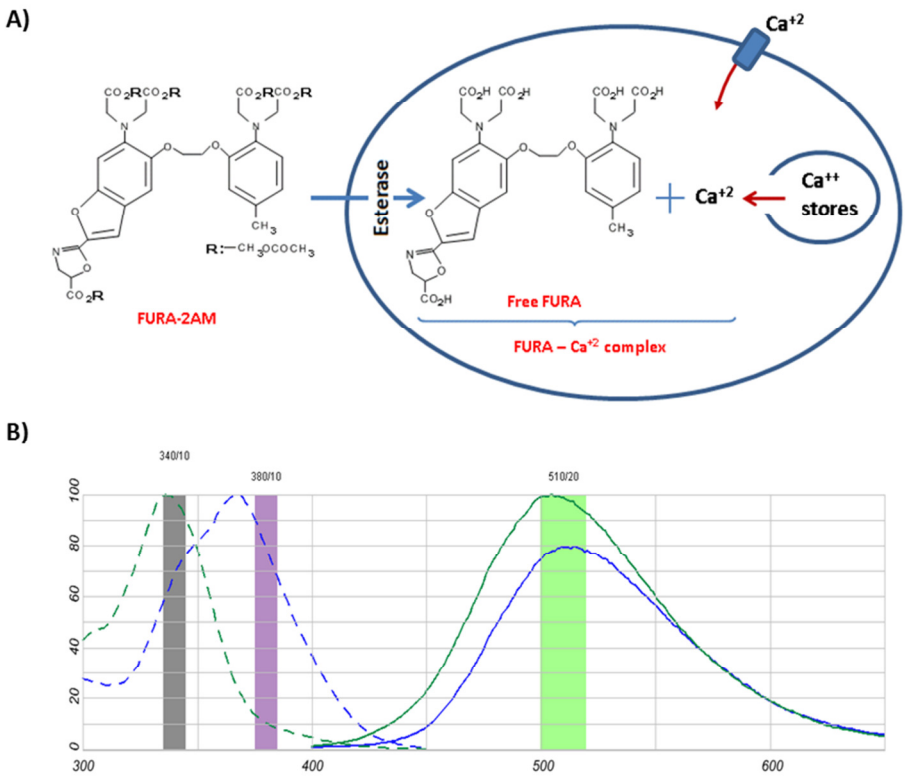

Figure 3.2: FURA-2AM as Ca^{2+} probe. A) Once FURA-2AM is loaded, cellular esterase cleaves the ester bonds to activate the FURA and become membrane impermeable. In this form it can binds the free Ca^{2+} to form FURA–Ca^{2+} complex. B) Fluorescence spectrum of FURA-2AM. Presence of Ca^{+2} increases fluorescence emission detected at 510nm (green line) when excited at 340nm (green dashed-line) and decreases fluorescence emission at 510nm (blue line) when excited at 380nm (blue dashed-line). (Source:http://www.invitrogen.com/site/us/en/home/support/Research-Tools/Fluorescence-SpectraViewer.html?fileId1=1200ca).

Ca^{2+} measurement was performed by detaching the cells first, then counting the cells, followed by loading the FURA to the cell suspension and finally measure Ca^{2+} influx. These steps are explained below.

3.3.5.2. Cells detaching

Under aseptic conditions the culture medium of the 70-80% confluent cells in the 10cm dishes were discarded and the cells were rinsed twice with 10ml of 1x PBS solution to remove the remaining culture medium. The cells were then incubated with 2ml 0.05% EDTA trypsin solution for 3 minutes at 37°C and 5% CO_2 incubator to detach the cells. Then, 10ml of culture medium supplemented with 10% FBS were added and the cell suspension was mixed gently using Gilson micropipette. The cell suspension was then transferred into a 50ml falcon tube and centrifuged at 1500 rpm for 3 minutes to remove the trypsin. The supernatant was discarded using vacosafe and the cell pellet was re-suspended using 10ml culture medium supplemented with 10ml FBS. The cell pellet was mixed gently using a pipette. The cells were then counted using the haemocytometer.

3.3.5.3. Loading FURA-2AM

Before performing the experiment, FURA-2AM (Cat # F0888, Sigma-Aldrich, UK) stock solution of 1mM was prepared in DMSO and away from light. This solution was kept under dark conditions and stored at -20°C. On the day of the experiment the stock solution was diluted in the media supplemented with 10% FBS to the required concentration.

Cells were detached and collected in 50ml falcon tube and centrifuged at 1500rpm for 3 minutes at room temperature. The cells pellet was washed and re-suspended using 10ml media supplemented with 10% FBS. The cell suspension was then left for 1hour in the incubator at 37°C and 5% CO_2 to recover from trypsin. An aliquot of this suspension was kept in 0.5ml eppendorf tube and was incubated at 37°C and 5% CO_2 to be used for blank measurement (cells with no FURA). The tube of the cells suspension was wrapped with aluminium foil then loaded with 250nM of FURA-2AM. This was performed in the dark. The cell suspension was then incubated for 30 minutes at 37°C and 5% CO_2. The cells suspension was mixed three times during the incubation period. Then, the cell suspension was centrifuged at 1500rpm for 3 minutes at room temperature to remove the excess FURA and the supernatant was discarded using the vacosafe. The cell pellet was washed and re-suspended in media supplemented with 10% FBS. The volume of media used was equal to the volume that is needed to obtain the required cell number ($1x10^6$ cells/ml). A volume of 100µl of cell suspension was then seeded in black 96-well culture

plate with clear bottom and were placed in the fluorescence plate reader to measure Ca^{+2} influx.

3.3.5.4. Preparing stock and work solutions of histamine, palcar and DHT for measuring Ca^{2+} influx

A stock solution of 27mM palcar (Cat # P4509, Sigma-Aldrich, UK) was prepared in DMSO. This stock solution was kept in a water bath at 37°C for 5 minutes. The stock solution of 100mM histamine (Cat # H7125-1G, Sigma-Aldrich, UK), the positive control, was prepared in de-ionized water. The DHT (Cat # 31573-100MG, Sigma-Aldrich, UK) stock solution of 3.44mM was prepared in DMSO. All stock solutions were prepared under aseptic conditions and at the end of each experiment; these solutions were stored at -20°C. The exception to this was the histamine stock solution, which was freshly prepared for every experiment of Ca^{2+} measurement since it is light and air sensitive.

Working solutions of DMSO (control), histamine (500µM), palcar (500µM) and DHT (10µM) were prepared in media supplemented with 10% FBS and placed in the reagent box of the plate reader to be used for priming the pumps and injecting the volume required to reach the final concentration into the cell suspension.

The plate reader is equipped with two pumps to be filled with work solutions and to be used for sample injection. The culture plate was placed in the fluorescence plate reader. In the OPTIMA software, the “fluorescence intensity” and “well mode” were selected. The protocol for measuring Ca^{+2} influx was set by determining the parameters in the “basic parameter”, the “Layout”, “Concentration/Volume/Shaking” and “Multichromatic” windows as shown in figure 3.3.

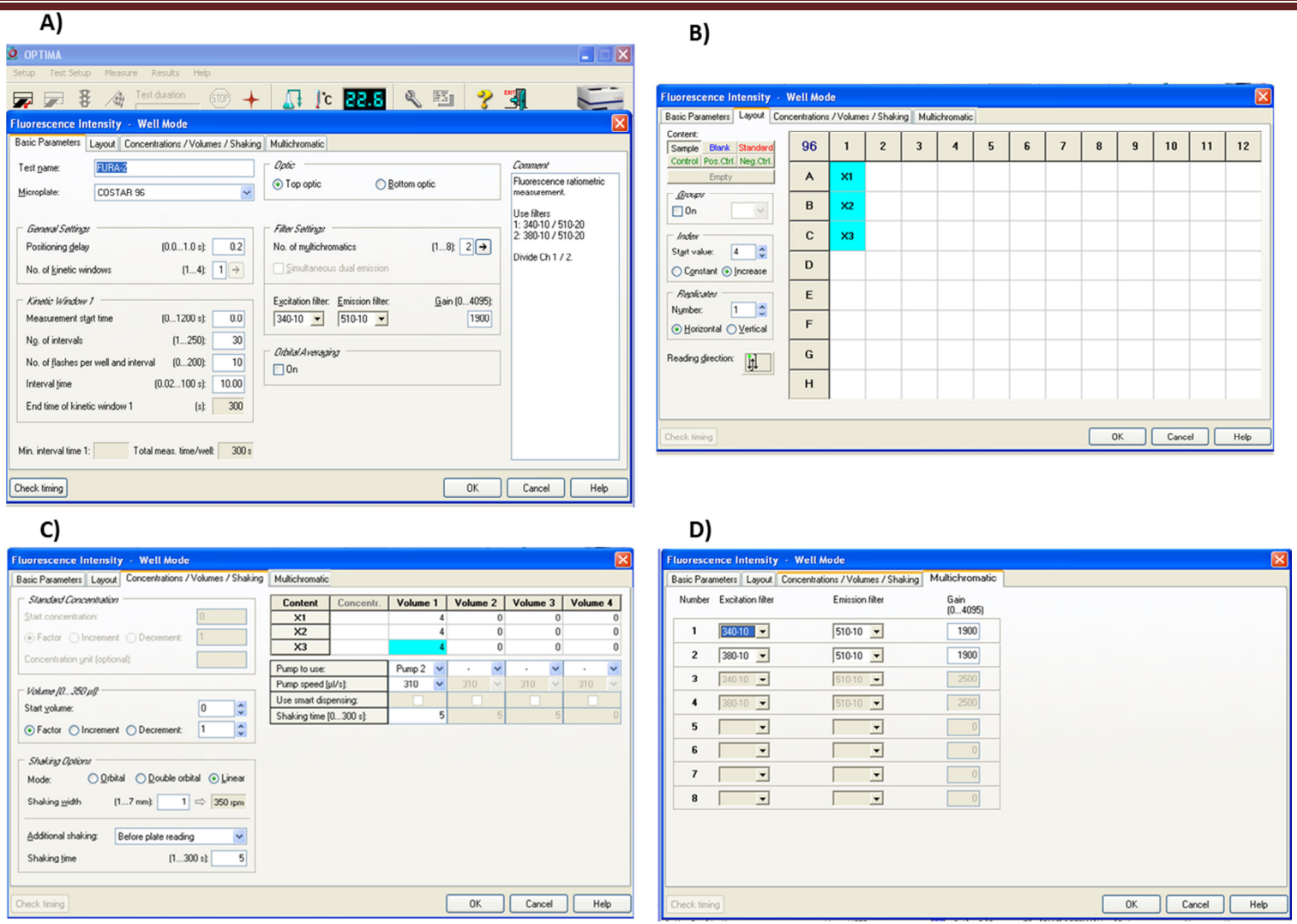

Figure 3.3: The "Fluorescence Intensity – Well mode" window of the OPTIMA software. In the figure is an example on preparing three samples. A) The basic parameters were determined as shown in A. B) The layout (position) of samples were selected. C) The volume of injection and the pump containing the treatment solution were determined (for example 4µl from pump 2). D) The multichromatic window, in which the gain and the filters for excitation and emission were determined. These windows are illustrated and explained in the manual of the FLUROstar optima plate reader.

Ca^{2+} influx in response to DMSO (control), histamine, palcar and DHT was measured by injecting the required illustrated in Table 3.1.

Table 3.1: Injection volumes needed from the work solutions.

Name	Concentration of work solution	Concentration required in wells	Injection volume form work solution
DMSO (control)			4µl
Histamine	500 µM	10 µM	2µl
		20 µM	4µl
Palcar	500 µM	5 µM	1µl
		10 µM	2µl
		20 µM	4µl
		50 µM	10µl
DHT	10µM	0.1µM	1µl
		1µM	10µl

Once control measurements were completed, the pump was washed with MilliQ water, then with 70% ethanol followed by MilliQ water again. The pump was then primed with the palcar working solution and Ca^{+2} measurements were performed as mentioned above. The washing step was repeated once palcar readings were completed. This process of washing was repeated when DHT was used.

3.3.6. Measuring Ca^{2+} influx

PNT1A, BPH-1, DU145 and PC3 cells were seeded in 10cm dishes and once growth had reached 70% confluence, cells were harvested, collected, counted as described earlier and used for the measurement of Ca^{2+} influx. The method of Ca^{2+} influx was developed using histamine as a positive control since it has been shown that it increased the $[Ca^{2+}]_i$ in PC3 cells [128, 129]. Cell suspensions were then loaded with 250nM FURA-2AM for 30 minutes at 37°C and excited at two wavelengths: 340nm and 380nm. Cells were injected with either DMSO, histamine (10 or 20µM), or palcar (5, 10, 20 or 50µM) after 50 seconds of the start of Ca^{2+} measurement. Following method optimisation, 2.5µM FURA for 45 minutes was chosen to measure Ca^{2+} influx in response to DHT (0.1and 1µM) as described in details above. The emission at 510nm was measured every 10 seconds for 5 minutes and the ratio of fluorescence was used to indicate the $[Ca^{2+}]_i$.

3.3.7. Statistical analysis

Cell growth in response to each palcar treatment in both PNT1A and PC3 cells was represented as the means ± SD of six biological replicates of one experiment. The levels of IL-6 secretion were represented as the means ± SD of three biological replicates of one experiment. To compare between the means of the different treatments within cell line, statistical analysis was performed with a one-way ANOVA followed by Bonferroni's multiple comparison post-test. To compare between the means of each treatment between two cell lines, statistical analysis was performed with two ways ANOVA followed by Bonferroni's multiple comparison post-test.

The findings of IL-6 gene expression were obtained from one experiment conducted in three biological replicates with three technical replicates each. The levels of IL-6 gene expression represent means ± SD of the three biological replicates of one experiment. In order to compare the fold change of IL-6 gene expression between the PNT1A and PC3 cells, statistical analysis were performed with a two way ANOVA followed by Bonferroni's multiple comparison post-test. To compare the fold change of IL-6 gene expression between each treatment within cell line, a one way ANOVA followed by Bonferroni's multiple comparison post-test was performed.

All statistical analyses above were performed using GraphPad Prism version 5.00 for Windows (GraphPad Software, San Diego California USA, www.graphpad.com).

The results of the kinetic measurement of Ca^{2+} influx represent the mean of three independent experiments. In order to compare between the effects of different treatments on kinetic Ca^{2+} influx in each cell line, statistical analysis were performed with mixed effect model using GenStat software 16th Edition.

The corrected ratio of fluorescence in each cell line in response to DHT injection were analysed with a one way ANOVA followed by Bonferroni's multiple comparison post-test using GraphPad Prism version 5.00 for Windows (GraphPad Software, San Diego California USA, www.graphpad.com).

3.4. Results

3.4.1. Cell viability in response to palcar in PNT1A and PC3 cells

The effect of palcar on the viability of both PNT1A and PC3 cells was tested prior to starting the investigation of palcar effect on IL-6 secretion and Ca^{2+} influx. Cell viability was examined using the WST-1 viability assay. Both cell lines were treated with

DMSO and palcar (5, 10, 50 and 100µM) for 24 hours at 37°C and 5% CO_2. Treatment with palcar (5–100µM) was not associated with any toxic effect in PNT1A cells compared with DMSO-treated cells (control) (P>0.05). However, high concentrations of palcar (50 and 100µM) were associated with a significant decrease in the viability of PC3 cells compared with the control (P≤0.05 and P≤0.01) and PNT1A cells (P≤0.05 and P≤0.01) (figure 3.4). However upon visual inspection, cells treated with palcar (50 and 100µM) were observed to cover the growth area of wells, and that the cells morphology and number of floating cells were the same as the cells treated with the DMSO (control).

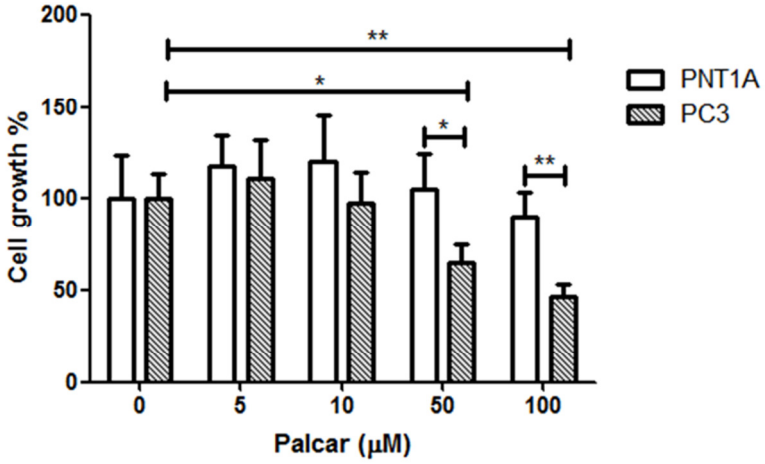

Figure 3.4: Viability assay in PNT1A and PC3 cells. Cells were seeded in 96-well plate and treated with DMSO (control), palcar (5, 10, 50 or 100µM) for 24 hours at 37°C and 5% CO_2. WST-1 reagent (10µl) was added and incubated for 30 minutes at 37°C and 5% CO_2. The absorbance was measured at 450nm. Palcar (50 and 100µM) significantly reduced the viability of PC3 cells compared to the control and PNT1A cells. Results represent means ± SD of six biological replicates of one experiment. Statistical analysis between PNT1A and PC3 cells were performed using a two way ANOVA followed by Bonferroni's multiple comparison post-test, and between each treatment in one cell line using a one way ANOVA followed by Tukey's multiple comparison post-test, *P≤0.05 and **P≤0.01.

3.4.2. Effect of palcar on IL-6

To assess the potential pro-inflammatory property of palcar in PNT1A and PC3 cells, the secretion of IL-6 was measured in response to treatments with 10, 50 and 100µM palcar for 24 hours. After 24 hours exposure of palcar, only high concentrations (50 and 100µM) were able to induce a significant increase in IL-6 secretion in PC3 cells

compared to the control (P≤0.01). Palcar treatment was not associated with any pro-inflammatory responses in the non-cancerous PNT1A cells (figure 3.5).

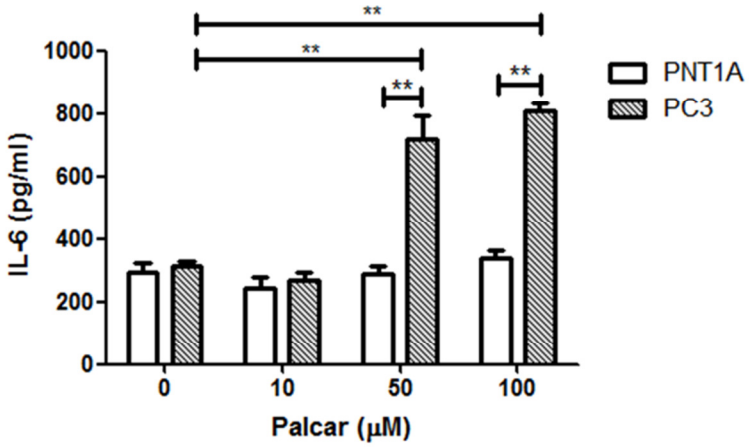

Figure 3.5: IL-6 secretion in PNT1A and PC3 cells in response to palcar. Cells were treated with DMSO or palcar (10, 50 and 100 µM) for 24 hours at 37°C and 5% CO_2. Culture medium was collected and IL-6 was measured using human IL-6 ELISA kit. Results represent means ± SD of three biological replicates. Palcar (50 and 100µM) induced a significant increase in IL-6 secretion in PC3 cells compared to control and PNT1A cells. Results represent means ± SD of three biological replicates of one experiment. Statistical analysis between PNT1A and PC3 cells were performed using a two way ANOVA followed by Bonferroni's multiple comparison post-test, and between each treatment in one cell line using a one way ANOVA followed by Bonferroni's multiple comparison post-test, **P≤0.01.

The reasons for the high levels of IL-6 secretions at high concentrations were either due to palcar induced gene expression of IL-6 or a palcar detergent effect on the cell membrane, in which it lyses the membrane causing the leakage of the cellular IL-6 into the media. Therefore, the gene expression of IL-6 in response to 24 hours treatment with palcar was investigated. Figure 3.6 represent palcar-induced IL-6 gene expression normalised to 18S. In PNT1A cells, 50 and 100µM palcar induced a significant two-fold increase in the IL-6 gene expression compared to the control (P≤0.001 and P≤0.01, respectively), but in PC3 cells, 50 and 100µM palcar induced a significant four-fold and six-fold increase in gene expression, respectively (P≤0.001; figure 3.6). This suggests that palcar was able to induce a pro-inflammatory response in PC3 cells as well as causing a modest increase in IL-6 gene levels in PNT1A cells. The results suggested that palcar at these concentrations was not associated with detergent effect on the cell-membrane of both PNT1A and PC3 cells.

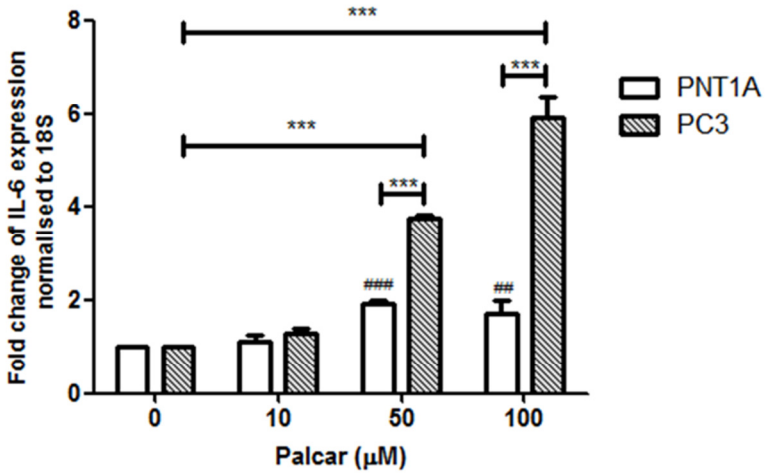

Figure 3.6: IL-6 gene expression in PNT1A and PC3 cells in response to palcar. Cells were treated with DMSO or palcar (10, 50 and 100 µM) for 24 hours at 37°C and 5% CO_2. Cells were collected and total RNA was extracted using the RNeasy kit. IL-6 Gene expression was quantified using real time RT-PCR. The expression of the housekeeping 18S gene was used for normalisation of the gene expression. Palcar (50 and 100µM) induced an increase in the fold change of IL-6 gene expression in both PNT1A and PC3 cells compared to the control. Results represent means ± SD of three biological replicates of one experiment. Statistical analysis between PNT1A and PC3 cells were performed using a two way ANOVA followed by Bonferroni's multiple comparison post-test, and between each treatment in one cell line using a one way ANOVA followed by Bonferroni's multiple comparison post-test, ***P<0.001 and $^{\#\#}$P<0.01, $^{\#\#\#}$P<0.001 versus control.

The effect of palcar on inducing IL-6 secretion in PC3 cells was compared with LPC, another lipid related compound derived from phosphatidylcholine and exhibiting an amphiphilic properties similar to that of palcar. In this experiment, cells were treated with LPC for 24 hours and the secretion of IL-6 was measured in PC3 cells. Figure 3.7 shows the levels of both LPC and palcar-induced IL-6 secretion (pg/ml). After 24 hours exposure to LPC and palcar, high concentrations of LPC (50 and 100µM) significantly reduced the secretion of IL-6 compared to the control (P<0.001). The observed effect of LPC was opposite to that of the effect of palcar in PC3 cells.

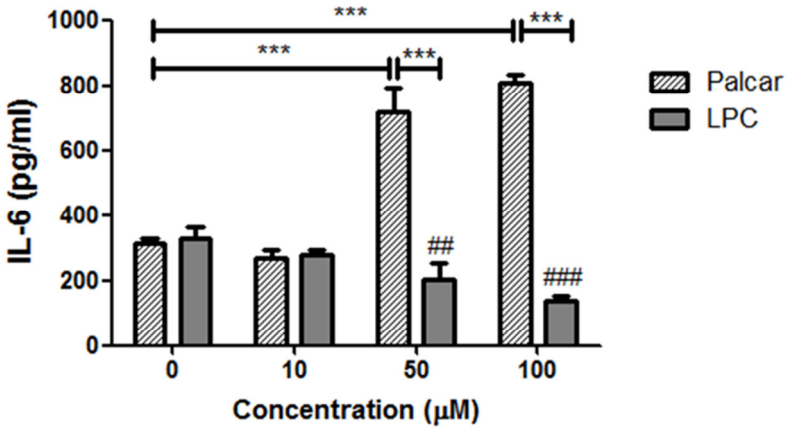

Figure 3.7: IL-6 secretion in response to palcar and LPC in PC3 cells. Cells were treated with DMSO, palcar (10, 50 or 100µM) or LPC (10, 50 or 100µM) for 24 hours at 37°C and 5% CO_2. Culture medium was collected, and IL-6 was measured using human IL-6 ELISA kit. Palcar (50 and 100µM) induced a significant increase in IL-6 secretion in PC3 cells in contrast to LPC (50 and 100µM), which significantly decreased the IL-6 secretion compared to control. Results represent means ± SD of three biological replicates of one experiment. Statistical analysis between palcar and LPC were performed using a two way ANOVA followed by Bonferroni's multiple comparison post-test, and within each palcar and LPC treatments using a one way ANOVA followed by Bonferroni's multiple comparison post-test, ***P<0.001, and $^{\#\#}$P<0.01, $^{\#\#\#}$P<0.001 versus control.

Since palcar is a lipid intermediate in fat oxidation, its effect on inducing IL-6 secretion was compared to that of DHT, which is a lipid-related hormone. Therefore both PNT1A and PC3 cells were treated with palcar and DHT for 24 hours and the IL-6 secretion was measured. The concentration range of DHT investigated in this study covered the physiologically relevant levels, 1 – 10nM [130]. Figure 3.8 showed that DHT treatment was not associated with IL-6 secretion in both PNT1A and PC3 cells contrary to the effect of palcar.

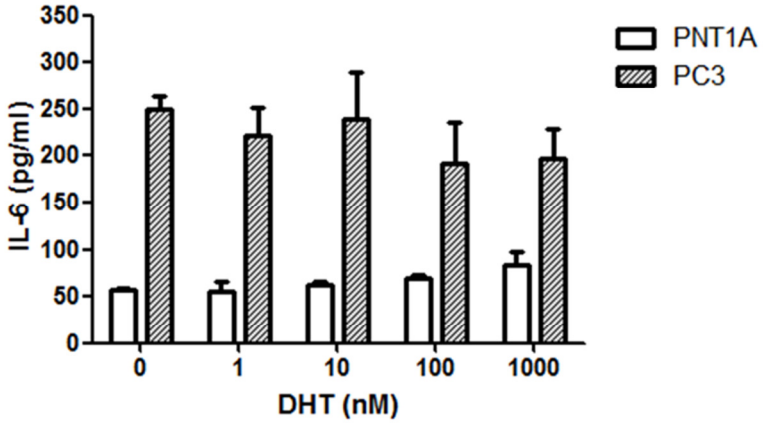

Figure 3.8: IL-6 secretion in PNT1A and PC3 cells in response to DHT. Cells were treated with DMSO or DHT (1, 10, 100 or 1000µM) for 24 hours at 37°C and 5% CO_2. Culture medium was collected, and IL-6 was measured using human IL-6 ELISA kit. DHT is not associated with any pro-inflammatory responses in either PC3 or PNT1A cells. Results represent means ± SD of three biological replicates of one experiment. Statistical analysis between PNT1A and PC3 cells were performed using a two way ANOVA followed by Bonferroni's multiple comparison post-test, and between each treatment in one cell line using a one way ANOVA followed by Bonferroni's multiple comparison post-test.

3.4.3. Ca^{2+} influx in prostate cell lines

3.4.3.1. Trypan blue viability assay

The effect of palcar on Ca^{2+} influx was measured for a 5 minute period. Since treatment with 50µM palcar for 24hour decreased the viability of PC3 cells to approximately 65%, the effect of this concentration of palcar on cell membrane integrity was investigated using the trypan blue viability assay. The Trypan blue assay was selected because it allows mimicking the experimental procedure of measuring the Ca^{2+} influx for 5 minutes, therefore testing whether palcar has an effect on cell membrane integrity during Ca^{2+} measurement.

The results indicate that palcar treatment for 5 minutes has no lethal effect on PC3 cells. The calculated viability percentage for 50µM palcar was very close to that of the control, which was approximately 78% and 80%, respectively. The 78% viable cells was an average of three replicates, which was consisting of 78%, 77% and 80% viable cells. These numbers were close to the counting of the viable cells in the control, which were 80%, 82% and 84%.

However, these values are considered low for a viability test and this could be attributed to the procedure of measuring Ca^{2+} influx, where the cells needed to be in a suspension state for one hour in the incubator (37°C and 5% CO_2). Figure 3.9 show the results of the trypan blue in response to 50µM palcar and DMSO; where the bright cells represent the viable cells and the blue stained cells represent the non-viable cells. The actual count of the cells present in these figures were higher than what it was shown in the figure 3.9, because the microscope used for this count has an extra magnification lens on the camera attached to it, which produce a photo taken from a section of the haemocytometer square where the count was performed and could not cover the whole area of the counting square (which consist of 16 smaller squares). This produces a photo that is more magnified compared with the other photos taken by other light microscopes using the same magnification lens.

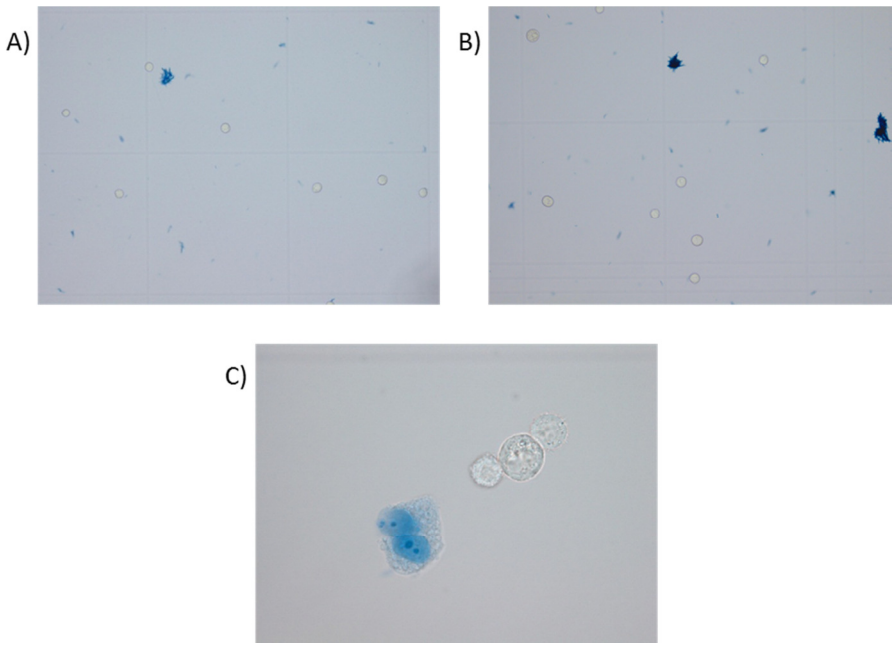

Figure 3.9: Trypan blue viability test in PC3 cells suspension. Cells were treated for 5 minutes with A) DMSO (x10) or B) 50µM palcar (x10). Bright and blue stained cells represent the viable and the non-viable cells, respectively. C) Higher magnification at the viable and the non-viable cells (x40). The photos are representative of three replicates.

3.4.3.2. Ca^{2+} influx in non-cancerous cell lines

3.4.3.2.1. Histamine effect on Ca^{2+} influx

In this experiment histamine was used as a positive control and therefore, the effect of palcar on Ca^{2+} influx was compared to the effect of histamine on both PNT1A and BPH-1 cells. In PNT1A cells, at the baseline and before injection with histamine the

fluorescence values of Ca^{2+}–saturated FURA (red line, figure 3.10) was less than that of the Ca^{2+}–free FURA (blue line, figure 3.10) indicating that there was no Ca^{2+} induced. Injection of 20µM histamine increased the fluorescence values of Ca^{2+}–saturated FURA with a concurrent decrease in the fluorescence values of Ca^{2+}–free FURA (figure 3.10A). This was also observed in BPH-1 cells (figure 3.10B), which suggest that histamine was able to induce Ca^{2+} influx and increase the cellular content of Ca^{2+}. This would suggest that Ca^{2+} bound with the FURA inside the cells leading to an increase in the levels of Ca^{2+}–saturated FURA, which in turn decreased the levels of Ca^{2+}–free FURA. The effects of histamine was represented by the rapid increase in the calculated fluorescence ratio that indicate $[Ca^{2+}]_i$. These results prove the validity of the protocol followed to measure palcar-induced Ca^{2+} influx.

3.4.3.2.2. Palcar effect on Ca^{2+} influx

In PNT1A and BPH-1 cells, injection of palcar after 50 seconds of the start of Ca^{2+} measurement, did not have any effect on Ca^{2+} influx. In figure 3.11A the fluorescence values in response to 50µM palcar injection in PNT1A cells shows that the fluorescence values of Ca^{2+}–free FURA are higher than the values of Ca^{2+}–saturated FURA before and after injection, suggesting that there was no Ca^{2+} induced to bind to the free FURA and become Ca^{2+}–saturated. This was reflected in the constant values of fluorescence ratios, which are similar to the ratios at the baseline. These results indicate that palcar injection was not able to induce any Ca^{2+} influx that could bind to the FURA inside the cells and increase the fluorescence levels of the Ca^{2+}–saturated FURA, therefore no increase in the fluorescence ratio was observed (figure 3.11A).

BPH-1 cells behaved in the same manner as the PNT1A cells in response to palcar, where palcar was not associated with any change in the ratio of fluorescence indicating no Ca^{2+} influx. Figure 3.11B shows the fluorescence values and ratios in BPH-1 cells after injection with 50µM palcar.

In PNT1A and BPH-1 cells, injection with different concentrations of palcar (5, 10, 20 and 50µM) was not associated with any change in the fluorescence values, unlike the Ca^{2+} influx in response to histamine, which showed a trend towards inducing a dose–dependent increase in Ca^{2+} influx (figure 3.12).

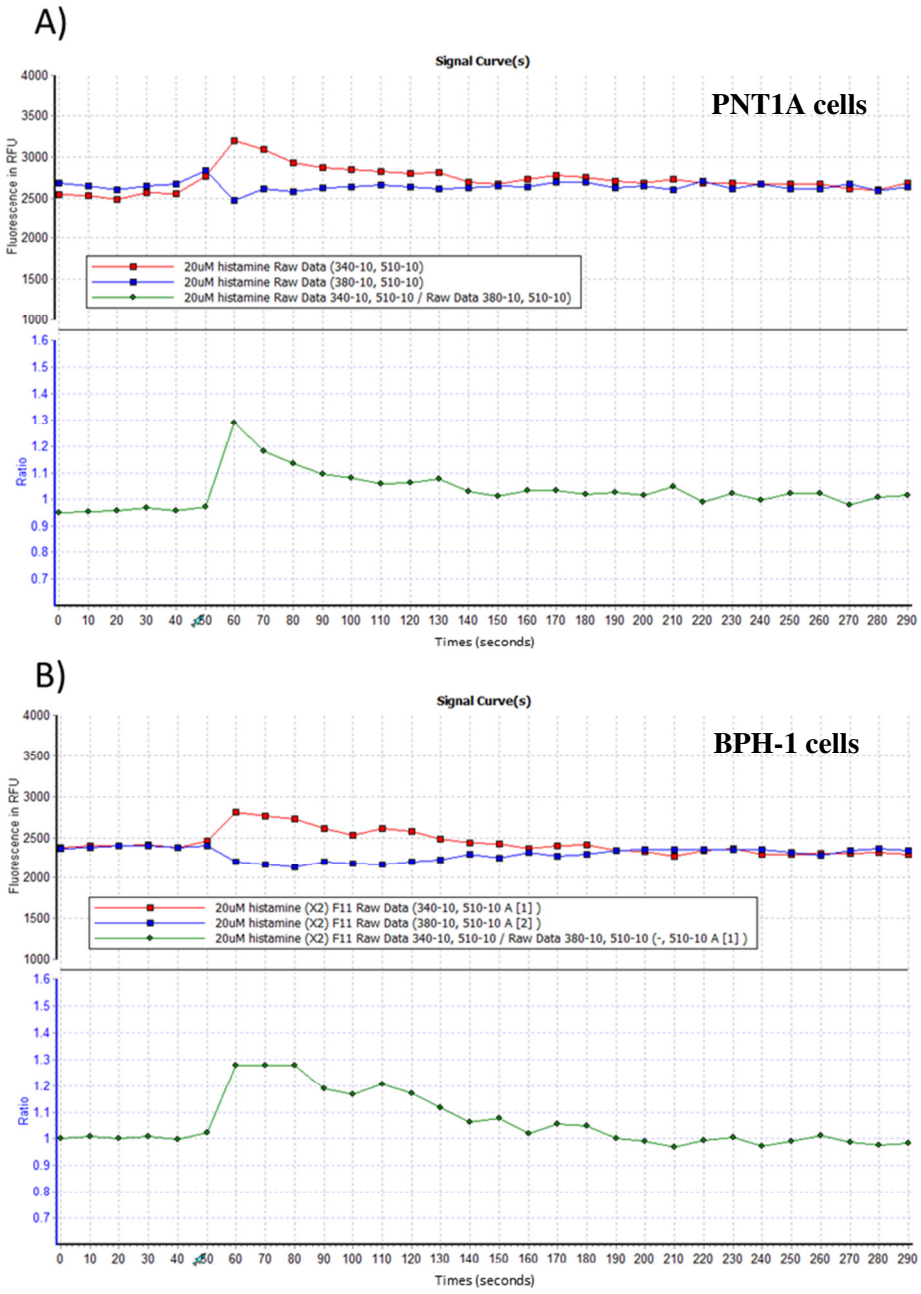

Figure 3.10: Representative fluorescence values in PNT1A and BPH-1 cells in response to histamine. FURA-loaded cells were excited at both 340nm (**red** line) & 380nm (**blue** line) and emission was detected at 510nm. Cells were injected with 20µM histamine after 50 seconds of the start of Ca^{2+} measurement. The increased ratio of fluorescence (**green** line) immediately following histamine injection in A) PNT1A and B) BPH-1 cells is indicative of Ca^{2+} influx.

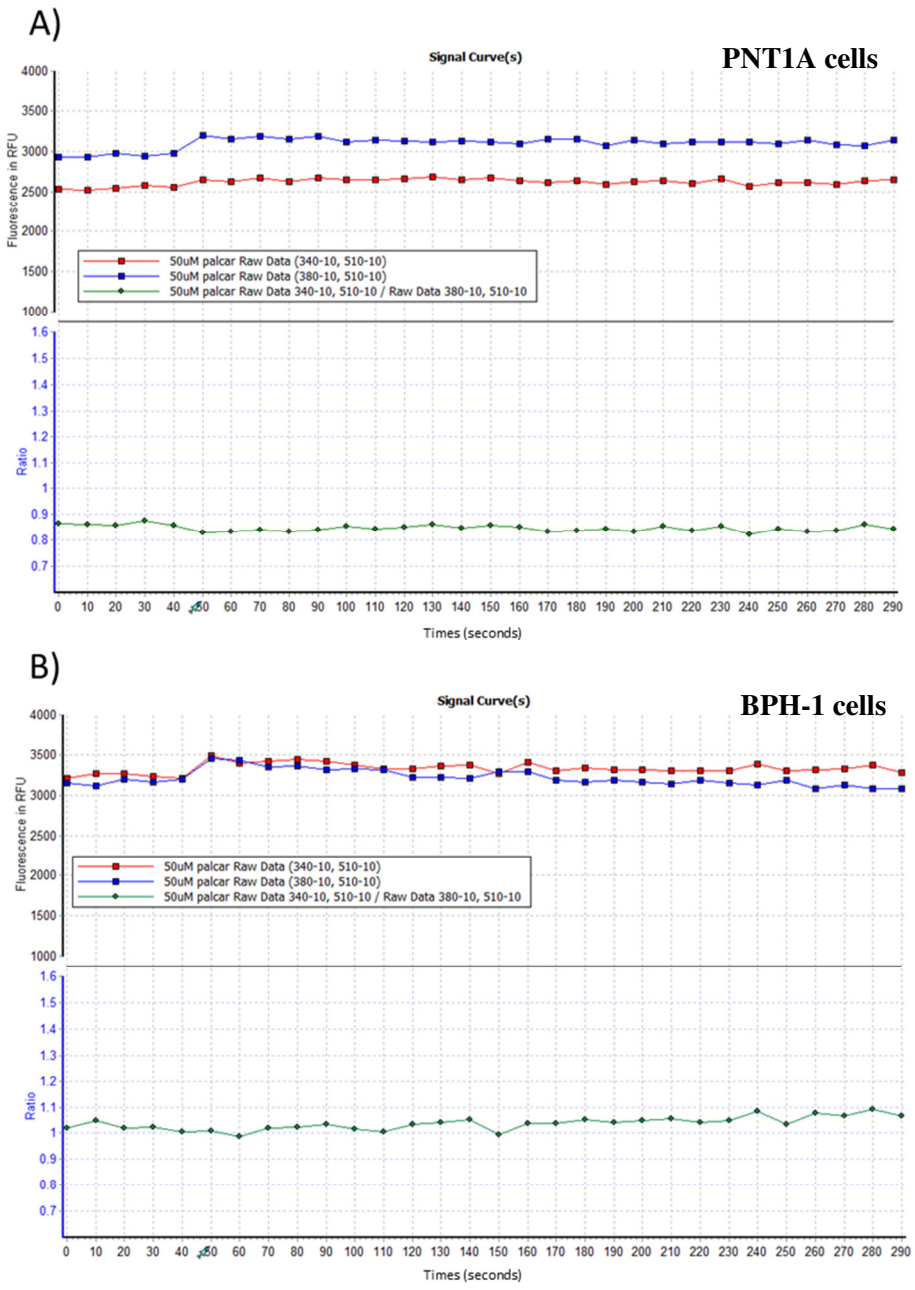

Figure 3.11: Representative fluorescence values in PNT1A and BPH-1 cells in response to palcar. FURA-loaded cells were excited at both 340nm (**red** line) & 380nm (**blue** line) and emission was detected at 510nm. Cells were injected with 50µM palcar after 50 seconds of the start of Ca^{2+} measurement. The unchanged ratio of fluorescence (**green** line) after DHT injection in A) PNT1A and B) BPH-1 cells is indicative of no Ca^{2+} influx.

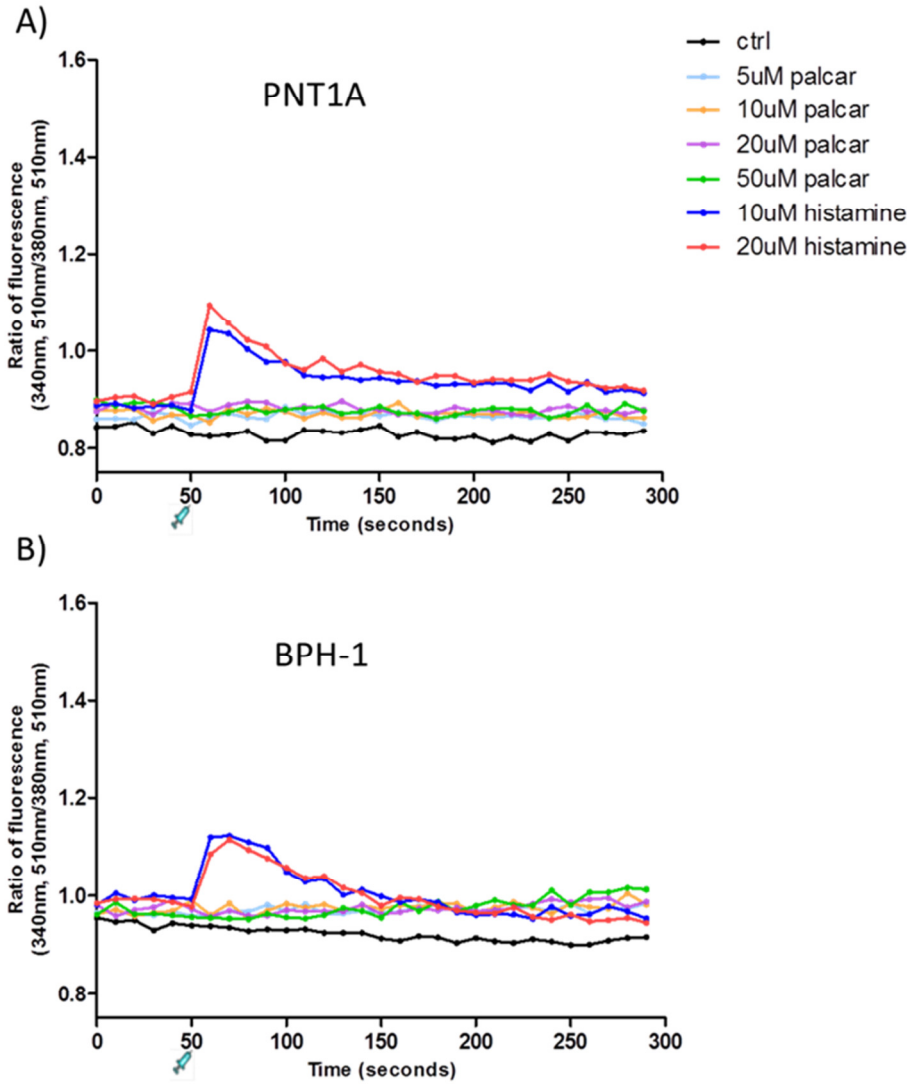

Figure 3.12: Ca^{2+} influx in PNT1A and BPH-1 cells in response to palcar and histamine. FURA (250nM)-loaded cells were injected with DMSO (control), histamine (10 or 20µM) or palcar (5, 10, 20 or 50µM) at 50 seconds. The ratio of fluorescence emission (510nm), excited at both 340nm & 380nm, indicated the $[Ca^{2+}]_i$. In PNT1A and BPH-1 cells, ratio of fluorescence after palcar (5, 10, 20 or 50µM) injection was not significantly different from the control (P = 0.110, 0.521, respectively), whereas it was significantly different after histamine (10 and 20µM) injection ($P \leq 0.001$ and $P \leq 0.05$, respectively). There were no significant differences between 10 and 20µM histamine on Ca^{2+} influx (P = 0.323 and 0.892, respectively). Data are means of three independent experiments. The statistical analysis was performed with mixed effect model test using the Genstat software.

3.4.3.2.3. DHT effect on Ca^{2+} influx

The unresponsiveness of both PNT1A and BPH-1 cells to palcar in terms of Ca^{2+} influx was compared to that in response to DHT, a hormone important for prostate growth and associated with the prostate cancer progression. This comparison was made to investigate whether DHT induced the same effect as palcar.

In both PNT1A and BPH-1 cells the fluorescence values of the Ca^{2+}–saturated FURA were elevated before injection. This is attributed to the procedure of measuring Ca^{2+} influx that require the cells in one well of the culture plate to be injected with the treatment followed by measuring Ca^{2+} influx for a duration of 5 minutes. Then this was repeated for the next treatment in the cells in the next well. During this time the levels of Ca^{2+} are subjected to a continuous change as they are dynamic ions that move into and out of the cells. Upon entry into the cells, Ca^{2+} may bind to the FURA leading to an increase in the levels of the Ca^{2+}–saturated FURA before injection. Having the levels of Ca^{2+}–saturated FURA higher than the levels of Ca^{2+}–free FURA leads to the high fluorescence ratio observed at the baseline levels (figure 3.13A). Although the fluorescence value of the Ca^{2+}–saturated FURA was high before injection, the calculated fluorescence ratios after 1µM DHT injection were the same as the values of the baseline levels, suggesting that DHT was not able to induce Ca^{2+} influx.

This was also true in BPH-1 cells, where injection of DHT did not lead to an increase in the calculated ratio of fluorescence (figure 3.13B). Therefore, these results suggest that 1µM DHT had no effect on PNT1A and BPH-1 cells, a similar effect to palcar.

Figure 3.14 showed the fluorescence ratios of both PNT1A and BPH-1 in response to different concentrations of DHT (0.1 and 1µM) in comparison to histamine. In this experiment, only one concentration of histamine (20µM) was investigated due to the observed increase in the levels of baseline. Because of this increase, the ratio of fluorescence was corrected to the baseline levels of each injection and was compared. The corrected ratio of fluorescence after DHT injection was not significantly different from that of the control ($P>0.05$) and that the increase in Ca^{2+} influx induced by histamine was significantly different from the control ($P<0.001$) (figure 3.14C).

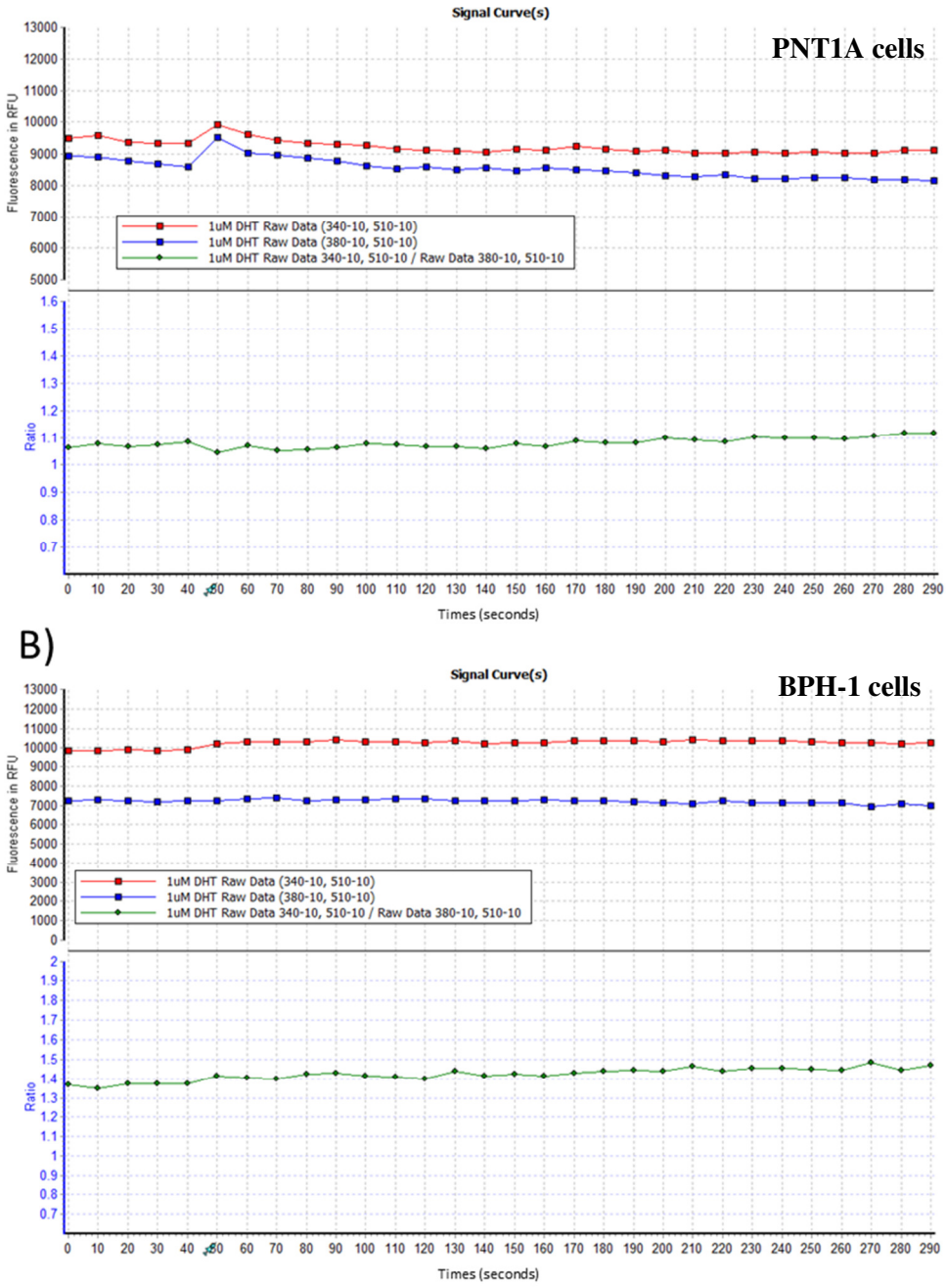

Figure 3.13: Representative fluorescence values in PNT1A and BPH-1 cells in response to DHT. FURA-loaded cells were excited at both 340nm (**red** line) & 380nm (**blue** line) and emission was detected at 510nm. Cells were injected with 1µM DHT after 50 seconds of the start of Ca^{2+} measurement. The unchanged ratio of fluorescence (**green** line) after DHT injection in A) PNT1A and B) BPH-1 cells is indicative of no Ca^{2+} influx.

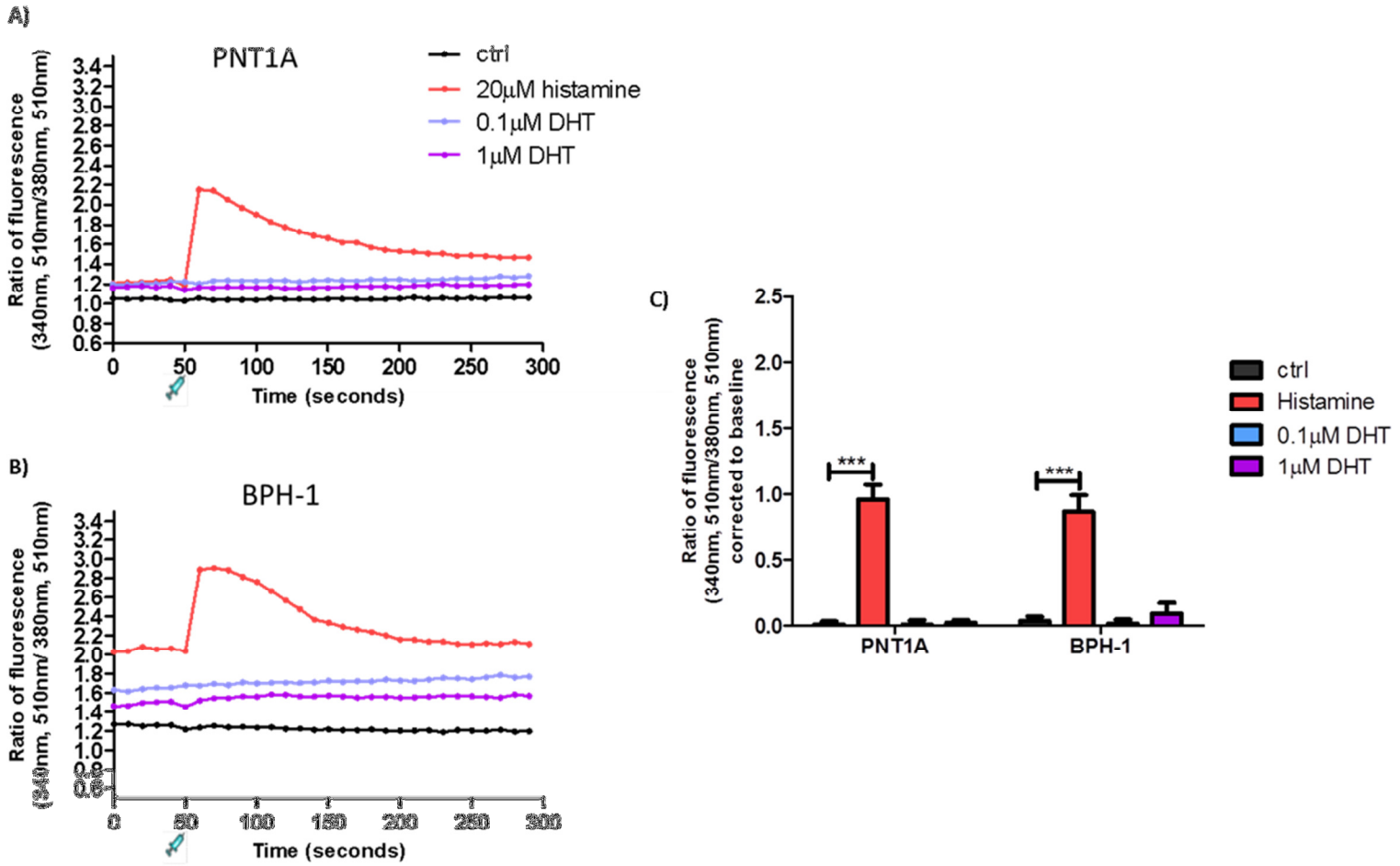

Figure 3.14: Ca^{2+} influx in PNT1A and BPH-1cells in response to DHT. FURA-loaded PNT1A (A) and BPH-1 (B) cells were injected with DMSO (control), 20μM histamine or DHT (0.1 or 1μM) at 50 seconds of the start of the Ca^{2+} measurement. The ratio of fluorescence emission (510nm), excited at both 340nm & 380 nm, indicated the $[Ca^{2+}]_i$. DHT (0.1 or 1μM) did not induce Ca^{2+} influx in PNT1A and BPH-1; Ca^{2+} influx was not significantly different to the control (C). Data represent means ± SD of three independent experiments. Statistical analysis was performed using two ways ANOVA followed by Bonferroni's post-test in each cell line.

3.4.3.3. Ca^{2+} influx in cancerous cell lines

3.4.3.3.1. Histamine effect on Ca^{2+} influx

As histamine was shown to induce Ca^{2+} in both PNT1A and BPH-1 cells, the effect of histamine on Ca^{2+} influx in DU145 and PC3 cells were investigated to assess the effect of palcar in the prostate cancerous cells. In DU145 and PC3 cells, there was no change in the ratio of fluorescence at the baseline (figure 3.15). In both cell lines injection of 20µM histamine immediately increased the fluorescence values of Ca^{2+}–saturated FURA and decreased the fluorescence values of Ca^{2+}–free FURA, therefore, increasing the ratio of fluorescence, which indicate an induction of Ca^{2+} influx. Interestingly, in DU145 cells, the levels of Ca^{2+} after histamine injection did not return to the baseline levels during the time of Ca^{2+} measurement (3.15A), as compared to PC3 cells (figure 3.15B). These results suggest that histamine was able to induce Ca^{2+} influx in these cells similar to PNT1A and BPH-1 cells and also indicate the validity of the protocol followed to measure Ca^{2+} influx in the cancerous cell lines.

3.4.3.3.2. Palcar effect on Ca^{2+} influx

In DU145 cells, injection with palcar was not associated with any change in Ca^{2+} influx. Figure 3.16A is a representative of fluorescence values in response to 50µM palcar injection, which indicates that after palcar injection the fluorescence values of Ca^{2+}–saturated FURA and Ca^{2+}–free FURA did not change, therefore, the fluorescence ratios were not affected. This was not observed in PC3 cells (figure 3.16B), where injection of 50µM palcar, after 50 seconds of the start of Ca^{2+} measurement, rapidly increased the fluorescence values of Ca^{2+}–saturated FURA with concurrent decrease in the fluorescence values of Ca^{2+}–free FURA. This indicates that palcar induced influx of Ca^{2+} leading to an increase in the levels of Ca^{2+} in the cells, thus binding with the FURA and increasing the levels of Ca^{2+}–saturated FURA (figure 3.16B). This effect of palcar followed the same pattern of histamine (figure 3.15B).

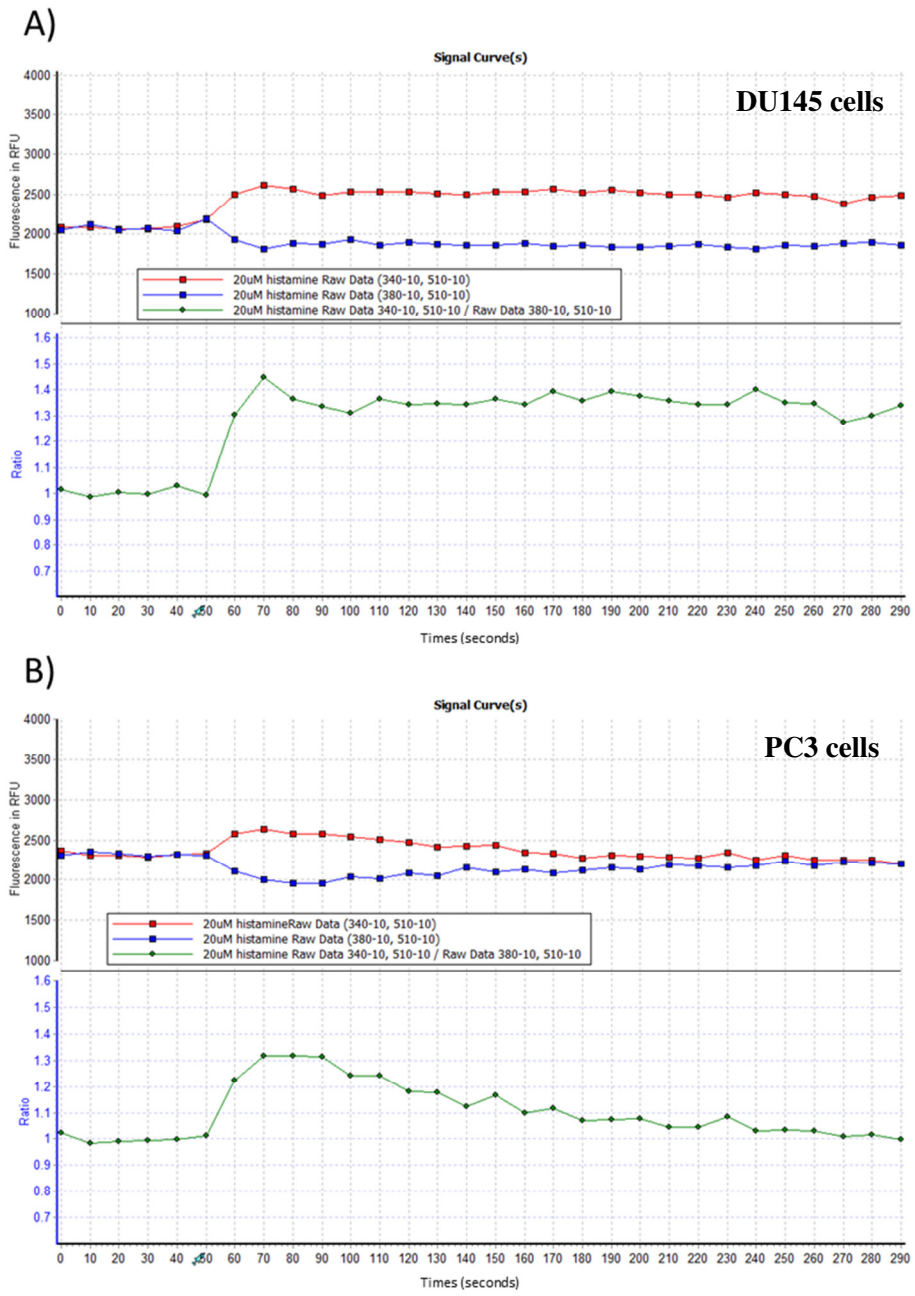

Figure 3.15: Representative fluorescence values in DU145 and PC3 cells in response to 20µM histamine. FURA-loaded cells were excited at both 340nm (**red** line) & 380nm (**blue** line) and emission was detected at 510nm. Cells were injected with 20µM histamine after 50 seconds of the start of Ca^{2+} measurement. The increased ratio of fluorescence (**green** line) immediately following histamine injection in A) DU145 and B) PC3 cells is indicative of Ca^{2+} influx.

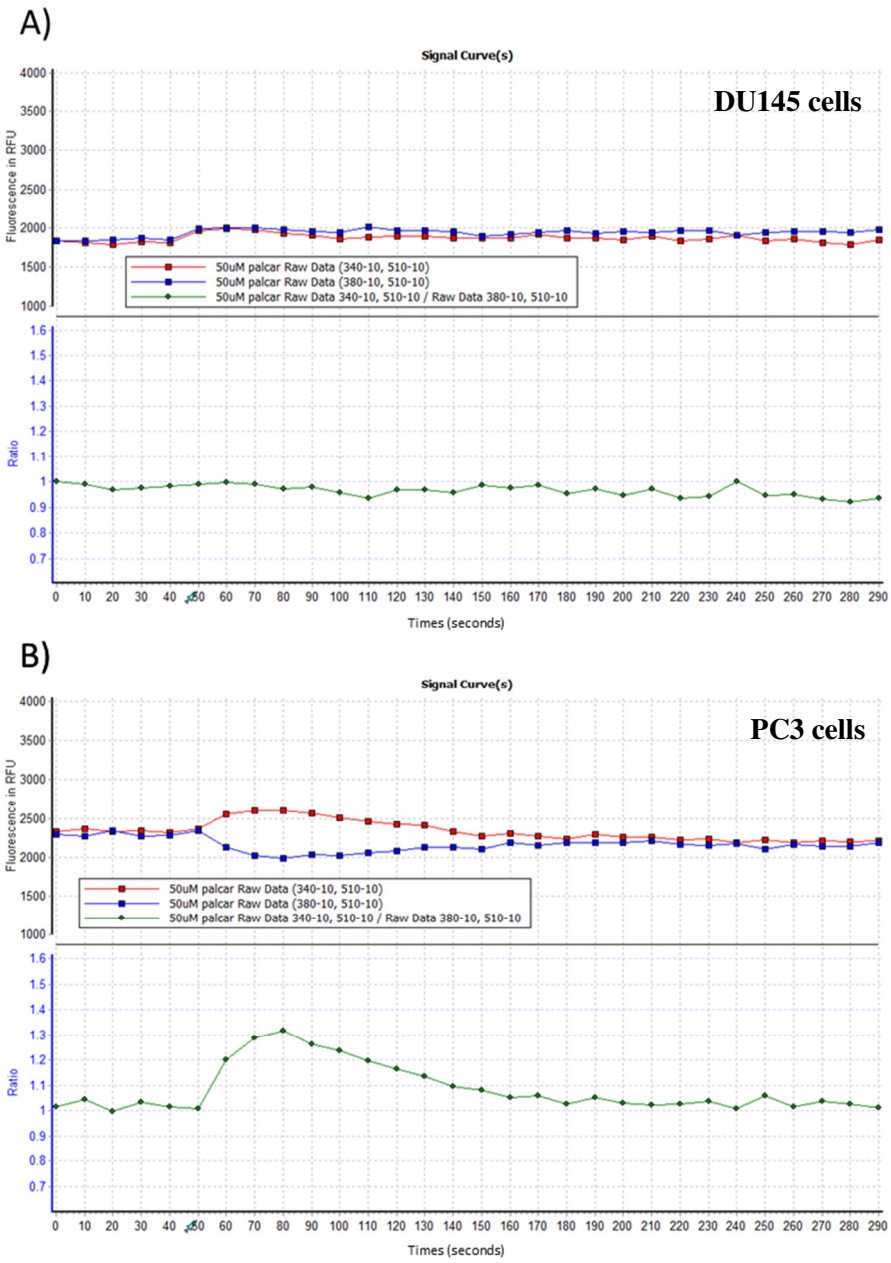

Figure 3.16: Representative fluorescence values in DU145 and PC3 cells in response to 50µM palcar. FURA-loaded cells were excited at both 340nm (**red** line) & 380nm (**blue** line) and emission was detected at 510nm. Cells were injected with 50µM histamine after 50 seconds of the start of Ca^{2+} measurement. Unchanged ratio of fluorescence (**green** line) following palcar injection in DU145 cells (A) is indicative of no Ca^{2+} influx, whereas in PC3 cells (B) the immediate increase in the ratio of fluorescence is indicative of Ca^{2+} influx.

In both DU145 and PC3 cells, the effect of different concentrations of palcar on Ca^{2+} influx was compared to that induced by histamine. In DU145 cells, different concentrations of palcar (5, 10, 20 and 50µM) had no effect on inducing

Ca^{2+} influx; the levels of Ca^{2+} influx were the same as the levels of the cells injected with DMSO (control) which was in contrast to the effect of histamine that showed a trend toward inducing a dose–dependent increase in Ca^{2+} influx (figure 3.17A). This pattern was also observed in PC3 cells, where histamine showed a dose–dependent increase in Ca^{2+} influx. In these cells, injection with different concentrations of palcar also induced a trend of a dose-response increase in Ca^{2+} influx (figure 3.17B). The effect of both histamine and palcar on Ca^{2+} levels in PC3 cells lasted for approximately two minutes before returning back to the baseline levels. In contrast, in DU145 cells histamine-induced Ca^{2+} influx sustained to the end of the experiment of measuring Ca^{2+} influx.

3.4.3.3.3. DHT effect on Ca^{2+} influx

In order to investigate whether the lipid nature of palcar has a role in Ca^{2+} influx, the effect of DHT on Ca^{2+} influx was studied since both palcar and DHT are lipid related compounds. In DU145 cells, 1µM DHT injection had no effect on Ca^{2+} influx, which was similar to the effect of palcar shown previously (figure 3.16). Although the fluorescence value of the Ca^{2+}–saturated FURA was high at the baseline due to the time that this sample had to wait before injection (see section 3.4.3.2.3), the calculated fluorescence ratios after 1µM DHT injection were the same as the values of the baseline levels before injection, which suggest that DHT injection did not induce any Ca^{2+} influx in these cells (figure 3.18A). However, in PC3 cells, the fluorescence values of the Ca^{2+}–saturated FURA were also high due to the same reason above, injection of 1µM DHT, after 50 seconds of the start of the Ca^{2+} measurement, induced a further increase in the Ca^{2+}–saturated FURA with a decrease in the Ca^{2+}–free FURA leading to an increase in the fluorescence ratio (figure 3.18B). These results suggest that DHT was able to induce Ca^{2+}influx leading to an increase in the levels of Ca^{2+} in the cells.

In both DU145 and PC3 cells, the effect of different concentrations of DHT (0.1 and 1µM) on Ca^{2+} influx was compared to that induced by histamine. In DU145 cells, DHT (0.1 and 1µM) has no effect on inducing any Ca^{2+} influx as compared to the effect of histamine (figure 3.19A), whereas in PC3 cells, injection with DHT induced a Ca^{2+} influx in pattern similar to that of histamine. In these cells, 0.1 and 1µM DHT induced a trend of a dose-response increase in Ca^{2+} influx (figure 3.19B). Only 1µM DHT induced a significant induction of Ca^{2+} influx compared to both the control ($P \leq 0.01$) and 0.1µM DHT ($P \leq 0.05$) (figure 3.19C).

The effect of DHT on Ca^{2+} levels last for approximately 3 minutes before returning to baseline levels, which was also observed after palcar injection.

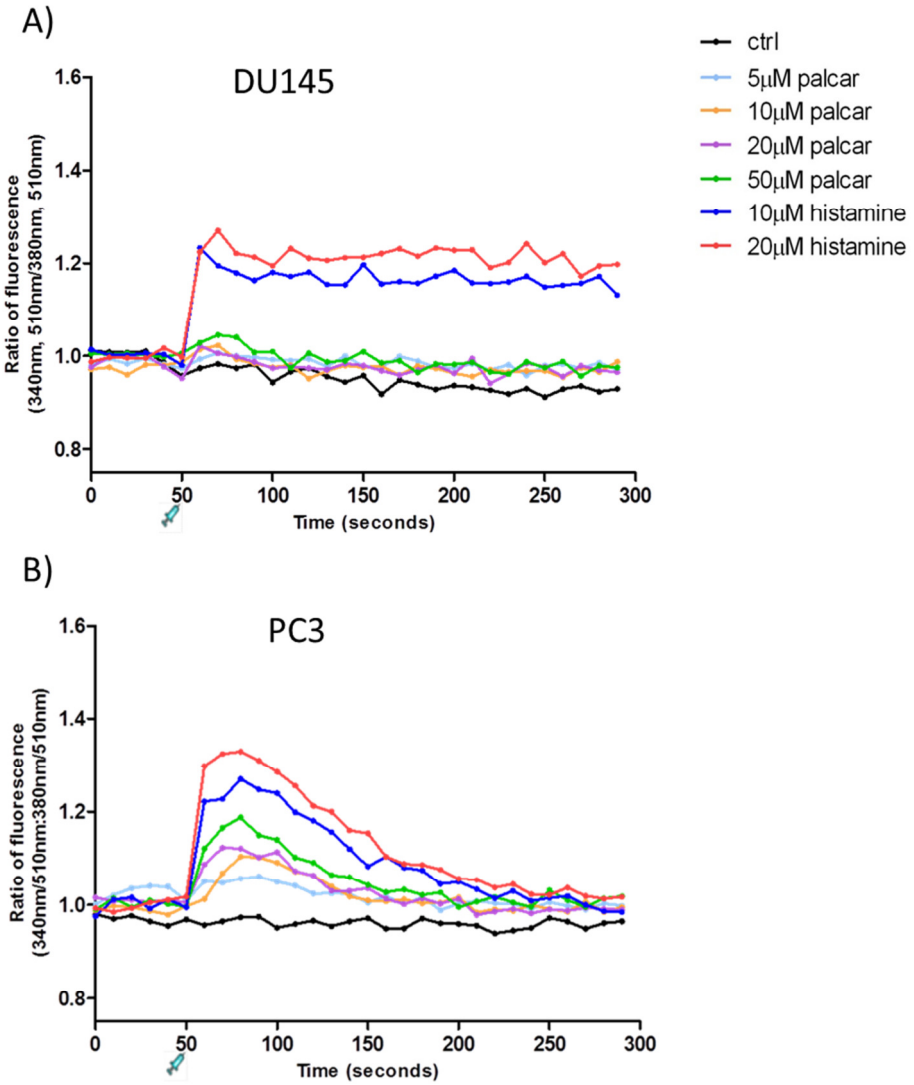

Figure 3.17: Ca^{2+} influx in DU145 and PC3 cells in response to palcar and histamine. FURA (250nM)-loaded cells were injected with DMSO (control), histamine (10 or 20μM) or palcar (5, 10, 20 or 50μM) at 50 seconds. The ratio of fluorescence emission (510nm), excited at both 340nm & 380nm, indicated the $[Ca^{2+}]_i$. A) In DU145 cells, palcar-induced Ca^{2+} influx was not significantly different compared to the control (P = 0.110). Histamine-induced Ca^{2+} influx was significant compared to the control (P=0.003), but there was no significant difference within the different concentrations of palcar or histamine. B) In PC3 cells, palcar and histamine-induced Ca^{2+} influx were significantly different from the control (P = 0.011 & 0.016, respectively), but there was no significant difference in Ca^{2+} influx within the different concentrations of palcar (P = 0.839) or histamine (P = 0.642). Data are means of three independent experiments. Statistical analysis was performed with mixed effect model test using the Genstat software.

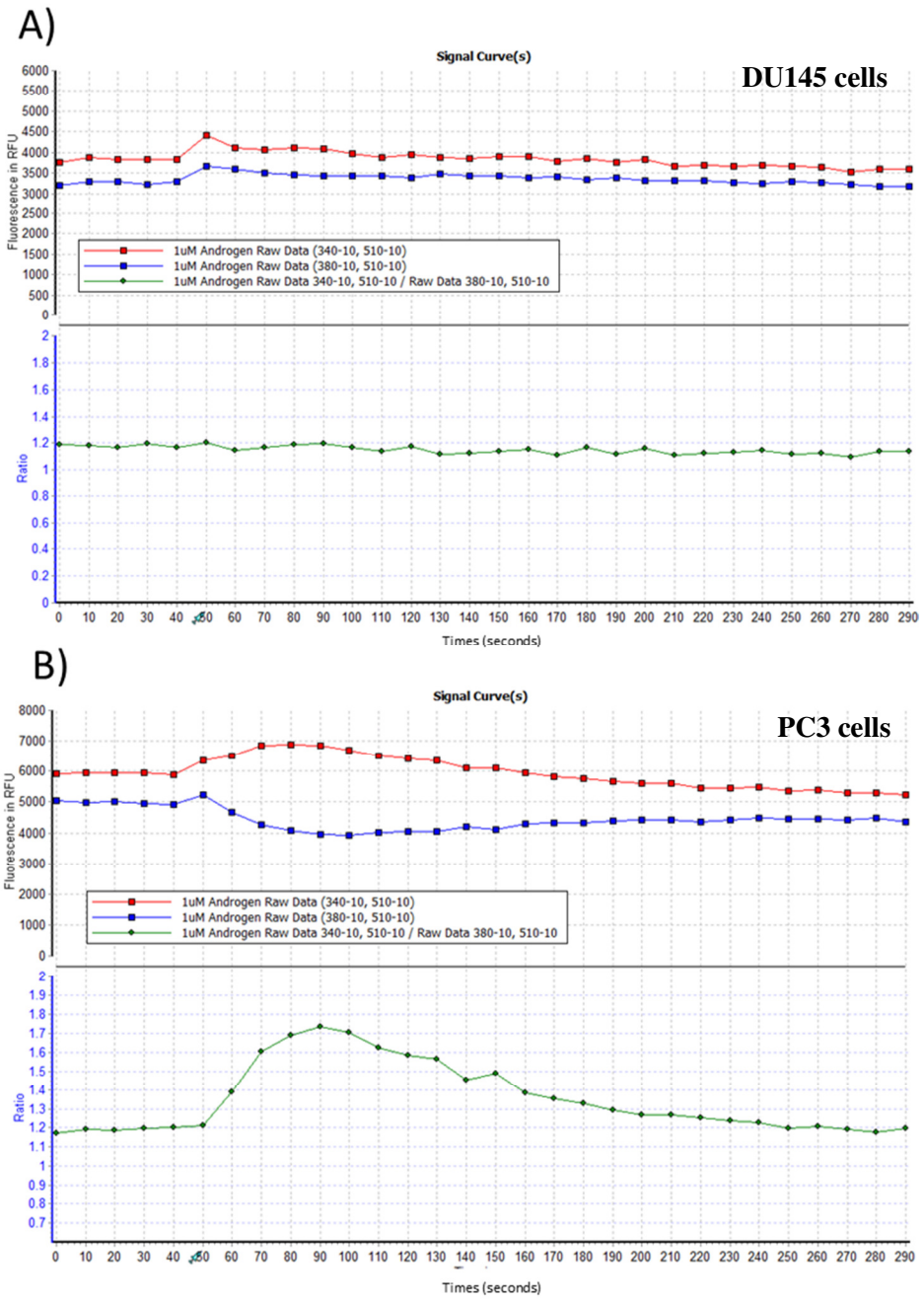

Figure 3.18: Representative fluorescence values in DU145 and PC3 cells in response to 1µM DHT. FURA-loaded cells were excited at both 340nm (**red** line) & 380nm (**blue** line) and emission was detected at 510nm. Cells were injected with 1µM DHT after 50 seconds of the start of Ca^{2+} measurement. Unchanged ratio of fluorescence (**green** line) following DHT injection in DU145 cells (A) is indicative of no Ca^{2+} influx, whereas in PC3 cells (B) the rapid increase in the fluorescence ratio is indicative of Ca^{2+} influx.

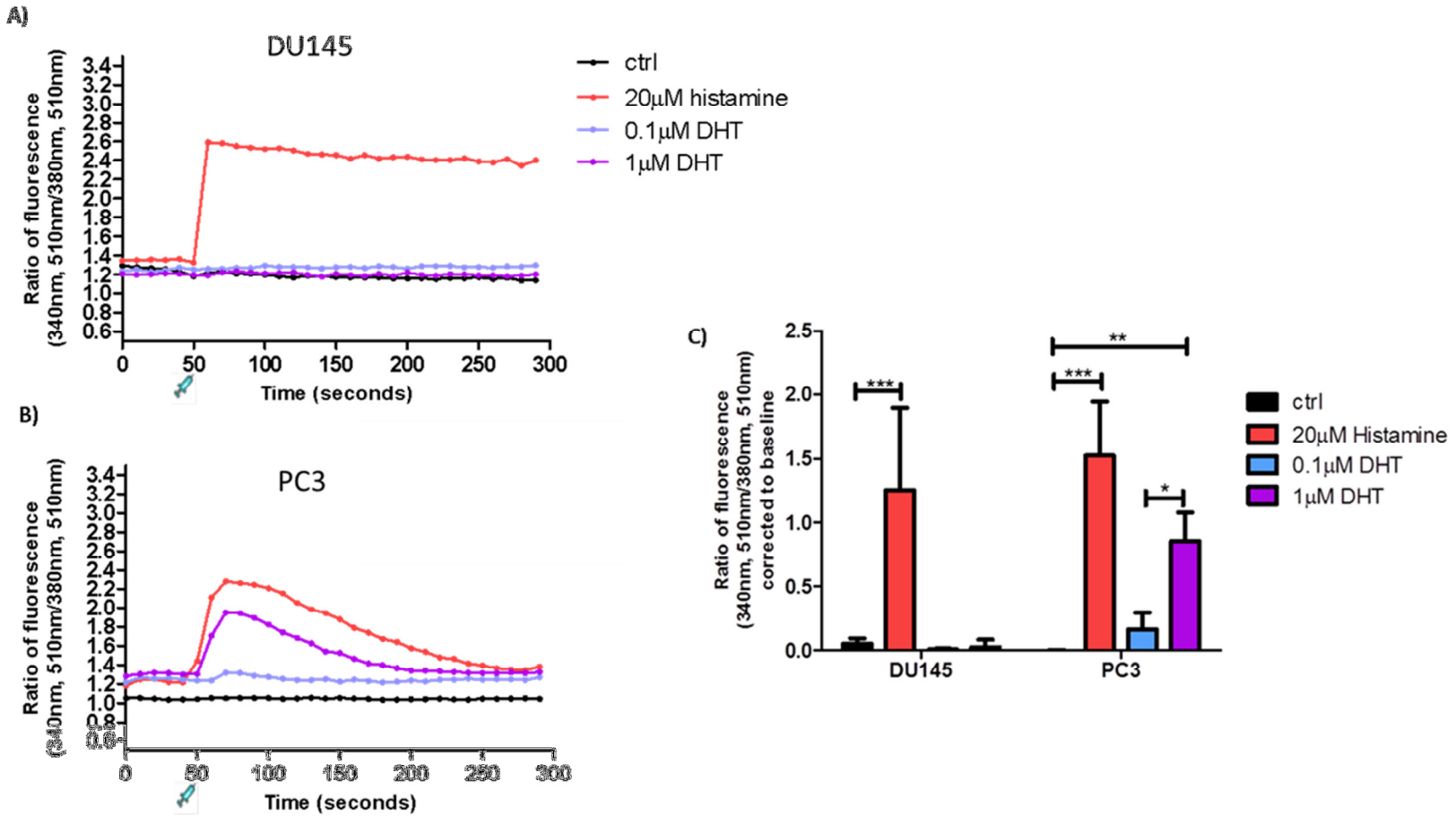

Figure 3.19: Ca^{2+} influx in DU145 and PC3 cells in response to DHT. FURA-loaded DU145 (A) and PC3 (B) cells were injected with DMSO, 20µM histamine or DHT (0.1 or 1µM) at 50 seconds. The ratio of fluorescence emission (510nm), excited at both 340nm & 380nm, indicated the $[Ca^{2+}]_i$. DHT (1µM) did not induce Ca^{2+} influx in DU145 (A) cells, but it did in PC3 cells (B) compared to the DMSO (control). In PC3 cells, the Ca^{2+} influx induced by 1µM DHT was significant compared to both control and 0.1µ DHT (C). Data represent means ± SD of three independent experiments. Statistical analysis was performed using one way ANOVA followed by Bonferroni's post-test in each cell line, $P \leq 0.05$, $P \leq 0.01$ and $P \leq 0.001$.

3.5. Discussion

In this chapter, the role of increased concentrations of palcar was investigated *in vitro* using prostate non-cancerous and cancerous cell lines. High concentrations of palcar was associated the induction of IL-6 gene expression in the non-cancerous PNT1A and PC3 cells, which was associated with IL-6 secretion in PC3 cells, but not in PNT1A cells, suggesting the pro-inflammatory role of palcar in PC3 cells. High concentrations were also associated with induction of Ca^{2+} influx in PC3 cells, but not in the cancerous DU145 cells and non-cancerous PNT1A and BPH-1 cells, which suggest that palcar induces changes in membrane permeability in PC3 cells. Induction of Ca^{2+} influx in PC3 cells in response to palcar was also observed for DHT.

3.5.1. Palcar potential pro-inflammatory property

A viability test against a range of palcar concentration (5, 10, 50 and 100µM) was investigated. This range of palcar was above those reported in plasma and tissues from humans (Table 2.1, Chapter 2). However, it has been shown that the plasma levels of other acylcarnitines in subjects who have a defect in metabolism is within this range [31]. Palcar at 50µM has been reported in ischemic heart of animal model, which is another form of metabolic dysfunction that involve a defect in fatty acid metabolism [103]. Therefore, high concentrations of palcar could be expected during prolonged accumulation. Furthermore, 50µM was previously studied *in vitro* and has been shown to be associated with functional changes in cell membrane properties [41, 123]. The highest concentration (100µM) was selected to study its effect on prostate cells and whether it is associated with a detergent effect since the effect of palcar in general was not investigated in prostate cells.

The results of the viability test showed that palcar did not affect PNT1A cell viability, but in PC3 cells 50 and 100µM palcar reduced the cells' viability to approximately 65% and 50% respectively, (figure 3.4). However, upon the visual examination of the cells at these two concentrations, cells morphology and growth were the same as the cells treated with DMSO (control) and that an increase in the number of the floating cells in comparison to the control was not observed, suggesting that at these two concentrations the remaining 35% of "unviable" cells were not died, but rather their growth was inhibited. This is because the WST-1 assay is a measure for the activity of the mitochondrial dehydrogenase enzyme; therefore an inhibition of the enzymatic activity of the dehydrogenase does not

necessary indicating cell death. Thus, suggesting that palcar at these two concentrations do not affect cell growth in PC3 cells.

The pro-inflammatory effect of palcar was investigated by studying the effect of palcar on IL-6, an inflammatory biomarker. Palcar at 50 and 100µM induced a significant increase in IL-6 secretion in PC3 cells (figure 3.5). Although the viability test in response to 50 and 100µM palcar observed in PC3 cells indicate that palcar at these concentrations may not be associated with cell death, the low cell viability (65%) accompanied with the increased IL-6 secretion in these cells suggest that this was either due to the detergent effect of palcar on the cell membrane, leading to the leakage of the cellular IL-6 into the media, or due to the induction of the gene expression of IL-6, which in this case might indicate that palcar was associated with a stress response in PC3 cells.

It seems unlikely that palcar within the concentration investigated (≥50µM) was associated with detergent effect on the cell membrane since the levels of palcar-induced IL-6 in PNT1A cells was close to that of the control. To confirm that palcar was not associated with a damaging effect on the cell membrane in PC3 cells, palcar-induced IL-6 gene expression was measured in PC3 cells and compared to that in PNT1A cells. Since in PNT1A cells, palcar did not affect the cell membrane integrity, as suggested by the data of IL-6 secretion, data from IL-6 gene expression in both cell lines would indicate that palcar is not associated with a detergent effect in PC3 cells, in that the increase in IL-6 secretion would be as a result of the induction of IL-6 gene expression. Indeed, the results showed that 50 and 100µM palcar induced a two- and six-fold increase in IL-6 gene expression, respectively, in PC3 cells (figure 3.6), suggesting that the increase in IL-6 secretion is due to the induction of IL-6 gene expression and not due to the loss of the membrane integrity and the release of IL-6 into the media. Interestingly, in PNT1A cells the results also show that palcar at 50 and 100µM was associated with an induction of IL-6 gene expression despite the lack of change in IL-6 secretion in these cells. This supports the hypothesis that high concentrations of palcar are associated pro-inflammatory activity via the induction of IL-6 and that this induction may indicate a stress response in prostate cells. It is unlikely that palcar-induced IL-6 secretion would suggest an apoptotic response since it has been shown that IL-6 protect gastric cancer from apoptosis [131] and inhibit apoptosis in malignant plasma cells [132] and human ovarian cancer cells [133]. In fact, IL-6 is associated with growth promotion in prostate cancer [49, 51].

The explanation for palcar-induced IL-6 in these cells might be related to the amphiphilic nature of palcar. This property allows palcar to interact with the phospholipid bilayer leading to a change in the physical state of the membrane, which affects the associated proteins leading to a change in their properties. This may trigger the inflammatory responses and the secretion of the pro-inflammatory cytokines. Therefore, the effect of the amphiphilic nature in inducing IL-6 was investigated by comparing palcar-induced IL-6 secretion to that of LPC, a compound that also exhibits amphiphilic properties. It has been observed that LPC induced the secretion of IL-6 in HUVEC cells [134]. The results of this Chapter showed that LPC treatment significantly reduced the levels of IL-6 compared to the control and 50μM palcar (figure 3.7), contrary to the effect of palcar. Hence, suggesting that palcar-induced IL-6 secretion in PC3 cells was not due to the amphiphilic property.

A further comparison was made with DHT, an androgen that promote prostate cancer. This comparison was made in order to investigate whether palcar has the same effect as that of DHT; especially that DHT is known to induce prostate growth. As stated above, IL-6 is known to promote the growth of prostate cancer [49, 51] and that the DHT effect on inducing prostate growth might be related to IL-6 secretion. Therefore if DHT induces IL-6 secretion, which was observed in response to palcar, this would indicate that palcar might induce prostate cancer progression indirectly through the induction of IL-6. The results indicate that DHT within the investigated physiological and pathophysiological levels neither increased nor decreased the levels of IL-6 in both PNT1A and PC3 cells compared to control, thus having no effect on the inflammatory responses (figure 3.8). It is important to note that the constitutive levels of IL-6 in PNT1A cells in figure 3.8 were not consistent with that observed in figure 3.5. This can be attributed to the high passage number of the cells used to measure the effect of DHT on IL-6.

Acylcarnitines have been previously observed to be associated with pro-inflammatory responses. In PBMCs isolated from healthy volunteers, short chain acylcarnitines induced the secretion of TNF-α [47]. In bone marrow-derived macrophages isolated from mice, medium chain acylcarnitines induced the secretion of pro-inflammatory cytokines [46]. These acylcarnitines increased the levels of the transcription factor NFκB [6], which is known to be a regulator of IL-6 synthesis [48]. The secretion of IL-6 has been linked to the progression of prostate cancer in humans [49, 51]. In prostate cancerous tissue the levels of IL-6

were higher than the benign non-cancerous tissue [49]. IL-6 has been found to induce the expression of AR [135]. AR signalling is considered essential for the development and proliferation of prostate epithelial cells, and since prostate cancer develops from the epithelial part of the prostate, AR maybe linked to the development of prostate cancer. Therefore, the effect of palcar in inducing IL-6 in PC3 cells, which represent the most aggressive metastatic form of prostate cancer, may indicate that palcar can be indirectly linked to the progression of prostate cancer.

3.5.2. Ca^{2+} influx in prostate cell lines

Structurally, the amphiphilic nature of palcar enables the molecule to interact with both the phospholipid bilayer and the proteins within the bilayer. This could, as mentioned previously, lead to changes in the membrane properties and alter protein functions, which could result in changes in the membrane permeability affecting the homeostasis of certain ions. One of these ions is Ca^{2+}. In this study, the effect of palcar on membrane permeability was determined by measuring the Ca^{2+} influx in PNT1A, BPH-1, DU145 and PC3 cells, and was compared to the effect of the positive control (histamine). Ca^{2+} influx within these cells was studied in 5 minutes duration. Although WST-1 assay showed that palcar was not associated with toxic effect, the effect of palcar on cell membrane during Ca^{2+} measurement was investigated using trypan blue. This assay was chosen to mimic the experimental procedure of palcar injection. The results showed that presence of 50µM palcar for 5 minutes was associated with approximately 78% viable cells compared to 80% viable cells injected with DMSO (control) (figure 3.9). Therefore, suggesting that incubation with 50µM palcar for 5 minutes has no major effect on the cell membrane integrity and that the Ca^{2+} influx is not due to the loss of membrane integrity. The low viability (approximately 78%) can be attributed to the procedure of measuring Ca^{2+} influx, which requires the cells to be in a suspension for one hour to recover from trypsin and then for another 30 – 45 minutes for FURA incubation, which might affect the cell viability.

3.5.2.1. Prostate non-cancerous cells: the effect of histamine versus palcar and DHT on Ca^{2+} influx

In order to evaluate the effect of palcar and DHT on Ca^{2+} influx, the Ca^{2+} influx should be compared to a positive control that is known to induce Ca^{2+} influx. In PC3 cells histamine has been reported to increase the $[Ca^{2+}]_i$ [128, 129]. There are two modes of action for histamine to induce Ca^{2+} increase: extracellular

Ca^{2+} entry and intracellular Ca^{2+} release. Extracellular Ca^{2+} entry involved second messenger-operated channels [129], while intracellular Ca^{2+} release involved the activation of H1 receptors in the cell-membrane, which in turn activated the phospholipase C (PLC). The latter can hydrolyse the phosphatidylinositol-4,5-bisphosphate (PIP_2) at the cytosolic surface of the cell membrane into inositol-1,4,5-triphosphate (IP_3) and diacylglycerol (DAG). IP_3 binds to the IP_3 sensitive Ca^{2+} stores to release Ca^{2+} into the cytosol and therefore increase $[Ca^{2+}]_i$ [128, 129]. Based on these studies histamine was used as a positive control for all prostate cells used in this study.

In FURA loaded PNT1A and BPH-1 cells, histamine injection induced an increase in the fluorescence values of Ca^{2+}–saturated FURA together with a decrease in the Ca^{2+}–free FURA (figure 3.10) suggesting that histamine increased the levels of Ca^{2+} inside the cells. This was demonstrated by an increase in the fluorescence ratio (an index of Ca^{2+} influx), thus an increase in $[Ca^{2+}]_i$. This increase was observed for approximately two minutes, after which it returned back to baseline levels. This recovery could be either due to Ca^{2+} being pumped out of the cells or back into the Ca^{2+} stores, which is important in maintaining the homeostatic levels of $[Ca^{2+}]_i$. These results indicate that the protocol followed to measure Ca^{2+} influx in these cells is valid and that histamine is a suitable positive control for the effect of palcar on Ca^{2+} influx.

Compared to histamine, injection with different concentrations of palcar (5, 10, 20 or 50µM) was not associated with any increase in the fluorescence ratios in the PNT1A and BPH-1 cells. This was clear from the fluorescence data illustrated in figure 3.11. Injection with 50µM palcar was associated with neither an increase in Ca^{2+}–saturated FURA nor decrease in Ca^{2+}–free FURA compared to the baseline levels, which suggests that palcar does not induce Ca^{2+} influx in either cell line. This pattern of unchanged fluorescence ratio was also observed after injection with 5, 10 and 20µM palcar (figure 3.12). This was also true for DHT (0.1 and 10µM) injection (figure 3.13 and 3.14).

3.5.2.2. Prostate cancerous cells: the effect of histamine versus palcar and DHT on Ca^{2+} influx

In DU145 and PC3 cells, histamine (10 or 20µM) was able to induce Ca^{2+} influx in a similar pattern to that observed in PNT1A and PBH-1 cells. Interestingly, the increase in Ca^{2+} influx in DU145 cells was maintained for the entire duration of measuring Ca^{2+} influx and did not return to baseline levels as

was observed in PC3 cells, where the effect was observed for approximately two minutes (figure 3.15). This may suggest that in DU145 cells, the number of Ca^{2+} stores may be higher than that in PNT1A, BPH-1 and PC3 cells.

Palcar did not induce any Ca^{2+} influx in DU145 cells. The fluorescence data of FURA loaded DU145 cells injected with 50μM palcar showed that fluorescence values at both 340 and 480nm were not changed as a result of palcar injection, and thus the resultant ratio of fluorescence was not changed (figure 3.16A). This was also the case with the injection of 5, 10 and 20μM palcar (figure 3.17A). However, in PC3 cells, palcar injection after 50 seconds induced an increase in Ca^{2+} influx, this was indicated from the fluorescence data illustrated in figure 3.15B, where injection with 50μM palcar caused an increase in Ca^{2+}–saturated FURA and a decrease in Ca^{2+}–free FURA. In these cells, 5, 10, 20 and 50μM palcar showed a trend of a dose-dependent increase in Ca^{2+} influx (figure 3.17B).

This ability of palcar to induce an increase in $[Ca^{2+}]_i$ has been previously observed in endothelial cells [136, 137], but this is the first time where it has been shown that palcar is able to induce Ca^{2+} influx in PC3 cells, which represent an aggressive form of prostate cancer. This effect of palcar may represent a stress response in these cells.

When comparing the effect of palcar in inducing Ca^{2+} influx with that of DHT in the prostate cancerous cells, the results showed that injection with 1μM DHT produced a similar effect to that of palcar. In DU145 cells, 1μM DHT did not induce Ca^{2+} influx; there was neither an increase in Ca^{2+}–saturated FURA nor a decrease in Ca^{2+}–free FURA after injection, hence, unchanged fluorescence ratio (figure 3.18A). This was not true in PC3 cells, which directly after DHT injection, Ca^{2+}–saturated FURA increased with a decrease in Ca^{2+}–free FURA, which produce an increase in the ratio of fluorescence (figure 3.18B). In these cells, injection with DHT (0.1 and 1μM) induced a trend of a dose-response influx (figure 3.19) and only 1μM DHT was associated with a significant Ca^{2+} influx compared to the control (figure 3.19C).

This effect of DHT on inducing Ca^{2+} influx has been previously observed in another prostate cancerous cell line; the LNCaP cells [45]. In these cells DHT-induced Ca^{2+} influx was due to the activation of a PTX-sensitive G-protein coupled receptor (GPCR) and L-type Ca^{2+} channels. The similarities between palcar and DHT in their abilities to induce an increase in Ca^{2+} influx in PC3 cells, may suggest that palcar's mode of action in changing membrane permeability may

include activation of a signalling pathway that is induced by DHT and only present in PC3 cells. This suggestion may explain the unresponsiveness of DU145, PNT1A and BPH-1 cells to both palcar and DHT. Another explanation for the unresponsiveness of DU145, PNT1A and BPH-1 cells to both palcar and DHT may include the existence of an efficient Ca^{2+} buffer system in these cells with a concentration that is high enough to balance the Ca^{2+} influx induced by either palcar or DHT [138].

It has been shown that incubation with palcar (>25µM) was associated with cell toxicity leading to a reduction in cell survival in renal cancer cells, but have less effect on the normal kidney cell [8]. In HUVEC and bovine aortic endothelial cells (BAEC), high concentrations of acylcarnitines (>20µM) were found to create a detergent-like effect on the cell membrane. This was also observed in heart muscle using concentrations higher than 10µM palcar [139]. The detergent effect was indicated by FURA leakage from the cells as a result of the damaged cell membrane and the drop of the fluorescence signal from both 340 and 380nm. However, in all prostate cells that were used in this study, palcar (5 – 50µM) injection was not associated with FURA leakage, since a drop of the fluorescence values from both 340 or 380nm was not observed (figure 3.11 and 3.16), which confirm again that palcar was not associated with any detergent effect.

Collectively, the results of this study highlight the ability of palcar, at high concentrations, to instigate the induction of IL-6 and Ca^{2+} influx in PC3 cells, which were not observed in DU145, PNT1A and BH-1 cells. These biological effects of palcar may represent a stress response in PC3 cells and since these effects were only observed in this cell line, it suggest that palcar could act as a signalling molecule in these cells to induce changes in the membrane proteins, which could be either ion channels or receptors that eventually linked to IL-6 secretion.

3.6. Conclusion

Palcar at high concentrations exert some biological roles in prostate cancer PC3 cells, these include its role as a pro-inflammatory mediator and its ability to change membrane permeability demonstrated by the induction of Ca^{2+} influx. These effects were observed at 50µM, which is a concentration that is higher than that reported in the human plasma, but occur under ischemic conditions reported

from animal model. However, from the results of the viability test this concentration was not associated with cellular death.

The pro-inflammatory effect of palcar was indicated by the induction of gene expression of IL-6 (a marker of inflammation), which was accompanied with IL-6 secretion in PC3 cells. In the non-cancerous PNT1A cells, palcar induced IL-6 gene expression, but not IL-6 secretion. This suggests that palcar may be associated with stress response in prostate cells. The increase in IL-6 in PC3 cells could be related to effect of palcar on inducing Ca^{2+} influx. In PC3 cells, palcar induced a trend of a dose-dependent increase in Ca^{2+} influx, but not in DU145, BPH-1 and PNT1A cells. The effect of palcar on inducing Ca^{2+} influx observed in these cells was the same as the effect of DHT; a lipid-related hormone that is synthesized from cholesterol and have a role in prostate cancer progression.

Ca^{2+} is a secondary messenger that is involved in stimulating pro-inflammatory responses, such as the induction of IL-6 secretion. Therefore, the results of this study suggest that palcar accumulation may mediate pro-inflammatory responses in the prostate cancerous PC3 cells and highlight the possibility that palcar could act as a signalling molecule in these cells. Further investigation into the mechanism by which palcar induces Ca^{2+} influx could be considered important in uncovering signalling pathways that may represent a target for future dietary interventions aiming to investigate the role of dietary components on reducing the effect of palcar accumulation in prostate cancer. Therefore in the next chapter, the mechanism by which palcar induces Ca^{2+} influx in PC3 cells is investigated.

Chapter 4

Mechanism of calcium influx in response to palmitoylcarnitine

4.1. Introduction

Previously, in Chapter 3 palcar was shown to have a potential pro-inflammatory effect through the induction of IL-6. This effect was observed in the prostate cancerous PC3 cells but not in the non-cancerous PNT1A cells. It was also shown that palcar has the ability to induce Ca^{2+} influx in PC3 cells, but not in prostate cancerous DU145 cells and prostate non-cancerous PNT1A and BPH-1 cell lines. Induction of Ca^{2+} influx in PC3 cells was also observed by DHT, a hormone that is associated with prostate cancer progression. The similarity between the effect of palcar and DHT could suggest that palcar induces the Ca^{2+} influx by the same mechanism as DHT. In this Chapter, the mechanisms of Ca^{2+} influx induced by palcar and DHT were therefore investigated.

Ca^{2+} is an important intracellular mediator for many reactions, therefore regulation of $[Ca^{2+}]_i$ is essential and maintained by signalling pathways that control the channels and pumps by which Ca^{2+} is transferred (figure 4.1).

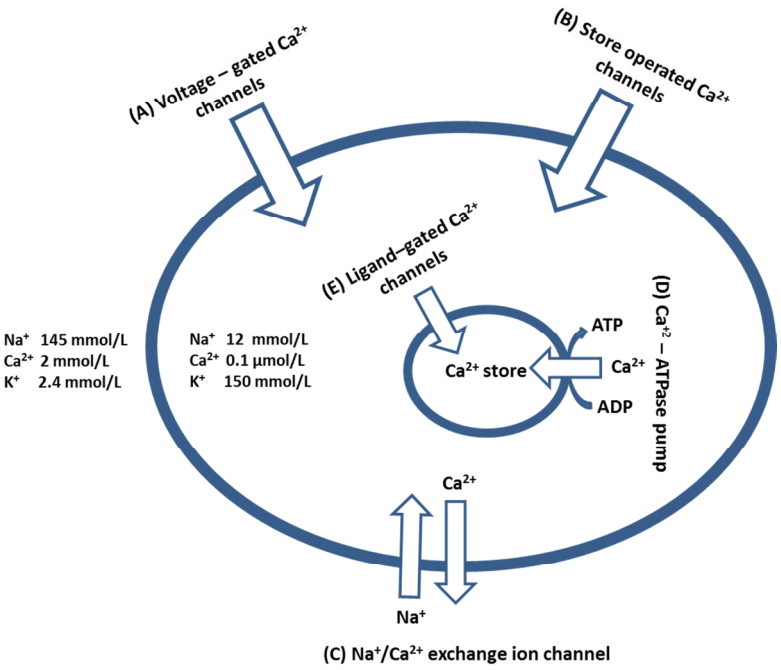

Figure 4.1: Ca^{2+} channels and pumps controlling the $[Ca^{2+}]_i$. Ca^{2+} can be transferred into and out of the cells by five means, which are (A) voltage–gated Ca^{2+} channels that open in response to membrane polarization, (B) store operated Ca^{2+} channels, which opens in response to Ca^{2+} store depletion, (C) Na^+/Ca^{2+} exchange ion channels; they couples the efflux of Ca^{2+} to influx of Na^+, (D) Ca^{2+}/ATPase pumps, which pumps the Ca^{+2} ions back to the stores and (E) ligand–gated Ca^{2+} channels that open the Ca^{2+} stores in response to ligand, such as IP_3 and ryanodine [140-142].

Some of these signalling pathways are associated with the activation of receptors that can couple to guanosine diphosphate (GDP)–binding proteins, also called G–proteins. G-proteins are heterotrimeric proteins consisting of three subunits; α, β and γ. These receptors use the G-proteins to transmit the signal to the cell interior, therefore they are called GPCRs [13, 14].

4.1.1. G-protein coupled receptors

GPCRs form the largest family of cell surface receptors. They are important for cellular communication in response to external stimuli. The signalling molecules that activate these receptors vary in structure and include proteins, small peptides, amino acid and fatty acid derivatives. Examples of fatty acid derivatives include lysophospholipids and their derivatives, such as lysophosphatidic acid (LPA) and sphingosine-1-phosphate, and arachidonic acid-derived eicosanoids, such as prostaglandins and leukotrienes [143]. Such ligands can be termed as bioactive lipids or lipid mediators. These ligands are not specific for one GPCR, but can activate several GPCR family members [142].

All GPCRs share the same structure, which consists of a single polypeptide chain that transverses the phospholipid bilayer back and forth seven times, thus they are described as seven trans-membrane helices or domains [13, 142].

Upon their activation, GPCRs undergo a conformational change that enables them to activate the trimeric G-proteins. The G-proteins are attached to the cytosolic face of the plasma membrane, and link the receptor to the appropriate intracellular targets known as effector proteins. These effector proteins can be gene regulatory proteins, a component of a metabolic pathway or a membrane bound protein, including an ion channel or an enzyme. An ion channel or an enzyme can be a part of a secondary messenger system, such as adenylyl cyclase or PLC [13, 14, 142]. In some cases, G-proteins can be physically attached to the receptor prior to receptor activation, and in other cases they bind only after receptor activation [142]. GPCR can be activated as a result of a chemical reaction such as palmitoylation. Palmitoylation is a reversible post-translational lipid modification, where a membrane-bound acyltransferase enzyme catalyses the transfer of a C16-carbon saturated fatty acyl chain to the cytoplasmic cysteine residue of a protein, and to a lesser extent to serine and threonine residues, through a thioester bond [144]. Palmitoylation can also occur through a non-enzymatic reaction [144, 145]. Some G-proteins were found to undergo palmitoylation, which modifies their structure and facilitates their transfer to the lipid raft [146]. The lipid raft is a

subdomain of the plasma membrane that is enriched with cholesterol and sphingolipids as well as GPCR [147]. This transfer increases the interaction between the hydrophilic G-proteins to form heterotrimeric molecule as well as increasing their interaction with the hydrophobic protein (the receptor), thus palmitoylation aids the recruitment of the soluble G-proteins the cytoplasmic face of the membrane and the receptor [148].

All G-proteins have identical basic structures and function in the same way. However, there are different types of G-proteins that are specific for a certain set of GPCR and for a particular set of target or effector proteins in the membrane. Gα-subunit has four subfamilies, the G_s, $G_{i/o}$, G_q & G_{12}. The signalling pathway ultimately induced by these G-proteins depends on ligand-binding and the type of Gα-subunit activated (figure 4.2).

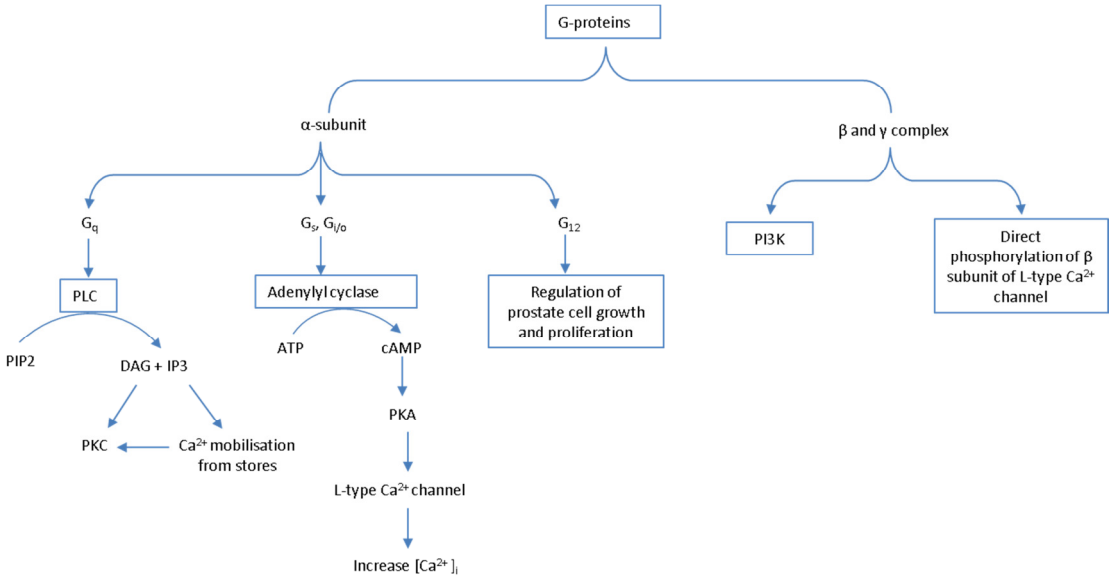

Figure 4.2: Pathways activated by the G-protein subunits. Gα subunit has four subfamilies; G_q, G_s, $G_{i/o}$ and G_{12}. The $G_q\alpha$ subunit involves in regulating the activity of PLC that catalyses the breakdown of PIP_2 into DAG and IP_3 [149]. DAG remains attached to the cell membrane due to hydrophobic interaction and drives the recruitment of protein kinase C (PKC) [150]. IP_3 binds to the receptor at the surface of endoplasmic reticulum and releases Ca^{2+}. The latter is required for the activation of PKC [150]. PKC can activate many proteins that stimulate proliferation and growth [151]. $G_s\alpha$ and $G_{i/o}\alpha$ regulate the activity of adenylyl cyclase. $G_s\alpha$ stimulates adenylyl cyclase activity to produce cyclic adenosine monophosphate (cAMP) from ATP, while $G_{i/o}\alpha$ inhibits the activity [152]. cAMP activates protein kinase A (PKA), which activates L-type Ca^{2+} channels to allow the influx of extracellular Ca^{2+} [150]. $G_{12}\alpha$ is involved in the regulation of prostate cancer growth and proliferation [149]. βγ complex can activate PI3K pathway and/or phosphorylate the β-subunit of the L-type Ca^{2+} channel.

In the inactive state, the α-subunit is bound to GDP. When the receptor is activated, it functions as a guanine nucleotide exchange factor and stimulates the Gα-subunit to exchange its GDP with guanosine triphosphate (GTP). The Gα-subunit then dissociates from both the receptor and the Gβγ complex [149, 153, 154]. The Gα-subunit together with the bound GTP (Gα-GTP) activates the effector proteins, such as PLC and adenylyl cyclase [149]. The dissociated Gβγ dimer can activate other signalling pathways, such as the PI3K pathway, or directly phosphorylate L-type Ca^{2+} channels, which upon their activation allow influx of Ca^{2+} from the extracellular space into the cells [155].

4.1.2. L-type Ca^{2+} channels

L-type Ca^{2+} channels belong to the voltage-dependent channels that allow the entrance of Ca^{2+} in both excitable and non-excitable cells in response to membrane depolarization [156]. Excitable cells are those that are able to produce action potentials, such as muscle and nerve cells [14]. L-type Ca^{2+} channels can regulate many intracellular processes, such as cell contraction and hormone secretion [157] and they are regulated by phosphorylation in response to secondary messengers [156].

From an electrophysiological and pharmacological perspective these channels can be classified into low voltage–activate (LVA) and high voltage–activate (HVA) channels. LVA channels require very low voltage (approximately –70mV) for their activation. They are characterised by transient current with a small conductance, therefore they are called T-type channels; "T" referring to "tiny". HVA channels are activated when the membrane voltage is high (≥ –30mV). There are different types of HVA channels and L-type Ca^{2+} channels are one of them [140]. L-type Ca^{2+} channels are located in the cell membrane of many cells and are important for providing Ca^{2+} required for excitable cells, such as cardiac and smooth muscle cells [140]. These channels are characterised by a large current, high activation threshold and slow inactivation, and therefore have long lasting effects, thus they were given the name "L"; referring to long [140]. These channels can be blocked by dihydropyridines (such as nifedipine), verapamil and diltiazem [140, 157].

L-type Ca^{2+} channels are protein complexes consisting of up to 5 subunits; α, β, γ, λ and δ [157]. The main subunit is α_1 and it is the voltage sensor of the channel as well as the pore forming subunit, which allows the passage of the ions.

It also contains the binding site for agonists and antagonists. The structure of α_1 is illustrated in figure 4.3.

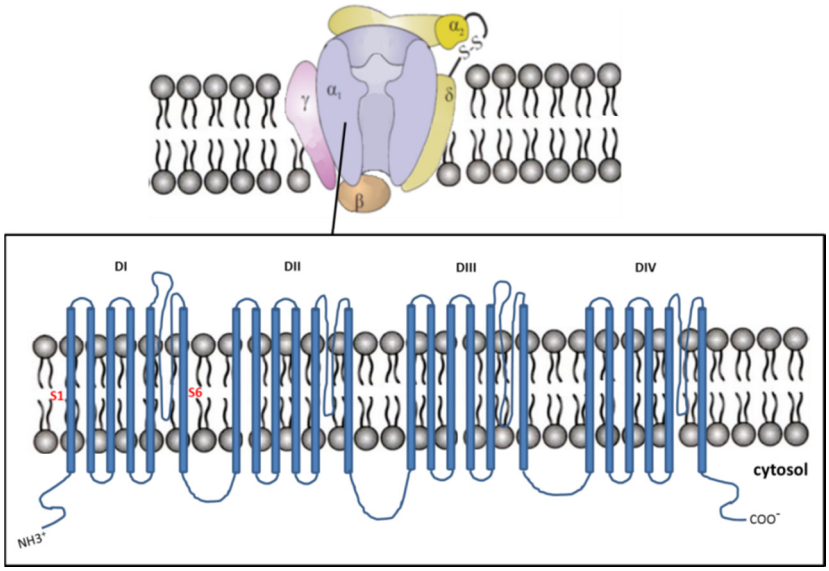

Figure 4.3: Structure of L-type Ca^{2+} channel. α_1-subunit is the main subunit of L-type Ca^{2+} channel and consists of four domains (DI – DIV), each domain have six transmembrane segments; S1 – S6 [157]. A link between S5 and S6 forms the channel pore. Adapted from Lacinova [158] and Splawski *et al* [159]).

It has been found that the gene of the α_1-subunit of the L-type Ca^{2+} channel ($Ca_v1.2$) was expressed in prostate tissue [159] and prostate cell lines [160].

In prostate LNCaP cancer cells an increase in $[Ca^{+2}]_i$ has been observed in response to DHT [45]. This increase in $[Ca^{+2}]_i$ is thought to be due to the activation of GPCR [45].

The role of GPCR-activated L-type Ca^{2+} channels in Ca^{2+} influx was reported in androgen-dependant prostate cancerous LNCaP cells [45]. In these cells, GPCRs were pertussis toxin (PTX)-sensitive. PTX is an exotoxin produced by the bacterium *Bordetella pertussis* and belongs to the A/B toxin family. From their name, A/B toxins consist of two parts; "A" and "B". "A" consists of one subunit called S1, while "B" consists of 4 subunits; S2 – S5. "A" behaves as an ADP-ribosyltransferase, whereas "B" responsible for the receptor–binding [161-163]. The mode of action of PTX involves the inhibition of the activity of Gα inhibitory ($G_i\alpha$)-subunit. The inhibition occurs by binding the "B" part of the toxin to the cellular receptor followed by the transfer of the S1 subunit to the cytosol. S1

catalyses the hydrolysis of the oxidized form of NADH, the NAD, present in the cytosol followed by the addition of the released ADP-ribose to the cysteine residue at the C-terminal of the $G_i\alpha$-subunit. This leads to a blocking of the $G_i\alpha$ subunit from exchanging its GDP with GTP, thus rendering the $G_i\alpha$ subunit in an inactive state and it uncouples from the receptor [161, 163, 164]. This uncoupling inactivates the signalling pathways induced by the GPCR [161, 163, 164] (figure 4.4).

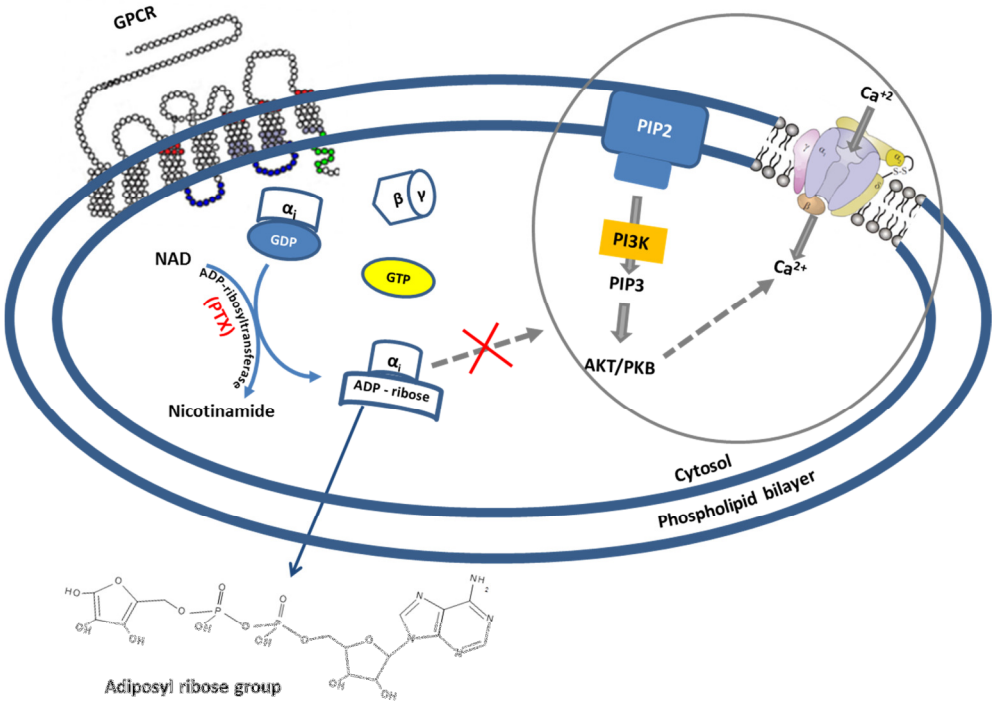

Figure 4.4: Inactivation of $G_i\alpha$ subunit by PTX treatment. ADP-ribosyltransferase of PTX catalyses the transfer of ADP-ribose from NAD to the $G_i\alpha$-subunit. This makes it unable to couple with both the receptor and the $G\beta\gamma$ complex, thus no signalling pathways are activated.

As shown previously in Chapter 3, DHT was able to induce Ca^{2+} influx in PC3 cells, thus it was hypothesized in this chapter that the mechanisms of Ca^{2+} influx in PC3 cells in response to palcar includes the activation of PTX-sensitive GPCR followed by the activation of L-type Ca^{2+} channel. In this Chapter, the mechanism of Ca^{2+} influx in response to palcar was compared to that of DHT.

4.2. Aims

– To investigate the mechanism by which palcar induces Ca^{2+} influx in PC3 cells via the activation of GPCR and L-type Ca^{2+} channel.

– To compare the mechanism of palcar-induced Ca^{2+} influx with that of DHT.

4.3. Materials and methods

4.3.1. Measuring Ca^{2+} influx through L-type Ca^{2+} channels

PC3 cells were seeded in 10cm dishes and when the growth reached 70% confluence, cells were harvested, counted (as described in Chapter 3, section 3.3.5.2) and incubated for 1 hour for trypsin recovery, then loaded with 2.5µM FURA-2AM (as described in Chapter 3, section 3.3.5.3) for a further 45 minutes at 37°C and 5% CO_2.

During the incubation period, nifedipine stock solution (50mM) was freshly prepared in DMSO in an opaque vial. After incubating for 45 minutes, the cell suspension was centrifuged at 1500 rpm for 3 minutes to remove the excess FURA. The cell pellet was washed and re-suspended with HAMS media supplemented with 10% FCS. The cell suspension ($1x10^6$ cells/ml) was then seeded in black 96-well culture plate with clear bottom followed by incubation with 1mM nifedipine for 5 minutes at room temperature before injection with the test compound. Nifedipine selectively binds to the α_1 subunit of the L-type Ca2+ channel in the inactive mode (zero mode), in which the channel is close, and thus interfering with the gating machinery of the channel and prevent it opening, therefore rendering the channel in the inactive state [140].

Since nifedipine is extremely photosensitive, it was applied to the cells in the plate away from light. DMSO, palcar, histamine or DHT were prepared at the start of the experiment as described in Chapter 3 (section 3.3.5.5) and applied in the cell suspension after 50 seconds to give a final concentration of 50, 20 or 1µM palcar, histamine or DHT, respectively. The fluorescence ratio of excitation at both 340 and 380nm (detected at 510nm) was measured, as described in chapter 3 (section 3.3.6), for 5 minutes and used to reflect the change in $[Ca^{2+}]_i$.

4.3.2. Measuring Ca^{2+} influx through PTX-sensitive GPCR

PC3 cells were seeded in 10cm dishes and when the growth reached 70% confluence, they were incubated with 200ng/ml PTX for 24 hour at 37°C and 5% CO_2. The stock solution of PTX was prepared by dissolving the content of the vial (50µg) in 500µl of buffer solution consisting of 100mM sodium phosphate and 500mM sodium chloride (pH 7.0). After 24 hours of PTX incubation, the cells were harvested and the cell suspension was loaded with 2.5µM FURA-2AM for 45

minutes at 37°C and 5% CO_2. During the incubation time, DMSO, palcar, histamine and DHT were prepared as described in Chapter 3 (section 3.3.5.5). The cell suspension was centrifuged and the cell pellet washed, re-suspended with HAMS media supplemented with 10% FCS and seeded ($1x10^6$ cells/ml) in black 96-well culture plate with clear bottom. Then, DMSO, palcar, histamine or DHT was applied to the cells to a final concentration of 50, 20 or 1µM palcar, histamine or DHT, respectively. The fluorescence ratio was measured for period of 5 minutes as described in chapter 3 (section 3.3.6).

4.3.3. Measuring Ca^{2+} influx through PI3K pathway

PC3 cells were seeded in 10cm dishes and when the growth reached 70% confluence, they were harvested as described in section 4.3.1. During trypsin recovery, the cell suspension was incubated with 50µM PI3K inhibitor (LY294002) for 1 hour at 37°C and 5% CO_2. After incubation, the cell suspension was treated with 10% FBS supplemented-HAMS media containing 2.5µM FURA-2AM and 50µM PI3K inhibitor and incubated for 45 minutes at 37°C and 5%CO_2. Then, the cell suspension was centrifuged and the cell pellet was washed, re-suspended with HAMS media supplemented with 10% FBS containing 50µM PI3K inhibitor and seeded ($1x10^6$ cells/ml) in black 96-well culture plate with clear bottom. Cells were then injected, after 50 seconds, with DMSO, palcar, histamine or DHT to a final concentration of 50, 20 or 1µM palcar, histamine or DHT, respectively. The fluorescence ratio was measured for 5 minutes as described in chapter 3 (section 3.3.6).

4.3.4. Constitutive gene expression of GPCRs

The gene expression of GPCRs was obtained from a microarray analysis of PC3, DU145, PNT1A and RWPE1 cells (experiment performed by Melchini and Sivapalan at the Institute of Food Research). Briefly, cells were cultured until 70% confluence and total RNA was extracted using the RNeasy mini kit (Qiagen) as described in Chapter 3 (section 3.3.4.2). The quantity and quality of RNA was determined using RNA 1000 Nanodrop (Agilent Technologies) as described in Chapter 3 (section 3.3.4.3). The analysis of the gene expression of these cells was performed as previously reported [165]. DMSO-treated cells were considered for comparing the baseline gene expression between all cell lines and were filtered for the expression of GPCRs. This was performed by extracting the $\log_2$ expression of all the GPCRs genes present in the Affymatrix human exon 1.0 ST array. There were 103 GPCRs genes out of a total of 18708 genes measured.

4.3.5. Measuring protein expression

4.3.5.1. Extraction of total cell proteins using RIPA lysis buffer

4.3.5.1.1. Background

Total cell proteins were extracted using radio immuno precipitation assay (RIPA) lysis buffer. This buffer lyses the cell membrane by the aid of sodium dodecyl sulphate (SDS) and sodium deoxycholate (DOC) contained within the buffer. SDS is an anionic denaturing detergent that disrupts membranes by breaking protein-protein interactions. The presence of DOC also assists in the process of disrupting and dissociating protein interactions. Once the lysis was started, the resulting polypeptides are susceptible to degradation; therefore, a protease inhibitor is added to inhibit the cellular proteases.

4.3.5.1.2. Extracting total cell proteins

Prostate non-cancerous PNT1A and BPH-1, and cancerous DU145 and PC3 cells were seeded in 6-well culture plates and when the growth reached 70% confluence, the plates were placed on ice after removing the media and washed twice with cold PBS (1x). Ice-cold lysis RIPA buffer (50µl) containing 4% SDS, 0.5% DOC and protease inhibitor (Roche tablet) was added to each well and left for approximately 2 minutes on ice. The cells were then scraped off the wells whilst still on ice using a plastic cell scraper. The cells lysates were pooled and gently transferred into pre-cooled micro-centrifuge tubes. The tubes were then vortexed for 20 seconds three times. The cells lysates were centrifuged for 13000rpm for 10 minutes at 4°C and the supernatants, which represent the total cell protein, were quantified using bicinchoninic acid (BCA) protein assay kit (Cat # BCA1 AND B9643, Sigma-Aldrich, UK). The protein lysates were stored at -20°C for further analysis.

4.3.5.2. Extraction of cell membrane proteins using transmembrane protein extraction kit

4.3.5.2.1. Background

Membrane proteins were extracted using ProteoExtract® Transmembrane Protein Extraction kit. The principle of using this kit relies on the use of a detergent free chemical reaction. This reaction consist of two steps: first, the cells are permeabilized with an extraction buffer that contain protease inhibitor to

protect the proteins from degradation once the lyses started, followed by centrifugation to remove the soluble protein leaving the insoluble proteins contained within the lipid bilayer. Second, membrane proteins are extracted from the lipid bilayer using transmembrane solubilising reagent. Using this kit has many advantages; it minimizes the potential protein loss that may results from severe vortexing, sonication or incubation at high temperatures that is used in other procedure for extracting membrane proteins.

4.3.5.2.2. Extracting membrane proteins

PNT1A, BPH-1, DU145 and PC3 cells were seeded in 6-well culture plates. When growth reached 70% confluence, plates were placed on ice and washed with twice with PBS (1x). Then, membrane proteins were isolated using ProteoExtract Transmembrane Protein Extraction Kit (Cat # 71772, Millipore LTD, UK) following the manufacturer's protocol (diagram 4.1). The protein concentration of both soluble and membrane fractions were determined immediately after extraction using the BCA protein assay kit (Sigma-Aldrich).

Diagram 4.1: Steps of protein separation using ProteoExtract® Transmembrane Protein Extraction kit.

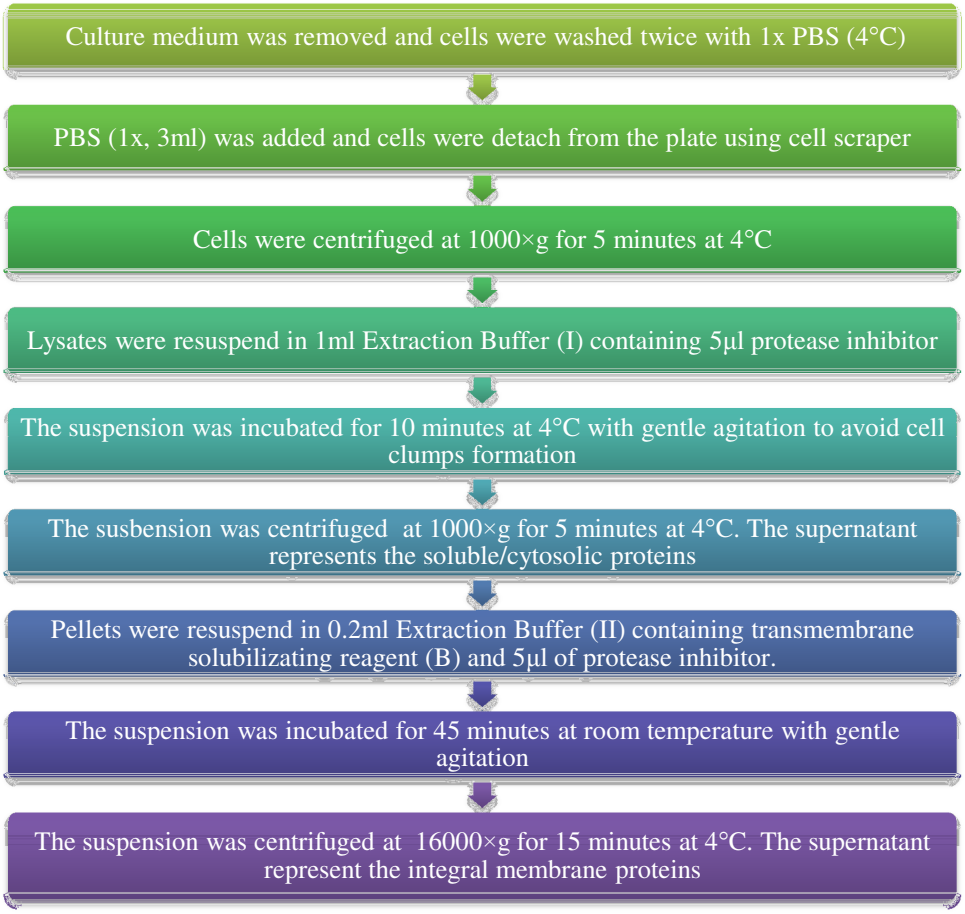

4.3.5.3. Quantifying protein concentrations using Bicinchoninic Acid (BCA)

4.3.5.3.1. Background

The principle of BCA assay depends on first, the formation of a Cu^{2+}–protein complex under alkaline conditions and second, the reaction of cuprous ion (Cu^{1+}) with the BCA reagent. In the first reaction, the peptide bond in a protein reduces the cupric ion (Cu^{2+}) in the cupric sulphate reagent into cuprous ion (Cu^{1+}). The amount of reduction is proportional to the amount of protein present in the sample. In the second reaction, the BCA reagent reacts with the resultant Cu^{1+} to form a stable purple–blue complex. The protein present in a sample can then be monitored by measuring the absorbance of the purple–blue complex and amount of protein can be calculated using a standard curve.

4.3.5.3.2. Determination of protein levels using BCA

The assay was performed by diluting the protein lysates into 1:6 using sodium phosphate buffer. Then, in a 96-well plate containing 200µl BCA reagent, 25µl of the diluted protein extract was added in duplicate. The plate was incubated at 37°C for 30 minutes and the absorbance of each sample was measured at 562nm using FLUROstar optima plate reader (BMG labtech). The amount of the protein was calculated using a standard curve of 0–1000µg/ml bovine serum albumin.

4.3.5.4. Measuring protein expression of $G_i\alpha 2$ subunit

Total cell protein lysates (40µg) from each PNT1A, BPH-1, DU145 and PC3 cells were prepared by mixing with sample loading buffer (Cat # NP0007, Invitrogen, UK) and reducing agent (Cat # NP0004, Invitrogen, UK) followed by denaturing at 70C° for 10 minutes. Protein lysates were then separated, under reducing conditions, onto 10% SDS-poly acrylamide gel electrophoresis (PAGE) in running buffer (Cat # NP0001, Invitrogen, UK) containing NuPAGE antioxidant (Cat # NP0005, Invitrogen, UK). MagicMark protein ladder (Cat # LC5602, Invitrogen, life technologies, UK) was loaded to determine the molecular weight of the protein on the gel. Gels were run for 50 minutes at 200V using the XCell SureLock system.

Proteins were then transferred into nitrocellulose membranes (Cat # 162-0112, BIO RAD, UK) using NuPAGE transfer buffer (Cat # NP00061, Invitrogen, UK) containing 10% methanol and 0.1% antioxidant. The transfer was run at 30V

for 60 minutes. Then the membrane was washed with 1x Tris buffer saline Tween20 (TBST) solution firstly for 5 minutes, secondly for 15 minutes and finally for another 5 minutes replacing the TBST each time. The membrane was then blocked for 1 hour in 10ml 5% skim milk in 1x TBST at room temperature with gentle agitation. Then the membrane was washed with 1x TBST solution as above and incubated overnight with gentle agitation at 4°C with primary rabbit anti-G protein alpha inhibitor 2 antibody (Cat # ab20392, Abcam LTD, UK), 1:500. The membrane was washed with 1x TBST as above and incubated with gentle agitation for 1 hour at room temperature with secondary anti-rabbit IgG horseradish peroxidase (HRP) linked antibody (Cat # 70745, New England Biolabs LTD, UK), 1:1000. The membrane was then washed with 1x TBST solution as above. Skimmed milk powder (5%) dissolved in 1x TBST was used to dilute the antibodies.

GAPDH was used as a loading control and was detected with primary GAPDH mouse monoclonal antibody (Cat # AM4300, Life Technologies LTD Invitrogen, UK) (1:1000) and secondary anti-mouse IgG HRP linked antibody (Cat # 7076S, Cell signalling, UK).

4.3.5.5. Measuring protein expression of GPCRs

Membrane proteins (30µg) from each PNT1A, BPH-1, DU145 and PC3 cells were prepared, separated on 10% SDS-PAGE gel and then transferred onto nitrocellulose membranes as described in section 4.3.5.4. After washing and blocking the membranes as described in section 4.3.5.4, GPR110, GPR87 and GPRC6A were detected using rabbit anti-GPR110 antibody (Cat # ab75306) (1:500), rabbit anti-GPR87 (Cat # ab77517) (1:500) and rabbit anti-GPRC6A (Cat # ab96504) (1:500), respectively. These antibodies were purchased from Abcam LTD, UK and were diluted as described in section 4.3.5.4. The membrane was incubated overnight with the primary antibody with gentle agitation at 4°C. Anti-rabbit IgG, HRP linked antibody (1:1000) was used as a secondary antibody.

Integrin β-1 protein was used as a loading control and was detected with primary rabbit anti-integrin β-1 antibody (Cat # 4706S, New England Biolabs LTD, UK), 1:500, and anti-rabbit IgG, HRP linked antibody was used as a secondary antibody. Protein was visualised using chemiluminescent substrate as described in next section 4.3.5.6.

4.3.5.6. Immunodetection

The Immunodetection was performed using chemiluminescent substrate working solution from SuperSignal West Pico Chemiluminescent Substrate (Cat # 34080, thermo scientific, USA) prepared by mixing 2ml of reagent A with 2ml of reagent B. The membranes were then incubated with the working solution for 5 minutes in the dark with gentle agitation. The HRP conjugated on the secondary antibody catalyses the oxidative degradation of the chemiluminescent substrate to produce light emitting luminescence molecule. The fluorescence intensity was then measured using Fluor-S MultiImager (Biorad Laboratories) and the protein bands were quantified using Quantity One software (Biorad Laboratories). The quantification of the protein bands is based on band density (volume) and the levels of the quantified protein were given as the percentage (%) of adjusted volume.

For re-probing of the membranes, the previous antibodies were stripped for 40 minutes at room temperature with gentle agitation using RestoreTM Western blot stripping buffer (Cat # 21059, thermo scientific, USA).

4.3.6. Statistical analysis

All experiments were repeated three times. Statistical analysis of the kinetic measurement of Ca^{2+} influx was performed with a mixed effect model using GenStat software 16th Edition. A mixed effect model was performed when the baseline levels of Ca^{2+} were approximately the same in all samples injected with different treatments in one experiment. When the baseline levels were not the same between the different treatments injections, the ratio of fluorescence was corrected to the baseline levels of each treatment injection and the data plotted represent the means ± SD of three independent experiments. In order to compare effect of one treatment on the corrected means of different treatment injections, statistical analyses were performed with one way ANOVA followed by Tukey's multiple comparison test.

To compare the quantified protein levels of GPR110, GPR87 and GPRC6A between the different cell lines, statistical analysis was performed using one way ANOVA followed by Tukey's multiple comparison test.

All statistical analysis performed with one way ANOVA followed by Tukey's multiple comparison test were accomplished by using GraphPad Prism

version 5.00 for Windows (GraphPad Software, San Diego California USA, www.graphpad.com).

4.4. Results

4.4.1. Ca^{2+} influx through L-type Ca^{2+} channels

4.4.1.1. Palcar

Palcar (50µM) induced Ca^{2+} influx in PC3 cells, but to a lesser extent than 20µM histamine, the positive control (figure 4.5A). Treatment with 1mM nifedipine for 5 minutes significantly blocked the influx of Ca^{2+} in cells injected, at 50 seconds, with both 50µM palcar and 20µM histamine (P=0.033 and P=0.016, respectively, figure 4.5A).

Because the baseline levels of Ca^{2+} varied between the different samples injected with different treatments in one experiment, the fluorescence ratios were corrected to the baseline levels. Correction was performed by subtracting the value of fluorescence ratio at maximum Ca^{2+} influx, which was observed at 80 seconds of treatment injection, from that of the baseline level at 50 seconds for each sample. Figure 4.5B illustrates the corrected ratios of fluorescence and is used to demonstrate the significant inhibitory effect of nifedipine on Ca^{2+} influx in response to both palcar and histamine.

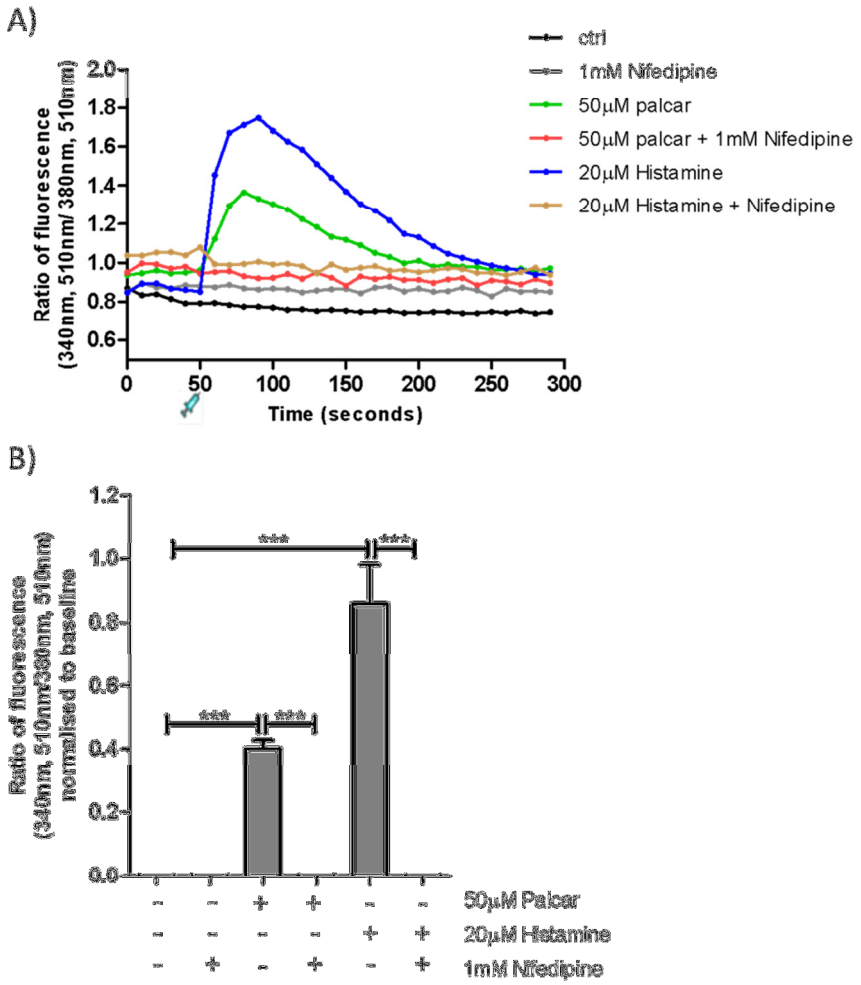

Figure 4.5: Palcar-induced Ca^{2+} influx in PC3 cells through L-type Ca^{2+} channels. Cell suspension was loaded with 2.5µM FURA-2AM for 45 minutes at 37°C and 5% CO_2 prior to treatment with 1mM Nifedipine for 5 minutes. The ratio of fluorescence emitted at 510nm and excited at both 340 & 380nm indicate $[Ca^{2+}]_i$. A) Both nifedipine treated and untreated cells were injected with DMSO, palcar or histamine at 50 seconds. B) Corrected ratio of fluorescence. Data represent means ± SD of three independent experiments. Statistical analysis was performed with mixed effect model test (A) and one way ANOVA followed by Tukey's post-test (B). Pre-treatment with 1mM nifedipine blocked Ca^{2+} influx in response to both palcar and histamine injections compared to nifedipine-untreated cells; P=0.033, P= 0.016, respectively (A). *** $P \leq 0.001$ (B).

4.4.1.2. DHT

In a separate experiment, 1mM nifedipine was also shown to block Ca^{2+} influx in response to 1µM DHT (figure 4.6A). The levels of Ca^{2+} influx in nifedipine-treated cells injected with 1µM DHT were significantly ($P \leq 0.001$) different from the levels of Ca^{2+} influx in nifedipine-untreated cells (figure 4.6B).

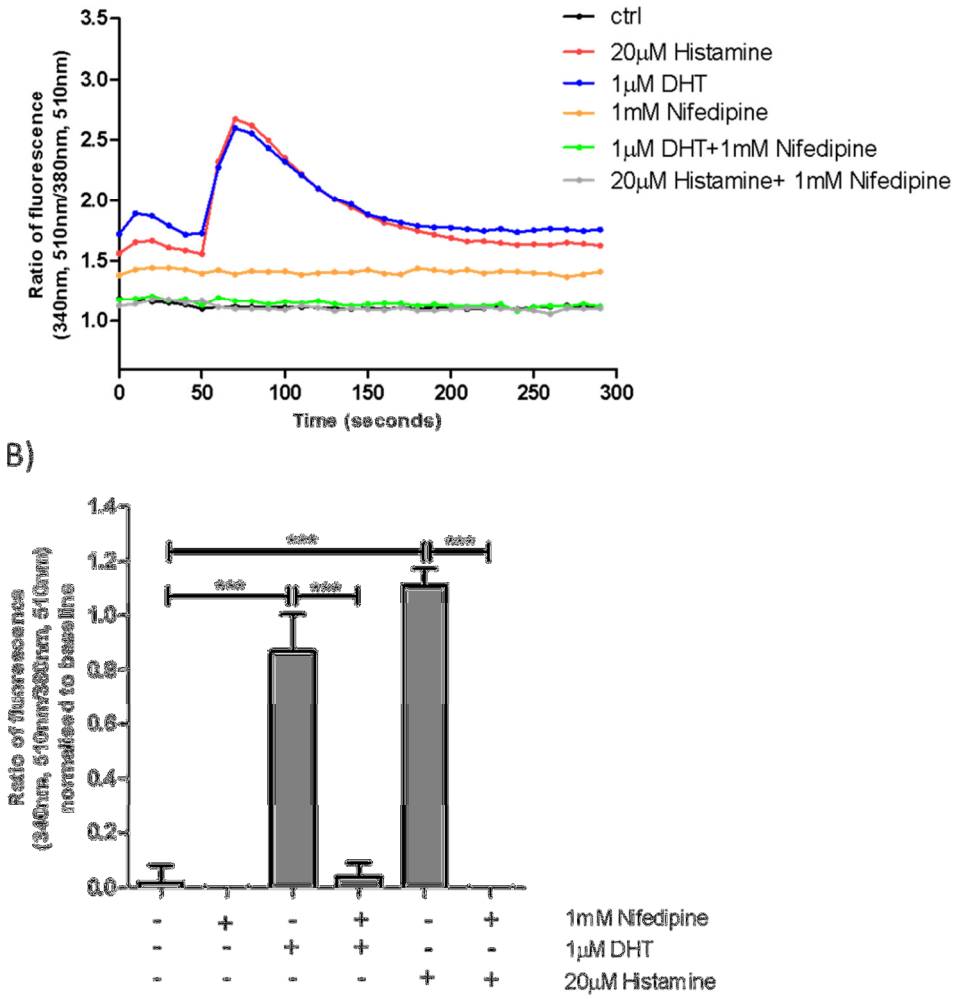

Figure 4.6: DHT-induced Ca^{2+} influx through L-type Ca^{2+} channels. PC3 cells suspension was loaded with 2.5µM FURA-2AM for 45 minutes at 37°C and 5% CO_2 prior to treatment with 1mM Nifedipine for 5 minutes at 37°C. The ratio of fluorescence emitted at 510nm and excited at both 340 & 380nm indicate $[Ca^{2+}]_i$. A) Both nifedipine-treated and untreated cells were injected with DMSO, DHT or histamine at 50 seconds. B) Corrected ratios of fluorescence. Data represent means ± SD of three independent experiments. Statistical analysis in B was performed with one way ANOVA followed by Tukey's post-test. Pre-treatment with 1mM nifedipine blocked Ca^{2+} influx in response to both DHT and histamine injection compared to nifedipine-untreated cells, *** P≤0.001.

4.4.2. Ca^{2+} influx through PTX-sensitive GPCRs

4.4.2.1. Palcar

PTX treatment was unable to block or reduce Ca^{2+} influx in response to 50µM palcar injection at 50 seconds (figure 4.7A, P>0.05; figure 4.7B). In contrast, PTX treatment significantly reduced the levels of Ca^{2+} influx in response to 20µM histamine (P≤0.05, figure 4.7B).

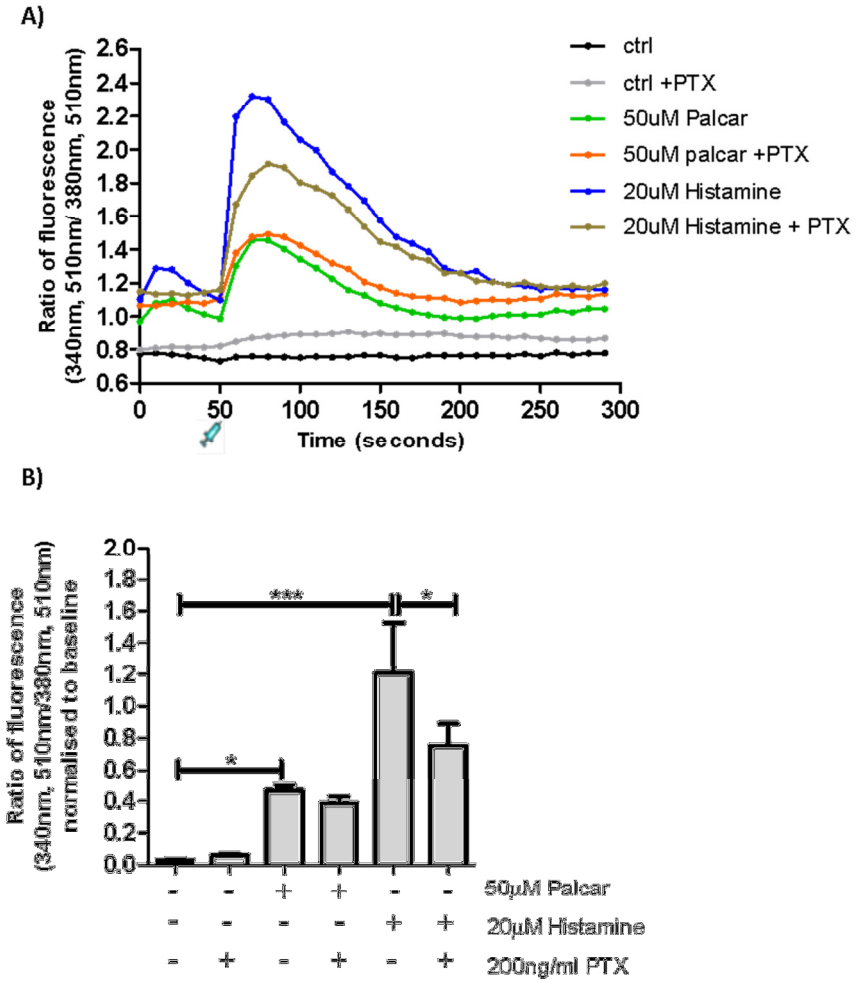

Figure 4.7: PTX-sensitive GPCR and palcar-induced Ca^{2+} influx in PC3 cells. Cells were treated with 200ng/ml PTX for 24 hour at 37°C and 5% CO_2 and then loaded with 2.5μM FURA-2AM for 45 minutes at 37°C and 5% CO_2. The ratio of fluorescence emitted at 510nm and excited at both 340 & 380nm indicate $[Ca^{2+}]_i$. PTX-treated and untreated cells were injected with DMSO, palcar or histamine at 50 seconds. B) Corrected ratios of fluorescence. Data represent means ± SD of three independent experiments. Statistical analysis in B was performed with one way ANOVA followed by Tukey's post-test. Palcar induces Ca^{2+} influx in both PTX- treated and untreated cells, ***P≤0.001 and *P≤0.05.

4.4.2.2. Constitutive levels of $G_i\alpha 2$ protein expression

In order to investigate the involvement of $G_i\alpha$ subunit in the mechanism of Ca^{2+} influx, protein expression of $G_i\alpha 2$ subunit was determined in PNT1A, BPH-1, DU145 and PC3 cells. As Ca^{2+} influx was only observed in PC3 cells, it may suggest that the $G_i\alpha 2$ subunit is more highly expressed in PC3 cells than the other cell lines, especially as it has been shown that $G_i\alpha 2$ subunit is the predominant subunit present in PC3 cells [164]; therefore the protein expression of $G_i\alpha 2$ subunit

was measured in PNT1A, BPH-1, DU145 and PC3 cells. However, no differences in the levels of expression was observed (figure 4.8).

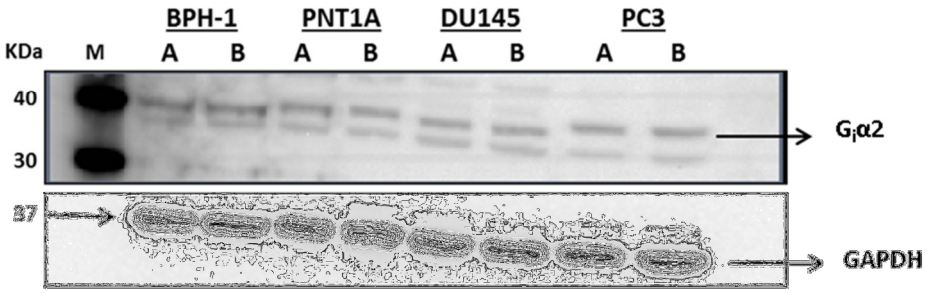

Figure 4.8: Western blot of $G_i\alpha2$ subunit expressed in PC3, DU145, PNT1A and BPH-1 cell lines. A band of 40kDa was detected in all cell lines. GAPDH was the loading control. M: Marker. The protein expression was performed in duplicates (A and B) in each cell line. This blot is a representative of three independent protein extracts.

4.4.2.3. DHT

Ca^{2+} influx through the PTX-sensitive GPCRs were also investigated in response to DHT. PTX treatment reduced the influx of Ca^{2+} in response to both DHT and histamine injection at 50 seconds (figure 4.9A). Figure 4.9B illustrate the significant effect of PTX-treatment on Ca^{2+} influx induced by both DHT ($P \leq 0.01$) and histamine ($P \leq 0.05$) injection compared to the PTX-untreated cells injected with DHT or histamine; respectively.

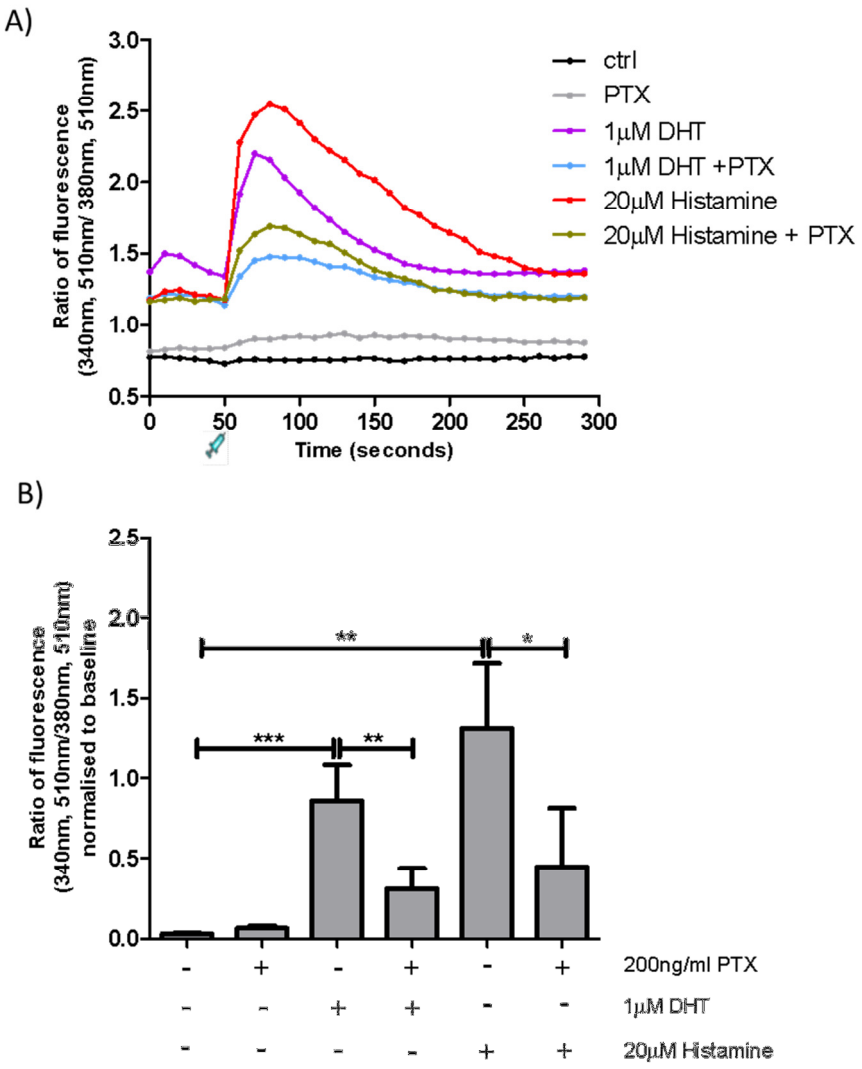

Figure 4.9: DHT-induced Ca^{2+} influx in PC3 cells through PTX-sensitive GPCR. Cells were treated with 200ng/ml PTX for 24 hour at 37°C and 5% CO_2 and then loaded with 2.5µM FURA-2AM for 45 minutes at 37°C and 5% CO_2. The ratio of fluorescence emitted at 510nm and excited at both 340 & 380nm indicate $[Ca^{2+}]_i$. PTX-treated and untreated cells were injected with DMSO, DHT or histamine after 50 seconds. B) Corrected ratios of fluorescence. Data represent means ± SD of three independent experiments. Statistical analysis in B was performed with one way ANOVA followed by Tukey's post-test. ***P≤0.001, **P≤0.01 and *P≤0.05.

4.4.3. Ca^{2+} influx through PI3K pathway

Treatment with PI3K inhibitor (LY294002) reduced the Ca^{2+} influx in response to 50µM palcar injection after 50 seconds (figure 4.10A). This reduction was significant when compared to the PI3K-uninhibited cells (P≤0.01, figure

4.10B). Treatment with PI3K inhibitor (LY294002) also significantly reduced the levels of Ca^{2+} influx in response to histamine (P≤0.05, figure 4.10B).

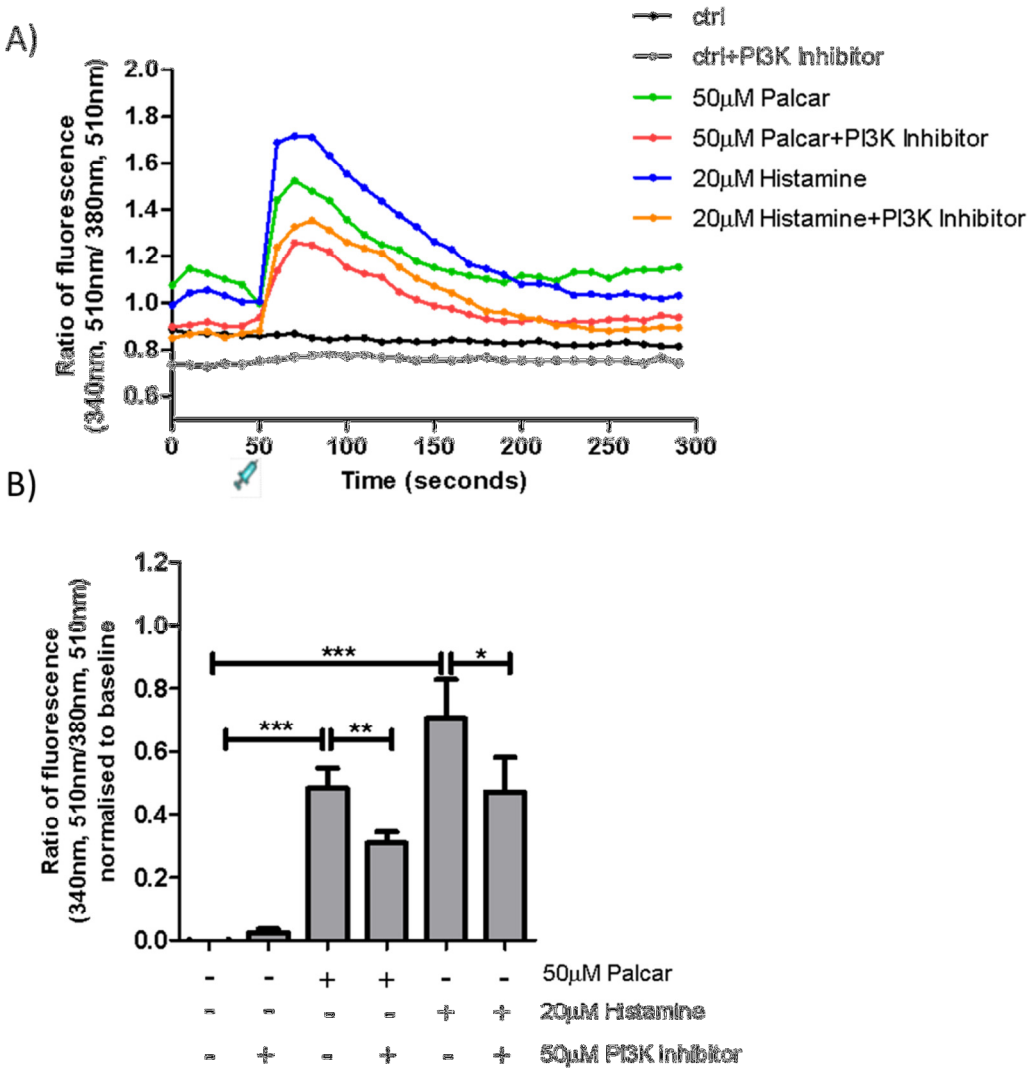

Figure 4.10: Palcar-induced Ca^{2+} influx in PI3K inhibited PC3 cells. Cell suspension was loaded with 2.5µM FURA-2AM for 45 minutes at 37°C and 5%CO_2 prior to incubation with 50µM P13K inhibitor for 1 hour at 37°C and 5% CO_2 and washed with PI3K inhibitor containing media. A) PI3K-inhibited and uninhibited cells were injected with DMSO, palcar or histamine at 50 seconds. B) Corrected ratios of fluorescence. Data represent means ± SD of three independent experiments. Statistical analysis in B was performed with one way ANOVA followed by Tukey's multiple comparison test. Treatment with PI3K inhibitor significantly reduced Ca^{2+} influx induced by both palcar and histamine compared to PI3K-uninhibited cells injected with palcar and histamine, respectively, ***P≤0.001, **P≤0.01, *P ≤0.05.

4.4.4. Constitutive gene expression of GPCRs in prostate non-cancerous and cancerous cell lines

The gene expression of GPCRs was analysed in the non-cancerous PNT1A and RWPE1, and cancerous DU145 and PC3 cells. From these data it was observed that certain GPCRs, such as GPR110, was highly expressed in PC3 cells, while others, such as GPR87 was highly expressed in PNT1A cells (figure 4.11).

When comparing the profile of the gene expression of GPCRs between PC3 and DU145 cells, certain genes were highly expressed in PC3, but not in DU145 cells (figure 4.12). The same pattern of the gene expression profile was observed when PC3 were compared to RWPE1 cells (figure 4.13).

The profile of the gene expression of GPRCs in DU145 in comparison to PNT1A cells (figure 4.14) was similar to that observed in DU145 compared to RWPE1 cells (figure 4.15).

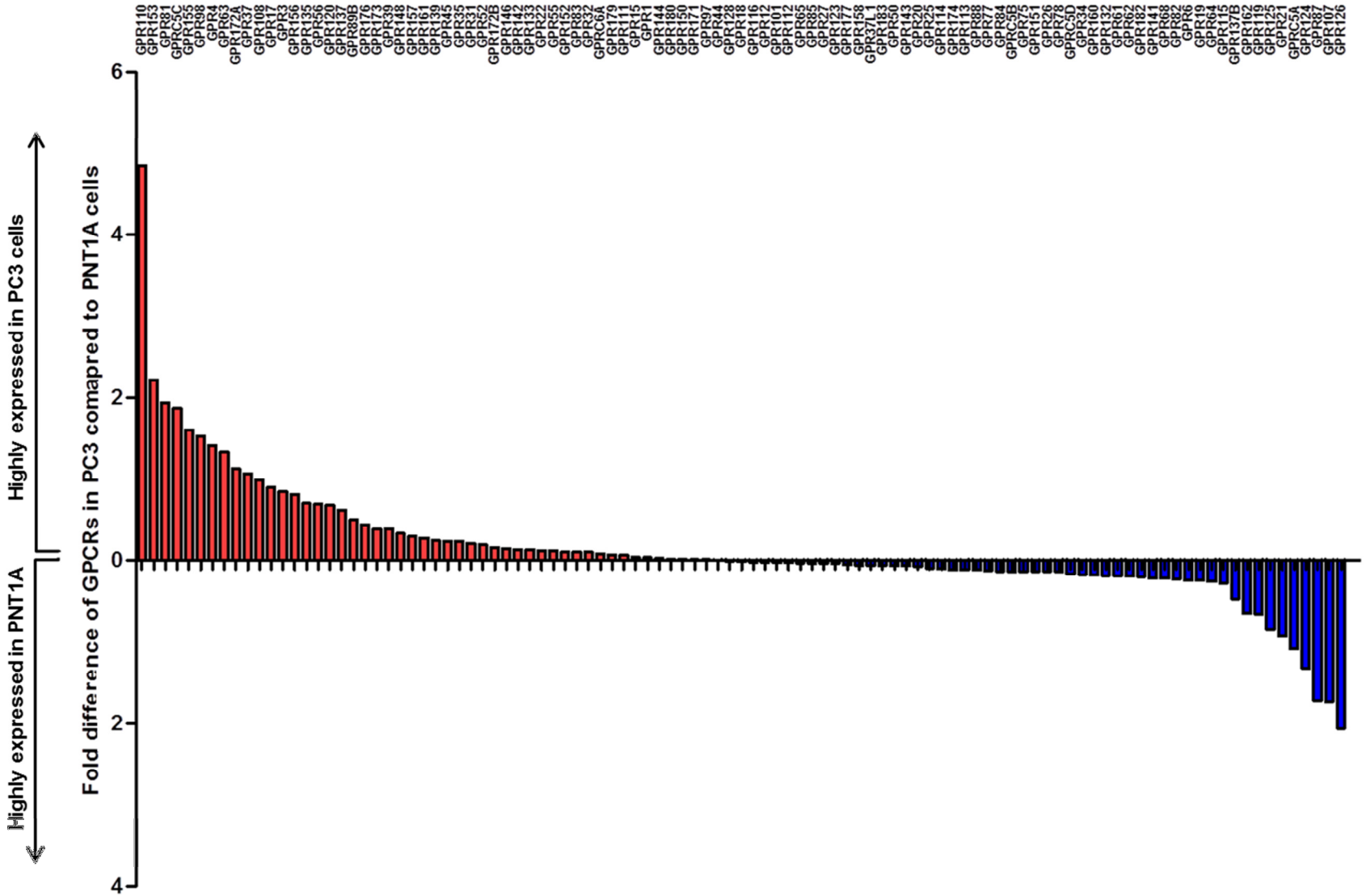

Figure 4.11: Fold difference of GPCR genes expressed in PC3 as compared to PNT1A cells. Red columns indicate genes highly expressed in PC3 as compared to PNT1A cells, whilst blue columns indicate genes highly expressed in PNT1A as compared to PC3 cells. The names of the genes are indicated at the top of the columns.

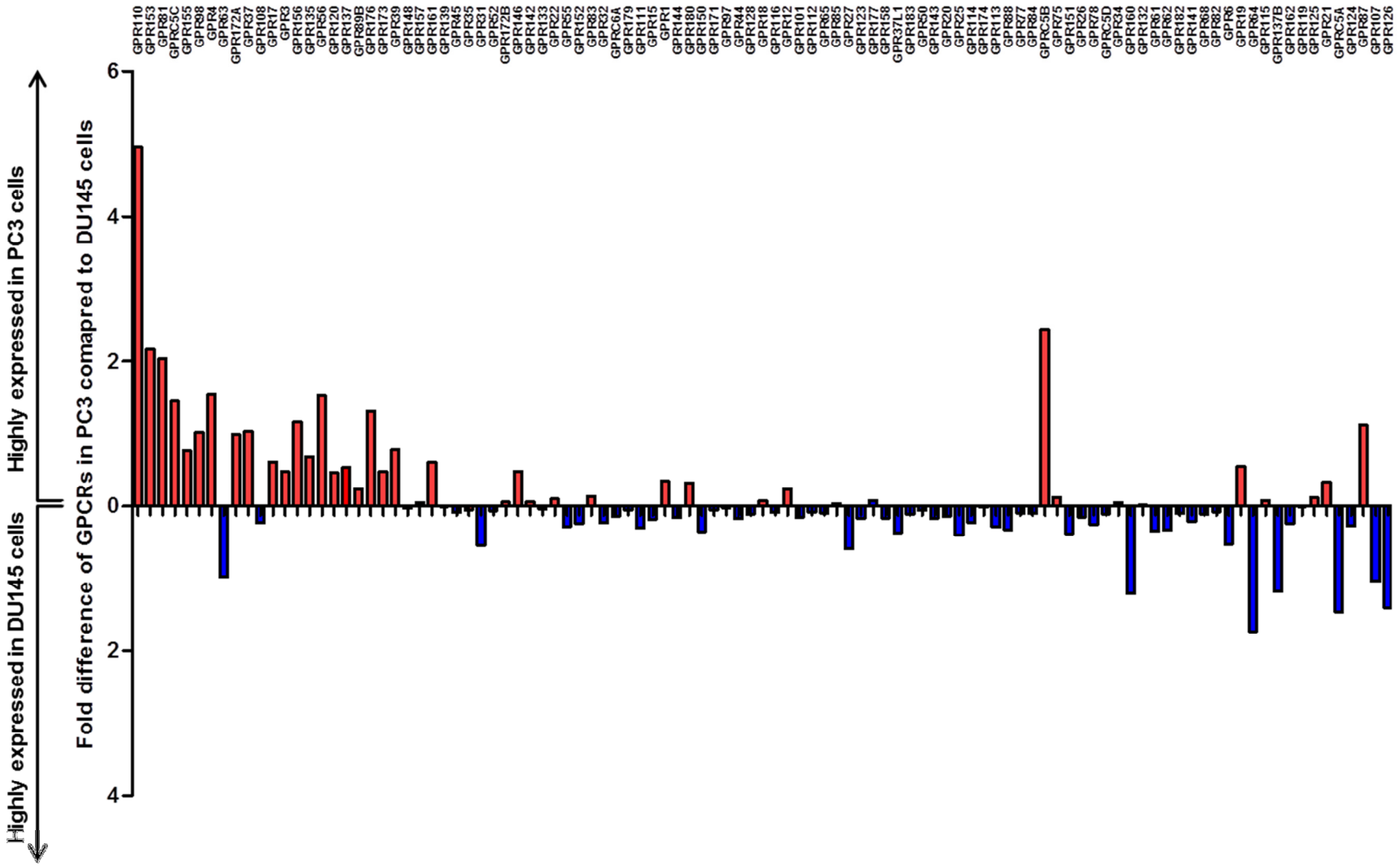

Figure 4.12: Fold difference of GPCR genes expressed in PC3 as compared to DU145 cells. Red columns indicate genes highly expressed in PC3 as compared to DU145 cells, whilst blue columns indicate genes highly expressed in DU145 as compared to PC3 cells. The names of the genes are indicated at the top of the columns.

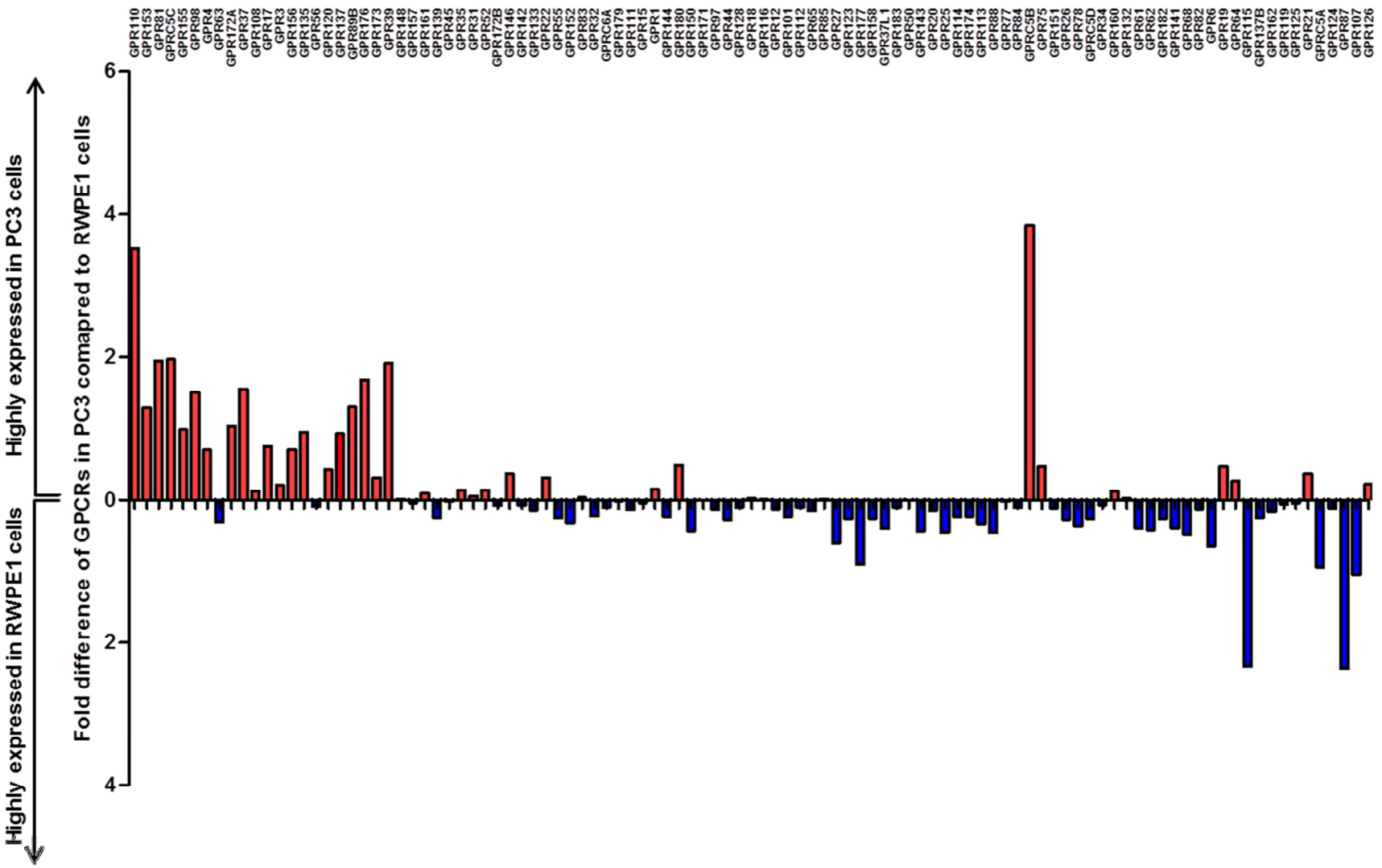

Figure 4.13: Fold difference of GPCR genes expressed in PC3 as compared to RWPE1 cells. Red columns indicate genes highly expressed in PC3 compared to RWPE1 cells, whilst blue columns indicate genes highly expressed in RWPE1 as compared to PC3 cells. The names of the genes are indicated at the top of the columns.

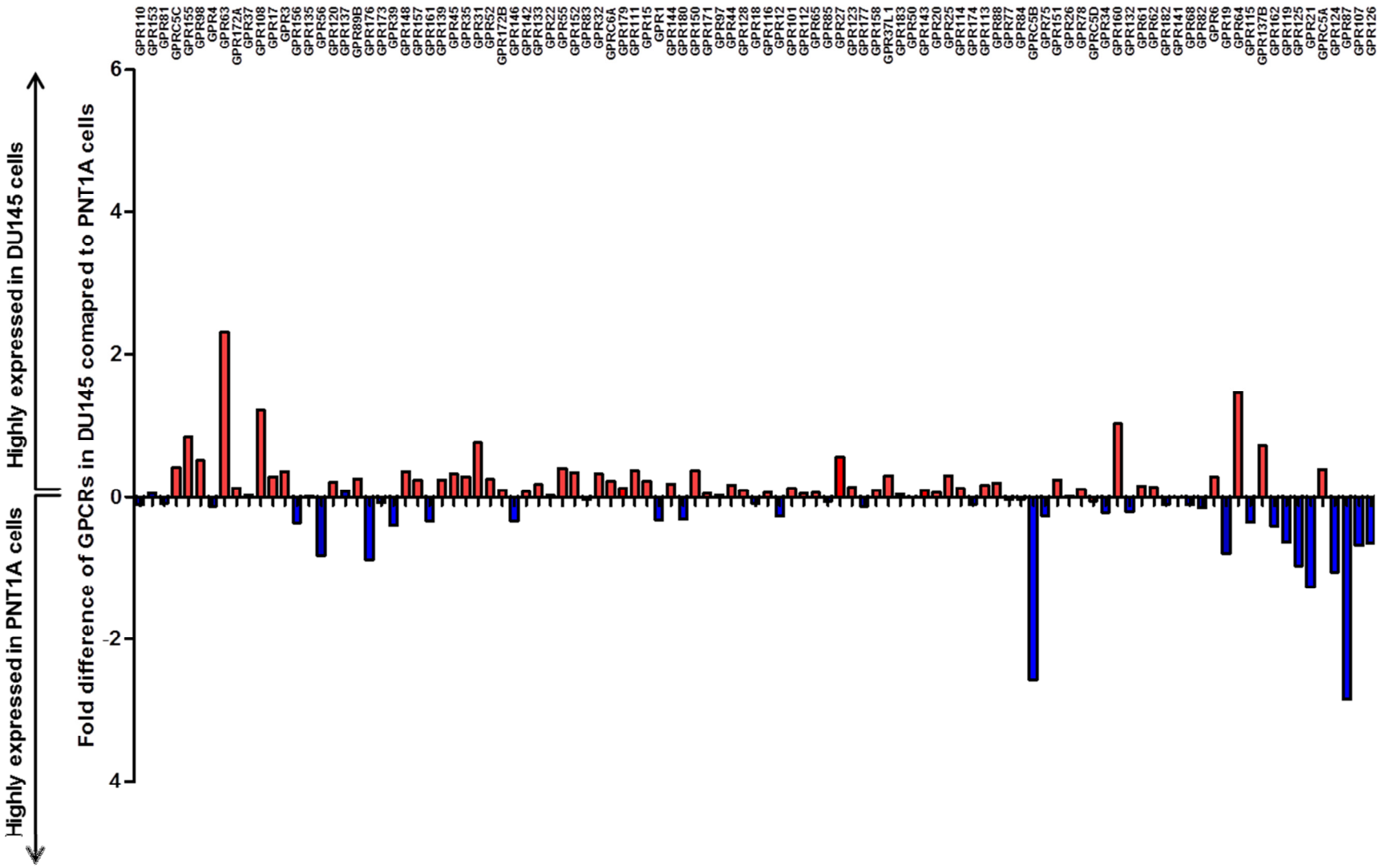

Figure 4.14: Fold difference of GPCR genes expressed in DU145 as compared to PNT1A cells. Red columns indicate genes highly expressed in DU145 as compared to PNT1A cells, whilst blue columns indicate genes highly expressed in PNT1A as compared to DU145 cells. The names of the genes are indicated at the top of the columns.

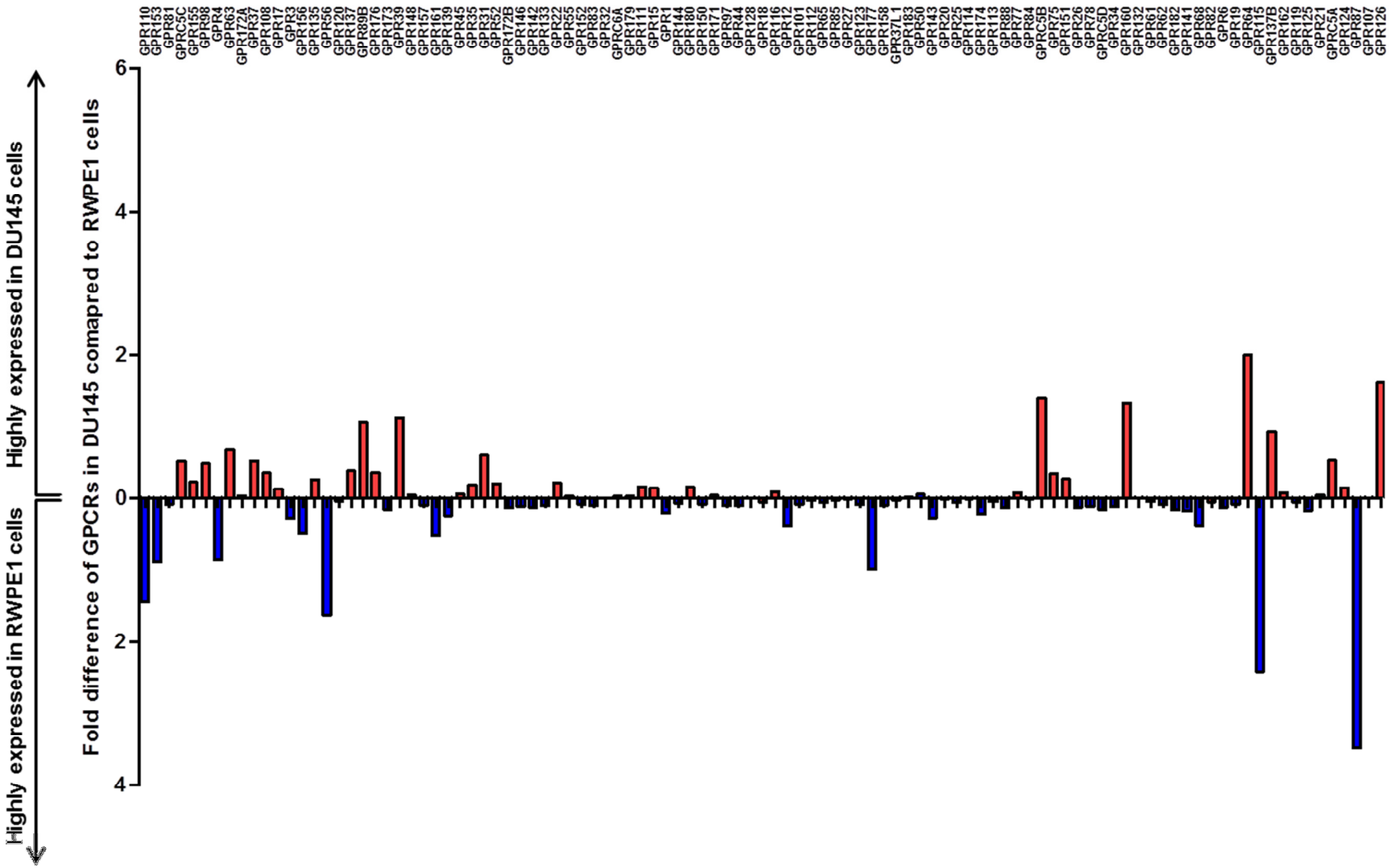

Figure 4.15: Fold difference of GPCR genes expressed in DU145 as compared to RWPE1 cells. Red columns indicate genes highly expressed in DU145 as compared to RWPE1 cells, whilst blue columns indicate genes highly expressed in RWPE1 as compared to DU145 cells. The names of the genes are indicated at the top of the columns.

4.4.5. Protein expression of GPCRs in prostate non-cancerous and cancerous cell lines

Protein expression of GPCRs; GPR110, GPR87 and GPRC6A was quantified using western blotting in PNT1A, BPH-1, DU145 and PC3 cells.

GPR110 protein (approximately 100kDa) was detected in the membrane protein fraction of the PC3 cells and had higher levels of expression as compared to PNT1A and BPH-1 cells, but was not detected in the cancerous DU145 cells (figure 4.16A). The number of protein bands detected for the loading control integrin β-1 varied with the different cell lines investigated. In BPH-1 cells, one strong protein band (120kDa) was detected as compared to PC3, DU145 and PNT1A cells, in which two bands (100 and 120kDa) were detected.

The protein expression of GPR87 (approximately 41kDa) and GPRC6A (approximately 95kDa) were detected in the membrane fractions of PNT1A, BPH-1, DU145 and PC3 cells (figure 4.12B and C, respectively). In DU145 cells, GPRC6A was less expressed as compared to the other investigated cell lines (figure 4.16C). The protein bands of GPR110, GPR87 and GPRC6A detected by western blot were quantified and presented as the percentage (%) of adjusted volume of each protein in each cell line (figure 4.16D). In PC3 cells, GPR110 was significantly ($P \leq 0.001$) more expressed when compared to GPR87 and GPRC6A, and more highly expressed than in the other investigated cell lines.

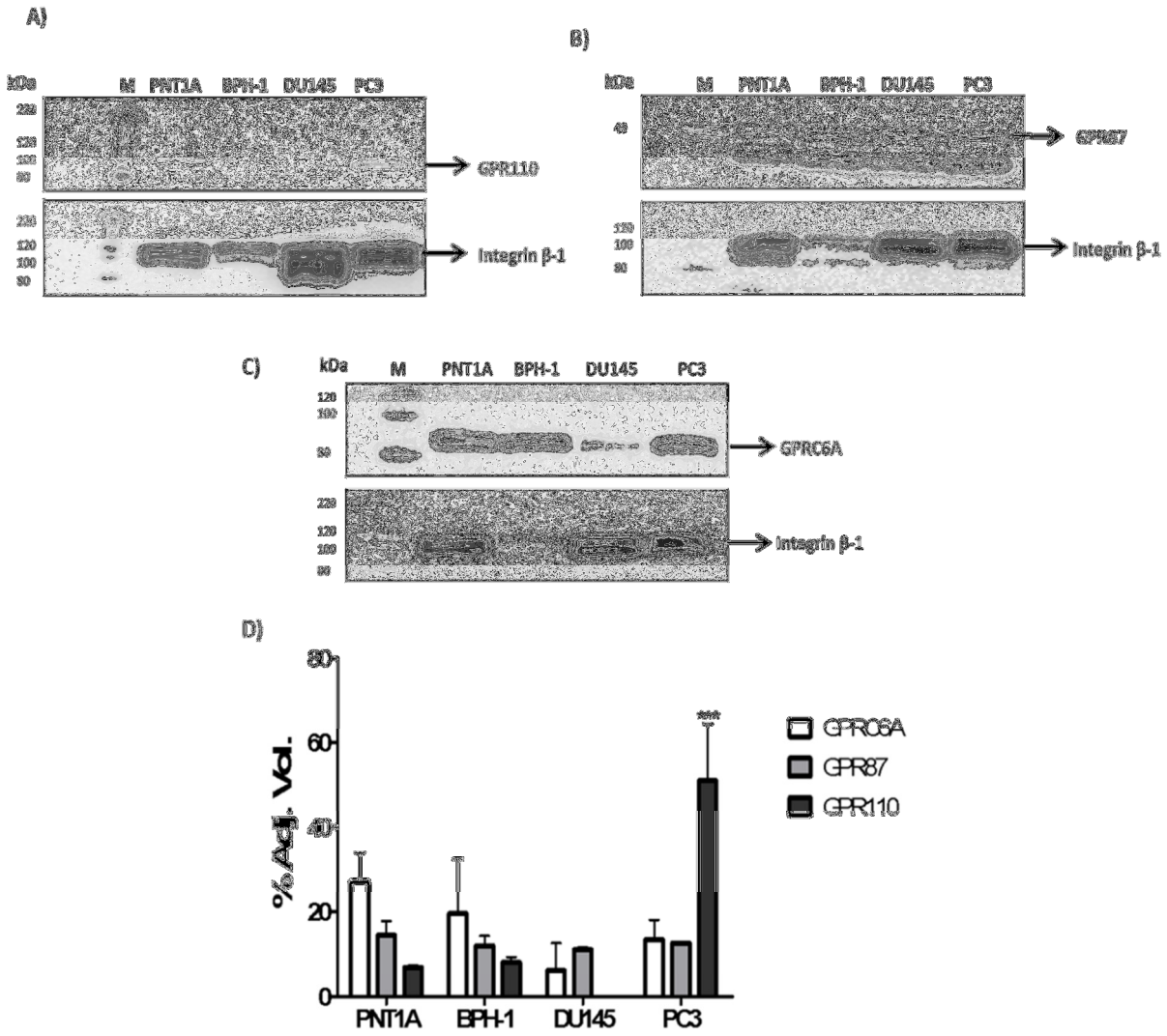

Figure 4.16: Protein expression of GPR110, GPR87 and GPRC6A in PNT1A, BPH-1, DU145 and PC3 cells. A) GPR110 is more highly expressed in PC3 cells than PNT1A and BPH-1, and not detected in DU145 cells. B) GPR87 was equally expressed in all cell lines tested. C) GPRC6A is expressed equally in PNT1A, BPH-1, PC3 cells and to lesser extend in DU145 cells. D) Protein quantification of GPR110, GPR87 and GPRC6A in PNT1A, BPH-1, DU145 and PC3 cells. These data are representative of three independent experiments. Statistical analysis was performed using one way ANOVA in each cell line followed by Tukey's multiple comparison test, ***P≤0.001.

4.5. Discussion

In this study, the mechanism by which palcar induces Ca^{2+} influx in PC3 cells was studied and was compared with that induced by DHT. The mechanism by which palcar induced Ca^{2+} influx was different from that induced by DHT and involve the stimulation of L-type Ca^{2+} channels, but not the activation of PTX-sensitive GPCRs. Also this influx was partly due to the activation of PI3K pathway. In contrast, DHT induced Ca^{2+} influx through the activation of PTX-sensitive GPCRs, which stimulate the L-type Ca^{2+} channels.

The mechanism by which DHT induces Ca^{2+} influx has previously been investigated in prostate androgen–dependent LNCaP cells [45] and implicated the involvement of PTX–sensitive GPCR. Since both DHT and palcar are lipid-related compounds and both PC3 and LNCaP cells are prostate cancerous cell-models, it was hypothesized that palcar may act through the same mechanism as DHT and therefore palcar activate PTX-sensitive GPCR, which then stimulate L-type Ca^{2+} channel. However, the results support the null hypothesis that palcar and DHT do not act through the same mechanism.

The mechanism of Ca^{2+} influx in PC3 cells was investigated by using three different inhibitors; nifedipine, PTX and PI3K inhibitor (LY294002). Ca^{2+} influx was then investigated in response to palcar, histamine (the positive control) and DHT. Table 4.1 summarise the findings of these treatments.

Table 4.1: Summary of the effect of different inhibitors on Ca^{2+} influx induced by palcar, histamine and DHT in PC3 cells.

Treatment	Nifedipine	PTX	PI3K inhibitor (LY294002)
Palcar	Blocked	No effect	Reduced
Histamine	Blocked	Reduced	Reduced
DHT	Blocked	Reduced	Not determined

In contrast to palcar the role of PI3K pathway was not investigated in response to DHT. Palcar-induced activation of PI3K pathway was studied to investigate the presence of a possible link between the activation of L-type Ca^{2+} channels and the GPCR, which would confirm the involvement of GPCR in the mechanism of palcar action and that the Ca^{2+} influx was not solely due to the activation of L-type Ca^{2+} channels. In contrast, the mechanism induced by DHT was clearer in that the involvement of GPCR was confirmed.

4.5.1. Activation of L-type Ca^{2+} channels

The investigation of the mechanism of Ca^{2+} influx started first by exploring the role of L-type Ca^{2+} channels since these channels are responsible for the majority of Ca^{2+} influx in most cells. This was performed by inhibiting the channels with 1mM nifedipine. Nifedipine is an L-type Ca^{2+} channel antagonist that blocks the entry of Ca^{2+} through the pore forming subunit; α_1-subunit [140]. The inability of each palcar, DHT and histamine to induce Ca^{2+} influx in nifedipine-treated cells suggests that the Ca^{2+} influx was via the activation of L-type Ca^{2+} channels (figure 4.5 and 4.6).

It was noticed that the levels of Ca^{2+} influx in response to histamine were higher than the levels induced by palcar (figure 4.5) suggesting that histamine is able to induce Ca^{2+} influx from the exterior of the cells, in addition to the release of Ca^{2+} from stores. Blocking Ca^{2+} influx by nifedipine suggests that histamine-induced Ca^{2+} influx was mostly due to the activation of L-type Ca^{2+} channels. The activation of these channels may stimulate a signalling pathway that induces the release of Ca^{2+} from stores.

Histamine was reported as a ligand for H1 [166] and H4 [167] receptors, in which their activation causes the stimulation of PLC, which catalyses the production of IP_3 and DAG from PIP_2. IP_3 can act as a key for the release of Ca^{2+} from Ca^{2+} stores [166, 167]. It has been found that the released Ca^{2+} along with DAG can activate PKA, which is involved in phosphorylating the L-type Ca^{2+} channel allowing the influx of Ca^{2+} into the cells [168].

The variation of the baseline levels of Ca^{2+} observed in figure 4.5 can be attributed to the time difference when the samples were injected with the different treatments, which is one of the drawbacks of using the plate reader for measuring Ca^{2+} influx. Despite the increase in the baseline levels, the ratio of fluorescence that indicate the change in $[Ca^{2+}]_i$ was not altered after injecting the cell suspension with histamine or palcar, which indicates that nifedipine blocked the Ca^{2+} influx.

4.5.2. PTX-sensitive GPCRs

Since L-type Ca^{2+} channels can be an effector protein for the activation of GPCRs, the effect of palcar on GPCR activation was investigated. This was achieved using 2.5µM FURA-2AM loaded PC3 cells treated with 200ng/ml PTX for 24 hours. The results showed that 50µM palcar induced an increase in Ca^{2+} influx in PTX-treated cells to the same degree as non PTX-treated cells (figure

4.7A) suggesting that in PC3 cells palcar-induced Ca^{2+} influx was not mediated via PTX-sensitive GPCR.

PTX treatment, nevertheless, significantly reduces the levels of Ca^{2+} influx in response to histamine compared to the non PTX-treated cells (figure 4.7B), which confirms the validity of the PTX stock solution used in the experiment. Since PTX treatment is only specific for the $G_i\alpha$ that can bind to the receptor, the insensitivity of palcar to the PTX treatment implies that $G_i\alpha$ was not involved in the mechanism of palcar-induced Ca^{2+} influx and that the downstream signalling pathways of $G_i\alpha$ subunit, such as PLC, would also be not involved in palcar–induced Ca^{2+} influx. This is supported by a work performed in prostate cancerous LNCaP cells, where it has been shown that the activation of PLC was not involved in changing the levels of Ca^{2+} influx and blocking the activity of PLC did not alter $[Ca^{2+}]_i$, thus the intracellular Ca^{2+} stores were not involved in changing the $[Ca^{2+}]_i$ [45]. Moreover, palcar was found to inhibit the activation of PKC purified from mouse brain, which is a downstream protein for the PLC [151]. It has also been shown that palcar does not activate PKC in rabbit aortic endothelial cells [136]. These observations support that the mechanism by which palcar induces Ca^{2+} influx in PC3 cells do not involve PLC.

The un-involvement of $G_i\alpha$ in the mechanism of action was confirmed by investigating the protein expression of $G_i\alpha$ in the four cell lines; PC3, DU145, PNT1A and BPH-1 cells, in which the Ca^{2+} influx was only observed in PC3 cells (Chapter 3). It was hypothesised that in PC3 cells the $G_i\alpha$ is overexpressed compared to the other cell lines. However, the western blot findings in figure 4.8 indicate that there were no differences in the protein expression of the $G_i\alpha$ subunit between the cell lines; the lack of involvement of $G_i\alpha$ subunit in the palcar mediated mechanism of Ca^{2+} influx is thus supported.

Since $G_i\alpha$ is only one type of the other $G\alpha$ subunit that can bind to the receptor and that palcar mode of action did not involve $G_i\alpha$, the mechanism of palcar action in PC3 cells may involve the recruitment of a different $G\alpha$ subunit, other than $G_i\alpha$, to bind with the receptor.

PTX treatment has a different effect in response to histamine; it significantly reduced the Ca^{2+} influx in PC3 cells (figure 4.7), suggesting that histamine induced Ca^{2+} influx observed via the activation of L-type Ca^{2+} channels was as a result of the activation of PTX-sensitive GPCRs.

Histamine-induced Ca^{2+} influx in PC3 cells agrees with that induced in human leukaemia and mast cells, in which histamine induces its effect via PTX-sensitive way through the activation of $G_i\alpha$ subunit [167], which has been linked to PLC [166, 167]. In contrast, histamine has been found to induce Ca^{2+} influx in bovine adrenal cells in a PTX-insensitive way through the activation of G_q subunit that is linked to PLC [169].

In this study presented in this thesis, the signalling pathway that link the activation of PTX-sensitive GPCRs and L-type Ca^{2+} channels in PC3 cells was not explored, thus need further investigations and may involve the activation of PLC.

The link between the activation of PLC and the Ca^{2+} released from stores may explain the high levels of Ca^{2+} influx induced by histamine compared to palcar.

In regards to DHT, PTX treatment significantly reduced the Ca^{2+} influx in PC3 cells (figure 4.9), which was similar to the effect of histamine, but not palcar, suggesting that DHT induced Ca^{2+} influx via the PTX-sensitive GPCRs and which support null hypothesis that palcar induces Ca^{2+} influx in a manner different from DHT.

The ability of DHT to induce Ca^{2+} influx via the activation of L-type Ca^{2+} channels and PTX-sensitive GPCR agrees with that of LNCaP cells from Sun *et al* study [45], in which DHT was able to induce Ca^{2+} influx following the same mechanism of activating L-type Ca^{2+} channels and PTX-sensitive GPCRs.

4.5.3. Activation of PI3K pathway in response to palcar and histamine

The PI3K pathway is a significant pathway in PC3 cells, since it has been found that the expression of PTEN, which negatively regulates PI3K pathway, is non-functional in PC3 cells in contrast to PNT1A and BPH-1 cells [170], therefore resulting in PI3K signalling being more dominant in PC3 cells [118]. Activation of the PI3K pathway has been found to activate L-type Ca^{2+} channels. Therefore, the PI3K pathway may play an important role in Ca^{2+} influx in PC3 cells.

To investigate the involvement of PI3K pathway, PC3 cells were treated with 50µM PI3K inhibitor (LY294002) for 1 hour. It has been shown that 1 hour treatment with 50µM PI3K inhibitor (LY294002) is able to completely inhibits the phosphorylation of AKT, which is also known as PKB, by PI3K enzyme in PC3 and PNT1A cells [165]. Other studies also show that using PI3K inhibitor

(LY294002) at 50µM inhibit the increase in $[Ca^{2+}]_i$, [171, 172]. The results of the work performed in this chapter regarding the role of PI3K pathway in Ca^{2+} influx showed that PI3K inhibitor (LY294002) reduced the levels of Ca^{2+} influx in response to palcar injection suggesting that the PI3K pathway was partly responsible for palcar-induced Ca^{2+} influx in PC3 cells (figure 4.10). Similar results were also found in response to histamine (figure 4.10), which indicate that the PI3K pathway may be partly responsible for linking the activation of PTX-sensitive GPCRs with the L-type Ca^{2+} channels.

Figure 4.17 illustrates the proposed mechanism for the Ca^{2+} influx in PC3 cells and the role of the PI3K pathway. The proposed mechanism includes the activation of GPCR by palmitoylation, which recruit G-proteins to bind the receptor. The receptor then activates the Gα subunit, regardless its subfamily, to exchange its GDP with GTP and dissociate from the Gβγ complex. The dissociated Gβγ complex can phosphorylate, and thus activate PI3K, which subsequently phosphorylates the β subunit of the L-type Ca^{2+} channel, activating the channel, and allowing the entrance of Ca^{2+}.

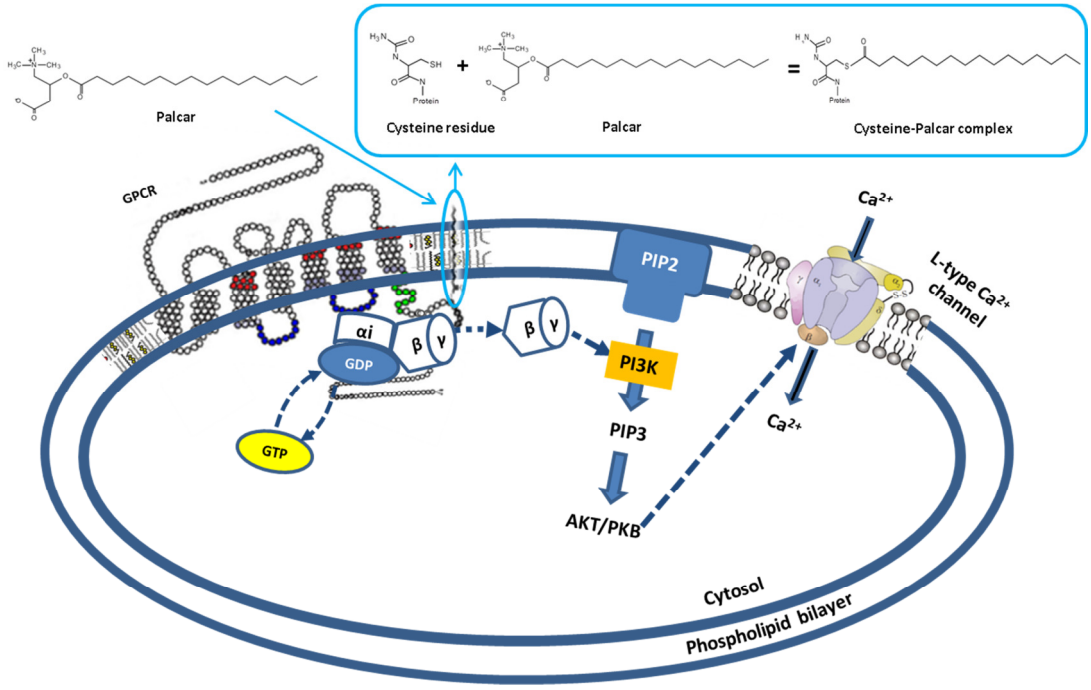

Figure 4.17: A schematic representation for the hypothesis of Ca^{2+} influx through GPCR, PI3K pathway and L-type Ca^{2+} channel in response to palcar. The presence of palcar induces the recruitment of G-proteins to bind to the GPCR. The $G_i\alpha$ subunit exchanges its GDP with GTP and dissociates from both the receptor and Gβγ complex. The Gβγ complex activates the PI3K pathway, which subsequently phosphorylates the β-subunit of the L-type Ca^{2+} channel and opens the channel for Ca^{2+} influx.

4.5.4. Protein expression of GPCRs

The stimulation of L-type Ca^{2+} channels in PC3 cells in response to palcar could be as a result of the activation of GPCR. PTX-sensitive GPCR was not involved in the mechanism; however other GPCRs may be involved.

GPCRs are large group of receptors and there might be a number of GPCRs on which palcar could act. Recently, lipids and lipid derivatives have been found to be possible ligands for several orphan GPCRs. Palcar is a lipid derivative compound and therefore might be a possible ligand for these receptors. In order to find GPCR candidates, the constitutive expression of numerous genes obtained by microarray analysis, performed in PC3, DU145, PNT1A and RWPE1cells, were filtered for GPCRs gene expression. The fold difference of the gene expression of all the GPCRs detected in all cell lines were plotted (figure 4.11, 4.12, 4.13, 4.14 and 4.15). The results show that GPCRs were differently expressed between PC3, DU145, PNT1A and RWPE1 cells.

There were certain GPCRs genes that were highly expressed in PC3 compared to PNT1A (figure 4.11), DU145 (figure 4.12) and RWPE1 cells (figure 4.13). In DU145 cells, the profile of the GPCRs were similar to that in PNT1A (figure 4.14) and RWPE1 (figure 4.15) cells. These results suggest that although DU145 cells are a metastatic cancerous cell line, the similarities in its GPCRs gene expression with PNT1A and RWPE1 may explain why DU145 cells have a similar response to that of PNT1A cells to palcar in regards the Ca^{2+} influx.

Based on the results of the profile of the GPCRs gene expression in PC3, DU145 and PNT1A cells, three candidate GPCRs were selected to measure the levels of their protein expression; these were GPR110, a GPCR that was highly expressed in PC3 as compared to PNT1A and DU145 cells, GPR87, a GPCR that was highly expressed in PNT1A compared to DU145 and PC3 cells, and finally GPRC6A, a GPCR that was equally expressed between all the cell lines. GPRC6A was selected to confirm the validity of the microarray data since the levels of gene expression did not necessarily imply the same levels of protein expression.

GPR107 and GPR126 were two genes that were highly expressed in PNT1A cells in comparison to PC3 cells. However, an association between the receptors encode by these two genes and Ca^{2+} influx has not been reported, therefore they were not selected for further protein quantification.

GPRC6A was one of the genes that were equally expressed between all the cell lines. Therefore, GPRC6A was selected for investigating the protein expression.

GPR87 was linked to the increase in $[Ca^{2+}]_i$ in response to LPA [173]. This receptor was expressed in mouse normal tissue of placenta, ovary, testis, prostate, brain, and skeletal muscle [173].

GPRC6A was also linked to the increase in $[Ca^{2+}]_i$ in response to amino acids in intestinal GLUTag cells via the activation of G_q protein, which activates PLC and increases $[Ca^{2+}]_i$ through IP_3-mediated release from the ER [174].

The immunoblotting with the appropriate antibodies in the work performed in this chapter revealed that GPR110 protein was most abundantly expressed in PC3 cells as compared to the other cell lines giving a band of approximately 100kDa (figure 4.16A). Also, the results showed that the protein expression of GPR110 was not detected in DU145 cell line. Although the microarray analysis performed in this study showed that GPR110 was expressed in very low levels in DU145 cells (figure 4.14), previous RT-PCR gene expression work has shown that this gene is absent in DU145 cells [175].

The findings of this chapter showed that GPR87 protein expression was equally expressed by all cell lines with a band of approximately 41kDa (figure 5.16B). The equal protein expression was also observed for GPRC6A that has a band of approximately 100kDa, except in DU145 cells, which has lower expression levels (figure 4.16C).

In this work, β-integrin-1 was used as a loading control for the membrane proteins based on the findings of Lum *et al* [175]. β-integrin-1 is heterodimeric cell surface receptor that has an essential role in cell adhesion and migration, as well as in growth and survival [176, 177]. The results of the protein expression of β-integrin-1 in this chapter showed that this protein was not the best choice for a loading control. BPH-1 cells showed a weak expression of β-integrin-1 across of three independent experiments. Another reason for β-integrin-1 being a poor choice of control is on western blot of DU145 cells three bands were detected for β-integrin-1, whereas only two bands were observed in PNT1A and PC3 cells, suggesting difference in the expression of β-integrin-1 between these cell types. However, the poor loading control did not affect the evaluation of the levels of the protein expression of GPR110, GPR87 and GPRC6A, because even though the

band for the β-integrin-1 in BPH-1 cells was weak, the protein expression of GPR87 and GPRC6A in this cell line still can be observed clearly and in levels that were very close to that in PNT1A and PC3 cells.

It is important to note that another membrane protein loading control Na^+/K^+–ATPase was investigated, however the expression of this protein was weak and only observed in PC3 and DU145 cells and not in the other cell lines. There are other loading controls that could be investigated, such as β-actin, however this was not possible due to the time limitation for the completion of this thesis.

Since palcar-induced Ca^{2+} influx was only observed in PC3 cells, this indicates the involvement of a GPCR that is present in PC3, but not in PNT1A and DU145 cells. The protein expression of both GPR87 and GPRC6A in PC3, PNT1A and DU145 cells, therefore implies that both GPR87 and GPRC6A receptors are unlikely to be involved in the mechanism of Ca^{2+} influx and thus suggest that GPR110 may be the gene that is linked to the Ca^{2+} influx in these cells.

Further research is needed to investigate the link between Ca^{2+} influx and the activation of GPR110 in addition to determining whether the activation of this receptor is induced by the presence of palcar, thus provide more insights on the mechanism by which palcar act in prostate cancer.

4.6. Conclusion

In this study, palcar induced Ca^{2+} influx in PC3 cells via the activation of L-type Ca^{2+} channels, but not PTX-sensitive GPCR. Since PTX treatment is specific for the $G_i\alpha$ subunit, the PTX insensitivity of Ca^{2+} influx in response to palcar suggested that $G_i\alpha$ subunit and its associated pathways were not involved in the mechanism of Ca^{2+} influx. However, different Gα subunits, other than $G_i\alpha$ subunit, could bind to the receptor leading to the activation of L-type Ca^{2+} channel. The results of this study suggested that the mechanism also includes a partial involvement of the PI3K pathway. The PI3K pathway may provide a link between the activation of GPCR and L-type Ca^{2+} channel.

In this study, the profile of the GPCRs gene expression investigated in PC3, DU145, PNT1A and RWPE1 cells showed that GPR110 was highly expressed in PC3 as compared to the other cell lines. GPR87 was highly expressed in PNT1A as

compared to PC3 and DU145 cells, and GPRC6A was equally expressed between all the cell lines. The protein expression of these receptors showed that GPR110 was more expressed in PC3 cells as compared to PNT1A, BPH-1 and DU145 cells. In addition, GPR110 was the most abundantly expressed protein as compared to the other GPCRs in PC3 cells, which suggests that this receptor might have a role in the Ca^{2+} influx observed in PC3 cells.

Collectively, although the concentration of palcar used in this study was above the reported human physiological levels in plasma and tissue, and that the effects of palcar may be related to a stress response, the results of this study highlight the potential importance of acylcarnitines, in particular palcar, under high concentrations as a signalling molecule in prostate cancer. However, the physiological role in signalling is unclear.

In the cell-model that was used in this chapter, the induction of Ca^{2+} influx was a biological consequence of using a high concentration of palcar, therefore this may raise a question of whether palcar at lower concentrations may have any other biological consequences. The answer to this question is to be addressed in the next chapter.

Chapter 5

Effect of palmitoylcarnitine at lower concentrations

5.1. Introduction

Previously, it was shown that palcar is associated with the induction of IL-6 gene expression in prostate non-cancerous PNT1A and cancerous PC3 cells. This was thought to be related to the effect of palcar on inducing Ca^{2+} influx. Ca^{2+} influx was also induced by DHT, which is a hormone associated with prostate cancer progression. The mechanism of Ca^{2+} influx in response to both palcar and DHT was investigated in Chapter 4, and it was found that palcar induced Ca^{2+} influx in a mechanism that was different to that of DHT. However, all of these changes occur with a high concentration of palcar that was higher than the levels detected in prostate cancerous tissue quantified in Chapter 2, as well as in plasma from individuals with metabolic disorders reported in the literature (table 2.1, Chapter 2). This raised a question of whether palcar at lower concentrations would have any effect on prostate cells. Therefore, in this Chapter, the effect of lower concentrations of palcar was investigated by quantifying the global gene expression using Affymetrix Human Exon 1.0 ST arrays in non-cancerous PNT1A prostate cells treated with increasing concentrations of palcar (0-5µM) and 10nM DHT. PNT1A cell line was selected to investigate the hypothesis that palcar may be associated with the induction of genes important for cell transformation and prostate cancer progression. In this study palcar was compared to DHT in order to investigate the hypothesis that palcar may have DHT-like activities and have a role in prostate cancer progression.

Studying the induction of genes by microarrays provides a general look at the behaviour of the cells in response to a specific compound. In prostate cells, studying the effect of palcar by microarray helps identify the patterns of gene activity in response to this compound. It may detect induced genes involved in certain signalling pathways that may have a role in initiating cancer, or may indicate an induction of protein, fat or carbohydrate synthesis or oxidation. In cancer cells, the induction of such processes may indicate cell proliferation through the induction of catabolic processes to provide energy for the proliferated cells as well as the induction of anabolic processes to provide the building blocks for these newly formed cells.

Since PC3 cells represent the most metastatic form of prostate cancer, palcar effect on inducing genes in both PNT1A and PC3 cells suggest that palcar may have a role in prostate cancer progression. Therefore, the genes that were shown to be induced in response to both palcar and DHT by microarray analysis in PNT1A

cells were further quantified in PC3 cells using real time RT-PCR and compared with that in PNT1A cells.

5.2. Aims

- To investigate the effect of low concentrations of palcar on global gene expression profiles of PNT1A cells.
- To compare the effect of palcar on gene expression profiles with that of DHT.
- To compare the effect of palcar and DHT-induced gene expression in both PNT1A and PC3 cells.

5.3. Materials and methods

5.3.1. Measuring gene expression using microarray (Affymetrix Human Exon 1.0 ST Array)

5.3.1.1. Background

The Affymetrix GeneChip® Human Exon 1.0ST array is a whole-transcript-based array for the profiling of gene expression. This array queries the entire transcript and is not specific for the 3' end in contrast to the old Affymetrix array.

This array contains more than 5.5 million individual probes. Four individual perfectly matched probes form one probe set. Therefore, this array has approximately 1.4 million probe sets. Each probe set represents an exon. A group of probe sets or exons form a transcript cluster, which corresponds to a gene. Therefore, analysis at the gene level is performed by considering all the probes within a single transcript cluster. Genes may have a number of transcripts and alternative splicing may produce different transcripts.

5.3.1.2. RNA extraction, quality and quantity

PNT1A cells were seeded in 6 well plates and once the growth reached 70% confluence, cells were treated with DMSO, palcar (0.005, 0.05, 0.5 or 5μM) or 10nM DHT for 8 hours at 37°C and 5% CO_2. RNA was extracted using RNeasy Mini kit as described in Chapter 3 (section 3.3.4.2). RNA quality and quantity were checked using RNA 1000 Nanodrop (Life Technologies) as described in Chapter 3 (section 3.3.4.3). RNA samples were stored at -80°C for later use.

Quality was checked on Agilent Bioanalyser, where all samples had RNA integrity number > 8.

5.3.1.3. Analysis of gene expression

Profiling of gene expression was performed using Affymetrix GeneChip Human Exon 1.0ST Array (Affymetrix Sana Clara, CA) at Nottingham Arabidopsis Stock Centre (Nottingham, UK) following the Affymetrix protocols. Data were analysed using R/Bioconductor [178] and the *aroma.affymetrix* package [179]. The raw signal intensity data was provided in .CEL files. The data were robust multiple average (RMA) background-corrected and quantile normalised. To obtain the gene-level summaries, linear probe level models were applied to the data. For annotation, the current custom CDF file available at the aroma.affymetrix Web site containing the core probe sets (18708 transcript clusters; 284258 probe sets) was used. To identify differentially expressed genes, subsequent statistical data analysis using benjamini hochberg multiple testing correction was performed using *limma*. Genes were identified as differentially expressed at $P \leq 0.05$. To identify pathways that were the most over represented in the lists of the differentially expressed genes, functional analyses was performed using the Database for Annotation, Visualization and Integrated Discovery v6.7 (DAVID; http://david.abcc.ncifcrf.gov/) [180].

Overlapping genes between treatments were identified using the *overLapped* package in R. The number of the common genes that is expected to be induced by chance was calculated using the following equation:

$$N_{chance} = \frac{N\ genes\ in\ list\ 1 \times N\ genes\ in\ list\ (n)}{(total\ N\ genes\ )^{n-1}}$$, where

N_{chance}: number of genes that is expected to be induced by chance

N genes: number of genes

N genes list (n): number of genes induced by treatment (n) compared to control.

5.3.2. Quantification of mRNAs using real-time reverse-transcription-polymerase chain reaction (RT-PCR)

PNT1A and PC3 cells were seeded in 6 well plates until growth reached 70% confluence. To validate the microarray results, PNT1A cells were treated with

DMSO, palcar (0.005, 0.05, 0.5 and 5µM) and 10nM DHT for 8 hours at 37°C and 5% CO_2. To investigate and compare the long term exposure of palcar and DHT on gene expression between PNT1A and PC3, cells were treated with DMSO, 5µM palcar and 10nM DHT for 24 hours at 37°C and 5% CO_2. RNA was extracted from cells using RNeasy Mini kit as described in Chapter 3 (section 3.3.4.2). The quantity and quality of RNA was determined using RNA 1000 Nanodrop (Life Technologies) as described in Chapter 3 (section 3.3.4.3). The RNA samples were stored at -80°C for later use.

HK2, aldehyde dehydrogenase 1 family, member A3 (ALDH1A3) and endothelin 1 (EDN1) gene expression was measured by real time RT-PCR performed using an Applied Biosystems OneStep Plus real time RT-PCR system carried out on a microamp optical 96-well plate in a total volume of 20µl pre well, containing TaqMan 1-step RT-PCR master mix reagent kit (Applied Biosystems), 20ng total RNA, and primers and probes of HK2 [forward sequence 5'-GCATCAAGGAGAACAAAGGC-3', 500nM, reverse sequence 5'-TCTTATATGTAGACGCTTGGCAA-3', 500nM and probe 5'-FAM/ACCGTCGACCCCAATAGTAGAGCG-TAMRA/-3'], ALDH1A3 [forward sequence 5'-CTCTGGAAGGCAACCTGTG-3', 500nM, reverse sequence 5'-GGAGCAAATATGTGAAGTGGAAG-3' and probe 5'-/FAM/AGATAAGCCCGACGTGGACAAGG-TAMRA/-3'] and EDN1 [forward sequence 5'-GATGCCAATGTGCTAGCCA-3', 500nM, reverse sequence 5'-CTTATGATTATTCCAGTCTTTCTCCA-3', 500nM and probe 5'-FAM/TCTTCAGCCCTGAGTTCTTTTCCTGC-TAMRA/-3']. All were purchased from Integrated DNA Technologies, USA. Reverse transcription was performed as described in Chapter 3 (section 3.3.4.4). Reactions were carried out in triplicate and were normalized against an endogenous housekeeping gene, 18S ribosomal RNA, as described in Chapter 3 (section 3.3.4.4).

Relative quantification of the gene expression in samples was based on the relative standard curve method, where a relative standard curve is prepared by serial dilutions made form a sample containing the highest RNA concentration. Standard curves were prepared for both the samples and the endogenous gene because quantitation is normalized to the endogenous gene.

5.3.3. Effect of androgen-free environment on changing the gene expression

Since in the literature a modified medium has always been used to measure the activity of DHT in LNCaP cells, the effect of using modified media on the gene expression was investigated in PNT1A, PC3 and LNCaP cells. Cells were seeded in 6 well plates using, first, RPMI media (RPMI-1640, Cat. # R8758, sigma-aldrich) supplemented with 10% FBS until growth reached 70%. Then they were switched to modified media of phenol-free RPMI media (RPMI-1640, Cat. # 11835-063, Invitrogen) supplemented with 10% Charcoal‑stripped FBS (CS‑FBS, Cat # F6765-500ML, sigma-aldrich). The phenol-free media were used to create a steroid–free environment, whereas charcoal-treated FBS was used to eliminate the endogenous steroids. Cells were kept for 48 hours in this media and then treated with DMSO, 5µM palcar and 10nM DHT for 24 hours at 37°C and 5% CO_2. RNA was extracted using RNeasy Mini kit as described in Chapter 3 (section 3.3.4.2). The quality and quantity of RNA were checked using UV absorbance determined by RNA 1000 Nanodrop (Life Technologies) as described in Chapter 3 (section 3.3.4.3). RNA samples were then kept in -80°C for later use.

The extracted RNA was used as a template for measuring the gene expression of HK2, ALDH1A3 and EDN1 and was performed using real time RT-PCR technique as described above (section 5.3.2).

5.3.4. Statistical analysis

In the microarray, to determine whether the genes in common between palcar and DHT were changed by the effect of treatments and not by chance, the proportion of genes in common were compared to the proportion of the genes expected to be changed by chance. Proportion is defined by the number of genes expected to be changed by chance (or by both treatments) divided by the total number of genes that changed significantly by treatment. Statistical analysis of the proportion was performed by a proportion test using R version 3.0.1.

Real time RT-PCR was performed in triplicate measuring of three biological replicates of one experiment. Data were normalised against an endogenous gene and the data plotted as means ± SD. Statistical analysis was performed by one way ANOVA followed by Tukey's multiple comparison post-test using GraphPad Prism version 5.00 for Windows (GraphPad Software, San Diego California USA, www.graphpad.com). Differences were considered significant at $P \leq 0.05$.

5.4. Results

5.4.1. Affymetrix Human Exon 1.0 ST gene expression of PNT1A cells in response to palcar and DHT

The gene expression profile of PNT1A cells treated with palcar (0.005, 0.05, 0.5 or 5µM) or 10nM DHT in three biological replicates were investigated by hybridisation of RNA samples to Affymetrix Human Exon 1.0 ST arrays. A total of 18 mRNA samples collected were hybridised to the array chip. A total of 18708 genes were compared and the number of genes altered in response to palcar or DHT treatment in comparison to control is shown in table 5.1. Initial analysis by multiple testing correction revealed that there were no genes differentially expressed (P≤0.05, benjamini hochberg multiple testing correction). However, due to the large number of analysed genes, it is expected that the multiple testing corrections would be very stringent and not allow the detection of real biological changes. Therefore, the gene expression values with uncorrected P-values were further analysed (P≤0.05, moderated t-statistic) to determine whether they have any biological significance.

In order to determine whether a gene was up- or down-regulated, $\log_2$ expression ratio was extracted and the fold change was calculated as the ratio of the gene expression value in either palcar (0.005, 0.05, 0.5 or 5µM) or 10nM DHT compared to DMSO (control). Positive or negative values represent up- or down-regulated genes, respectively, in comparison to control. Table 5.1 shows the number of genes altered in response to each treatment, where the green and red colours represent the up- and down-regulated genes, respectively.

Table 5.1: Number of genes differentially expressed in PNT1A in response to palcar and DHT treatment compared to control.

P-value	Palcar				DHT
	5nM	50nM	500nM	5µM	10nM
P ≤0.05[1]	334 (213, 121)[2]	73 (42, 31)	180 (107, 73)	346 (198, 148)	605 (235, 370)
P≤0.005	30 (25, 5)	3 (2, 1)	9 (6, 3)	23 (19, 4)	66 (30, 36)

[1] P-value is calculated using moderated t-statistic.
[2] Number of genes up regulated (green) and down regulated (red).

The data in table 5.1 showed that more genes were altered in response to the highest palcar concentration (5µM) compared to the other concentrations (0.005, 0.05, 0.5µM). There were a total number of 346 genes altered in response to 5µM

palcar at P≤0.05. These genes are shown in annex I ranked in a descending order according to fold change levels.

Functional pathway analysis with DAVID was performed for the genes altered by the 5μM palcar treatment. There were four over represented pathways affected by palcar treatment at P≤0.05 (table 5.2); one of them was the glycolytic pathway, which has highest fold enrichment value along with the metabolism of xenobiotic pathway. Fold enrichment is a term that describes the degree of enrichment, for example if a pathway has a fold enrichment of 4, this means that 4 times the number of genes expected by chance within the pathway were identified. It has been proposed that a value of ≥1.5 is considered as an interesting finding [180].

Table 5.2: Functional pathway analysis after 5μM palcar treatment for 8 hours (P≤0.05) arranged according to the fold enrichment in descending order.

Pathway	# genes	P-value[1]	Fold Enrichment
Glycolysis / Gluconeogenesis	5	0.038	3.888
Metabolism of xenobiotics by cytochrome P450	5	0.038	3.888
Olfactory transduction	16	0.013	1.969
Cytokine-cytokine receptor interaction	11	0.050	1.959

[1]P value = Fisher Exact P-Value.

The total number of genes that belong to the glycolytic pathway and were altered in response to palcar treatment was 5 genes (table 5.3). The genes that were altered in the other pathways are presented in annexes II – IV with their fold change levels.

Table 5.3: Genes involved in pathway of glycolysis/gluconeogenesis affected by 5μM palcar treatment for 8 hours arranged according to the fold change in descending order.

Accession	Gene description	Gene name	Fold change	P-value
NM_000693	aldehyde dehydrogenase 1 family, member A3	ALDH1A3	1.161	0.003
NM_000189	hexokinase 2	HK2	1.156	0.040
NM_002633	phosphoglucomutase 1	PGM1	-1.133	0.049
NM_000691	aldehyde dehydrogenase 3 family, member A1	ALDH3A1	-1.148	0.025
NM_006066	aldo-keto reductase family 1, member A1 (aldehyde reductase)	AKR1A1	-1.163	0.022

Pathway analysis was also performed for the genes altered by 10nM DHT treatment. There were a total of three pathways that were significantly affected (table 5.4). Both pathways of glycolysis/gluconeogenesis and sulphur metabolism were potentially altered by DHT.

Table 5.4: Functional pathway analysis after 10nM DHT treatment for 8 hours (P≤0.05) arranged according to the fold enrichment in descending order.

Pathway	# genes	P-value	Fold Enrichment
Sulfur metabolism	3	0.076	6.42
Porphyrin and chlorophyll metabolism	5	0.037	3.891
Tyrosine metabolism	6	0.026	3.502
TGF-beta signalling pathway	9	0.019	2.657
Glycolysis / Gluconeogenesis	6	0.081	2.568

Glycolytic pathway was altered in response to palcar and potentially in response to DHT treatment. The DHT-altered genes involved in glycolytic pathway were identified in order to determine whether DHT affect the same genes that were altered by palcar. The DHT-altered genes are shown in table 5.5 and ranked according to the fold change value.

Table 5.5: Genes involved in the glycolytic / gluconeogentic pathway affected by 10nM DHT treatment for 8 hours arranged according to the fold change in descending order.

Accession	Gene title	Short name	Fold change	P-value
NM_000693	aldehyde dehydrogenase 1 family, member A3	ALDH1A3	1.257	0.0001
NM_000189	hexokinase 2	HK2	1.168	0.030
NM_000691	aldehyde dehydrogenase 3 family, member A1	ALDH3A1	-1.146	0.027
NM_002633	phosphoglucomutase 1	PGM1	-1.150	0.030
NM_004563	phosphoenolpyruvate carboxykinase 2 (mitochondrial)	PCK2	-1.166	0.044
NM_006066	aldo-keto reductase family 1, member A1 (aldehyde reductase)	AKR1A1	-1.238	0.002

ALDH1A3 and HK2 genes were up regulated in response to both palcar and DHT treatment (table 5.3 and 5.5). ALDH1A3 and HK2 have an induction of approximately 1.2 fold increase in their expression level in comparison to their control.

The genes altered in the other pathways in response to DHT are presented in annex V, VI, VII and VIII.

5.4.1.1. Genes in common between palcar and DHT

Because it was observed that the glycolytic pathway was altered by DHT and palcar treatments, and there were two genes, which belong to this pathway and altered by both treatments, the genes in common affected by all palcar concentrations (0.005, 0.05, 0.5 and 5 µM) were determined first and then the genes in common between all palcar concentrations and DHT was investigated, this is in order to answer the question of whether palcar might have DHT-like biological activities in PNT1A cells. There were a total of six genes affected by all palcar concentrations (figure 5.1); these genes are listed in table 5.6.

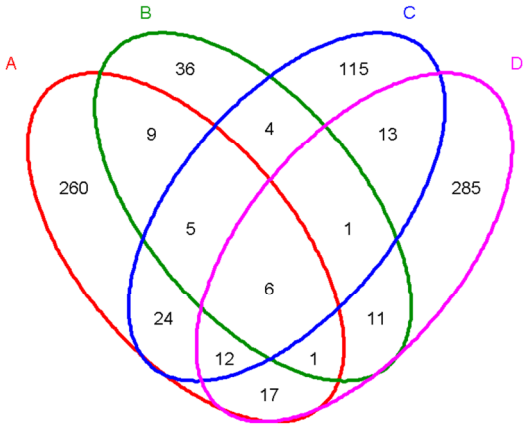

Figure 5.1: Venn diagram of the total genes in common detected across varying concentrations of palcar in PNT1A cells treated for 8 hours. A, B, C and D represent the genes changed by varying concentrations of palcar compared to control; where A: 0.005µM palcar, B: 0.05µM palcar, C: 0.5µM palcar and D: 5µM palcar.

Table 5.6: Genes in common between all palcar concentrations (0.005, 0.05, 0.5 and 5µM) arranged according to the fold change in descending order.

Accession	Gene title	Short name
NM_000693	aldehyde dehydrogenase 1 family, member A3	ALDH1A3
NM_004613	transglutaminase 2 (C polypeptide, protein-glutamine-gamma-glutamyltransferase)	TGM2
NM_005242	coagulation factor II (thrombin) receptor-like 1	F2RL1
NM_001955	endothelin 1	EDN1
NM_002068	guanine nucleotide binding protein (G protein), alpha 15 (Gq class)	GNA15
NM_174976	zinc finger, DHHC-type containing 22	ZDHHC22

When DHT was incorporated in the Venn diagram, the common number of genes across all treatments becomes five (figure 5.2). These genes are presented in table 5.7.

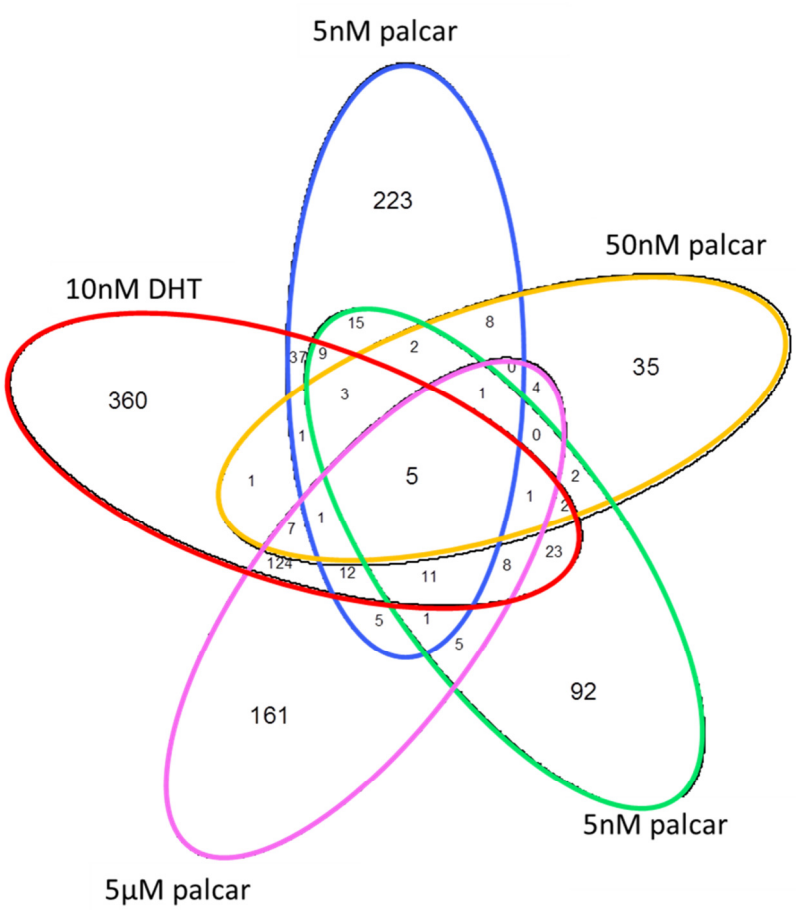

Figure 5.2: Venn diagram of the genes in common detected across varying concentrations of palcar and 10nM DHT treatment in PNT1A cells treated for 8 hours.

Table 5.7: Genes in common between palcar (0.005, 0.05, 0.5 and 5µM) and 10nM DHT treatment arranged according to the fold change in descending order.

Accession	Gene title	Short name	Fold change	P-value
NM_000693	aldehyde dehydrogenase 1 family, member A3	ALDH1A3	1.257	6.0E-05
NM_004613	transglutaminase 2 (C polypeptide, protein-glutamine-gamma-glutamyltransferase)	TGM2	1.219	0.001
NM_005242	coagulation factor II (thrombin) receptor-like 1	F2RL1	1.207	0.007
NM_002068	guanine nucleotide binding protein (G protein), alpha 15 (Gq class)	GNA15	1.118	0.028
NM_174976	zinc finger, DHHC-type containing 22	ZDHHC22	-1.322	0.001

The genes that were induced by all palcar concentrations and DHT belong to different pathways and thus have different functions. TGM2 is a gene that encodes for the production of the protein transglutaminase 2. This protein has a role in the modification of other proteins by forming an inter- or intramolecular bond that is highly resistant to proteolysis. This reaction is Ca^{2+} dependent. Forming such a bond is important for cell adhesion, which is essential in cancer development. Moreover, TMG2 has a role in GTP-binding/hydrolysing process [181].

Since this gene was induced by both DHT and palcar, the functions of this gene may provide more insights into the role of DHT in prostate cells, which include its mediatory effect in the deamination of the glutamate to form α-ketoglutarate, which is important for the TCA cycle. Also the induction of TGM2 means the formation of a proteolysis-resistant bond between proteins, which is as mentioned earlier is a requirement for cell adhesion. This may indicate the mediatory role of both DHT and palcar in cancer development. In addition, the role of TGM2 in the GTP-binding/hydrolysing process might provide information about the role of DHT and palcar in the activation of GPCR.

EDN1 is a gene that encodes for the production of preproendothelin-1, which can be proteolytically converted into endothelin 1 [182]. This protein is released by endothelial cells and behaves as a vasoconstrictor; therefore it was associated with hypertension. This gene has been found to be involved in many diseases, such as CVD, reproductive, and renal diseases in addition to cancer [183]. Moreover, this gene has been found to have a role in controlling the blood flow in the epididymis, which is necessary for the movement of the sperms [184]. Gene orthology revealed that this gene can be activated as a consequence of stimulating NFκB and HIF-1–dependant pathways.

The other gene that was induced by all palcar concentrations and DHT is F2RL1. It is a gene that encodes the production of coagulation factor II (thrombin) receptor-like 1, also known as GPR11 and PAR2, thus it is a member of the GPCR family and the protease-activated receptor family. It is involved in the inflammatory pathways and has a role in the sensory system, in which it acts as a sensor for proteolytic enzymes generated during infection [185]. The induction of this gene, therefore, indicates that both palcar and DHT might be involved in inflammatory responses in the prostate cells.

GNA15 was induced by all palcar concentrations. It is the gene that encodes for G protein, alpha 15 (Gq class). This GPCR is activated in response to

nuerotransmitters and hormones. The activation of this receptor stimulates the dissociation of $G\alpha_q$ subunit, which is able to activate PLC. The latter stimulates the release of Ca^{2+} from Ca^{2+} stores via IP_3 and does not involve the activation of L-type Ca^{2+} channels [186]. Because L-type Ca^{2+} channels are not involved in the mode of action of GNA15, the possibility of the contribution of GNA15 to the mechanism of action induced by palcar was not considered. However, it can be involved in the mechanism by which DHT induces Ca^{2+} influx since the levels of DHT-induced Ca^{2+} influx (shown in Chapter 3, figure 3.19 B and C) was higher than that induced by palcar, which indicate the involvement of the Ca^{2+} stores in DHT mechanism of action.

The last gene that was induced by all palcar concentrations is the zinc finger DHHC-type containing 22 (ZDHHC22) gene. Gene ontology annotations related to this gene revealed that this gene has transferase activity and is involved in transferring acyl groups [187]. This role of the gene may indicate a possible role in transferring the acyl group from palcar to the GPCR and also has a role in transferring palcar into the mitochondrial matrix for β-oxidation.

The genes overlapped between each individual palcar concentration and DHT was investigated and illustrated in figure 5.3. There were a total of 79, 21, 62 and 196 genes common between DHT and 0.005, 0.05, 0.5 and 5μM palcar, respectively (figure 5.3A).

The number of the common genes that are expected to be induced by chance is illustrated in the table in figure 5.3B. It is clear that the number of the genes induced by treatment was significantly higher than the number of genes that could be induced by chance, which indicate that this effect was due to the treatment in and not by chance.

The largest number of common genes was between 5μM palcar and 10nM DHT, which were 169 genes. These genes are listed annex IX.

A)

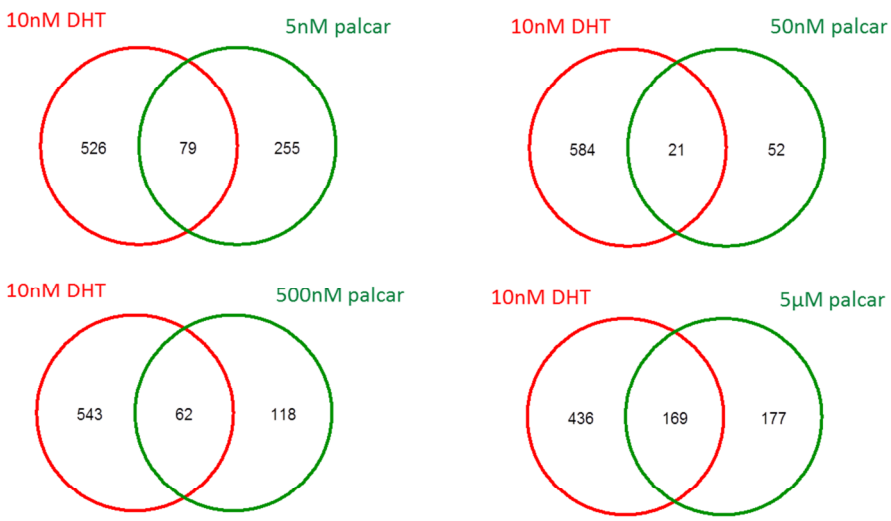

B)

Treatment	# genes expected to be induced by chance	# genes induced by treatment (detected)
0.005µM palcar and DHT	11	79 (P<0.001)
0.05µM palcar and DHT	2	21 (P<0.001)
0.5µM palcar and DHT	6	62 (P<0.001)
5µM palcar and DHT	11	169 (P<0.001)

Figure 5.3: Genes in common across palcar and DHT treatment in PNT1A cells treated for 8 hours. A) Venn diagram of genes across each palcar (5, 50, 500 and 5000nM) and 10nM DHT treatments. B) A comparison between the numbers of the genes expected to be induced by chance and treatment. P values are calculated using a proportion test [188].

Some of the 169 genes were up-regulated and some down-regulated. Figure 5.4 represents the fold change of DHT compared to control against the fold change of palcar compared to control. This figure show that palcar have DHT-like activities in the prostate cell.

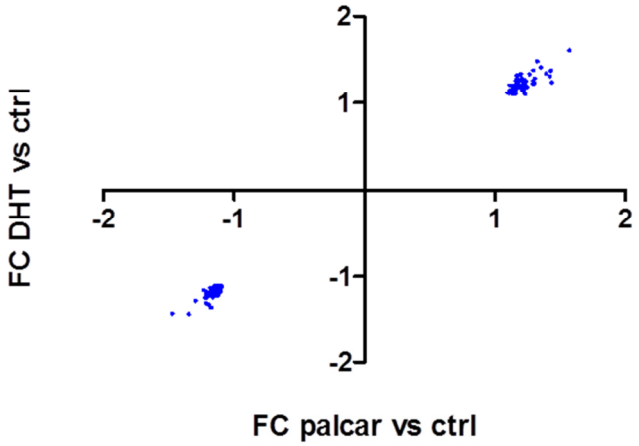

Figure 5.4: Fold change of DHT compared to control against fold change of palcar compared to control. The genes that are up-regulated by palcar are also up-regulated by DHT and vice versa. FC: fold change, ctrl: control, vs: versus.

5.4.2. Real time RT-PCR measurement of gene expression

To confirm the validity of the gene expression obtained by microarray, two genes were selected for further analysis by real-time RT-PCR. These genes were ALDH1A3 and HK2. They were selected because they demonstrated the highest level of expression in response to palcar and DHT in comparison to their controls ($P \leq 0.05$, table 5.3 and 5.5). EDN1 gene was also selected, which is a gene that is common between all palcar treatments, but not induced by DHT treatment in this experiment; however, it has been reported to be induced by DHT treatment previously [184]. Therefore, a total of three genes were selected to be further analysed by real-time RT-PCR. In this study, DHT was considered as a positive control for the effect of palcar as it has been reported previously to induce both HK2 and ALDH1A3 [189, 190]. The real time RT-PCR results showed that ALDH1A3, HK2 and EDN1 gene expression were not induced in response to palcar (0.005, 0.05, 0.5 and 5µM) or DHT, except for ALDH1A3, which was down-regulated (figure 5.5) by DHT. These results therefore, confirm the microarray data that palcar and DHT were not associated with an induction of gene expression.

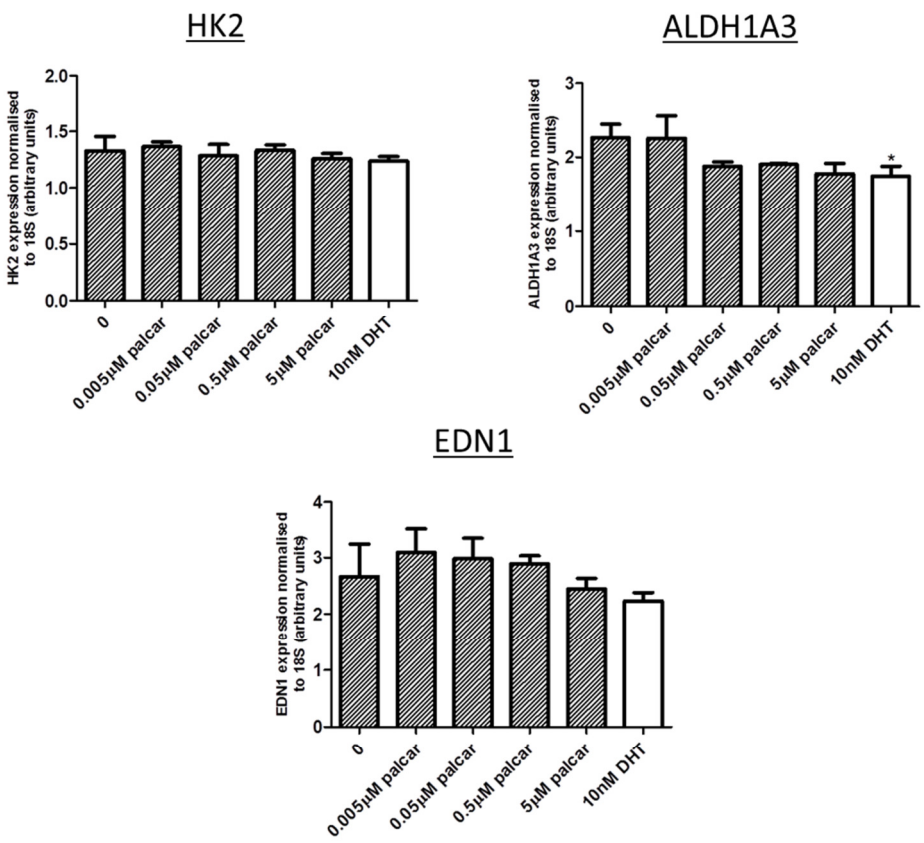

Figure 5.5: Real time RT-PCR analysis of HK2, ALDH1A3 and EDN1 mRNA expression in PNT1A cells. Cells were cultured in RPMI media supplemented with 10% FBS at 37°C and 5% CO_2. Cells were treated with DMSO, 5µM palcar or 10nM DHT for 8 hours. Data represent means ± SD of three biological replicates. Statistical analysis was performed using one way ANOVA followed by Tukey's post-test. Neither palcar (0.005, 0.05, 0.5 and 5µM) nor 10nM DHT induces an induction of HK2, ALDH1A3 or EDN1 genes expression.

5.4.3. Effect of palcar and DHT on HK2, ALDH1A3 and EDN1 gene expression in PNT1A and PC3 cells in response to 24 hours

To investigate whether longer incubation of palcar would result in inducing the expression of the above genes, the effect of the highest palcar concentration (5µM) for 24 hours was determined in PNT1A cells and were compared to that in PC3 cells. In PNT1A cells, DHT significanlty induced HK2 and EDN1 gene expression ($P \leq 0.01$), but not ALDH1A3, while palcar treatment had no effect (figure 5.6). However, in PC3 cells, DHT did not induce gene expression of ALDH1A3 and EDN1, but there was a trend to induce HK2 although it did not reach a statisticaly significant level (figure 5.6 A). In contrast, 5µM palcar

treatment significantly induced HK2 (P≤0.05), but not ALDH1A3 and EDN1 genes in PC3 cells.

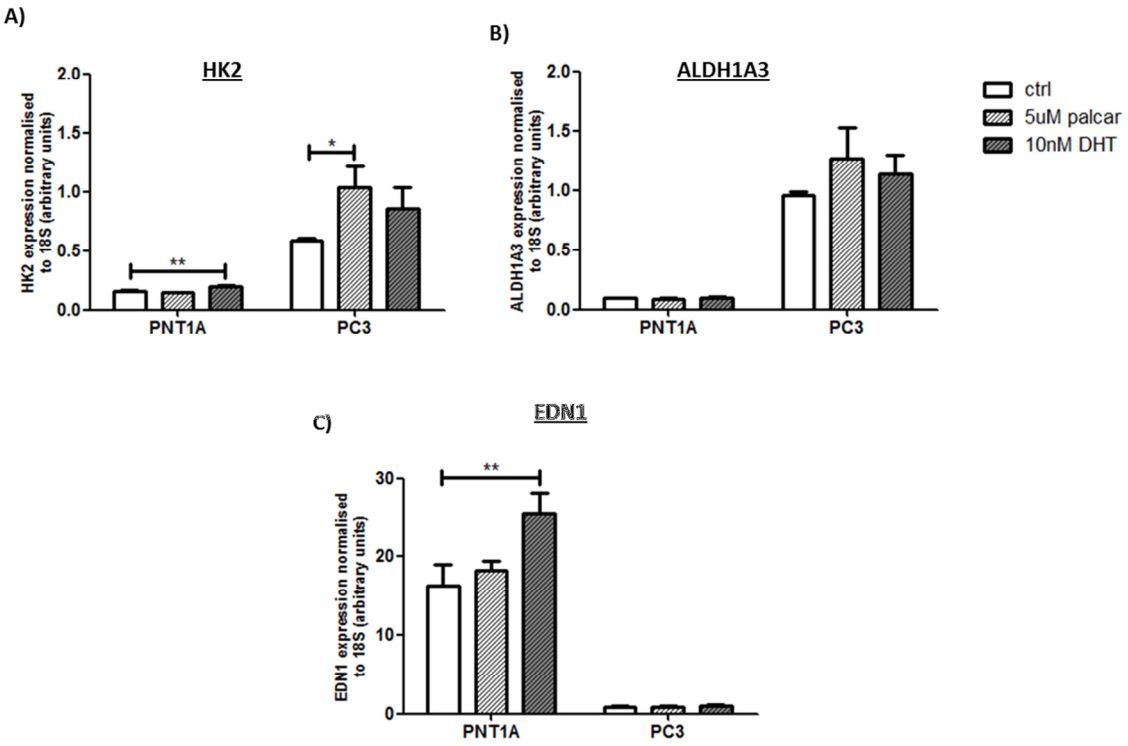

Figure 5.6: Real time RT-PCR analysis of HK2, ALDH1A3 and EDN1 mRNA expression in PNT1A and PC3 cells. Cells were cultured in RPMI media supplemented with 10% FBS at 37°C and 5% CO_2. Cells were treated with DMSO, 5µM palcar or 10nM DHT for 24 hours. Data represent means ± SD of three biological replicates. Statistical analysis was performed using one way ANOVA followed by Tukey's post-test performed in each PNT1A and PC3 cells separately. Palcar (5µM) treatment for 24 hours only induced the gene expression of HK2 in PC3 cells, but not in PNT1A, while 10nM DHT treatment induced the induction of EDN1 gene expression only in PNT1A cells. **P≤0.01.

5.4.4. Effect of androgen-free environment on palcar and DHT-induced gene expression

The lack of change in ALDH1A3 gene expression in response to DHT in both PNT1A and PC3 cells as well as the gene expression of HK2 in PC3 cells were thought to be due to the media that was used, which contains steroids. Steroids can be converted by cells into androgens that can bind with cellular receptors and induce changes to the gene expression, thus presence of androgen in the media used to culture these cells may prevent the observation of any effect of

DHT added from the treatment, which may affect the results of the gene expression and may explain why palcar did not have an effect. Therefore, the effect of a DHT free environment was investigated by using another type of media that is free of steroids; also a charcoal-stripped FBS was used to adsorb any endogenous lipid-related compounds including androgens. This media was called modified media. Since DHT was reported to induce gene expression in the prostate cancerous LNCaP cells, DHT effect was also investigated in this cell line and compared to that in PNT1A and PC3 cells cultured in the modified media. The results showed that changing the type of media where the cells were cultured prior to the addition of DHT from the treatment has no effect on the gene expression of HK2, ALDH1A3 and EDN1 in PNT1A and PC3 cells (figure 5.7).

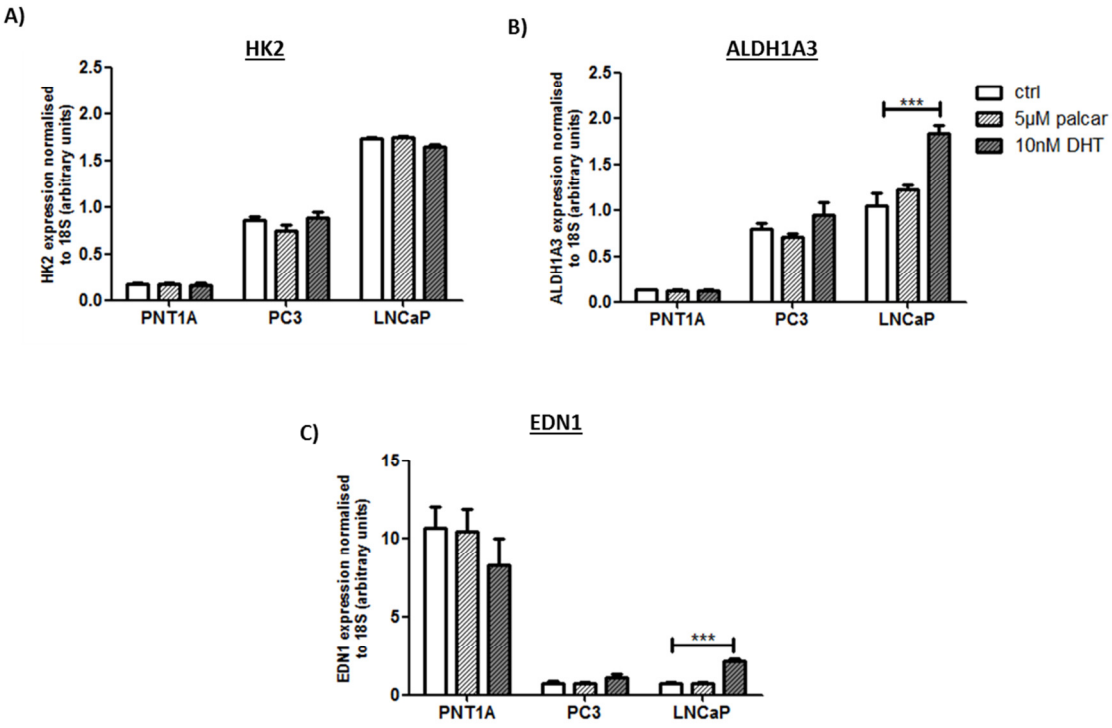

Figure 5.7: Real time RT-PCR analysis of HK2, ALDH1A3 and EDN1 mRNA expression in PNT1A, PC3 and LNCaP cells. Cells were cultured in RPMI media until growth reached 70% confluence and then switched to phenol-free RPMI media supplemented with charcoal-stripped FBS for 48 hours at 37°C and 5% CO_2. Cells were treated with DMSO, 5μM palcar or 10nM DHT for 24 hours. Data represent means ± SD of three biological replicates. Statistical analysis was performed using one way ANOVA followed by Tukey's post-test performed in each cell line separately. Changing the media did not induce a detectable gene expression in PNT1A, PC3 and LNCaP cells in response to 5μM palcar, but it induced a significant gene expression of ALDH1A3 (B) and EDN1 (C) in LNCaP cells in response to DHT treatment. *** $P \leq 0.001$.

In fact, using this media abolished the effect of palcar in inducing HK2 gene expression observed in PC3 cells, in addition to the effect of DHT on HK2 and EDN1 gene expression in PNT1A cells. However, in LNCaP cells, the gene expression of ALDH1A3 and EDN1 were significantly different compared to control in response to DHT, but not palcar.

5.5. Discussion

Following from the previous findings in this thesis showing that palcar induced Ca^{2+} influx and IL-6 at supra-physiological levels (Chapter 3); this Chapter investigate the effect of lower concentrations of palcar, and it was hypothesized that palcar at physiological concentrations is associated with changes on the gene expression. The results indicate that palcar was not associated with any changes on the gene expression of PNT1A cells, after 8 hours, measured by microarray study. This was also confirmed by real time RT-PCR.

The concentration range of palcar used in the microarray study performed in this Chapter was based on the levels of palcar previously quantified in Chapter 2 in both normal and cancerous prostate tissue (figure 2.7A, Chapter 2). Therefore, PNT1A cells were treated with DMSO, palcar (0.005, 0.05, 0.5 and 5µM) or 10nM DHT. The latter was investigated since it was found to induce Ca^{2+} influx in the same pattern as that of palcar (figure 3.19 B, Chapter 3), therefore a comparison of the effect of palcar with that of DHT would be interesting and might provide indication that palcar may have a DHT-like effect.

In this study, the analysis of the Affymetrix Human Exon 1.0 ST gene expression revealed that in PNT1A cells, both palcar (at all concentrations) and DHT treatments induced the expression of a number of genes (table 5.1) only when uncorrected, which support that notion that the changes induced by palcar was real since they occur for all concentrations rather than for only one or two concentrations. The largest number of the altered genes was caused by the DHT treatment, whereas 5µM palcar was associated with the largest number of altered genes compared to the other palcar concentrations. At this concentration palcar induced 346 genes compared to the control ($P \leq 0.05$). These genes are listed annex I. Functional pathway analysis performed on the list of genes altered by 5µM palcar showed that most of the genes belong to the glycolysis/gluconeogenesis and the metabolism of xenobiotics by cytochrome P450 pathways (table 5.2). The genes that were up regulated are HK2 and ALDH1A3. However, the fold change of these genes was only 1.161 (table 5.3), which is considered very small to

describe that certain compound induce an effect on the gene expression and make it difficult for any interpretation, therefore confirming that palcar did not induce any gene expression. When compared to palcar, DHT potentially altered the glycolysis/gluconeogenesis pathway (table 5.4), and the genes belong to this pathway and up regulated by DHT were the same as those altered by palcar with a fold change of 1.168 and 1.257 for HK2 and ALDH1A3, respectively (table 5.5), which also considered very low for an indication of an alteration in gene expression. Therefore, these results suggest that both palcar and DHT were not associated with alteration in the gene expression in PNT1A cells.

Since both palcar and DHT were shown to have the same effect of inducing Ca^{2+} influx in PC3 cells and therefore palcar might have a DHT-like effect in these cells (Chapter 3), the DHT-like property of palcar was also investigated on the gene expression in PNT1A cells. This was determined using Venn diagram. There were a total of six gene s affected by all palcar concentrations (figure 5.1); these genes are listed in table 5.6. Then, when DHT was incorporated, a total of five genes were found in common between all palcar concentrations and DHT (figure 5.2), these genes were given in table 5.7. These results indicate that all genes induced by all palcar concentrations were also induced by DHT treatment, except one gene, which is EDN1. However, EDN1 gene has been shown to be induced by androgen treatment [191], therefore this suggests that EDN1 may have missed the significance threshold, and thus was not detected.

When studying the number of genes in common between each individual palcar concentration and DHT, different concentrations altered different numbers of genes in common with DHT. However, the largest number of common genes in common was found between DHT and 5µM palcar, which was 169 genes (figure 5.3). The number of the overlapped genes was not due to chance (the P values are indicated in the table within figure 5.2), but rather due to the treatment. Therefore, these data may provide preliminary support to the notion that palcar might have a DHT-like effect. In order to support this notion further follow up research is needed, where some of the genes in common between palcar and DHT can be selected for further investigation gene and protein expression in response to palcar and DHT.

5.5.1. Confirmation of the gene expression by real time RT-PCR

Real time RT-PCR is a routine follow up experiment conducted following microarray study in order to confirm the validity of the microarray study. Three

genes were selected for this purpose; ALDH1A3, HK2 and EDN1. These genes were selected because they were up regulated by palcar and DHT, although their low fold change. ALDH1A3 and HK2 genes were induced in response to both palcar and DHT, while EDN1 gene was induced in response to all palcar concentrations, but not induced by DHT; however, it was selected because it has been found to be induced by DHT in the published literature [191].

The results indicate that 8 hours treatment with palcar (0.005, 0.05, 0.5 or 5µM) or 10nM DHT did not induce the gene expression of HK2, ALDH1A3 and EDN1 in PNT1A cells (figure 5.5), which confirm the microarray data that both palcar and DHT were not associated with an alteration in gene expression.

It has been shown that in prostate cancerous LNCaP cells, DHT induced the gene expression of HK2 and ALDH1A3 after 24 and 48 hours treatment, respectively [189, 190]. Thus, the lack of changes in the gene expression in PNT1A cells in response to both palcar and DHT was thought to be due to the incubation time. Therefore, the gene expression was measured in PNT1A cells in response to 24 hours treatment of palcar and DHT. In these cells, 24 hours treatment with 5µM palcar did not induce the gene expression of HK2, ALDH1A3 and EDN1, while 10nM DHT induced the gene expression of HK and EDN1, but not ALDH1A3 (figure 5.6). These results again confirm the inability of palcar to induce the gene expression of HK2, ALDH1A3 and EDN1 in PNT1A cells even when higher incubation time was used, but in contrast show that DHT was able to induce HK2 and EDN1 gene expression in these cells. These results, therefore, support the null hypothesis that palcar at low concentrations do not have an effect on the gene expression.

5.5.2. Palcar and DHT effect on the gene expression of PNT1A and PC3 cells detected by real time RT-PCR

Since the effect of palcar was previously observed in the cancerous PC3 cells, the gene expression of HK2, ALDH1A3 and EDN1 were performed in PC3 cells in response to 5µM palcar and 10nM DHT for 24 hours and were compared to that in PNT1A cells. In PC3 cells, palcar treatment induced the gene expression of HK2, but not ALDH1A3 and EDN1. When compared to palcar, DHT was not associated with any effect on the expression of these genes. The lack of alteration in the gene expression in response to DHT in PC3 cells may be due to the unresponsiveness of these cells to DHT due to the absence of ARs. In PNT1A cells, palcar has no effect on the three genes; in contrast DHT induced the gene

expression of HK2 and EDN1, but not ALDH1A3 (figure 5.6), suggesting that palcar effect in PC3 cells might be similar to the effect of DHT in PNT1A cells.

5.5.3. Effect of androgen-free media on palcar- and DHT-induced gene expression

Since the effect of DHT was not observed on ALDH1A3 gene expression in PNT1A cells, which has previously been shown to be induced by DHT in LNCaP cells [189, 190], the effect of using androgen-free environment on the levels of the gene expression was investigated in PNT1A, PC3 and LNCaP cells. LNCaP cells were used as a positive control to compare the effect of this environment on the gene expression in PNT1A and PC3 cells and determine the validity of the procedure followed. The results showed that culturing PNT1A cells in phenol-free media supplemented with charcoal-stripped serum did not affect the gene expression of ALDH1A3, HK2 and EDN1 in response to palcar and DHT (figure 5.7). In PC3 cells, changing the environment did not affect the previous results of the gene expression of ALDH1A3, but affected the gene expression of HK2 in response to palcar. However, in LNCaP cells, this environment induced an increase in the gene expression of ALDH1A3and EDN1compared to the control ($P \leq 0.001$) in response to DHT, but not in response to palcar. DHT effect in these cells agrees with the previous published result [189]. These results suggest that culturing PNT1A and PC3 cells in androgen-free environment had no effect on enhancing the responsiveness of these cells to palcar or DHT treatment, but may be important if LNCaP cells are to be investigated. Moreover, the lack of the effect of this androgen-free media on the gene expression confirm the validity of the microarray experiment since the media used to treat the cells from which RNA were extracted to be used for microarray was not an androgen-free media.

The results of both microarray and real time RT-PCR did not support the hypothesis that palcar at lower concentration is associated with alteration in the gene expression in PNT1A cells, and therefore may not be associated with the induction of gene expression important for transforming the cells into the cancerous stage. However, the results of the real time RT-PCR conducted in PC3 and PNT1A cells indicate that in PC3 cells 24 hour treatment with palcar was associated with the induction of the gene expression of HK2, which is a gene that encodes for the production of HK enzyme. HK enzyme is a regulatory enzyme that is essential for the initiation of the glycolysis by phosphorylating glucose using one molecule of ATP into glucose-6-phosphate (figure 5.8).

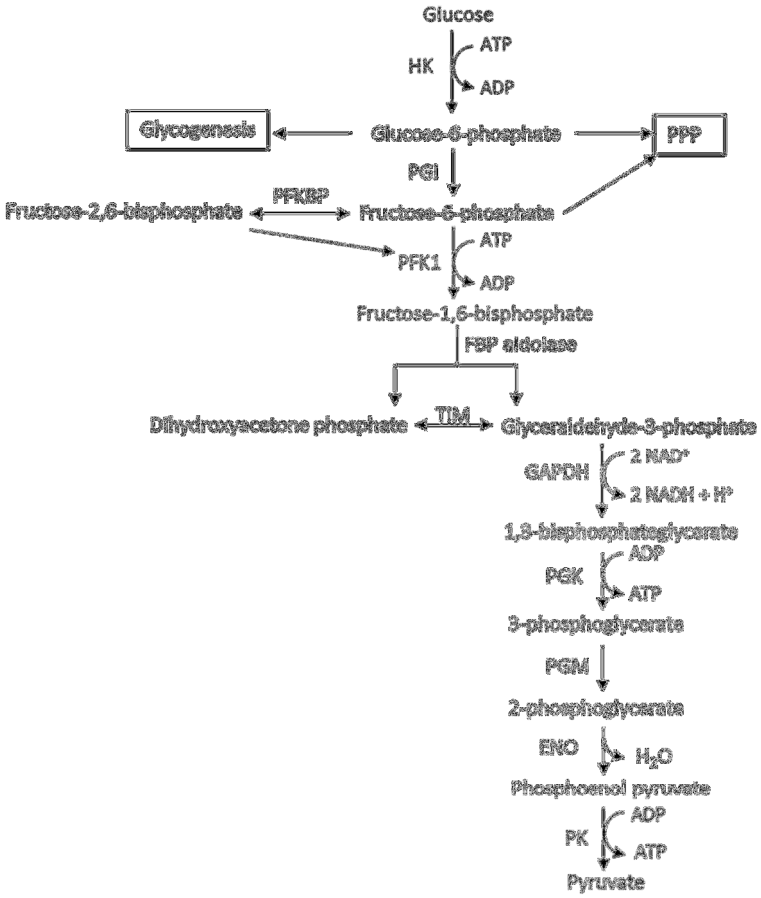

Figure 5.8: Conversion of glucose into pyruvate during glycolysis. Glucose is converted into pyruvate by series of enzyme-catalysed reactions. The regulatory enzymes of glycolytic pathway include HK, PFK and PK. HK. (Based on Devlin and Devlin [13]).

Once the latter has formed, it gets trapped inside the cells and used for energy production through glycolysis, glycogen synthesis, or a substrate for PPP. The latter is important for providing the reducing molecules of NADH and $FADH_2$ required for the anabolic processes as well as the production of pentose sugar that is a component of fundamental cellular compounds, such as ATP, CoA, NAD, FAD, RNA, and DNA [13]. In prostate cancerous cells, induction of glycolysis is important to provide the carbon skeleton required for the lipogenesis [5]. In this process, pyruvate resulted from glycolysis is converted into acetylCoA, which is shifted away from TCA cycle and excreted into the cytosol to be used as a substrate for lipid and cholesterol synthesis [5], in this process acetylCoA can be converted into acetylcarnitine, which can be transported into the cytosol and to reform acetylCoA. The resultant acetylCoA can be converted into malonylCoA, which is used along with other molecules of malonylCoA to produce fatty acids by

the aid of FASN. It is unlikely that the formation of malonylCoA is associated with the inhibition of CPTI enzyme since malonylCoA is not accumulated in case of prostate cancer, but rather being used to produce fatty acids, which are considered the building blocks for cell membrane formation and supporting the proliferated cells. In fact this does not goes against fatty acid-glucose cycle as it has been shown that exposure to long chain fatty acids is associated with a decrease in PDH activity in cultured rat islets in addition to an inhibition of PFK, leading to a decrease in glucose oxidation and an increase in the levels of glucose-6-phosphate [192]. In prostate cancer cells, *PFKFB4* is up regulated and associated with a decrease in the levels of Fru-2,6-BP, which is a regulator of PFK1 [87]. Diverting glucose from entering TCA cycle highlights the importance of fatty acids as the main energy source in these cells. Therefore, as a consequence of the stimulated fatty acid oxidation in PC3 cells along with the metabolic disruption in these cells, the resultant intermediates of incomplete fatty acid oxidation such as palcar, may act as a signalling molecule to induce the expression of HK2, which induces glycolysis to produce the carbon skeleton required for providing the building blocks for the proliferating cells. Thus, palcar-induced HK2 gene expression in PC3 cells may suggest that palcar may have a potential role in the induction of cellular proliferation through the induction of glycolysis. However, the mechanism by which palcar induces HK2 gene expression and thus glycolysis need further investigation.

5.6. Conclusion

In this study, the effect of low concentrations of palcar on the gene expression was investigated and compared to that of DHT. In the microarray experiment performed in PNT1A cells, multiple testing revealed that there were no genes altered by either DHT or palcar at any concentrations. However, to investigate the biological importance of the data, analysis of the uncorrected P values was conducted and indicated that there were a number of altered genes in common between palcar and DHT treatments including HK2 and ALDH1A3. However, these results were not confirmed by real time RT-PCR in PNT1A cells. Nevertheless, real time RT-PCR indicated that in PC3 cells a low concentration of palcar was able to induce HK2 gene expression. HK2 is a gene that encodes for the production of a rate limiting enzyme that drive glycolysis, which suggest a potential role for palcar to induce glycolysis. Induction of glycolysis in these cells

is important for providing the carbon skeleton required for anabolic processes, such as lipogenesis and PPP. Therefore, suggesting a possible potential role of palcar in enhancing prostate cancer progression.

Chapter 6

General discussion

6.1. General discussion

The rationale behind this thesis was influenced by previous work [66], which had primarily focussed on investigating the effect of a diet rich in high GSLs broccoli on reducing the risk of developing CVD. This diet had been found to reduce the accumulation of acylcarnitines [66]. Acylcarnitines are metabolites of fatty acid oxidation that accumulate as a result of a mitochondrial dysfunction. High levels of plasma acylcarnitines have been detected in chronic disorders, such as obesity and DM type 2 [7], in which a metabolic disturbance has been observed. Accumulation of acylcarnitines has also been observed in kidney cancer tissue [8]. However, there are no reports currently in regards to their levels in prostate cancer. Therefore, this thesis focuses on investigating the accumulation of palcar, a long chain acylcarnitine, in prostate cancer tissue and the effects of high levels of palcar on prostate non-cancer and cancer cell models.

In this chapter I will discuss the main findings of the four results chapters and their contributions to my original thesis aims, also their context within the wider field of research and finally the future plans for this work. The original aims of my thesis as stated out in Chapter 1 were:

- To test the hypothesis that palcar accumulates in the prostate cancer tissue as compared to the non-cancerous tissue, thus providing a biomarker for the metabolic dysfunction in prostate cancer (Chapter 2).

- To test the hypothesis that the accumulation of palcar is associated with induction of IL-6 and Ca^{2+} influx in prostate epithelial cancer cells (Chapter 3).

- To test the hypothesis that the mechanism by which palcar induces Ca^{2+} influx involves the activation of PTX-sensitive GPCR and L-type Ca^{2+} channels (Chapter 4).

- To investigate the hypothesis that low concentrations of palcar are associated with changes in gene expression in prostate epithelial cells (Chapter 5).

6.1.1. Levels of palcar in prostate cancer tissues

The first aim of my thesis was to quantify the levels of palcar in prostate non-cancer and cancer tissue. Prostate cancer has been shown to be associated with metabolic disturbances [111]. With this in mind, I quantified the levels of palcar in

prostate non-cancerous and cancerous tissue to determine whether the metabolic disturbances were linked to accumulation of acylcarnitines. In cancer tissue the levels were higher than the non-cancer tissue (figure 2.7, Chapter 2). Therefore, suggesting that palcar could represent a potential biomarker for the metabolic dysfunction associated with prostate cancer. The exact reason for the accumulation of palcar in prostate cancer need further investigation and may include either a defect or less efficient TCA cycle, which affect the rate of β-oxidation, or a defect in CPTII enzyme. However, the small sample size of prostate tissue samples (n=20) considered a limitation since having more tissue samples would give a more robust assessment for the potential role of palcar as a diagnostic tool. In this work, I was not able to measure total acylcarnitine due to the lack of the internal standards required for the quantification process by LC-MS/MS. Knowing that fatty acid oxidation represents the main energy source for the prostate cells; quantifying total acylcarnitines may have provided information on the type of fatty acids consumed for energy production. Short and medium chain fatty acids are oxidized via β-oxidation in the mitochondria, whereas long and branch chain are oxidized via β-oxidation in the peroxisome.

6.1.2. Effect of high concentrations of palcar *in vitro*: effect on IL-6 and Ca^{2+} influx

Accumulation of palcar in cancer tissue indicate that the plasma membrane of the cancer cells is exposed to increased levels of palcar, therefore, the question of whether the presence of palcar in prostate cancer only represents a potential biomarker for the metabolic disturbances or induces other effects was investigated. Therefore, the next aim of this thesis was to investigate the effects of palcar. This was performed using *in vitro* cell models of prostate non-cancer and cancer cells. The use of a cell model is more appropriate for studying the effect and the molecular mechanism of a compound than using human tissue as it eliminates the large inter-variability from different donors, therefore ensuring greater reproducibility of the results.

In this study it was shown that palcar was able to induce its effect at high concentrations that were not reported in the human plasma or tissues, however, has been within the range reported in ischemic heart of animal model [103]. In PC3 cells, 50μM palcar induced IL-6 secretion (figure 3.4, Chapter 3), which was associated with the induction of IL-6 gene expression (figure 3.5, Chapter 3). The induction of IL-6 gene expression indicates that palcar was not associated with

detergent effect. This was also supported from the data of the fluorescence signals; where there was no reduction in the fluorescence values from both 340 and 380nm, which is an indication of a FURA leakage as a result of a damaged cell membrane. In endothelial cells, a concentration higher than 10μM was associated with a detergent effect indicated from the leakage of FURA [44], which suggest that palcar effect is a dependent on the cell type being investigated. The ability of palcar to induce IL-6 gene expression and protein secretion suggest that palcar may act as a potential pro-inflammatory mediator in prostate cells.

The effect of acylcarnitine at high concentrations, notably palcar, has been previously investigated [6-8] and they have been shown to be associated with an alteration of membrane proteins that act as ion channel and pumps, such as Na^+/K^+ pump and Ca^{2+} pump [39, 41, 42]. Altering the functions of these channels leads to a change in membrane permeability, which changes the concentrations of ions that may be involved in signalling pathways. This could trigger signal transduction mechanisms that may eventually initiate immune responses. It has been shown that acylcarnitines at high concentrations are associated with the induction of pro-inflammatory cytokines [46] as well as the induction of Ca^{2+} influx [136]. Indeed, in addition to its ability to induce IL-6 at high concentration, palcar was able to induce Ca^{2+} influx in PC3 cells, but not in DU145, PNT1A and BPH-1 cells (figure 3.11. and 3.16, Chapter 3). There are no reported studies in the literature regarding the biological activities of palcar in prostate cells. However, there is only one published study in prostate cancerous LNCaP cells, where they measure Ca^{2+} influx in response to DHT (10 – 1000nM) [45]. DHT is the potent form of the hormone testosterone and synthesized by 5α-reductase present in the prostate, testes, hair follicles and adrenal gland [14]. It is important for the growth and development of prostate gland [14] and associated with prostate cancer progression [190]. In my study, DHT did not have an effect on IL-6 secretion (figure 3.7, Chapter 3), but induced Ca^{2+} influx in PC3 cells in response to 1μM DHT (figure 3.18, Chapter 3), which is above the reported physiological levels. However, no effect was observed for DHT in DU145, PNT1A and BPH-1 cells. The Ca^{2+} influx induced by DHT followed the same pattern of that induced by palcar and histamine, which is known to induce Ca^{2+} influx [166, 167].

Ca^{2+} is an important secondary ion that is involved in many signalling pathways, some of which are related to inflammatory responses [193]. It has been shown that inhibiting Ca^{2+} influx was associated with a decrease in IL-6 production in response to endothelin-1 [193]. IL-6 has been shown to be

associated with prostate cancer progression through the activation of AR due to its DHT-like effect [135, 194]. The ability of palcar to induce both Ca^{2+} influx and IL-6 secretion at high concentrations suggest that palcar has no effect on cultured prostate cancer cells at physiological concentrations and therefore it is difficult to interpret that palcar would represent a potential biomarker for the development of prostate cancer.

In this study, I measured Ca^{2+} influx using a plate reader and one of its limitations is the increase in the baseline levels of Ca^{2+} influx, which was observed in some samples of this study. The increase in the baseline levels is caused by the time delay between the samples. The procedure for measuring the fluorescence ratio required that the cell suspension is seeded in the wells first and then the fluorescence ratio is measured in each well subsequently for 5 minutes per well. Also, another limitation is the variability in the fluorescence values that could results from uneven number of the cells in each well. Although the cells were seeded in uniform cell density, the seeding process may lead to a slight difference in the number of the cells seeded in each well. Despite the technical difficulty in measuring Ca^{2+} influx, the technique was able to show that palcar induced Ca^{2+} influx in PC3 cells similar to the effect of DHT.

Since Ca^{2+} influx was measured in PNT1A, BPH-1, DU145 and PC3 cells, it would be of great value if IL-6 secretion in BPH-1 and DU145 cells was also measured. This would give an interesting comparison of the effect of palcar at high concentrations on IL-6 secretion in different prostate cells and gives information of whether the effect of palcar on IL-6 would be the same as its effect on Ca^{2+} influx.

The mechanism underlying palcar-induced IL-6 production via Ca^{2+} influx in PC3 cells has not been investigated yet. It is possible that the increase in $[Ca^{2+}]_i$ is important for the activation of transcription factors, such as NFκB, which is known to regulate IL-6 secretion. Further studies are needed to investigate the downstream events of Ca^{2+} induced signalling on IL-6 secretion in PC3 cells.

6.1.3. Mechanism of Ca^{2+} influx in PC3 cells in response to high levels of palcar

It has been previously shown that in LNCaP cells DHT induces Ca^{2+} influx by activating PTX-sensitive GPCR and L-type Ca^{2+} channels [45]. Since both palcar and DHT showed a similar effect in inducing Ca^{2+} influx in PC3 cells, although at high concentrations, I hypothesized in Chapter 4 that palcar may act as

a signalling molecule and activate specific pathways that are induced by DHT. However the results indicate that DHT and palcar at high concentration activate different pathways. DHT induced the activation of L-type Ca^{2+} channels and PTX-sensitive GPCR (figures 4.6 and 4.9, Chapter 4). Palcar also activated L-type Ca^{2+} channels, but not PTX-sensitive GPCRs (figure 4.5 and 4.7, Chapter 4), with a possible involvement of PI3K pathway (figure 4.10, Chapter 4), which provides a possible link to connects the activation of GPCR with the L-type Ca^{2+} channels. Figure 4.17, Chapter 4 illustrates the proposed mechanism.

It is important to note that PC3 cells are an androgen-independent cell line, which implies that these cells do not have an active AR or low levels of AR [80, 85, 195], therefore, the growth of these cells is induced by the activation of signalling pathways that bypass AR, such as PI3K.

The PI3K pathway is negatively regulated by the PTEN pathway. In PC3 cells, the PTEN pathway is functionally inactive in contrast to PNT1A and BPH-1 cells [170], which result in PI3K /AKT signalling pathway being more dominant in PC3 cells [118]. Activation of the PI3K pathway has been associated with fatty acid and cholesterol synthesis [196]. The mechanism of lipogenesis induced by the PI3K pathway includes the loss of PTEN activity in PC3 cells with subsequent activation of the PI3K/AKT pathway, activating the transcription factors that regulate lipogenesis [196]. The results of my study showed that high concentrations of palcar induced Ca^{2+} influx through the activation of the PI3K/AKT pathway, suggesting that palcar induced the activation of the PI3K/AKT pathway, and therefore palcar may indirectly mediate lipogenesis that is essential for prostate cancer progression. However, palcar-induced lipogenesis in PC3 cells need further investigation. One approach would be to investigate palcar-induced gene and protein expression of a rate limiting enzyme involved in lipogenesis, such as fatty acid synthase.

6.1.4. The profile of the gene expression of GPCRs

Although palcar did not activate PTX-sensitive GPCR, it may activate PTX-insensitive GPCRs, especially that L-type Ca^{2+} channel are known to be an effector protein for the GPCR. GPCRs is a large group of receptors, and therefore to investigate which receptor might be involved in Ca^{2+} influx, I analysed the gene expression obtained from a separate microarray study performed DMSO-treated PC3, DU145, PNT1A and RWPE1 cells. The array analysis revealed that the profile of GPCR gene expression in PC3 cells was different to that in DU145 cells

with DU145 gene expression profile similar to that observed in PNT1A and RWPE1 cells. Although DU145 cells are metastatic cancerous cell line, the similarities of the profile of GPCRs gene expression between DU145 and both PNT1A and RWPE1 cells may explain the similar reaction of DU145 and PNT1A cells in the lack of response to palcar.

The profile of the gene expression also revealed that GPR110 was highly expressed in PC3 cells as compared to RWPE1, PNT1A and DU145 cells. GPR87 was highly expressed in PNT1A in comparison to DU145 and PC3 cells. Additionally, GPRC6A was one of the genes that were equally expressed between all cell lines (figure 4.11, 4.12, 4.13, 4.14 and 4.15, Chapter 4). Therefore, based on these results I measured the protein expression of GPR110, GPR87 and GPRC6A by western blot in PNT1A, BPH-1, DU145 and PC3 cells. This revealed that the level of protein expression of GPR110 was higher in PC3 cells as compared to the other cell lines (figure 4.16, Chapter 4) as well as higher than the levels of GPR87 and GPRC6A (figure 4.16, Chapter 4), suggesting that GPR110 may represent a potential receptor by which palcar could induce its effect.

Nevertheless, one difficulty with the loading control was observed. In this study, I used integrin β-1 as a loading control for the membrane proteins. There were differences in the expression of this protein in DU145 cells and BPH-1 cells compared to PNT1A and PC3 cells, which results in differences in the number and the band size of the protein (figure 4.16, Chapter 4). However, the poor loading control did not affect the estimation of the levels of the protein expression of GPR110, GPR87 and GPRC6A. Yet, one possible loading control that could be further investigated and alternatively used is β-actin.

The potential receptor involved in the mechanism of Ca^{2+} influx in response to palcar may not only limited to GPR110 as the profile of the GPCRs gene expression in PC3 cells revealed a number of GPCRs, other than GPR110, that were highly expressed in PC3 cells compared to DU145 and PNT1A. However, GPR110 was considered a potential biomarker for the development of both lung and prostate cancer since the gene and protein expression of GPR110 were detected in the tissue and cell lines of both cancer types [175]. This is considered important since lung cancer is the number one cause of deaths in the UK followed by prostate cancer [1]. This may suggest the importance of investigating the role of GPR110 in Ca^{2+} influx. Due to the time limit for the completion of the work involved in this thesis, I did not investigate palcar-induced activation of GPCR as

well as the link between the activation of GPCR and Ca^{2+} influx. Studying these would provide a clearer image of the mechanism of Ca^{2+} influx induced by palcar in PC3 cells.

Although the supraphysiological concentration of palcar used to induce the Ca^{2+} influx would make the physiological relevance questionable, studying the mechanism by which palcar induces Ca^{2+} influx may uncover a signalling pathway that represents a target for future dietary intervention aiming to investigate the role of dietary components on reducing the effect palcar accumulation in prostate cancer. As mentioned earlier a diet rich in high GSL broccoli was able to reduce the levels of acylcarnitines. The active component that may induce this effect is SF. SF may increase the anti-oxidant capacity of the cells by increasing the concentration of the reduced form of glutathione, which in turn can reduce the levels of ROS that negatively affecting the efficiency of TCA cycle. Therefore, it is interesting to study to the effect of SF on the mechanism of Ca^{2+} influx, thus providing a more understanding of the mechanism by which SF induces its effect.

6.1.5. The effect of low concentration of palcar on the profiles of gene expression *in vitro*

The final aim of the thesis was to identify whether low concentrations of palcar were associated with changes in the gene expression of prostate epithelial cells. I investigated this by conducting a microarray study in PNT1A cells followed by real time RT-PCR in both PNT1A and PC3 cells, in which the effect of palcar was compared to that of DHT. The range of concentration selected for palcar was based on the levels of palcar obtained from the prostate non-cancer and cancer tissue (figure 2.7, Chapter 2). The highest concentration of palcar (5µM) was selected since it was the highest concentration of acylcarnitine, other than palcar, that was reported in the literature and it was reported in subjects with metabolic dysfunction [31]. Therefore, it was thought that the accumulation of palcar under metabolic dysfunction may reach to this level, thus the effect of this concentration was investigated. The concentration of DHT that was selected in this study represents a physiologically relevant dose. Since DHT is known to be associated with prostate cancer progression, the findings of my study might aid in understanding whether palcar have a DHT-like effects. The rationale behind the use of PNT1A cells was to investigate whether palcar may have a role in inducing malignant transformation of the cells by inducing genes involved in signalling pathways that are associated with cancer progression or induction of anabolic or

catabolic processes essential for the biology of cancer, such as glycolysis and lipogenesis.

The results of the microarray revealed that low concentrations of palcar were associated with changes in the gene expression of a number of genes in PNT1A cells (table 5.1, Chapter 5) only when uncorrected P value was used, which make the effect of both DHT and palcar on the gene expression questionable. However, with the use of uncorrected P value, 5μM palcar was associated with the largest number of significantly altered genes. When pathway analysis was performed, 5μM palcar was associated with the induction of glycolysis/gluconeogenesis and metabolism of xenobiotic pathways (table 5.3, Chapter 5). Glycolysis/gluconeogenesis was also potentially induced by 10nM DHT (table 5.5, Chapter 5). Two genes involved in the glycolytic pathway (ALDH1A3 and HK2) were induced by both DHT and palcar (table 5.4 and 5.6, Chapter 5), however their fold change was only 1.161, which suggest that both palcar and DHT were not associated with the induction of these genes. The pattern of the gene expression between palcar and DHT was similar (figure 5.4).

Real time RT-PCR confirmed that both palcar and DHT were not associated with any induction of the gene expression. The genes selected for this purpose were HK2, ALDH1A3 and EDN1 (figure 5.5, Chapter 5). However, due to the lack effect of palcar and DHT after 8 hours, the expression of these three genes was measured after 24 hours treatment in PNT1A and was compared to that in PC3 cells. In PNT1A cells, 24 hours treatment with 5μM palcar has no effect on the gene expression of ALDH1A3, HK2 and EDN1. DHT, in contrast, induced the gene expression of HK2 and EDN1. The results of the DHT-induced gene expression of HK2 in PNT1A cells agree with the previously reported results in LNCaP cells [190].

In PC3 cells, palcar induced the gene expression of HK2, but not ALDH1A3 and EDN1, whereas DHT has no effect (figure 5.6, Chapter 5). The unresponsiveness of PC3 cells to DHT may be explained by the un-functional or absence of AR in these cells. There are some studies reported that both PNT1A and PC3 cells do not express the AR [80, 85] and that PC3 cells might express AR, but it is functionally inactive [195]. However, the effect of DHT in PNT1A cells suggest that AR may present in these cells and DHT either induced its effect through this receptor or other receptors in which DHT could be a possible ligand. The variation in the effect of DHT on the gene expression of HK2, ALDH1A3 and

EDN1 in PNT1A and lack of its effect in PC3 cells was thought to be as a result of receptor saturation with the androgen already present in the media or synthesized by the cells themselves. Cells were therefore cultured in an androgen-free environment and the effect of DHT in these cells were compared to that in LNCaP cells, in which DHT has been reported to induce the gene expression of HK2, EDN1 and ALDH1A3. Using such environment did not affect the gene expression in PNT1A and PC3 cells. In LNCaP cells, however an androgen-free environment induced the expression of ALDH1A3 in response to DHT after 24 hours, which disagrees with the previously reported results, in which it has been shown that 24 hour was not sufficient to induce the gene expression of ALDH1A3, and thus it was observed after 48 hours [189].

6.2. Future plans

The work described in this thesis investigates the role of high concentrations of palcar in prostate cancer. There are some aspects that are considered important for the completion of this work, which were not investigated due to the time limitation for the completion of this thesis. These include first, the profile of total acylcarnitines in prostate tissue. Second, the role of Ca^{2+} influx in IL-6 secretion in prostate cancer cells, and finally the role of GPR110 in Ca^{2+} influx and whether the activation of this receptor is induced by the presence of palcar. Research to investigate the above issues will provide evidence whether palcar at high concentrations has a mediatory effect on the development and progression of prostate cancer. The concentration of palcar used to induce these effects was within the concentration range reported in ischemic heart of animal model, however, because it was higher than those reported in the human plasma, it would make the physiological relevance of these studies questionable.

The profile of total acylcarnitines in prostate cancer has not been investigated. Studying total acylcarnitines would provide information as to the type of fatty acids consumed for energy production. Accumulation of palcar in prostate tissue might be related to a defect in CPT II enzyme, part of a large family of transferases that transfer fatty acid from C12 – C18 acylcarnitines. Therefore, measuring total acylcarnitines may provide an insight into the metabolic disturbance in these tissue samples.

The second aspect is the link between Ca^{2+} and IL-6. Since palcar induced both Ca^{2+} influx and IL-6 secretion, studying the association between Ca^{2+} influx and IL-6 may aid in understanding the role of palcar in prostate cancer cells. There

are some studies that addressed the role of changing $[Ca^{2+}]_i$ in IL-6 secretion, however, there are no published studies regarding this issue in prostate cells. One approach, which can be used to investigate this includes treating the cells with nifedipine to block Ca^{2+} influx and then measure the secretion of IL-6 using commercially available ELISA kits. However, because Ca^{2+} is a dynamic ion that is important for many cellular functions, blocking Ca^{2+} influx may lead to less viable cells, therefore affecting the levels of IL-6 secreted, thus a method optimisation to determine the concentration and time of nifedipine incubation is needed prior to investigating the role of Ca^{2+} influx on palcar-induced IL-6 secretion.

The third important aspect of this research is the role of palcar in activating GPR110 and whether it is linked to the Ca^{2+} influx. This can be investigated by using a specific antibody for that receptor, however, because there are no published studies regarding the role of GPR110 in Ca^{2+} influx in prostate cancer, it is important first to determine the concentration and the incubation time of the antibody required to completely block the receptor prior to measuring palcar-induced Ca^{2+} influx.

Since the effects of palcar were shown in PC3 cells, a microarray study using PC3 cells treated with 5µM palcar for 24 hours would provide much information about what and how genes changed in response to palcar. This will give a broader image of the effect of palcar on the different pathways affected in these cells.

The effects of palcar in this research were measured using *in vitro* cell models of prostate non-cancerous and cancerous cells. However, it would be interesting to investigate whether palcar would induce the same effects in *ex. vivo* human prostate tissue, which could provide evidence as to the effect of palcar *in vivo*.

In conclusion, the findings of the work presented in this thesis suggest that accumulation of palcar, the most abundant acylcarnitine, in prostate cancer tissue may represent a potential biomarker for the metabolic disturbance associated with prostate cancer. However, more tissue samples are needed to confirm the potential role of palcar to be a diagnostic tool. Palcar was not associated with any effects in the non-cancerous cell models used in this study including an effect on the gene expression profile. Nevertheless, in the most aggressive form of the prostate cancerous cells, palcar at high concentrations induced physiological changes

including gene expression that could be related to prostate cancer progression. Some of these effects were in common with DHT, suggesting a possible DHT-like property of palcar in these cells. However, since these effects were not observed at physiological levels, this study conclude that palcar has no effect on the cultured prostate cancer cells at physiological concentrations, and therefore it is difficult to conclude any physiological relevance of the effect of palcar in these cells.

Annex I

A list of genes altered in PNT1A cells after 5μM palcar treatment for 8 hours (P≤0.05) arranged according to the fold change in descending order.

Accession	Gene description	Gene name	Fold change
NM_018728	myosin VC	MYO5C	0.91
NM_182643	deleted in liver cancer 1	DLC1	0.91
NM_015589	sterile alpha motif domain containing 4A	SAMD4A	0.91
NM_198531	ATPase, class II, type 9B	ATP9B	0.91
NM_001964	early growth response 1	EGR1	0.90
NM_004196	cyclin-dependent kinase-like 1 (CDC2-related kinase)	CDKL1	0.90
NM_000393	collagen, type V, alpha 2	COL5A2	0.90
NM_014391	ankyrin repeat domain 1 (cardiac muscle)	ANKRD1	0.90
NM_014011	suppressor of cytokine signaling 5	SOCS5	0.90
NM_001554	cysteine-rich, angiogenic inducer, 61	CYR61	0.90
NM_199441	zinc finger protein 334	ZNF334	0.90
NM_173354	salt-inducible kinase 1	SIK1	0.89
NM_002784	pregnancy specific beta-1-glycoprotein 9	PSG9	0.89
NM_005737	ADP-ribosylation factor-like 4C	ARL4C	0.89
NM_031938	beta-carotene oxygenase 2	BCO2	0.89
NM_003268	toll-like receptor 5	TLR5	0.89
ENST00000342887	chromosome 12 open reading frame 63	C12orf63	0.89
NM_020348	cyclin M1	CNNM1	0.89
NM_058237	protein phosphatase 4, regulatory subunit 4	PPP4R4	0.88
NM_152597	fibrous sheath interacting protein 1	FSIP1	0.88
NM_173039	aquaporin 11	AQP11	0.88
NM_002068	guanine nucleotide binding protein (G protein), alpha 15 (Gq class)	GNA15	0.88
NM_022842	CUB domain containing protein 1	CDCP1	0.88
NM_145016	glycine-N-acyltransferase-like 2	GLYATL2	0.88
NM_007069	phospholipase A2, group XVI	PLA2G16	0.88
NR_027786	serine hydrolase-like hydrolase-like 2	SERHL	0.88
NM_001083602	patched 1	PTCH1	0.88
NM_002356	myristoylated alanine-rich protein kinase C substrate	MARCKS	0.88
NM_002298	lymphocyte cytosolic protein 1 (L-plastin)	LCP1	0.88
NM_199254	transmembrane phosphoinositide 3-phosphatase and tensin homolog 2	TPTE2	0.88
NM_032387	WNK lysine deficient protein kinase 4	WNK4	0.88
NM_024764	cation channel, sperm-associated, beta	CATSPERB	0.87
AK127870	FLJ45974 protein	FLJ45974	0.87
BC026884	chromosome 9 open reading frame 43	C9orf43	0.87
NM_176880	nuclear receptor 2C2-associated protein	NR2C2AP	0.87
NM_058187	chromosome 21 open reading frame 63	C21orf63	0.87
NM_174891	chromosome 14 open reading frame 79	C14orf79	0.87
NM_004190	lipase, gastric	LIPF	0.87
NM_139171	StAR-related lipid transfer (START) domain containing 6	STARD6	0.87
NM_005542	insulin induced gene 1	INSIG1	0.87
NM_022475	hedgehog interacting protein	HHIP	0.87
NM_002019	fms-related tyrosine kinase 1 (vascular endothelial growth factor/vascular permeability factor receptor)	FLT1	0.87
NM_080817	G protein-coupled receptor 82	GPR82	0.87

NM_003247	thrombospondin 2	THBS2	0.87
NM_001097579	G protein-coupled receptor 34	GPR34	0.87
NM_031955	spermatogenesis associated 16	SPATA16	0.87
NM_153267	MAM domain containing 2	MAMDC2	0.87
NM_199136	chromosome 7 open reading frame 46	C7orf46	0.87
NM_000189	hexokinase 2	HK2	0.87
NM_024688	chromosome 10 open reading frame 68	C10orf68	0.86
NM_023016	ankyrin repeat domain 57	ANKRD57	0.86
NM_025015	heat shock 70kDa protein 12A	HSPA12A	0.86
NM_138812	DPY30 domain containing 1	DYDC1	0.86
NM_000527[1]	low density lipoprotein receptor	LDLR	0.86
NM_004613	transglutaminase 2 (C polypeptide, protein-glutamine-gamma-glutamyltransferase)	TGM2	0.86
NM_003897	immediate early response 3	IER3	0.86
NM_000693[1]	aldehyde dehydrogenase 1 family, member A3	ALDH1A3	0.86
NM_213599	anoctamin 5	ANO5	0.86
NM_000212	integrin, beta 3 (platelet glycoprotein IIIa, antigen CD61)	ITGB3	0.86
NM_003567	breast cancer anti-estrogen resistance 3	BCAR3	0.86
NM_152779	GLI pathogenesis-related 1 like 1	GLIPR1L1	0.86
NR_026838	Down syndrome critical region gene 8	DSCR8	0.86
NR_027713	keratin 8 pseudogene	FLJ46111	0.86
NM_002982	chemokine (C-C motif) ligand 2	CCL2	0.86
NM_001005205	olfactory receptor, family 8, subfamily J, member 1	OR8J1	0.86
NM_021992	thymosin beta 15a	TMSB15A	0.86
NM_002658	plasminogen activator, urokinase	PLAU	0.86
NM_000767	cytochrome P450, family 2, subfamily B, polypeptide 6	CYP2B6	0.86
NM_058229	F-box protein 32	FBXO32	0.85
NM_001993	coagulation factor III (thromboplastin, tissue factor)	F3	0.85
NM_024514	cytochrome P450, family 2, subfamily R, polypeptide 1	CYP2R1	0.85
NM_002228	jun proto-oncogene	JUN	0.85
NM_030763	high-mobility group nucleosome binding domain 5	HMGN5	0.85
NM_170723	chromodomain protein, Y-linked, 1	CDY1	0.85
NM_199289	NIMA (never in mitosis gene a)-related kinase 5	NEK5	0.85
NM_021624	histamine receptor H4	HRH4	0.85
NM_003714	stanniocalcin 2	STC2	0.85
NM_006446	solute carrier organic anion transporter family, member 1B1	SLCO1B1	0.85
NM_001955	endothelin 1	EDN1	0.85
NM_000880	interleukin 7	IL7	0.85
NM_001163560	chromosome 16 open reading frame 73	C16orf73	0.85
NM_001764	CD1b molecule	CD1B	0.85
NM_001340	cylicin, basic protein of sperm head cytoskeleton 2	CYLC2	0.85
NM_001924	growth arrest and DNA-damage-inducible, alpha	GADD45A	0.85
NM_014344	four jointed box 1 (Drosophila)	FJX1	0.84
NM_001136505	coiled-coil domain containing 79	CCDC79	0.84
NM_005842	sprouty homolog 2 (Drosophila)	SPRY2	0.84
NM_152251	defensin, beta 106A	DEFB106A	0.84
NM_144594	gametocyte specific factor 1	GTSF1	0.84
NR_024060	family with sequence similarity 27, member A	FAM27A	0.84
NM_175878	XK, Kell blood group complex subunit-related family, member 3	XKR3	0.84
NM_003813	ADAM metallopeptidase domain 21	ADAM21	0.84
NR_027263	chromosome 14 open reading frame 128	C14orf128	0.84

NM_139167	sarcoglycan, zeta	SGCZ	0.84
NM_006566	CD226 molecule	CD226	0.84
ENST00000400419	hypothetical protein MGC5590	MGC5590	0.84
NM_003140	sex determining region Y	SRY	0.83
NM_001165	baculoviral IAP repeat-containing 3	BIRC3	0.83
NM_001143668	adhesion molecule with Ig-like domain 2	AMIGO2	0.83
NM_018327	serine palmitoyltransferase, long chain base subunit 3	SPTLC3	0.83
NR_026825	ribosomal protein SA pseudogene 52	RPSAP52	0.83
NM_012472	leucine rich repeat containing 6	LRRC6	0.83
NM_152505	Leber congenital amaurosis 5-like	LCA5L	0.83
NM_181610	keratin associated protein 19-4	KRTAP19-4	0.83
NM_015714	G0/G1switch 2	G0S2	0.83
NM_003469	secretogranin II	SCG2	0.83
NM_001008391	coiled-coil domain containing 73	CCDC73	0.83
NM_001508	G protein-coupled receptor 39	GPR39	0.83
NM_001004730	olfactory receptor, family 5, subfamily AR, member 1	OR5AR1	0.83
NR_026693	zinc finger protein 487, pseudogene	ZNF487P	0.83
AL831934	zinc finger protein 663	ZNF663	0.83
NM_004780	transcription elongation factor A (SII)-like 1	TCEAL1	0.83
NM_001143	amelogenin, Y-linked	AMELY	0.83
NM_152323	Spi-C transcription factor (Spi-1/PU.1 related)	SPIC	0.83
NM_003007	semenogelin I	SEMG1	0.82
NM_000074	CD40 ligand	CD40LG	0.82
NM_001143811	brain-derived neurotrophic factor	BDNF	0.82
NM_001004461	olfactory receptor, family 10, subfamily A, member 6	OR10A6	0.82
NM_002546[1]	tumor necrosis factor receptor superfamily, member 11b	TNFRSF11B	0.82
NM_001443	fatty acid binding protein 1, liver	FABP1	0.82
NM_003540[1]	histone cluster 1, H4f	HIST1H4F	0.82
NM_152647	chromosome 15 open reading frame 33	C15orf33	0.82
NM_005810	killer cell lectin-like receptor subfamily G, member 1	KLRG1	0.82
NM_001195234	tripartite motif-containing 49-like 2	TRIM49L2	0.82
NM_213658	killer cell lectin-like receptor subfamily C, member 1	KLRC1	0.82
NM_001001961	olfactory receptor, family 13, subfamily C, member 3	OR13C3	0.81
NM_005242[1]	coagulation factor II (thrombin) receptor-like 1	F2RL1	0.81
NM_021966	T-cell leukemia/lymphoma 1A	TCL1A	0.81
NM_153444	olfactory receptor, family 5, subfamily P, member 2	OR5P2	0.81
NM_000133	coagulation factor IX	F9	0.81
NM_001004726	olfactory receptor, family 4, subfamily X, member 1	OR4X1	0.81
NM_005118	tumor necrosis factor (ligand) superfamily, member 15	TNFSF15	0.81
NM_206998	secretoglobin, family 1D, member 4	SCGB1D4	0.81
NM_001098272	3-hydroxy-3-methylglutaryl-CoA synthase 1 (soluble)	HMGCS1	0.81
NM_005635	synovial sarcoma, X breakpoint 1	SSX1	0.81
NR_002776[1]	MCM3AP antisense RNA (non-protein coding)	MCM3AP-AS	0.81
NM_001005204	olfactory receptor, family 8, subfamily U, member 1	OR8U1	0.81
NM_024775	gem (nuclear organelle) associated protein 6	GEMIN6	0.81
NM_002240	potassium inwardly-rectifying channel, subfamily	KCNJ6	0.81

	J, member 6		
NM_005059	relaxin 2	RLN2	0.81
NM_032330	calpain, small subunit 2	CAPNS2	0.81
NM_001005197	olfactory receptor, family 8, subfamily D, member 4	OR8D4	0.81
NM_001192	tumor necrosis factor receptor superfamily, member 17	TNFRSF17	0.80
NM_000891[1]	potassium inwardly-rectifying channel, subfamily J, member 2	KCNJ2	0.80
NM_002175	interferon, alpha 21	IFNA21	0.80
NM_001145465	NANOG neighbor homeobox	NANOGNB	0.80
NM_017680	asporin	ASPN	0.80
NM_002424	matrix metallopeptidase 8 (neutrophil collagenase)	MMP8	0.80
NM_031457	membrane-spanning 4-domains, subfamily A, member 8B	MS4A8B	0.80
NM_000686	angiotensin II receptor, type 2	AGTR2	0.79
NM_013243	secretogranin III	SCG3	0.79
NM_005292	G protein-coupled receptor 18	GPR18	0.79
NR_024004	DEAD/H (Asp-Glu-Ala-Asp/His) box polypeptide 11 like 2	DDX11L2	0.79
NM_176891	interferon, epsilon	IFNE	0.79
NM_173857	vomeronasal 1 receptor 4	VN1R4	0.79
NM_001001960	olfactory receptor, family 5, subfamily W, member 2	OR5W2	0.79
NM_001039916	zinc finger protein 384	ZNF384	0.79
NM_172312	sperm associated antigen 8	SPAG8	0.78
NR_026983[1]	basic transcription factor 3 pseudogene 11	BTF3P11	0.78
NM_000371	transthyretin	TTR	0.78
NM_032461	SPANX family, member B1	SPANXB1	0.77
NM_021225	proline rich, lacrimal 1	PROL1	0.77
NM_033057[1]	olfactory receptor, family 2, subfamily B, member 2	OR2B2	0.77
NM_001004756	olfactory receptor, family 51, subfamily M, member 1	OR51M1	0.77
NM_020903	ubiquitin specific peptidase 29	USP29	0.77
NM_207339	P antigen family, member 2 (prostate associated)	PAGE2	0.77
NR_026935	hypothetical LOC158696	LOC158696	0.77
ENST00000325812	chromosome 14 open reading frame 177	C14orf177	0.77
AF210651	NAG18 mRNA	NAG18	0.77
NM_000575[1]	interleukin 1, alpha	IL1A	0.77
NM_001005329	olfactory receptor, family 51, subfamily A, member 2	OR51A4	0.76
NM_002173[1]	interferon, alpha 16	IFNA16	0.76
NM_006205	phosphodiesterase 6H, cGMP-specific, cone, gamma	PDE6H	0.76
NM_001004735	olfactory receptor, family 5, subfamily D, member 14	OR5D14	0.75
NM_033048	CPX chromosome region, candidate 1	CPXCR1	0.75
NM_001005167[1]	olfactory receptor, family 52, subfamily E, member 6	OR52E6	0.75
NM_001005182	olfactory receptor, family 6, subfamily C, member 1	OR6C1	0.74
NM_178455	serine peptidase inhibitor, Kunitz type 4	SPINT4	0.74
NM_145662[1]	SPANX family, member A2	SPANXA2	0.74
BC021580	nuclear apoptosis inducing factor 1	NAIF1	0.72
NM_020646	achaete-scute complex homolog 3 (Drosophila)	ASCL3	0.72
NM_013318[1]	HLA-B associated transcript 2-like 1	BAT2L1	0.70
AF165185	LSM14B, SCD6 homolog B (S. cerevisiae)	LSM14B	0.70

NM_001001922[1]	olfactory receptor, family 52, subfamily N, member 5	OR52N5	0.70
NM_138331[1]	ribonuclease, RNase A family, 8	RNASE8	0.70
NM_001134657	proline rich 23C	PRR23C	0.66
NM_130388	ankyrin repeat and SOCS box-containing 12	ASB12	0.66
NR_026813[1]	chromosome 15 open reading frame 5	C15orf5	0.64
NR_002308[1]	ubiquinol-cytochrome c reductase binding protein pseudogene	LOC442454	0.61
NM_033439[1]	interleukin 33	IL33	0.56
NM_033198	phosphatidylinositol glycan anchor biosynthesis, class S	PIGS	-1.09
NM_015060	AVL9 homolog (S. cerevisiase)	AVL9	-1.10
NM_006076	ArfGAP with FG repeats 2	AGFG2	-1.10
NM_025155	proteasomal ATPase-associated factor 1	PAAF1	-1.10
NM_006809	translocase of outer mitochondrial membrane 34	TOMM34	-1.10
NM_005469	acyl-CoA thioesterase 8	ACOT8	-1.10
NM_014773	KIAA0141	KIAA0141	-1.10
NM_017849	transmembrane protein 127	TMEM127	-1.11
NM_001109903	ring finger protein, transmembrane 2	RNFT2	-1.11
NM_170607	MAX-like protein X	MLX	-1.11
NR_026728	ER degradation enhancer, mannosidase alpha-like 2	EDEM2	-1.11
NM_017873	ankyrin repeat and SOCS box-containing 6	ASB6	-1.11
NM_001610	acid phosphatase 2, lysosomal	ACP2	-1.11
NM_053064	guanine nucleotide binding protein (G protein), gamma 2	GNG2	-1.11
NM_201540	NDRG family member 2	NDRG2	-1.11
NM_145799	septin 6	Sep-06	-1.11
NM_016099	golgin A7	GOLGA7	-1.11
NM_001033549	chromosome 19 open reading frame 62	C19orf62	-1.11
NM_032635	transmembrane protein 147	TMEM147	-1.11
NM_015476	chromosome 18 open reading frame 10	C18orf10	-1.11
NM_057161	kelch domain containing 3	KLHDC3	-1.11
NM_006896	homeobox A7	HOXA7	-1.12
NM_018283	nudix (nucleoside diphosphate linked moiety X)-type motif 15	NUDT15	-1.12
NM_003079	SWI/SNF related, matrix associated, actin dependent regulator of chromatin, subfamily e, member 1	SMARCE1	-1.12
NM_016243	cytochrome b5 reductase 1	CYB5R1	-1.12
NM_014306	chromosome 22 open reading frame 28	C22orf28	-1.12
NM_015651	PHD finger protein 19	PHF19	-1.12
NM_001039673	Yip1 interacting factor homolog B (S. cerevisiae)	YIF1B	-1.12
NM_153713	Lix1 homolog (mouse)-like	LIX1L	-1.12
NM_178148	solute carrier family 35, member B2	SLC35B2	-1.12
NM_014604	Tax1 (human T-cell leukemia virus type I) binding protein 3	TAX1BP3	-1.12
NM_213601	transmembrane emp24 protein transport domain containing 8	TMED8	-1.12
NM_153273	inositol hexakisphosphate kinase 1	IP6K1	-1.12
NR_002786	cell death-inducing DFFA-like effector c pseudogene	CIDECP	-1.12
NM_024592	steroid 5 alpha-reductase 3	SRD5A3	-1.12
NM_005698	secretory carrier membrane protein 3	SCAMP3	-1.12
NM_198563	transmembrane protein 110	TMEM110	-1.12
NM_004231	ATPase, H+ transporting, lysosomal 14kDa, V1 subunit F	ATP6V1F	-1.12
NM_001135021	ELMO/CED-12 domain containing 3	ELMOD3	-1.12

NM_176783	proteasome (prosome, macropain) activator subunit 1 (PA28 alpha)	PSME1	-1.13
NM_203413	chromosome 17 open reading frame 81	C17orf81	-1.13
NM_007067	MYST histone acetyltransferase 2	MYST2	-1.13
NM_001105203	RUN and SH3 domain containing 1	RUSC1	-1.13
NM_005015	oxidase (cytochrome c) assembly 1-like	OXA1L	-1.13
NM_153002	G protein-coupled receptor 156	GPR156	-1.13
NM_001184768	armadillo repeat containing, X-linked 6	ARMCX6	-1.13
NM_025202	EF-hand domain family, member D1	EFHD1	-1.13
NM_003309	TSPY-like 1	TSPYL1	-1.13
NM_022823	fibronectin type III domain containing 4	FNDC4	-1.13
NM_014971	EFR3 homolog B (S. cerevisiae)	EFR3B	-1.13
NM_006841	solute carrier family 38, member 3	SLC38A3	-1.13
NR_026582	inhibitor of DNA binding 2B, dominant negative helix-loop-helix protein (pseudogene)	ID2B	-1.13
NM_173659	RNA pseudouridylate synthase domain containing 3	RPUSD3	-1.13
NM_199249	chromosome 19 open reading frame 48	C19orf48	-1.13
NM_002633	phosphoglucomutase 1	PGM1	-1.13
NM_001005333	melanoma antigen family D, 1	MAGED1	-1.13
NM_012279	zinc finger protein 346	ZNF346	-1.13
NM_001167820	bladder cancer associated protein	BLCAP	-1.13
NM_000543	sphingomyelin phosphodiesterase 1, acid lysosomal	SMPD1	-1.14
NM_024584	coiled-coil domain containing 121	CCDC121	-1.14
NM_004577	phosphoserine phosphatase	PSPH	-1.14
NM_000304	peripheral myelin protein 22	PMP22	-1.14
NM_006623	phosphoglycerate dehydrogenase	PHGDH	-1.14
NM_024095	ankyrin repeat and SOCS box-containing 8	ASB8	-1.14
NM_032015	ring finger protein 26	RNF26	-1.14
NM_007039	protein tyrosine phosphatase, non-receptor type 21	PTPN21	-1.14
NM_004095	eukaryotic translation initiation factor 4E binding protein 1	EIF4EBP1	-1.14
NM_016506	kelch repeat and BTB (POZ) domain containing 4	KBTBD4	-1.14
NR_028450	branched chain amino-acid transaminase 2, mitochondrial	BCAT2	-1.14
NM_002923	regulator of G-protein signaling 2, 24kDa	RGS2	-1.14
NM_001080473	major facilitator superfamily domain containing 2B	MFSD2B	-1.15
NM_032385	chromosome 5 open reading frame 4	C5orf4	-1.15
NM_032336	GINS complex subunit 4 (Sld5 homolog)	GINS4	-1.15
NM_030821	phospholipase A2, group XIIA	PLA2G12A	-1.15
NM_024887	dehydrodolichyl diphosphate synthase	DHDDS	-1.15
NM_005736	ARP1 actin-related protein 1 homolog A, centractin alpha (yeast)	ACTR1A	-1.15
NM_052875[1]	vacuolar protein sorting 26 homolog B (S. pombe)	VPS26B	-1.15
NM_004548	NADH dehydrogenase (ubiquinone) 1 beta subcomplex, 10, 22kDa	NDUFB10	-1.15
NM_003525	histone cluster 1, H2bi	HIST1H2BI	-1.15
NM_000691	aldehyde dehydrogenase 3 family, member A1	ALDH3A1	-1.15
AY568085	chromosome 6 open reading frame 125	C6orf125	-1.15
NM_032342	chromosome 9 open reading frame 125	C9orf125	-1.15
NM_004776	UDP-Gal:betaGlcNAc beta 1,4-galactosyltransferase, polypeptide 5	B4GALT5	-1.15
NM_004528	microsomal glutathione S-transferase 3	MGST3	-1.15
NM_177528	sulfotransferase family, cytosolic, 1A, phenol-preferring, member 2	SULT1A2	-1.15
NM_018379	family with sequence similarity 63, member A	FAM63A	-1.15
NM_000137[1]	fumarylacetoacetate hydrolase	FAH	-1.15

	(fumarylacetoacetase)		
NM_006221	peptidylprolyl cis/trans isomerase, NIMA-interacting 1	PIN1	-1.15
NM_016952	Cdon homolog (mouse)	CDON	-1.15
NM_022453	ring finger protein 25	RNF25	-1.15
NM_033204	zinc finger protein 101	ZNF101	-1.16
NM_018208	ethanolamine kinase 2	ETNK2	-1.16
NM_017777	Meckel syndrome, type 1	MKS1	-1.16
NM_001312	cysteine-rich protein 2	CRIP2	-1.16
NM_194296	spermatogenesis associated 24	SPATA24	-1.16
NM_020438	dolichyl pyrophosphate phosphatase 1	DOLPP1	-1.16
NM_006503	proteasome (prosome, macropain) 26S subunit, ATPase, 4	PSMC4	-1.16
NM_005227	ephrin-A4	EFNA4	-1.16
NM_006066	aldo-keto reductase family 1, member A1 (aldehyde reductase)	AKR1A1	-1.16
NM_006118	HCLS1 associated protein X-1	HAX1	-1.16
NM_025263	proline rich 3	PRR3	-1.17
NM_006245	protein phosphatase 2, regulatory subunit B', delta	PPP2R5D	-1.17
NM_032377	elongation factor 1 homolog (S. cerevisiae)	ELOF1	-1.17
NM_182491	zinc finger, AN1-type domain 2A	ZFAND2A	-1.17
NM_016060	mediator complex subunit 31	MED31	-1.17
NM_020154	chromosome 15 open reading frame 24	C15orf24	-1.17
NM_138573	neuregulin 4	NRG4	-1.17
NM_000784	cytochrome P450, family 27, subfamily A, polypeptide 1	CYP27A1	-1.18
NM_032822	family with sequence similarity 136, member A	FAM136A	-1.18
NM_053045	transmembrane protein 203	TMEM203	-1.18
NM_198849	seven in absentia homolog 3 (Drosophila)	SIAH3	-1.18
NM_016440	vaccinia related kinase 3	VRK3	-1.18
NM_001338	coxsackie virus and adenovirus receptor	CXADR	-1.18
NM_012412	H2A histone family, member V	H2AFV	-1.18
NM_001077351	RNA binding motif protein 23	RBM23	-1.18
NM_032940	polymerase (RNA) II (DNA directed) polypeptide C, 33kDa	POLR2C	-1.18
NM_001353	aldo-keto reductase family 1, member C1 (dihydrodiol dehydrogenase 1; 20-alpha (3-alpha)-hydroxysteroid dehydrogenase)	AKR1C1	-1.19
NM_174976	zinc finger, DHHC-type containing 22	ZDHHC22	-1.19
NM_004234	zinc finger protein 235	ZNF235	-1.19
NM_032505	kelch repeat and BTB (POZ) domain containing 8	KBTBD8	-1.20
NM_012446	single-stranded DNA binding protein 2	SSBP2	-1.20
NM_001170423	protease, serine, 35	PRSS35	-1.20
NM_006945	small proline-rich protein 2D	SPRR2D	-1.20
NM_017414	ubiquitin specific peptidase 18	USP18	-1.20
NM_014365	heat shock 22kDa protein 8	HSPB8	-1.20
NR_036639	Yip1 domain family, member 1	YIPF1	-1.21
NM_014206	chromosome 11 open reading frame 10	C11orf10	-1.21
NM_003754	eukaryotic translation initiation factor 3, subunit F	EIF3F	-1.21
NM_198179	pyroglutamylated RFamide peptide receptor	QRFPR	-1.22
NM_002167	inhibitor of DNA binding 3, dominant negative helix-loop-helix protein	ID3	-1.22
NR_002722	zinc finger protein 204, pseudogene	ZNF204P	-1.22
NM_001001317	trypsin X3	TRYX3	-1.22
NM_004405	distal-less homeobox 2	DLX2	-1.22
NM_005740[1]	dynein, axonemal, light chain 4	DNAL4	-1.23
NM_002124	major histocompatibility complex, class II, DR beta 1	HLA-DRB1	-1.25

NM_006156	neural precursor cell expressed, developmentally down-regulated 8	NEDD8	-1.25
NM_017700	Rho guanine nucleotide exchange factor (GEF) 38	ARHGEF38	-1.26
NM_001001918	olfactory receptor, family 14, subfamily C, member 36	OR14C36	-1.27
NM_007227	G protein-coupled receptor 45	GPR45	-1.28
NR_024277	non-protein coding RNA 241	NCRNA00241	-1.29
NM_175886	phosphoribosyl pyrophosphate synthetase 1-like 1	PRPS1L1	-1.29
NM_181619	keratin associated protein 21-1	KRTAP21-1	-1.34
NM_019120[1]	protocadherin beta 8	PCDHB8	-1.35
NM_001496	GDNF family receptor alpha 3	GFRA3	-1.36
NM_019599	taste receptor, type 2, member 1	TAS2R1	-1.37
NM_005285	neuropeptides B/W receptor 1	NPBWR1	-1.47
NM_002500	neurogenic differentiation 1	NEUROD1	-1.73

[1] Genes those were significant at $P \leq 0.005$ in table 5.1 in Chapter 5. There were 9 genes removed from this list as they were not annotated in the latest national centre for biotechnology information (NCBI) build 2009-01-31. However, they were all up-regulated, with approximately 0.8 fold increase in gene expression compared to control except one, which had a 1.24 fold reduction in gene expression compared to control.

Annex II

Genes altered in the "Metabolism of xenobiotics by cytochrome P450 pathway" in response to 5μM palcar treatment for 8 hours:

Accession	Gene title	Short name	Fold change	P-value
NM_000693	aldehyde dehydrogenase 1 family, member A3	ALDH1A3	1.161	0.00276
NM_000691	aldehyde dehydrogenase 3 family, member A1	ALDH3A1	-1.148	0.024582
NM_001353	aldo-keto reductase family 1, member C1 (dihydrodiol dehydrogenase 1; 20-alpha (3-alpha)-hydroxysteroid dehydrogenase)	AKR1C1	-1.191	0.008281
NM_004528	microsomal glutathione S-transferase 3	MGST3	-1.151	0.028535
NM_000767	cytochrome P450, family 2, subfamily B, polypeptide 6	CYP2B6	1.169	0.045439

Annex III

Genes that were affected in olfactory transduction pathway in response to 5µM palcar treatment for 8 hours:

Accession	Gene title	Short name	Fold change	P-value
NM_001004461	olfactory receptor, family 10, subfamily A, member 6	OR10A6	1.218	0.041
NM_001005167	olfactory receptor, family 52, subfamily E, member 6	OR52E6	1.341	0.003
NM_001004726	olfactory receptor, family 4, subfamily X, member 1	OR4X1	1.231	0.032
NM_001005204	olfactory receptor, family 8, subfamily U, member 1	OR8U1	1.236	0.014
NM_001001961	olfactory receptor, family 13, subfamily C, member 3	OR13C3	1.228	0.038
NM_001004756	olfactory receptor, family 51, subfamily M, member 1	OR51M1	1.294	0.007
NM_001004735	olfactory receptor, family 5, subfamily D, member 14	OR5D14	1.325	0.025
NM_001005205	olfactory receptor, family 8, subfamily J, member 1	OR8J1	1.168	0.041
NM_001001922	olfactory receptor, family 52, subfamily N, member 5	OR52N5	1.427	0.001
NM_001004730	olfactory receptor, family 5, subfamily AR, member 1	OR5AR1	1.206	0.044
NM_033057	olfactory receptor, family 2, subfamily B, member 2	OR2B2	1.293	0.004
NM_153444	olfactory receptor, family 5, subfamily P, member 2	OR5P2	1.230	0.035
NM_001005197	olfactory receptor, family 8, subfamily D, member 4	OR8D4	1.241	0.044
NM_001001918	olfactory receptor, family 14, subfamily C, member 36	OR14C36	-1.273	0.040
NM_001005182	olfactory receptor, family 6, subfamily C, member 1	OR6C1	1.345	0.046
NM_001005329	olfactory receptor, family 51, subfamily A, member 4	OR51A4	1.315	0.006

Annex IV

Genes that were affected in cytokine-cytokine receptor interaction pathway in response to 5µM palcar treatment for 8 hours:

Accession	Gene title	Short name	Fold change	P-value
NM_001192	tumor necrosis factor receptor superfamily, member 17	TNFRSF17	1.243	0.023
NM_000880	interleukin 7	IL7	1.180	0.006
NM_000074	CD40 ligand	CD40LG	1.216	0.025
NM_002173	interferon, alpha 16	IFNA16	1.317	0.001
NM_002546	tumor necrosis factor receptor superfamily, member 11b	TNFRSF11B	1.219	0.004
NM_002175	interferon, alpha 21	IFNA21	1.247	0.038
NM_000575	interleukin 1, alpha	IL1A	1.306	0.003
NM_005118	tumor necrosis factor (ligand) superfamily, member 15	TNFSF15	1.231	0.026
NM_002982	chemokine (C-C motif) ligand 2	CCL2	1.167	0.017
NM_002019	fms-related tyrosine kinase 1 (vascular endothelial growth factor/vascular permeability factor receptor)	FLT1	1.151	0.048
NM_176891	interferon, epsilon	IFNE	1.267	0.029

Annex V

Genes altered in the Sulfur metabolic pathway in response to 10nM DHT treatment for 8 hours:

Accession	Gene title	Short name	Fold change	P-value
NM_177528	sulfotransferase family, cytosolic, 1A, phenol-preferring, member 2	SULT1A2	-1.161	0.008041
NM_003166	sulfotransferase family, cytosolic, 1A, phenol-preferring, member 3	SULT1A3	-1.124	0.048171
NM_000456	sulfite oxidase	SUOX	-1.290	0.000384

Annex VI

Genes that were affected in the porphyrin and chlorophyll metabolic pathway in response to 10nM DHT treatment for 8 hours:

Accession	Gene title	Short name	Fold change	P-value
NR_036510	uroporphyrinogen decarboxylase	UROD	-1.120	0.026
NM_000713	biliverdin reductase B (flavin reductase (NADPH))	BLVRB	-1.159	0.046
NM_000031	aminolevulinate dehydratase	ALAD	-1.167	0.004
NM_001303	COX10 homolog, cytochrome c oxidase assembly protein, heme A: farnesyltransferase (yeast)	COX10	-1.132	0.043
NM_001012515	ferrochelatase	FECH	-1.181	0.010

Annex VII

Genes that were affected in the tyrosine metabolic pathway in response to 10nM DHT treatment for 8 hours:

Accession	Gene title	Short name	Fold change	P-value
NM_000693	aldehyde dehydrogenase 1 family, member A3	ALDH1A3	1.257	0.0001
NM_002415	macrophage migration inhibitory factor (glycosylation-inhibiting factor)	MIF	1.157	0.025
NM_000137	fumarylacetoacetate hydrolase (fumarylacetoacetase)	FAH	-1.143	0.005
NM_000691	aldehyde dehydrogenase 3 family, member A1	ALDH3A1	-1.146	0.027
NM_000754	catechol-O-methyltransferase	COMT	-1.165	0.026
NM_016173	HemK methyltransferase family member 1	HEMK1	-1.185	0.008

Annex VIII

Genes that were affected in the TGF-beta signalling pathway in response to 10nM DHT treatment for 8 hours:

Accession	Gene title	Short name	Fold change	P-value
NM_002467	v-myc myelocytomatosis viral oncogene homolog (avian)	MYC	1.159	0.019
NM_003246	thrombospondin 1	THBS1	1.136	0.035
NM_002167	inhibitor of DNA binding 3, dominant negative helix-loop-helix protein	ID3	-1.240	0.009
NM_001719	bone morphogenetic protein 7	BMP7	-1.144	0.015
NM_003247	thrombospondin 2	THBS2	1.162	0.006
NM_001720	bone morphogenetic protein 8b	BMP8B	-1.197	0.046
NM_153426	paired-like homeodomain 2	PITX2	-1.157	0.025
NM_001135599	transforming growth factor, beta 2	TGFB2	1.251	0.009
NM_001127217	SMAD family member 9	SMAD9	-1.136	0.033

Annex IX

The list of the 169 genes in common between 10nM DHT and 5µM palcar in PNT1A cells after treatment for 8 hours (P≤0.05) arranged according to the fold change in descending order.

Accession	Gene description	Gene name	Fold change of palcar vs ctrl	Fold change of DHT vs ctrl
NR_026813	chromosome 15 open reading frame 5	C15orf5	1.569	1.613
NM_138331	ribonuclease, RNase A family, 8	RNASE8	1.434	1.240
NM_001001922	olfactory receptor, family 52, subfamily N, member 5	OR52N5	1.427	1.382
AF165185	LSM14B, SCD6 homolog B (S. cerevisiae)	LSM14B	1.426	1.372
NM_013318	HLA-B associated transcript 2-like 1	BAT2L1	1.420	1.308
NM_020646	achaete-scute complex homolog 3 (Drosophila)	ASCL3	1.395	1.346
NM_178455	serine peptidase inhibitor, Kunitz type 4	SPINT4	1.352	1.412
NM_001004735	olfactory receptor, family 5, subfamily D, member 14	OR5D14	1.325	1.486
NM_000575	interleukin 1, alpha	IL1A	1.306	1.284
AF210651	NAG18 mRNA	NAG18	1.305	1.239
NM_020903	ubiquitin specific peptidase 29	USP29	1.295	1.380
NM_001004756	olfactory receptor, family 51, subfamily M, member 1	OR51M1	1.294	1.256
NM_033057	olfactory receptor, family 2, subfamily B, member 2	OR2B2	1.293	1.223
NM_176891	interferon, epsilon	IFNE	1.267	1.336
NM_017680	asporin	ASPN	1.249	1.186
NM_024775	gem (nuclear organelle) associated protein 6	GEMIN6	1.238	1.253
NR_002776	MCM3AP antisense RNA (non-protein coding)	MCM3AP-AS	1.233	1.100
NM_005118	tumor necrosis factor (ligand) superfamily, member 15	TNFSF15	1.231	1.267
NM_005242	coagulation factor II (thrombin) receptor-like 1	F2RL1	1.229	1.207
NM_213658	killer cell lectin-like receptor subfamily C, member 1	KLRC1	1.223	1.170
NM_152647	chromosome 15 open reading frame 33	C15orf33	1.221	1.142
NM_003540	histone cluster 1, H4f	HIST1H4F	1.221	1.195
NM_002546	tumor necrosis factor receptor superfamily, member 11b	TNFRSF11B	1.219	1.132
NM_001004461	olfactory receptor, family 10, subfamily A, member 6	OR10A6	1.218	1.256
NM_001143811	brain-derived neurotrophic factor	BDNF	1.217	1.261
NM_000074	CD40 ligand	CD40LG	1.216	1.236
NM_003007	semenogelin I	SEMG1	1.214	1.244
NM_004780	transcription elongation factor A (SII)-like 1	TCEAL1	1.210	1.149
AL831934	zinc finger protein 663	ZNF663	1.209	1.195

NM_001008391	coiled-coil domain containing 73	CCDC73	1.206	1.179
NM_015714	G0/G1switch 2	G0S2	1.205	1.288
NR_026825	ribosomal protein SA pseudogene 52	RPSAP52	1.201	1.174
NM_001143668	adhesion molecule with Ig-like domain 2	AMIGO2	1.200	1.337
NM_001165	baculoviral IAP repeat-containing 3	BIRC3	1.199	1.334
NM_144594	gametocyte specific factor 1	GTSF1	1.188	1.207
NM_005842	sprouty homolog 2 (Drosophila)	SPRY2	1.187	1.333
NM_014344	four jointed box 1 (Drosophila)	FJX1	1.184	1.264
NM_001924	growth arrest and DNA-damage-inducible, alpha	GADD45A	1.183	1.253
NM_001163560	chromosome 16 open reading frame 73	C16orf73	1.182	1.247
NM_000880	interleukin 7	IL7	1.180	1.250
NM_003714	stanniocalcin 2	STC2	1.179	1.182
NM_002228	jun proto-oncogene	JUN	1.172	1.314
NM_001993	coagulation factor III (thromboplastin, tissue factor)	F3	1.170	1.290
NM_002658	plasminogen activator, urokinase	PLAU	1.168	1.322
NM_001005205	olfactory receptor, family 8, subfamily J, member 1	OR8J1	1.168	1.253
NM_002982	chemokine (C-C motif) ligand 2	CCL2	1.167	1.329
NR_026838	Down syndrome critical region gene 8	DSCR8	1.165	1.196
NM_000212	integrin, beta 3 (platelet glycoprotein IIIa, antigen CD61)	ITGB3	1.162	1.169
NM_213599	anoctamin 5	ANO5	1.162	1.149
NM_000693	aldehyde dehydrogenase 1 family, member A3	ALDH1A3	1.161	1.257
NM_003897	immediate early response 3	IER3	1.161	1.176
NM_004613	transglutaminase 2 (C polypeptide, protein-glutamine-gamma-glutamyltransferase)	TGM2	1.160	1.219
NM_024688	chromosome 10 open reading frame 68	C10orf68	1.157	1.109
NM_000189	hexokinase 2	HK2	1.156	1.168
NM_001097579	G protein-coupled receptor 34	GPR34	1.154	1.158
NM_003247	thrombospondin 2	THBS2	1.154	1.162
NM_080817	G protein-coupled receptor 82	GPR82	1.152	1.177
NM_022475	hedgehog interacting protein	HHIP	1.150	1.199
NM_004190	lipase, gastric	LIPF	1.148	1.163
NM_058187	chromosome 21 open reading frame 63	C21orf63	1.147	1.124
NM_024764	cation channel, sperm-associated, beta	CATSPERB	1.144	1.139
NM_199254	transmembrane phosphoinositide 3-phosphatase and tensin homolog 2	TPTE2	1.140	1.103
NM_002356	myristoylated alanine-rich protein kinase C substrate	MARCKS	1.138	1.194
NR_027786	serine hydrolase-like	SERHL	1.136	1.140
NM_022842	CUB domain containing protein 1	CDCP1	1.135	1.200
NM_002068	guanine nucleotide binding protein (G protein), alpha 15 (Gq class)	GNA15	1.134	1.118
NM_020348	cyclin M1	CNNM1	1.129	1.110
NM_031938	beta-carotene oxygenase 2	BCO2	1.124	1.154
NM_001554	cysteine-rich, angiogenic inducer, 61	CYR61	1.114	1.121

NM_014011	suppressor of cytokine signaling 5	SOCS5	1.114	1.148
NM_014391	ankyrin repeat domain 1 (cardiac muscle)	ANKRD1	1.114	1.207
NM_004196	cyclin-dependent kinase-like 1 (CDC2-related kinase)	CDKL1	1.110	1.112
NM_001964	early growth response 1	EGR1	1.106	1.126
NM_182643	deleted in liver cancer 1	DLC1	1.097	1.114
NM_033198	phosphatidylinositol glycan anchor biosynthesis, class S	PIGS	-1.094	-1.108
NM_015060	AVL9 homolog (S. cerevisiase)	AVL9	-1.097	-1.125
NM_006076	ArfGAP with FG repeats 2	AGFG2	-1.101	-1.153
NM_005469	acyl-CoA thioesterase 8	ACOT8	-1.104	-1.175
NM_014773	KIAA0141	KIAA0141	-1.105	-1.163
NM_017849	transmembrane protein 127	TMEM127	-1.107	-1.124
NM_001109903	ring finger protein, transmembrane 2	RNFT2	-1.108	-1.127
NM_170607	MAX-like protein X	MLX	-1.108	-1.119
NM_017873	ankyrin repeat and SOCS box-containing 6	ASB6	-1.109	-1.127
NM_001610	acid phosphatase 2, lysosomal	ACP2	-1.111	-1.166
NM_201540	NDRG family member 2	NDRG2	-1.112	-1.137
NM_145799	septin 6	SEPT6	-1.114	-1.149
NM_032635	transmembrane protein 147	TMEM147	-1.114	-1.107
NM_003079	SWI/SNF related, matrix associated, actin dependent regulator of chromatin, subfamily e, member 1	SMARCE1	-1.117	-1.108
NM_014306	chromosome 22 open reading frame 28	C22orf28	-1.117	-1.119
NM_015651	PHD finger protein 19	PHF19	-1.119	-1.177
NM_001039673	Yip1 interacting factor homolog B (S. cerevisiae)	YIF1B	-1.119	-1.201
NM_153713	Lix1 homolog (mouse)-like	LIX1L	-1.120	-1.155
NM_014604	Tax1 (human T-cell leukemia virus type I) binding protein 3	TAX1BP3	-1.120	-1.134
NM_178148	solute carrier family 35, member B2	SLC35B2	-1.120	-1.125
NM_153273	inositol hexakisphosphate kinase 1	IP6K1	-1.120	-1.141
NR_002786	cell death-inducing DFFA-like effector c pseudogene	CIDECP	-1.121	-1.181
NM_005698	secretory carrier membrane protein 3	SCAMP3	-1.123	-1.124
NM_198563	transmembrane protein 110	TMEM110	-1.123	-1.206
NM_001135021	ELMO/CED-12 domain containing 3	ELMOD3	-1.125	-1.220
NM_176783	proteasome (prosome, macropain) activator subunit 1 (PA28 alpha)	PSME1	-1.126	-1.116
NM_203413	chromosome 17 open reading frame 81	C17orf81	-1.126	-1.157
NM_007067	MYST histone acetyltransferase 2	MYST2	-1.128	-1.134
NM_001105203	RUN and SH3 domain containing 1	RUSC1	-1.128	-1.195
NM_153002	G protein-coupled receptor 156	GPR156	-1.129	-1.128
NM_025202	EF-hand domain family, member D1	EFHD1	-1.130	-1.132
NM_003309	TSPY-like 1	TSPYL1	-1.130	-1.136

NM_022823	fibronectin type III domain containing 4	FNDC4	-1.131	-1.144
NM_014971	EFR3 homolog B (S. cerevisiae)	EFR3B	-1.131	-1.141
NM_006841	solute carrier family 38, member 3	SLC38A3	-1.132	-1.132
NM_173659	RNA pseudouridylate synthase domain containing 3	RPUSD3	-1.133	-1.222
NM_002633	phosphoglucomutase 1	PGM1	-1.133	-1.150
NM_199249	chromosome 19 open reading frame 48	C19orf48	-1.133	-1.223
NM_001167820	bladder cancer associated protein	BLCAP	-1.135	-1.107
NM_004577	phosphoserine phosphatase	PSPH	-1.137	-1.138
NM_000304	peripheral myelin protein 22	PMP22	-1.137	-1.112
NM_006623	phosphoglycerate dehydrogenase	PHGDH	-1.140	-1.216
NM_024095	ankyrin repeat and SOCS box-containing 8	ASB8	-1.141	-1.176
NM_032015	ring finger protein 26	RNF26	-1.141	-1.165
NM_004095	eukaryotic translation initiation factor 4E binding protein 1	EIF4EBP1	-1.142	-1.202
NM_016506	kelch repeat and BTB (POZ) domain containing 4	KBTBD4	-1.142	-1.164
NR_028450	branched chain amino-acid transaminase 2, mitochondrial	BCAT2	-1.142	-1.186
NM_001080473	major facilitator superfamily domain containing 2B	MFSD2B	-1.145	-1.181
NM_032385	chromosome 5 open reading frame 4	C5orf4	-1.146	-1.211
NM_024887	dehydrodolichyl diphosphate synthase	DHDDS	-1.147	-1.189
NM_005736	ARP1 actin-related protein 1 homolog A, centractin alpha (yeast)	ACTR1A	-1.147	-1.106
NM_052875	vacuolar protein sorting 26 homolog B (S. pombe)	VPS26B	-1.148	-1.112
NM_004548	NADH dehydrogenase (ubiquinone) 1 beta subcomplex, 10, 22kDa	NDUFB10	-1.148	-1.147
NM_000691	aldehyde dehydrogenase 3 family, member A1	ALDH3A1	-1.148	-1.146
NM_032342	chromosome 9 open reading frame 125	C9orf125	-1.149	-1.118
NM_177528	sulfotransferase family, cytosolic, 1A, phenol-preferring, member 2	SULT1A2	-1.151	-1.161
NM_018379	family with sequence similarity 63, member A	FAM63A	-1.152	-1.181
NM_000137	fumarylacetoacetate hydrolase (fumarylacetoacetase)	FAH	-1.152	-1.143
NM_033204	zinc finger protein 101	ZNF101	-1.156	-1.155
NM_017777	Meckel syndrome, type 1	MKS1	-1.157	-1.130
NM_001312	cysteine-rich protein 2	CRIP2	-1.157	-1.200
NM_194296	spermatogenesis associated 24	SPATA24	-1.159	-1.217
NM_020438	dolichyl pyrophosphate phosphatase 1	DOLPP1	-1.160	-1.140
NM_006503	proteasome (prosome, macropain) 26S subunit, ATPase, 4	PSMC4	-1.160	-1.155
NM_005227	ephrin-A4	EFNA4	-1.161	-1.236
NM_006066	aldo-keto reductase family 1, member A1 (aldehyde reductase)	AKR1A1	-1.163	-1.238

NM_006118	HCLS1 associated protein X-1	HAX1	-1.164	-1.169
NM_025263	proline rich 3	PRR3	-1.165	-1.138
NM_006245	protein phosphatase 2, regulatory subunit B', delta	PPP2R5D	-1.166	-1.225
NM_032377	elongation factor 1 homolog (S. cerevisiae)	ELOF1	-1.168	-1.221
NM_138573	neuregulin 4	NRG4	-1.174	-1.359
NM_000784	cytochrome P450, family 27, subfamily A, polypeptide 1	CYP27A1	-1.175	-1.221
NM_032822	family with sequence similarity 136, member A	FAM136A	-1.175	-1.169
NM_053045	transmembrane protein 203	TMEM203	-1.179	-1.202
NM_198849	seven in absentia homolog 3 (Drosophila)	SIAH3	-1.181	-1.163
NM_016440	vaccinia related kinase 3	VRK3	-1.182	-1.213
NM_001077351	RNA binding motif protein 23	RBM23	-1.183	-1.177
NM_032940	polymerase (RNA) II (DNA directed) polypeptide C, 33kD	POLR2C	-1.184	-1.127
NM_174976	zinc finger, DHHC-type containing 22	ZDHHC22	-1.192	-1.322
NM_032505	kelch repeat and BTB (POZ) domain containing 8	KBTBD8	-1.196	-1.182
NM_017414	ubiquitin specific peptidase 18	USP18	-1.204	-1.198
NM_014365	heat shock 22kDa protein 8	HSPB8	-1.204	-1.179
NR_036639	Yip1 domain family, member 1	YIPF1	-1.205	-1.239
NM_014206	chromosome 11 open reading frame 10	C11orf10	-1.209	-1.193
NM_003754	eukaryotic translation initiation factor 3, subunit F	EIF3F	-1.214	-1.304
NM_002167	inhibitor of DNA binding 3, dominant negative helix-loop-helix protein	ID3	-1.216	-1.240
NR_002722	zinc finger protein 204, pseudogene	ZNF204P	-1.217	-1.216
NM_004405	distal-less homeobox 2	DLX2	-1.222	-1.245
NM_005740	dynein, axonemal, light chain 4	DNAL4	-1.231	-1.156
NM_175886	phosphoribosyl pyrophosphate synthetase 1-like 1	PRPS1L1	-1.294	-1.280
NM_019120	protocadherin beta 8	PCDHB8	-1.347	-1.433
NM_005285	neuropeptides B/W receptor 1	NPBWR1	-1.472	-1.430

Three genes were not annotated in the latest NCBI build 2009-01-31, therefore they were removed from this list. However, they were all up-regulated, with approximately 1.3 fold increase in gene expression compared to control.

References

1. IARC. *GLOBOCAN 2008*. 2010; Data from WHO]. Available from: http://globocan.iarc.fr/factsheets/populations/factsheet.asp?uno=900.
2. Statistics, O.f.N. *Cancer registrations in England, 2010*. 2012; Available from: http://www.ons.gov.uk/ons/dcp171778_263537.pdf.
3. Kirby, R.S. and M.I. Patel, *Prostate Cancer*. 2011: Health Press Limited.
4. Giovannucci, E. and D. Michaud, *The role of obesity and related metabolic disturbances in cancers of the colon, prostate, and pancreas.* Gastroenterology, 2007. **132**(6): p. 2208-25.
5. Zadra, G., C. Photopoulos, and M. Loda, *The fat side of prostate cancer.* Biochim Biophys Acta, 2013.
6. Adams, S.H., et al., *Plasma acylcarnitine profiles suggest incomplete long-chain fatty acid beta-oxidation and altered tricarboxylic acid cycle activity in type 2 diabetic African-American women.* J Nutr, 2009. **139**(6): p. 1073-81.
7. Mihalik, S.J., et al., *Increased levels of plasma acylcarnitines in obesity and type 2 diabetes and identification of a marker of glucolipotoxicity.* Obesity (Silver Spring), 2010. **18**(9): p. 1695-700.
8. Ganti, S., et al., *Urinary acylcarnitines are altered in human kidney cancer.* Int J Cancer, 2012. **130**(12): p. 2791-800.
9. Liu, Y., L.S. Zuckier, and N.V. Ghesani, *Dominant uptake of fatty acid over glucose by prostate cells: a potential new diagnostic and therapeutic approach.* Anticancer Res, 2010. **30**(2): p. 369-74.
10. Santos, C.R. and A. Schulze, *Lipid metabolism in cancer.* FEBS Journal, 2012. **279**(15): p. 2610-2623.
11. Jones, L.L., D.A. McDonald, and P.R. Borum, *Acylcarnitines: role in brain.* Prog Lipid Res, 2010. **49**(1): p. 61-75.
12. Ebert, D., R.G. Haller, and M.E. Walton, *Energy Contribution of Octanoate to Intact Rat Brain Metabolism Measured by 13C Nuclear Magnetic Resonance Spectroscopy.* The Journal of Neuroscience, 2003. **23**(13): p. 5928-5935.
13. Devlin, K.J. and T.M. Devlin, *Textbook of Biochemistry: With Clinical Correlations and Student Survey Set*. 1999: John Wiley & Sons Australia, Limited.
14. Vander, A.J.L., D. S. and Sherman, J. H. , *Human Physiology: The Mechanisms of Body Function*. 8th ed. 2001, Boston, MA: The McGraw−Hill Companies, 2001.
15. Corr, P., R. Gross, and B. Sobel, *Amphipathic metabolites and membrane dysfunction in ischemic myocardium.* Circulation Research, 1984. **55**(2): p. 135-154.
16. Zammit, V.A., et al., *Carnitine, mitochondrial function and therapy.* Advanced Drug Delivery Reviews, 2009. **61**(14): p. 1353-1362.
17. Kler, R.S., et al., *Quantitation of acyl-CoA and acylcarnitine esters accumulated during abnormal mitochondrial fatty acid oxidation.* J Biol Chem, 1991. **266**(34): p. 22932-8.
18. Indiveri, C., et al., *The mitochondrial carnitine/acylcarnitine carrier: Function, structure and physiopathology.* Mol Aspects Med, 2011. **32**(4-6): p. 223-33.

19. Palmieri, F. and C.L. Pierri, *Mitochondrial metabolite transport.* Essays in biochemistry, 2010. **47**: p. 37-52.
20. Foster, D.W., *The Role of the Carnitine System in Human Metabolism.* Annals of the New York Academy of Sciences, 2004. **1033**(1): p. 1-16.
21. Idell-Wenger, J.A., L.W. Grotyohann, and J.R. Neely, *Coenzyme A and carnitine distribution in normal and ischemic hearts.* Journal of Biological Chemistry, 1978. **253**(12): p. 4310-4318.
22. Indiveri, C., A. Tonazzi, and F. Palmieri, *The reconstituted carnitine carrier from rat liver mitochondria: evidence for a transport mechanism different from that of the other mitochondrial translocators.* Biochimica et Biophysica Acta (BBA) - Biomembranes, 1994. **1189**(1): p. 65-73.
23. Reuter, S.E. and A.M. Evans, *Long-chain acylcarnitine deficiency in patients with chronic fatigue syndrome. Potential involvement of altered carnitine palmitoyltransferase-I activity.* Journal of Internal Medicine, 2011. **270**(1): p. 76-84.
24. Koves, T.R., et al., *Mitochondrial Overload and Incomplete Fatty Acid Oxidation Contribute to Skeletal Muscle Insulin Resistance.* Cell Metabolism, 2008. **7**(1): p. 45-56.
25. Houten, S.M. and R.J. Wanders, *A general introduction to the biochemistry of mitochondrial fatty acid β-oxidation.* Journal of inherited metabolic disease, 2010. **33**(5): p. 469-77.
26. Chegary, M., et al., *Mitochondrial long chain fatty acid beta-oxidation in man and mouse.* Biochim Biophys Acta, 2009. **1791**(8): p. 806-15.
27. Zha, S., et al., *Peroxisomal branched chain fatty acid beta-oxidation pathway is upregulated in prostate cancer.* Prostate, 2005. **63**(4): p. 316-23.
28. Brière, J.-J., et al., *Tricarboxylic acid cycle dysfunction as a cause of human diseases and tumor formation.* American Journal of Physiology - Cell Physiology, 2006. **291**(6): p. C1114-C1120.
29. McCormack, J. and R. Denton, *The role of Ca2+ ions in the regulation of intramitochondrial metabolism and energy production in rat heart.* Molecular and Cellular Biochemistry, 1989. **89**(2): p. 121-125.
30. Bourgeron, T., et al., *Mutation of the fumarase gene in two siblings with progressive encephalopathy and fumarase deficiency.* The Journal of Clinical Investigation, 1994. **93**(6): p. 2514-2518.
31. Peng, M., et al., *Measurement of free carnitine and acylcarnitines in plasma by HILIC-ESI-MS/MS without derivatization.* J Chromatogr B Analyt Technol Biomed Life Sci, 2013. **932C**: p. 12-18.
32. Minkler, P.E., et al., *Quantification of carnitine and acylcarnitines in biological matrices by HPLC electrospray ionization-mass spectrometry.* Clin Chem, 2008. **54**(9): p. 1451-62.
33. Ha, C.Y., et al., *The association of specific metabolites of lipid metabolism with markers of oxidative stress, inflammation and arterial stiffness in men with newly diagnosed type 2 Diabetes.* Clinical Endocrinology, 2011: p. no-no.
34. Newgard, C.B., et al., *A Branched-Chain Amino Acid-Related Metabolic Signature that Differentiates Obese and Lean Humans*

and Contributes to Insulin Resistance. Cell Metabolism, 2009. **9**(4): p. 311-326.
35. Krebs, M., et al., *Mechanism of Amino Acid-Induced Skeletal Muscle Insulin Resistance in Humans.* Diabetes, 2002. **51**(3): p. 599-605.
36. Lundbæk, J.A., R.E. Koeppe, and O.S. Andersen, *Amphiphile regulation of ion channel function by changes in the bilayer spring constant.* Proceedings of the National Academy of Sciences, 2010. **107**(35): p. 15427-15430.
37. LAMERS, J.M.J., et al., *On the possible role of long chain fatty acylcarnitine accumulation in producing functional and calcium permeability changes in membranes during myocardial ischaemia.* Cardiovascular Research, 1987. **21**(5): p. 313-322.
38. Chien, K.R., et al., *Fatty acylcarnitine accumulation and membrane injury in ischemic canine myocardium.* Am J Cardiol, 1983. **52**(7): p. 893-7.
39. Fink, K. and R. Gross, *Modulation of canine myocardial sarcolemmal membrane fluidity by amphiphilic compounds.* Circulation Research, 1984. **55**(5): p. 585-594.
40. Inoue, N., et al., *Palmitoyl-L-carnitine modifies the function of vascular endothelium.* Cardiovasc Res, 1994. **28**(1): p. 129-34.
41. Adams, R.J., et al., *In vitro effects of palmitylcarnitine on cardiac plasma membrane Na,K-ATPase, and sarcoplasmic reticulum Ca2+-ATPase and Ca2+ transport.* J Biol Chem, 1979. **254**(24): p. 12404-10.
42. Wood, J.M., et al., *Inhibition of bovine heart Na+,K+-ATPase by palmitylcarnitine and palmityl-CoA.* Biochemical and Biophysical Research Communications, 1977. **74**(2): p. 677-684.
43. el-Hayek, R., et al., *Activation of the Ca2+ release channel of skeletal muscle sarcoplasmic reticulum by palmitoyl carnitine.* Biophys J, 1993. **65**(2): p. 779-89.
44. Muraki, K. and Y. Imaizumi, *A novel action of palmitoyl-L-carnitine in human vascular endothelial cells*. Vol. 92. 2003. 252-8.
45. Sun, Y.H., et al., *Androgens induce increases in intracellular calcium via a G protein-coupled receptor in LNCaP prostate cancer cells.* J Androl, 2006. **27**(5): p. 671-8.
46. Sampey, B.P., et al., *Metabolomic profiling reveals mitochondrial-derived lipid biomarkers that drive obesity-associated inflammation.* PLoS One, 2012. **7**(6): p. e38812.
47. Kouttab, N.M. and C. De Simone, *Modulation of cytokine production by carnitine.* Mediators Inflamm, 1993. **2**(7): p. S25-8.
48. Kutikov, A., et al., *Interleukin-6: a potential biomarker of resistance to multitargeted receptor tyrosine kinase inhibitors in castration-resistant prostate cancer.* Urology, 2011. **78**(4): p. 968 e7-11.
49. Cansino Alcaide, J.R., et al., *[Prostatic specific antigen (PS), pro-inflammatory cytokines, and prostatic pathology (benign prostatic hyperplasia and cancer). Relationship with malignancy].* Arch Esp Urol, 2009. **62**(5): p. 359-66.
50. Siegsmund, M.J., H. Yamazaki, and I. Pastan, *Interleukin 6 receptor mRNA in prostate carcinomas and benign prostate hyperplasia.* J Urol, 1994. **151**(5): p. 1396-9.

51. Royuela, M., et al., *Immunohistochemical analysis of the IL-6 family of cytokines and their receptors in benign, hyperplasic, and malignant human prostate.* J Pathol, 2004. **202**(1): p. 41-9.
52. Murillo, G. and R.G. Mehta, *Cruciferous vegetables and cancer prevention.* Nutr Cancer, 2001. **41**(1-2): p. 17-28.
53. Papi, A., et al., *Cytotoxic and antioxidant activity of 4-methylthio-3-butenyl isothiocyanate from Raphanus sativus L. (Kaiware Daikon) sprouts.* J Agric Food Chem, 2008. **56**(3): p. 875-83.
54. Traka, M. and R. Mithen, *Glucosinolates, isothiocyanates and human health.* Phytochemistry Reviews, 2009. **8**(1): p. 269-282.
55. Joshipura, K.J., et al., *Fruit and vegetable intake in relation to risk of ischemic stroke.* JAMA, 1999. **282**(13): p. 1233-9.
56. London, S.J., et al., *Isothiocyanates, glutathione S-transferase M1 and T1 polymorphisms, and lung-cancer risk: a prospective study of men in Shanghai, China.* Lancet, 2000. **356**(9231): p. 724-9.
57. Ambrosone, C.B., et al., *Breast cancer risk in premenopausal women is inversely associated with consumption of broccoli, a source of isothiocyanates, but is not modified by GST genotype.* J Nutr, 2004. **134**(5): p. 1134-8.
58. Epplein, M., et al., *Urinary isothiocyanates; glutathione S-transferase M1, T1, and P1 polymorphisms; and risk of colorectal cancer: the Multiethnic Cohort Study.* Cancer Epidemiol Biomarkers Prev, 2009. **18**(1): p. 314-20.
59. Yang, G., et al., *Isothiocyanate exposure, glutathione S-transferase polymorphisms, and colorectal cancer risk.* The American Journal of Clinical Nutrition, 2010. **91**(3): p. 704-711.
60. Tang, L., et al., *Intake of cruciferous vegetables modifies bladder cancer survival.* Cancer Epidemiol Biomarkers Prev, 2010. **19**(7): p. 1806-11.
61. Giovannucci, E., et al., *A prospective study of cruciferous vegetables and prostate cancer.* Cancer Epidemiol Biomarkers Prev, 2003. **12**(12): p. 1403-9.
62. Kolonel, L.N., et al., *Vegetables, fruits, legumes and prostate cancer: a multiethnic case-control study.* Cancer Epidemiol Biomarkers Prev, 2000. **9**(8): p. 795-804.
63. Jain, M.G., et al., *Plant foods, antioxidants, and prostate cancer risk: findings from case-control studies in Canada.* Nutr Cancer, 1999. **34**(2): p. 173-84.
64. Steevens, J., et al., *Vegetables and fruits consumption and risk of esophageal and gastric cancer subtypes in the Netherlands Cohort Study.* Int J Cancer, 2011. **129**(11): p. 2681-93.
65. Annema, N., et al., *Fruit and vegetable consumption and the risk of proximal colon, distal colon, and rectal cancers in a case-control study in Western Australia.* J Am Diet Assoc, 2011. **111**(10): p. 1479-90.
66. Armah, C.N., et al., *A diet rich in high-glucoraphanin broccoli interacts with genotype to reduce discordance in plasma metabolite profiles by modulating mitochondrial function.* Am J Clin Nutr, 2013. **98**(3): p. 712-22.
67. Li, W. and A.N. Kong, *Molecular mechanisms of Nrf2-mediated antioxidant response.* Mol Carcinog, 2009. **48**(2): p. 91-104.

68. Maheo, K., et al., *Inhibition of cytochromes P-450 and induction of glutathione S-transferases by sulforaphane in primary human and rat hepatocytes.* Cancer Res, 1997. **57**(17): p. 3649-52.
69. May, D.H., et al., *Metabolomic profiling of urine: response to a randomised, controlled feeding study of select fruits and vegetables, and application to an observational study.* Br J Nutr, 2013. **110**(10): p. 1760-70.
70. Menni, C., et al., *Targeted metabolomics profiles are strongly correlated with nutritional patterns in women.* Metabolomics, 2013. **9**(2): p. 506-514.
71. Chen, C., et al., *Induction of detoxifying enzymes by garlic organosulfur compounds through transcription factor Nrf2: effect of chemical structure and stress signals.* Free Radic Biol Med, 2004. **37**(10): p. 1578-90.
72. Boettler, U., et al., *Coffee constituents as modulators of Nrf2 nuclear translocation and ARE (EpRE)-dependent gene expression.* J Nutr Biochem, 2011. **22**(5): p. 426-40.
73. Consultation, R.o.a.J.F.W.E., *Diet, nutrition and the prevention of chronic diseases*, in *WHO Technical Report Series, No. 916*. 2003, World Health Organization: Geneva.
74. Notara, M. and A. Ahmed, *Benign prostate hyperplasia and stem cells: a new therapeutic opportunity.* Cell Biol Toxicol, 2012. **28**(6): p. 435-42.
75. Dasgupta, P. and R.S. Kirby, *ABC of Prostate Cancer*. 2011: Wiley.
76. De Nunzio, C., et al., *The correlation between metabolic syndrome and prostatic diseases.* Eur Urol, 2012. **61**(3): p. 560-70.
77. Oh WK, H.M., D'Amico AV, et al. , *Biology of Prostate Cancer*, in *Holland-Frei Cancer Medicine*, P.R. Kufe DW, Weichselbaum RR, et al., Editor. 2003, Hamilton (ON): BC Decker.
78. Kumar, A., et al., *Expression of Pro Form of Prostate-specific Antigen by Mammalian Cells and Its Conversion to Mature, Active Form by Human Kallikrein 2.* Cancer Research, 1997. **57**(15): p. 3111-3114.
79. Clinic, M.G. *Anatomy and physiology*. Available from: http://www.prostate.com.ph/anatomy.htm.
80. Mitchell, S., et al., *Phenotypic and genotypic characterization of commonly used human prostatic cell lines.* BJU Int, 2000. **85**(7): p. 932-44.
81. Mydlo, J.H. and C.J. Godec, *Prostate Cancer: Science and Clinical Practice*. 2003: Elsevier Science.
82. Horoszewicz, J.S., et al., *The LNCaP cell line--a new model for studies on human prostatic carcinoma.* Prog Clin Biol Res, 1980. **37**: p. 115-32.
83. Stone, K.R., et al., *Isolation of a human prostate carcinoma cell line (DU 145).* Int J Cancer, 1978. **21**(3): p. 274-81.
84. Kaighn, M.E., et al., *Establishment and characterization of a human prostatic carcinoma cell line (PC-3).* Invest Urol, 1979. **17**(1): p. 16-23.
85. Cussenot, O., et al., *Immortalization of human adult normal prostatic epithelial cells by liposomes containing large T-SV40 gene.* J Urol, 1991. **146**(3): p. 881-6.

86. Hayward, S.W., et al., *Establishment and characterization of an immortalized but non-transformed human prostate epithelial cell line: BPH-1.* In Vitro Cell Dev Biol Anim, 1995. **31**(1): p. 14-24.
87. Ros, S., et al., *Functional metabolic screen identifies 6-phosphofructo-2-kinase/fructose-2,6-biphosphatase 4 as an important regulator of prostate cancer cell survival.* Cancer Discov, 2012. **2**(4): p. 328-43.
88. Costello, L.C. and R.B. Franklin, *Aconitase activity, citrate oxidation, and zinc inhibition in rat ventral prostate.* Enzyme, 1981. **26**(6): p. 281-7.
89. Anastasiou, D., et al., *Inhibition of Pyruvate Kinase M2 by Reactive Oxygen Species Contributes to Cellular Antioxidant Responses.* Science, 2011. **334**(6060): p. 1278-1283.
90. Kim, J.W., et al., *HIF-1-mediated expression of pyruvate dehydrogenase kinase: a metabolic switch required for cellular adaptation to hypoxia.* Cell Metab, 2006. **3**(3): p. 177-85.
91. Yao, H., et al., *Sulforaphane inhibited expression of hypoxia-inducible factor-1alpha in human tongue squamous cancer cells and prostate cancer cells.* Int J Cancer, 2008. **123**(6): p. 1255-61.
92. Minchenko, O., et al., *Hypoxia induces transcription of 6-phosphofructo-2-kinase/fructose-2,6-biphosphatase-4 gene via hypoxia-inducible factor-1alpha activation.* FEBS Lett, 2004. **576**(1-2): p. 14-20.
93. Higgins, L.H., et al., *Hypoxia and the metabolic phenotype of prostate cancer cells.* Biochim Biophys Acta, 2009. **1787**(12): p. 1433-43.
94. Vaz, C.V., et al., *Androgen-responsive and nonresponsive prostate cancer cells present a distinct glycolytic metabolism profile.* Int J Biochem Cell Biol, 2012. **44**(11): p. 2077-84.
95. Liu, Y., *Fatty acid oxidation is a dominant bioenergetic pathway in prostate cancer.* Prostate Cancer Prostatic Dis, 2006. **9**(3): p. 230-4.
96. Kuhajda, F.P., et al., *Fatty acid synthesis: a potential selective target for antineoplastic therapy.* Proc Natl Acad Sci U S A, 1994. **91**(14): p. 6379-83.
97. Swinnen, J.V., et al., *Overexpression of fatty acid synthase is an early and common event in the development of prostate cancer.* Int J Cancer, 2002. **98**(1): p. 19-22.
98. Swinnen, J.V., et al., *Selective activation of the fatty acid synthesis pathway in human prostate cancer.* Int J Cancer, 2000. **88**(2): p. 176-9.
99. Carvajal, K. and R. Moreno-Sanchez, *Heart metabolic disturbances in cardiovascular diseases.* Arch Med Res, 2003. **34**(2): p. 89-99.
100. Effert, P., et al., *Expression of glucose transporter 1 (Glut-1) in cell lines and clinical specimens from human prostate adenocarcinoma.* Anticancer Res, 2004. **24**(5A): p. 3057-63.
101. Rashed, M.S., et al., *Diagnosis of inborn errors of metabolism from blood spots by acylcarnitines and amino acids profiling using automated electrospray tandem mass spectrometry.* Pediatr Res, 1995. **38**(3): p. 324-31.
102. Vieira Neto, E., et al., *Analysis of acylcarnitine profiles in umbilical cord blood and during the early neonatal period by electrospray*

ionization tandem mass spectrometry. Braz J Med Biol Res, 2012. **45**(6): p. 546-56.
103. Moore, K.H., A.E. Koen, and F.E. Hull, *beta-Hydroxy fatty acid production by ischemic rabbit heart.* J Clin Invest, 1982. **69**(2): p. 377-83.
104. Liedtke, A.J., *Alterations of carbohydrate and lipid metabolism in the acutely ischemic heart.* Prog Cardiovasc Dis, 1981. **23**(5): p. 321-36.
105. Whitmer, J.T., *L-carnitine treatment improves cardiac performance and restores high-energy phosphate pools in cardiomyopathic Syrian hamster.* Circ Res, 1987. **61**(3): p. 396-408.
106. Frye, R.E., S. Melnyk, and D.F. Macfabe, *Unique acyl-carnitine profiles are potential biomarkers for acquired mitochondrial disease in autism spectrum disorder.* Transl Psychiatry, 2013. **3**: p. e220.
107. Sun, D., et al., *Measurement of stable isotopic enrichment and concentration of long-chain fatty acyl-carnitines in tissue by HPLC-MS.* J Lipid Res, 2006. **47**(2): p. 431-9.
108. Santa, T., *Derivatization in liquid chromatography for mass spectrometric detection.* Drug Discov Ther, 2013. **7**(1): p. 9-17.
109. Ghoshal, A.K., et al., *Rapid measurement of plasma acylcarnitines by liquid chromatography-tandem mass spectrometry without derivatization.* Clin Chim Acta, 2005. **358**(1-2): p. 104-12.
110. Kivilompolo, M., et al., *Rapid quantitative analysis of carnitine and acylcarnitines by ultra-high performance-hydrophilic interaction liquid chromatography-tandem mass spectrometry.* J Chromatogr A, 2013. **1292**: p. 189-94.
111. Schulze, A. and A.L. Harris, *How cancer metabolism is tuned for proliferation and vulnerable to disruption.* Nature, 2012. **491**(7424): p. 364-373.
112. Vander Heiden, M.G., L.C. Cantley, and C.B. Thompson, *Understanding the Warburg Effect: The Metabolic Requirements of Cell Proliferation.* Science, 2009. **324**(5930): p. 1029-1033.
113. Lligona-Trulla, L., et al., *Acetyl-L-carnitine flux to lipids in cells estimated using isotopomer spectral analysis.* Journal of Lipid Research, 1997. **38**(7): p. 1454-62.
114. Brass, E.P., *Supplemental carnitine and exercise.* Am J Clin Nutr, 2000. **72**(2 Suppl): p. 618S-23S.
115. Giri, D., M. Ozen, and M. Ittmann, *Interleukin-6 Is an Autocrine Growth Factor in Human Prostate Cancer.* The American Journal of Pathology, 2001. **159**(6): p. 2159-2165.
116. Siegall, C.B., et al., *Expression of the Interleukin 6 Receptor and Interleukin 6 in Prostate Carcinoma Cells.* Cancer Research, 1990. **50**(24): p. 7786-7788.
117. Spiotto, M.T. and T.D. Chung, *STAT3 mediates IL-6-induced growth inhibition in the human prostate cancer cell line LNCaP.* Prostate, 2000. **42**(2): p. 88-98.
118. Shukla, S., et al., *Activation of PI3K-Akt signaling pathway promotes prostate cancer cell invasion.* Int J Cancer, 2007. **121**(7): p. 1424-32.

119. Vignozzi, L., et al., *Fat boosts, while androgen receptor activation counteracts, BPH-associated prostate inflammation.* Prostate, 2013. **73**(8): p. 789-800.
120. Norata, G.D., et al., *Dihydrotestosterone decreases tumor necrosis factor-alpha and lipopolysaccharide-induced inflammatory response in human endothelial cells.* J Clin Endocrinol Metab, 2006. **91**(2): p. 546-54.
121. Death, A.K., et al., *Dihydrotestosterone promotes vascular cell adhesion molecule-1 expression in male human endothelial cells via a nuclear factor-kappaB-dependent pathway.* Endocrinology, 2004. **145**(4): p. 1889-97.
122. Hougee, S., et al., *Decreased pro-inflammatory cytokine production by LPS-stimulated PBMC upon in vitro incubation with the flavonoids apigenin, luteolin or chrysin, due to selective elimination of monocytes/macrophages.* Biochemical Pharmacology, 2005. **69**(2): p. 241-248.
123. Lamers, J.M., et al., *The effect of lipid intermediates on Ca2+ and Na+ permeability and (Na+ + K+)-ATPase of cardiac sarcolemma. A possible role in myocardial ischemia.* Biochim Biophys Acta, 1984. **774**(1): p. 127-37.
124. Heusinkveld, H.J. and R.H. Westerink, *Caveats and limitations of plate reader-based high-throughput kinetic measurements of intracellular calcium levels.* Toxicol Appl Pharmacol, 2011. **255**(1): p. 1-8.
125. Zaidi, M., et al., *Cytosolic Free Calcium Measurements in Single Cells Using Calcium-Sensitive Fluorochromes*, in *Biomembrane Protocols*. 1994, Springer New York. p. 279-293.
126. Simpson, A.W., *Fluorescent measurement of [Ca2+]c: basic practical considerations.* Methods in molecular biology (Clifton, N.J.), 2006. **312**: p. 3-36.
127. Morgan, A.J. and A.P. Thomas, *Single-cell and subcellular measurement of intracellular Ca(2)+ concentration.* Methods Mol Biol, 2005. **312**: p. 87-117.
128. Huang, C.J., et al., *Desipramine-induced Ca2+ movement and cytotoxicity in PC3 human prostate cancer cells.* Toxicol In Vitro, 2007. **21**(3): p. 449-56.
129. Lee, K.C., et al., *Mechanism underlying histamine-induced intracellular Ca2+ movement in PC3 human prostate cancer cells.* Pharmacol Res, 2001. **44**(6): p. 547-52.
130. Heinlein, C.A. and C. Chang, *Androgen receptor in prostate cancer.* Endocr Rev, 2004. **25**(2): p. 276-308.
131. Lin, M.-T., et al., *IL-6 inhibits apoptosis and retains oxidative DNA lesions in human gastric cancer AGS cells through up-regulation of anti-apoptotic gene mcl-1.* Carcinogenesis, 2001. **22**(12): p. 1947-1953.
132. Lichtenstein, A., et al., *Interleukin-6 inhibits apoptosis of malignant plasma cells.* Cell Immunol, 1995. **162**(2): p. 248-55.
133. Ishioka, S., et al., *Effects of interleukin-6 (IL-6) on chemotherapy-induced apoptosis in human ovarian cancer cell lines.* International Journal of Clinical Oncology, 1999. **4**(2): p. 84-89.

134. Takabe, W., et al., *Lysophosphatidylcholine enhances cytokine production of endothelial cells via induction of L-type amino acid transporter 1 and cell surface antigen 4F2.* Arterioscler Thromb Vasc Biol, 2004. **24**(9): p. 1640-5.
135. Lin, D.L., et al., *Interleukin-6 induces androgen responsiveness in prostate cancer cells through up-regulation of androgen receptor expression.* Clin Cancer Res, 2001. **7**(6): p. 1773-81.
136. Taki, H., et al., *Mechanisms of the palmitoylcarnitine-induced response in vascular endothelial cells.* Pflugers Arch, 1999. **438**(4): p. 463-9.
137. Muraki, K. and Y. Imaizumi, *A novel action of palmitoyl-L-carnitine in human vascular endothelial cells.* Journal of pharmacological sciences, 2003. **92**(3): p. 252-258.
138. Brown, E.M. and R.J. MacLeod, *Extracellular Calcium Sensing and Extracellular Calcium Signaling.* Physiological Reviews, 2001. **81**(1): p. 239-297.
139. Clarke, B., et al., *On the roles of long-chain acyl carnitine accumulation and impaired glucose utilization in ischaemic contracture development and tissue damage in the guinea-pig heart.* J Mol Cell Cardiol, 1996. **28**(1): p. 171-81.
140. Rang, H.P., et al., *Rang and Dale's Pharmacology*. 6th edition ed. 2007: Churchill Livingstone.
141. Parekh, A.B. and J.W. Putney, *Store-Operated Calcium Channels.* Physiological Reviews, 2005. **85**(2): p. 757-810.
142. Alberts, B., *Molecular Biology of the Cell: Reference edition*. 2008: Garland Science.
143. Yin, H., et al., *Lipid G Protein-coupled Receptor Ligand Identification Using β-Arrestin PathHunter™ Assay.* Journal of Biological Chemistry, 2009. **284**(18): p. 12328-12338.
144. Smotrys, J.E. and M.E. Linder, *PALMITOYLATION OF INTRACELLULAR SIGNALING PROTEINS: Regulation and Function.* Annual Review of Biochemistry, 2004. **73**(1): p. 559-587.
145. Leventis, R., et al., *Acyl-CoA binding proteins inhibit the nonenzymic S-acylation of cysteinyl-containing peptide sequences by long-chain acyl-CoAs.* Biochemistry, 1997. **36**(18): p. 5546-53.
146. Duncan, J.A. and A.G. Gilman, *Autoacylation of G Protein α Subunits.* Journal of Biological Chemistry, 1996. **271**(38): p. 23594-23600.
147. Chini, B. and M. Parenti, *G-protein coupled receptors in lipid rafts and caveolae: how, when and why do they go there?* J Mol Endocrinol, 2004. **32**: p. 325 - 338.
148. Zheng, H., et al., *Palmitoylation and membrane cholesterol stabilize mu-opioid receptor homodimerization and G protein coupling.* BMC Cell Biol, 2012. **13**: p. 6.
149. Xia, C., et al., *Identification of a prostate-specific G-protein coupled receptor in prostate cancer.* Oncogene, 2001. **20**(41): p. 5903-7.
150. Yassin, G. and J.S. Dawson, *Pharmacology*. 3rd edition ed. Mosby's crash course. 2007, Edinburgh Mosby Elsevier.
151. Nakadate, T. and P.M. Blumberg, *Modulation by palmitoylcarnitine of protein kinase C activation.* Cancer Res, 1987. **47**(24 Pt 1): p. 6537-42.

152. Mangmool, S. and H. Kurose, *G(i/o) protein-dependent and -independent actions of Pertussis Toxin (PTX).* Toxins (Basel), 2011. **3**(7): p. 884-99.
153. Raj, G.V., et al., *Guanosine phosphate binding protein coupled receptors in prostate cancer: a review.* J Urol, 2002. **167**(3): p. 1458-63.
154. Cherfils, J. and M. Zeghouf, *Regulation of small GTPases by GEFs, GAPs, and GDIs.* Physiol Rev, 2013. **93**(1): p. 269-309.
155. Kamp, T.J. and J.W. Hell, *Regulation of cardiac L-type calcium channels by protein kinase A and protein kinase C.* Circ Res, 2000. **87**(12): p. 1095-102.
156. Catterall, W.A., *Structure and regulation of voltage-gated Ca2+ channels.* Annu Rev Cell Dev Biol, 2000. **16**: p. 521-55.
157. Welling, A., *Voltage-Dependant Calcium Channels* BIOTREND Reviews, 2009. **4**.
158. Lacinova, L., *Voltage-dependent calcium channels.* Gen Physiol Biophys, 2005. **24 Suppl 1**: p. 1-78.
159. Splawski, I., et al., *Ca(V)1.2 calcium channel dysfunction causes a multisystem disorder including arrhythmia and autism.* Cell, 2004. **119**(1): p. 19-31.
160. Chen, R., et al., *Ca1.3 channel alpha protein is overexpressed and modulates androgen receptor transactivation in prostate cancers.* Urol Oncol, 2013.
161. Carbonetti, N.H., *Pertussis toxin and adenylate cyclase toxin: key virulence factors of Bordetella pertussis and cell biology tools.* Future Microbiol, 2010. **5**(3): p. 455-69.
162. Williamson, Y.M., et al., *Mass spectrometric analysis of multiple pertussis toxins and toxoids.* J Biomed Biotechnol, 2010. **2010**: p. 942365.
163. Locht, C., *Molecular aspects of Bordetella pertussis pathogenesis.* Int Microbiol, 1999. **2**(3): p. 137-44.
164. Zhong, M., et al., *The Essential Role of Gialpha2 in Prostate Cancer Cell Migration.* Mol Cancer Res, 2012.
165. Melchini, A., et al., *Enhanced in vitro biological activity of synthetic 2-(2-pyridyl) ethyl isothiocyanate compared to natural 4-(methylsulfinyl) butyl isothiocyanate.* J Med Chem, 2012. **55**(22): p. 9682-92.
166. Hagelüken, A., et al., *Histamine receptor-dependent and/or -independent activation of guanine nucleotide-binding proteins by histamine and 2-substituted histamine derivatives in human leukemia (HL-60) and human erythroleukemia (HEL) cells.* Biochemical Pharmacology, 1995. **49**(7): p. 901-914.
167. Hofstra, C.L., et al., *Histamine H4 receptor mediates chemotaxis and calcium mobilization of mast cells.* J Pharmacol Exp Ther, 2003. **305**(3): p. 1212-21.
168. van der Heyden, M.A., T.J. Wijnhoven, and T. Opthof, *Molecular aspects of adrenergic modulation of cardiac L-type Ca2+ channels.* Cardiovasc Res, 2005. **65**(1): p. 28-39.
169. Currie, K.P. and A.P. Fox, *Voltage-dependent, pertussis toxin insensitive inhibition of calcium currents by histamine in bovine adrenal chromaffin cells.* J Neurophysiol, 2000. **83**(3): p. 1435-42.

170. El Sheikh, S.S., et al., *Phosphorylation of both EGFR and ErbB2 is a reliable predictor of prostate cancer cell proliferation in response to EGF.* Neoplasia, 2004. **6**(6): p. 846-53.
171. Rameh, L.E., et al., *Phosphoinositide 3-Kinase Regulates Phospholipase Cγ-mediated Calcium Signaling.* Journal of Biological Chemistry, 1998. **273**(37): p. 23750-23757.
172. Pasquet, J.M., et al., *A collagen-related peptide regulates phospholipase Cgamma2 via phosphatidylinositol 3-kinase in human platelets.* Biochem J, 1999. **342 (Pt 1)**: p. 171-7.
173. Tabata, K.-i., et al., *The orphan GPCR GPR87 was deorphanized and shown to be a lysophosphatidic acid receptor.* Biochemical and Biophysical Research Communications, 2007. **363**(3): p. 861-866.
174. Oya, M., et al., *The G Protein-coupled Receptor Family C Group 6 Subtype A (GPRC6A) Receptor Is Involved in Amino Acid-induced Glucagon-like Peptide-1 Secretion from GLUTag Cells.* Journal of Biological Chemistry, 2013. **288**(7): p. 4513-4521.
175. Lum, A.M., et al., *Orphan receptor GPR110, an oncogene overexpressed in lung and prostate cancer.* BMC Cancer, 2010. **10**: p. 40.
176. Hynes, R.O., *Integrins: Bidirectional, Allosteric Signaling Machines.* Cell, 2002. **110**(6): p. 673-687.
177. Hannigan, G.E., et al., *Regulation of cell adhesion and anchorage-dependent growth by a new beta 1-integrin-linked protein kinase.* Nature, 1996. **379**(6560): p. 91-6.
178. Gentleman, R.C., et al., *Bioconductor: open software development for computational biology and bioinformatics.* Genome Biol, 2004. **5**(10): p. R80.
179. Bengtsson, H., et al., *{aroma.affymetrix}: A generic framework in {R} for analyzing small to very large {Affymetrix} data sets in bounded memory.* 2008.
180. Huang da, W., B.T. Sherman, and R.A. Lempicki, *Systematic and integrative analysis of large gene lists using DAVID bioinformatics resources.* Nat Protoc, 2009. **4**(1): p. 44-57.
181. Facchiano, F., A. Facchiano, and A.M. Facchiano, *The role of transglutaminase-2 and its substrates in human diseases.* Front Biosci, 2006. **11**: p. 1758-73.
182. Beghetti, M., S.M. Black, and J.R. Fineman, *Endothelin-1 in congenital heart disease.* Pediatr Res, 2005. **57**(5 Pt 2): p. 16r-20r.
183. Stow, L.R., et al., *Endothelin-1 gene regulation.* Faseb j, 2011. **25**(1): p. 16-28.
184. Hamzeh, M. and B. Robaire, *Identification of early response genes and pathway activated by androgens in the initial segment and caput regions of the regressed rat epididymis.* Endocrinology, 2010. **151**(9): p. 4504-14.
185. Vesey, D.A., et al., *PAR2-induced inflammatory responses in human kidney tubular epithelial cells.* Am J Physiol Renal Physiol, 2013. **304**(6): p. F737-50.
186. Wettschureck, N. and S. Offermanns, *Mammalian G proteins and their cell type specific functions.* Physiol Rev, 2005. **85**(4): p. 1159-204.

187. Tian, L., et al., *Distinct acyl protein transferases and thioesterases control surface expression of calcium-activated potassium channels.* J Biol Chem, 2012. **287**(18): p. 14718-25.
188. Newcombe, R.G., *Interval estimation for the difference between independent proportions: comparison of eleven methods.* Stat Med, 1998. **17**(8): p. 873-90.
189. Trasino, S.E., E.H. Harrison, and T.T. Wang, *Androgen regulation of aldehyde dehydrogenase 1A3 (ALDH1A3) in the androgen-responsive human prostate cancer cell line LNCaP.* Exp Biol Med (Maywood), 2007. **232**(6): p. 762-71.
190. Massie, C.E., et al., *The androgen receptor fuels prostate cancer by regulating central metabolism and biosynthesis.* EMBO J, 2011. **30**(13): p. 2719-33.
191. Das, K., et al., *Differential expression of steroid 5alpha-reductase isozymes and association with disease severity and angiogenic genes predict their biological role in prostate cancer.* Endocr Relat Cancer, 2010. **17**(3): p. 757-70.
192. Liu, Y.Q., K. Tornheim, and J.L. Leahy, *Glucose-fatty acid cycle to inhibit glucose utilization and oxidation is not operative in fatty acid-cultured islets.* Diabetes, 1999. **48**(9): p. 1747-53.
193. Iwata, S., et al., *Regulation of endothelin-1-induced interleukin-6 production by Ca2+ influx in human airway smooth muscle cells.* European Journal of Pharmacology, 2009. **605**(1–3): p. 15-22.
194. Yang, L., et al., *Interleukin-6 differentially regulates androgen receptor transactivation via PI3K-Akt, STAT3, and MAPK, three distinct signal pathways in prostate cancer cells.* Biochem Biophys Res Commun, 2003. **305**(3): p. 462-9.
195. Alimirah, F., et al., *DU-145 and PC-3 human prostate cancer cell lines express androgen receptor: Implications for the androgen receptor functions and regulation.* FEBS Letters, 2006. **580**(9): p. 2294-2300.
196. Yue, S., et al., *Cholesteryl Ester Accumulation Induced by PTEN Loss and PI3K/AKT Activation Underlies Human Prostate Cancer Aggressiveness.* Cell Metabolism, 2014. **19**(3): p. 393-406.